



Characterising the Intra- Host Spread of Clinical Human Cytomegalovirus

A thesis submitted in candidature for the degree of
DOCTOR OF PHILOSOPHY

By

Lauren Elizabeth Kerr

November 2021

Division of Infection and Immunity,
School of Medicine,
Cardiff University

Acknowledgements

Firstly I would like to say thank you to my supervisors for their continued support during my PhD. Dr Richard Stanton, thank you for your patience and guidance through the last four years, especially for pushing me during periods where nothing seemed to go right and helping me get through to the other side. Your support has helped me to develop both professionally and personally. Thank you also to Prof Ian Humphreys and Prof Gavin Wilkinson, who have both always shown great interest in my research and for their helpful insights.

I am deeply grateful to the members of the HCMV lab, not only for their support professionally but also for their friendship and kindness. Dr Evelina Statkute, Anzelika Rubina and Dawn Roberts, thank you for becoming my support group and empathising when experiments didn't work, and for going to Personal Pole outside of work. Thanks to everyone else in UG10 for pleasantly distracting conversations, especially Pragati Sabberwal for sharing my enthusiasm for Halloween and Christmas decorations.

I would also like to thank colleagues outside of the HCMV group who assisted in obtaining data for the project including Dr Chris von Ruhland, Dr Michael Weekes, Dr Lior Sodai, Dr Maria Harkiolaki and those at Diamond Light Source Institute who have been involved in preparing samples for cryo-soft X-ray tomography. Thanks also to the Systems Immunity Research Institute, for funding the project.

To my friends and family, thank you for supporting me for the past four years, and Lee, thanks for telling me to “do my homework” at every opportunity during my writing up period! To my Mam, I really appreciate how proud you are of what I have achieved since leaving school (and the embarrassing Facebook posts that you make on my birthday). Gran, thank you for your support, even when that includes telling strangers about the time I presented at a conference in Tennessee.

Finally, I would like to thank my fiancé Tom. Thank you for your encouragement and for standing by me through all of the stressful times, the late nights, and the gruelling write-up period. Thank you for bragging about me to friends, family and your customers, even though you aren't entirely sure what I do in the lab. Thank you for doing your best to bring me up on my down days, and making me laugh when I don't feel like it. And thank you for just being you.

Summary

In vivo, Human Cytomegalovirus (HCMV) spreads predominantly via direct cell-cell contact, as do recent clinical isolates. *In vitro*, HCMV mutants are selected that produce higher levels of cell-free infectivity. Hence, laboratory strains predominantly spread via cell-free virions, and cell-cell spread has been less well characterised. The Merlin strain accurately recapitulates this mode of spread, enabling us to characterise it in more detail.

I found that cell-cell transfer is equivalent to an extremely high MOI infection, potentially providing an explanation for the ‘immune-evasive’ properties of this method of viral infection. Furthermore, infectious virions accumulated at cell-cell contacts between cells – potentially forming a virological synapse that protect virions from neutralising antibodies. As HCMV is able to superinfect individuals and recombine within the host, we investigated whether the higher number of genomes delivered by cell-cell spread affected recombination rates. However recombination was barely detectable following co-infection, even by the cell-cell route.

The interactions between HCMV and primary immature dendritic cells (DCs) were able to be explored as the Merlin strain enables efficient cell-cell infection of DCs with a virus expressing the full repertoire of viral genes. Proteomic analysis of DCs infected via the cell-cell route revealed modulation of proteins involved in the antiviral immune response, therefore providing novel insight into how HCMV manipulates the immune response to infection.

Finally, we also discovered that DCs mount two distinct responses to interfere with the Merlin strain’s ability to undergo a full lytic cycle. One leading to caspase-mediated death, and a second which halted the replication cycle at the stage of genome replication. These may represent previously unrecognised routes that the host uses to limit virus spread.

Table of Contents

Acknowledgements	I
Summary	III
Table of Contents	V
List of Figures	XI
List of Tables.....	XXIII
Abbreviations	XXV
Chapter 1. Introduction	1
1.1 Human Cytomegalovirus (HCMV).....	2
1.1.1 Herpesviruses	2
1.1.2 Human Cytomegalovirus Genome.....	4
1.1.3 Discovery and Isolation	10
1.1.4 Seroprevalence Rates	10
1.1.5 Congenital HCMV Infection.....	11
1.1.6 Clinical Presentation in AIDS Patients and Transplant Recipients	11
1.1.7 Current Therapeutics and Vaccines	12
1.2 Virion Structure.....	14
1.2.1 Capsid.....	15
1.2.2 Tegument	17
1.2.3 Envelope.....	17
1.3 Life Cycle	19
1.3.1 Cell Entry	19
1.3.2 Replication	25
1.3.3 Latent Infection and Reactivation.....	27
1.4 Evasion of the Immune Response	29
1.4.1 Innate Immunity	29
1.4.2 Adaptive Immunity	30

1.4.3 Dendritic Cells	31
1.5 Aims	34
Chapter 2. Methods and Materials	37
2.1 Tissue Culture	38
2.1.1 Cell Maintenance.....	38
2.1.2 Cell Counting.....	39
2.1.3 Long-Term Storage of Cell Lines.....	39
2.1.4 Dendritic Cells.....	40
2.1.5 Knock-down of Cellular Proteins using siRNA	41
2.1.6 Lentivirus Transduction.....	41
2.1.7 Cell Sorting.....	42
2.2 Virology	44
2.2.1 Generation of Viral Stocks	44
2.2.2 Titration of HCMV by Plaque Assay	46
2.2.3 Infecting Cell Lines with HCMV	47
2.2.4 Co-Cultures.....	47
2.2.5 HCMV Genome Delivery Assay.....	48
2.2.6 Viral DNA Extraction for Sequencing	49
2.3 Microscopy.....	50
2.3.1 Live Cell Imaging.....	50
2.3.2 Transmission Electron Microscopy	50
2.3.3 Immunofluorescence Assay.....	51
2.4 Flow Cytometry.....	53
2.4.1 Surface Staining for Flow Cytometry.....	53
2.4.2 Intracellular Staining for Flow Cytometry	53
2.5 Proteomics	55
2.5.1 Biotinylation of Dendritic Cell Plasma Membrane	55

2.5.2 Single Shot and Fractionation of Samples.....	56
2.6 Polymerase Chain Reaction (PCR)	57
2.6.1 Standard PCR.....	57
2.6.2 Quantitative Polymerase Chain Reaction (qPCR).....	58
2.6.3 RT-PCR	58
2.7 Western Blotting.....	60
2.8 Molecular Biology.....	62
2.8.1 Buffers and Solutions	62
2.8.2 Purification of DNA.....	62
2.8.3 TOPO TA Cloning.....	63
2.8.4 Antibody Cloning	63
2.8.5 Recombineering.....	67
2.8.6 <i>En Passant</i> Mutagenesis	68
2.8.7 Minipreparation of BAC DNA	70
2.8.8 Restriction Digest	70
2.8.9 Sequencing.....	70
2.8.10 Generation of Glycerol Stocks.....	71
2.8.11 Maxipreparation BAC DNA.....	71
2.9 Statistical Analysis	72
2.10 Primer Sequences	73
Chapter 3. Mechanisms of Cell-Cell Transmission of the Merlin Strain.....	83
3.1 Visualising Cell-Cell Transfer.....	85
3.1.1 The Generation of Fluorescent Viruses	85
3.1.2 Cell-Cell Transmission in Live Cells.....	89
3.1.3 Formation of a “Virological Synapse”.....	95
3.2 Quantifying Cell-Cell Transfer.....	99
3.2.1 Delivery of Viral Genomes Following Cell-Cell or Cell-Free Infection...99	

3.2.2 Potent Neutralising Antibodies.....	100
3.3 HCMV Superinfection	104
3.3.1 The Ability of HCMV to Superinfect Cells Over Time	104
3.3.2 Superinfection via Cell-Cell vs Cell-Free Transmission.....	107
3.3.3 Recombination Following Superinfection.....	113
3.4 Summary	115
Chapter 4. HCMV Manipulation of Dendritic Cells Following Cell-Cell Transfer	117
4.1 Preparation of Samples for Proteomic Analysis	119
4.1.1 Obtaining Pure Populations of HCMV-Infected DCs	119
4.1.2 Optimisation of Separation Protocols	122
4.1.3 Preparing Dendritic Cells for Proteomic Analysis.....	130
4.2 Quantitative Proteomics of Wildtype HCMV-Infected Dendritic Cells ...	131
4.2.1 Whole Cell Lysate.....	131
4.2.2 Plasma Membrane.....	132
4.2.3 Positive Controls.....	132
4.2.4 DAVID Pathway Analysis.....	134
4.2.5 Target Proteins	134
4.2.6 Validation of Target Proteins.....	139
4.3 Interactions between Single Deletion Mutants and ICOSL and ALCAM	150
4.4 Summary	157
Chapter 5. Intrinsic Antiviral Mechanisms in Dendritic Cells	159
5.1 Caspase-Mediated Apoptosis and Necroptosis	161
5.1.1 Investigation into Cause of Dendritic Cell Death.....	161
5.1.2 Z-VAD & Nec-1s.....	165
5.1.3 Multiple Caspase Inhibitors	167
5.2 Late Gene Expression.....	177
5.2.1 Immunofluorescence Assay	178

5.2.2	Intracellular Flow Cytometry	180
5.2.3	Comparing Infection Methods	182
5.2.4	APOBEC3A	184
5.3	Summary	188
Chapter 6. General Discussion.....		191
6.1	Cell-Associated Infection	192
6.1.1	Fluorescently-Tagged Virions	192
6.1.2	The Mechanism of Cell-Associated Infection	195
6.1.3	Superinfection and Recombination.....	197
6.2	Manipulation of Proteins in Dendritic Cells.....	199
6.3	Are DCs Able to Block the Lytic Cycle?	205
6.3.1	Premature Cell Death.....	205
6.3.2	Inhibition of Late Gene Expression	209
6.4	Future Directions and Concluding Remarks	211
Chapter 7. Appendix		215
Chapter 8. References		219

List of Figures

Figure 1.1 – Phylogenetic tree for the Betaherpesvirinae subfamily, adapted from Wilkie et al³. Based on concatenated amino acids of the core genes: U38, U39, U40, U41, U57, U60, U77 and U81.

Figure 1.2 – Types of herpesvirus genome structure (not to scale), adapted from Davison^{1,4}. Only repeats shown in the same colour and shade within the same structure are identical, repeats with the same colour and shade in other structures are not necessarily related. Unique regions within the same structure are unrelated to each other. Type E structure: a copy of the direct repeat (a) at the genome termini is also present internally as an inverted copy (a'). Yellow = unique regions; blue = direct repeats; red = inverted repeats. TR/IR = terminal/internal inverted repeats; L/S = long/short.

Figure 1.3 – The HCMV strain Merlin genome arrangement, adapted from Gatherer et al⁹. Inverted repeats (TRL, IRL, IRS, TRS) shown as grey blocks. Core genes are those conserved among α-, β-, and γ-herpesviruses; subcore genes are those conserved among β- and γ-herpesviruses; other genes grouped into gene families. UL72 is both a core gene and member of the DURP family.

Figure 1.4 – Combinations of seropositive or seronegative donors and recipients and the risk of developing HCMV disease following solid organ transplantation.

Figure 1.5 – The structure of a herpesvirus virion, adapted from a cryo-electron tomographic image of a HSV-1 virion⁸⁶. Black dot is a 10nm gold particle that was used as a fiducial marker.

Figure 1.6 – Transmission electron microscopy (TEM) image of a cellular junction between an infected human foetal foreskin fibroblast (HFFF) and a dendritic cell (DC) taken by Chris Von Ruhland. Red circle = mature enveloped infectious virion; green circle = NIEP; blue circle = dense body. Bar represents 2μm.

Figure 1.7 – Formation process of the three distinct types of capsids generated by HCMV, adapted from Reddehase et al⁹¹.

Figure 1.8 – Schematic showing the lytic lifecycle of HCMV in a host cell, from Crough et al.¹⁰⁴

Figure 1.9 – Directional and non-directional cell-cell spread, adapted from Zhong et al¹¹⁶. This diagram shows the difference between: A) cell-associated infection via surface tension (non-directional); and B) polarisation (directional).

Figure 1.10 – Diagram of the potential mechanisms of transfer for cell-cell spread in HCMV, that have been observed in HTLV-1 (adapted from Pique et al¹²³).

Figure 1.11 – The HCMV assembly complex in an infected fibroblast. HFFF were infected at an MOI 5 with a virus expressing GFP-tagged tegument protein UL32, 72hrs post-infection the cells were stained with Hoescht and imaged using a Zeiss microscope (Axio Observer Z1 with a XL Multi S1 Incubator) and APOTOME. AC = assembly complex; N = nucleus; Scale bar = 50µm.

Figure 3.1 – UL32-GFP/UL36-P2A-BFP/gM-(linker)mCherry virus. A) Schematic of pAL2479 construct. UL100 = gM. B) HFFF were infected with the supernatant from pAL2479-infected fibroblasts (MOI unknown), 72hrs post-infection the cells were imaged using a Zeiss microscope (Axio Observer Z1 with a XL Multi S1 Incubator) and APOTOME. Panels show fluorescence of individual markers and an overlay of all three. Scale bar = 10µm.

Figure 3.2 – Schematic of pAL2566 (top) and pAL2605 (bottom) constructs. UL75 = gH; UL55 = gB.

Figure 3.3 – UL32-GFP/gB-mCherry virus in HFFFs imaged using a Zeiss microscope 19 days post-transfection. A) One of three plaques. Scale bar = 50µm. B) Two cells within the plaque, white arrow indicates the virion assembly complex. Scale bar = 10µm.

Figure 3.4 – UL32-GFP/UL36-P2A-BFP/gM-mCherry-gM virus. A) Schematic of pAL2624, and image of HFFF infected with pAL2624 taken with Zeiss microscope. B)Schematic of pAL2759 construct. Scale bar = 10µm.

Figure 3.5 – HFFFs imaged using 2x2 binning, 20ms exposure, 50% power, every 30 mins. In the second image, taken 10 hours after the first, the cell on the left, which appeared healthy at 0hrs, can be seen breaking up into fragments, indicative of apoptosis, while the cell on the right remains intact. Scale bar = 50µm.

Figure 3.6 – HFFFs infected with UL32-GFP then stained with Hoescht (10ng/ml) and imaged using 1x1 binning, 30ms exposure, 25% power, every 30 minutes. A) Images that were taken at 0hr, 2hr, 4hr and 6hr time points selected. Scale bar = 50µm. B)Phase contrast image of the well after imaging. Bi) Higher magnification of the area highlighted by the black box in Bi.

Figure 3.7 – RPE-1 cells infected with UL32-GFP/gM-mCherry (pAL2624) imaged every 30 minutes for 48hrs. White boxes indicate a cell forming an assembly complex during the time course. Scale bar = 50µm.

Figure 3.8 – Structures formed by infected RPE-1 cells. Left and middle images, UL32-GFP; right image, UL32-GFP/gM-mCherry. Scale bar = 50 μ m.

Figure 3.9 – Electron microscopy image taken by Chris Von Ruhland, showing structure formed between HFFF and DC at 6hrs post co-culture. A) Lower magnification showing structure formed between the membranes of adjacent HFFF (right) and DC (centre). Scale bar = 10 μ m. B) Higher magnification of the area highlighted by the red square, shows HCMV particles between the two cells; DC right; HFFF left. Red circle = mature virion; black circle = dense body. Scale bar = 2 μ m.

Figure 3.10 – Image of a LifeAct GFP HFFF cell taken during pre-mapping at Diamond Light Source.

Figure 3.11 – Cryo-SXT imaging progression of DCs co-cultured with HFFFs. Non-fluorescent HFFF cells infected with UL32-GFP HCMV were co-cultured with DCs for 3hrs, DCs were stained with Hoechst prior to co-culture. A) Close up brightfield and fluorescence images taken during pre-mapping. Bi) X-ray mosaic of the area identified in A (bar = 16 μ m). Bii) A single field or view X-ray projection of area 5 in Bi. Data collected at B24 by Maria Harkiolaki and colleagues.

Figure 3.12 – Magnetic-activated cell sorting (MACS) of newly-infected HFFFs. Negative enrichment of mCherry-negative HFFFs, followed by enrichment of RatCD2-positive (infected) HFFFs.

Figure 3.13 – Genome delivery following co-culture or cell-free infection measured by gB copies per cell. HFFFs were infected with a UL36-P2A-RatCD2 virus for 24hrs either cell-free at a range of MOIs or by co-culture (four uninfected HFFFs per infected HFFF). Newly infected HFFFs were purified using MACS, DNA was extracted from the cells and gB and GAPDH quantified using QPCR. Results are representative of 3 independent experiments. Error bars refer to mean + SD of triplicate samples. ****P < 0.0001, by 1-way ANOVA.

Figure 3.14 - Treatment with potent neutralising antibodies reduces infection rates following cell-cell transfer. RPE-1 cells were infected for 24hrs with a UL36-P2A-RatCD2 virus by co-culture with HFFF-His cells. 200 μ g/ml antibody added at the same time as the co-culture. RPE-1 cells purified from HFFF-His cells 24hrs post co-culture using MACS, and analysed using flow cytometry. Results are representative of 2 independent experiments. Error bars refer to mean + SD of triplicate samples. ****P < 0.0001, by 1-way ANOVA.

Figure 3.15 – Genome delivery following co-culture +/- treatment with potent neutralising antibodies. RPE-1 cells were infected for 24hrs with a UL36-P2A-RatCD2 virus by co-culture with HFFF-His cells. 200 μ g/ml antibody added at the same time as the co-culture. Newly infected RPE-1s were purified using MACS, DNA was extracted from the cells and gB and GAPDH quantified using QPCR. Results are representative of 2 independent experiments. Error bars refer to mean + SD of triplicate samples. **P < 0.01, by 1-way ANOVA.

Figure 3.16 – Genome delivery to nucleus following co-culture +/- treatment with potent neutralising antibodies. RPE-1 cells were infected for 24hrs with a UL36-P2A-RatCD2 virus by co-culture with HFFF-His cells. 200 μ g/ml antibody added at the same time as the co-culture. Newly infected RPE-1s were purified using MACS, DNA was extracted from the nuclei and gB and GAPDH quantified using QPCR. A and B represent two independent experiments. Error bars refer to mean + SD of triplicate samples. ****P < 0.0001, ***P < 0.001, by 1-way ANOVA.

Figure 3.17 – Median fluorescence intensity (MFI) of PDGFR α on HCMV-infected HFFFs. HFFFs were infected with UL36-GFP Merlin at MOI 5 for 24hr in duplicate. Cells were harvested at 24hr intervals and surface stained with a primary anti-PDGFR α antibody and secondary anti-mouse AF647 antibody before fixing. The MFI of PDGFR α was calculated. Error bars refer to mean + SD of duplicate samples.

Figure 3.18 – Fluorescent tag expression time course. HFFFs were infected at an MOI 5 for 24hrs with either UL36-GFP Merlin (pAL2270) or US28-mCherry Merlin (pAL2988). Cells were harvested at 24hr intervals and fluorescence analysed by flow cytometry. A) Time course of UL36-GFP expressed in pAL2270-infected cells. B) Time course of US28-mCherry expressed in pAL2988-infected cells. Mock cells are uninfected HFFFs.

Figure 3.19 – Percentage of cells expressing GFP and mCherry at 96hrs post-US28-mCherry infection. HFFFs infected at MOI 5 for 24hrs with US28-mCherry (pAL2988), these cells were also infected with UL36-GFP (pAL2270) at MOI 5 either at the same time or at 24hr intervals following US28-mCherry infection. Cells were harvested and analysed by flow cytometry at 96hrs post US28-mCherry infection. Error bars refer to mean + SD of triplicate samples. *P < 0.05 by 1-way ANOVA.

Figure 3.20 – Infecting HFFFs using a co-culture system does not increase the percentage of cells that become superinfected. HFFFs infected with US28-mCherry Merlin at MOI 5, then either infected cell-free with UL36-GFP Merlin immediately or

72hrs later, or co-cultured with UL36-GFP-infected HFFFs at 72hrs post-infected. Ai) Percentage of cells expressing GFP, mock is uninfected HFFFs co-cultured with infected HFFF-His cells (UL36-GFP); ii) percentage of cells expressing both GFP and mCherry following cell-free and cell-cell infection. B) Gating strategy for identifying double positive cells in the co-culture. Error bars refer to mean + SD of triplicate samples.

Figure 3.21 – Percentage of cells expressing GFP 72hrs post co-culture. HFFFs were infected with US28-mCherry (pAL2988) with MOI 5 for 24hrs before being stained with a violet dye and co-cultured with late stage UL36-GFP-infected cells (72hrs post-infection) and analysed by flow cytometry 72hrs post co-culture to determine the percentage of mCherry+ or mock cells that obtained GFP fluorescence during the co-culture. Mock cells were uninfected cells co-cultured with late stage UL36-GFP infected HFFFs. Error bars refer to mean + SD of triplicate samples.

Figure 3.22 – Gating strategy to identify US28-mCherry (pAL2988)-infected cells that became GFP+ following co-culture with UL36-GFP (pAL2270)-infected cells. HFFFs were infected with US28-mCherry (pAL2988) with MOI 5 for 24hrs before being stained with a violet dye and co-cultured with late stage UL36-GFP-infected cells (72hrs post-infection) and analysed by flow cytometry 72hrs post co-culture.

Figure 3.23 – Co-infection reduces the intensity of UL36-GFP. HFFFs were infected with either US28-mCherry Merlin, UL36-GFP Merlin, or both for 24hrs at MOI 5 before being analysed by flow cytometry at 72hrs post-infection. A) GFP and mCherry intensity for mock (uninfected), US28-mCherry, UL36-GFP and cells co-infected with both viruses at 0hrs (cell-free). B) Histogram demonstrating a “middle intensity” peak for cells co-infected at 0hrs, compared to mock and UL36-GFP-infected cells. C) Histogram demonstrating GFP intensity in cells superinfected at 24hrs post-infection. Figure 3.24 – Primary HFFFs infected with supernatant from superinfected HFFFs to determine if recombination occurred. Primary HFFFs infected with varying quantities of supernatants for 24hrs before being overlayed with 2X DMEM/2% Avicel. A) Cells were imaged with Zeiss microscope two weeks after infection, each dilution represents two replicates. B) Plaques counted in 100 μ l wells. Error bars refer to mean + SD of triplicate samples.

Figure 4.1 – Use of MACS to separate fibroblasts from DCs, then infected from uninfected DCs.

Figure 4.2 – Dot plots showing the benefit of resting the DCs between separations. DCs that have undergone two separations immediately after each other show a significant shift in FSC/SSC (A), compared to those that are rested for 4hr between separations (B). C) HFFFs killed by washing in 100% ethanol, demonstrating that dead cells shift to the left on FSC.

Figure 4.3 – Flow cytometric analysis of mCherry expression in HIS-tagged mCherry expressing HFFF cell line. A) Comparing expression in an early passage cell line to the same cell line after multiple passages. B) Analysis following MACS of multiple passage cell line co-cultured with regular HFFFs.

Figure 4.4 – Sort report of mCherry high- and low-expressing cells by Mrs Kelly Miners. HFFF-His cells that were shown to have two mCherry peaks were harvested and sorted using a BD FACSAria to purify each population within the cell culture. i) Pre-sorted sample. ii) Post-sorting, mCherry high and mCherry low samples.

Figure 4.5 – Flow cytometric analysis comparing mCherry expression (A) and anti-His antibody binding (B) expression in different cell lines. Following purification of the mCherry high and mCherry low-expressing cells, these cell lines along with an early passage of the parental line and non-mCherry expressing HFFFs were stained with an anti-His and anti-Mouse AF647 and analysed by flow cytometry.

Figure 4.6 – Expression of RatCD2 on the surface of UL36-RatCD2 infected HFFFs.

Figure 4.7 – Five UL36 constructs containing epitope tags. A) Single FLAG tag inserted before RatCD2. B) Triple FLAG tag inserted before RatCD2. C) RatCD2 replaced with triple HA tag, linked to eGFP and GPI anchor. D) RatCD2 and exogenous signal peptide replaced with eGFP and triple FLAG tag with a transmembrane domain. E) RatCD2 replaced with a triple HA tag, linked to GFP and a transmembrane domain.

Figure 4.8 – Expression of the new UL36 tags in HFFFs is poor compared to the UL36-P2A-RatCD2 tag. HFFFs were infected with the supernatant from cells transfected with the constructs shown and analysed by flow cytometry (including surface staining for FLAG, HA and RatCD2). A) UL36-P2A-FLAG-RatCD2 (pAL2544). B) UL36-P2A-3xFLAG-RatCD2 (pAL2545). C) UL36-P2A-3xHA-eGFP-GPI (pAL2546). D) UL36-P2A-eGFP-3xFLAG (pAL2547). E) UL36-P2A-3xHA-GFP (pAL2550). F) UL36-P2A-RatCD2 (pAL2310).

Figure 4.9 – Infected DCs and bystanders separated 72 hours after co-culture and passed through two LS columns. DCs were co-cultured with UL36-P2A-RatCD2

infected HFFF-His cells for 24hrs before being separated by MACS, infected and bystander DCs were kept in culture until 72hrs post co-culture when they were then stained with anti-PE and anti-IgG beads for MACS. When the purity of the desired population is <90%, the retained sample was passed through another LS column.

Figure 4.10 – Bystander DCs shift towards the RatCD2+ population during culture. DCs were co-cultured with UL36-P2A-RatCD2 infected HFFF-His cells for 24hrs before being separated by MACS, infected and bystander DCs were kept in culture and samples taken for flow cytometry at 24hr intervals and stained with anti-RatCD2-PE antibody.

Figure 4.11 – Infected DC population purity can be improved by separating from bystanders at 24hrs post co-culture. Infected DCs and bystanders separated 24 hours after co-culture (2hrs rest after HFFF separation) using anti-PE and anti-IgG beads and MACS, separation required passing the cells through only one LS column.

Figure 4.12 – Hierarchical cluster of DC whole cell lysate. This shows the relative abundance of proteins across all samples.

Figure 4.13 – Hierarchical cluster of DC plasma membrane. This shows the relative abundance of proteins across all samples.

Figure 4.14 – Relative abundance of several proteins in dendritic cells, which are known to be downregulated by HCMV^{192, 193, 194, 195}

Figure 4.15 – DAVID pathway analysis of fractionated DC whole cell lysate and plasma membrane samples shows enrichment of proteins involved in the immune response.

Figure 4.16 – Flow diagram of selection criteria for target proteins identified in proteomics data sets.

Figure 4.17 – Validation of ALCAM downregulation using flow cytometry. A) Modulation seen in proteomics data sets. B) ALCAM expression in bystander, mock and infected DC samples.

Figure 4.18 – Validation of Caspase 10 downregulation using flow cytometry. A) Modulation seen in proteomics data sets. B) Caspase 10 expression in bystander, mock and infected DC samples.

Figure 4.19 – Validation of CD84 downregulation using flow cytometry. A) Modulation seen in proteomics data sets. B) CD84 expression in bystander, mock and infected DC samples.

Figure 4.20 – Validation of Dectin-1 downregulation using flow cytometry. A) Modulation seen in proteomics data sets. B) Dectin-1 expression in bystander, mock and pAL2344-infected DC samples.

Figure 4.21 – Validation of ICAM3 downregulation using flow cytometry. A) Modulation seen in proteomics data sets. B) ICAM3 expression in bystander, mock and infected DC samples.

Figure 4.22 – Validation of ICOSL downregulation using flow cytometry. A) Modulation seen in proteomics data sets. B) ICOSL expression in bystander, mock and infected DC samples.

Figure 4.23 – Validation of IRF7 using IFA. DCs were co-cultured with UL36-RatCD2 infected HFFF-His cells for 24hrs before being separated by MACS; infected and bystander DCs were separated by MACS 2hrs after HFFF separation. DCs were seeded onto glass-bottomed 96-well plates treated with poly-D-lysine hydrobromide before being fixed, permeabilised and stained with RatCD2-PE, rabbit anti-IRF7, anti-rabbit AF488 and DAPI after 24hrs.

Figure 4.24 – Modulation of IRF7 seen in whole cell proteomics data set.

Figure 4.25 – Validation of LAG3 downregulation using flow cytometry. A) Modulation seen in proteomics data sets. B) LAG3 expression in bystander, mock and infected DC samples.

Figure 4.26 – Validation of c-Met upregulation using flow cytometry. A) Modulation seen in proteomics data sets. B) c-Met expression in bystander, mock and infected DC samples.

Figure 4.27 – Validation of OSCAR downregulation using flow cytometry. A) Modulation seen in proteomics data sets. B) OSCAR expression in bystander, mock and infected DC samples.

Figure 4.28 – Validation of PECAM1 downregulation using flow cytometry. A) Modulation seen in proteomics data sets. B) PECAM1 expression in bystander, mock and infected DC samples.

Figure 4.29 – Validation of SCIMP downregulation using flow cytometry. A) Modulation seen in proteomics data sets. B) SCIMP expression in bystander, mock and infected DC samples.

Figure 4.30 – Validation of SECTM1 downregulation using flow cytometry. A) Modulation seen in proteomics data sets. B) SECTM1 expression in bystander, mock and infected DC samples.

Figure 4.31 – Validation of Semaphorin-4A downregulation using flow cytometry. A) Modulation seen in proteomics data sets. B) Semaphorin-4A expression in bystander, mock and infected DC samples.

Figure 4.32 – Validation of Leukosialin downregulation using flow cytometry. A) Modulation seen in proteomics data sets. B) Leukosialin expression in bystander, mock and infected DC samples.

Figure 4.33 – The HCMV strain Merlin genome arrangement, adapted from Gatherer et al⁹. Red rectangles indicate groups of genes that were removed in the block deletion mutants.

Figure 4.34 - Example of analysis of the sequenced block deletion mutant genomes using Geneious. ΔUS16 virus (pAL3060) aligned to the Merlin genome, A) the whole alignment; B) a close up of the US16 gene, showing no reads in the area of the deletion.

Figure 4.35 – Using single deletion mutants to confirm the genes responsible for downregulating ICOSL and ALCAM. DCs were co-cultured for 24hrs with infected HFFF-His cells, protein expression in mock, infected and bystander DCs was analysed by flow cytometry at 48hrs post co-culture. A) Manipulation of ICOSL with pAL2310 (WT), pAL3080 (Δ US16 & Δ US20), pAL2993 (Δ US18), pAL3186 (Δ US18 & Δ US20), and pAL3132 (Δ US20). B) Manipulation of ALCAM with pAL2310 (WT), pAL3080 (Δ US16 & Δ US20), pAL2993 (Δ US18), and pAL3132 (Δ US20).

Figure 5.1 – Diagram depicting the stages of the co-culture and separation process that were modified when investigating the cause of DC death.

Figure 5.2 – HCMV infection rates in immature and mature DCs. DCs were co-cultured with UL36-GFP infected HFFF-His cells for 24hrs before separation of HFFFs and DCs. The percentage of infected cells calculated from live cells at each time point, by staining the DCs with a viability stain and analysing fluorescence using flow cytometry. DCs were matured with either LPS or TNF- α 24hrs prior to co-culture.

Figure 5.3 – Survival of immature DCs infected with HCMV-GFP via co-culture, up to 96hrs post co-culture. DCs were co-cultured with UL36-GFP infected HFFF-His cells for 24hrs before separation of HFFFs and DCs. The percentage of GFP+ cells was calculated from live dendritic cells at each time point, by staining the DCs with a viability stain and analysing fluorescence using flow cytometry. Representative of two donors.

Figure 5.4 – Survival of HCMV-infected DCs following treatment with caspase and necroptosis inhibitors. DCs were co-cultured with UL36-GFP infected HFFF-His cells for 24hrs before separation of HFFFs and DCs. Z-VAD and Nec-1s were added to the media of the DCs immediately after separation from HFFFs. The percentage of infected cells was calculated from live dendritic cells at each time point, by staining the DCs with a viability stain and analysing fluorescence using flow cytometry.

Figure 5.5 – Simple schematic of caspase-dependent apoptosis and the stimuli which trigger the cascade.

Figure 5.6 – Modulation of Caspase 2 seen in DC whole cell lysate proteomics dataset. DCs were co-cultured with UL36-RatCD2 infected HFFF-His cells for 24hrs before separation of HFFFs and DCs, and separation of infected and bystander DCs. DCs were lysed and the whole cell lysates analysed for protein abundance.

Figure 5.7 – Modulation of Caspase 3 seen in DC whole cell lysate proteomics dataset. DCs were co-cultured with UL36-RatCD2 infected HFFF-His cells for 24hrs before separation of HFFFs and DCs, and separation of infected and bystander DCs. DCs were lysed and the whole cell lysates analysed for protein abundance.

Figure 5.8 – Modulation of Caspase 6 seen in DC whole cell lysate proteomics dataset. DCs were co-cultured with UL36-RatCD2 infected HFFF-His cells for 24hrs before separation of HFFFs and DCs, and separation of infected and bystander DCs. DCs were lysed and the whole cell lysates analysed for protein abundance.

Figure 5.9 – Modulation of Caspase 7 seen in DC whole cell lysate proteomics dataset. DCs were co-cultured with UL36-RatCD2 infected HFFF-His cells for 24hrs before separation of HFFFs and DCs, and separation of infected and bystander DCs. DCs were lysed and the whole cell lysates analysed for protein abundance.

Figure 5.10 – Modulation of Caspase 8 seen in DC whole cell lysate proteomics dataset. DCs were co-cultured with UL36-RatCD2 infected HFFF-His cells for 24hrs before separation of HFFFs and DCs, and separation of infected and bystander DCs. DCs were lysed and the whole cell lysates analysed for protein abundance.

Figure 5.11 – Modulation of Caspase 10 seen in DC whole cell lysate proteomics dataset. DCs were co-cultured with UL36-RatCD2 infected HFFF-His cells for 24hrs before separation of HFFFs and DCs, and separation of infected and bystander DCs. DCs were lysed and the whole cell lysates analysed for protein abundance.

Figure 5.12 - Survival of HCMV-infected DCs following treatment with caspase inhibitors. Dendritic DCs were co-cultured with UL36-GFP infected HFFF-His cells

for 24hrs before separation of HFFFs and DCs. Caspase inhibitors were added to the DC media immediately after separation from HFFFs. The percentage of GFP+ cells was calculated from live dendritic cells at each time point, by staining the DCs with a viability stain and analysing fluorescence using flow cytometry. Untreated, Z-VAD, Z-IETD and Z-AEVD samples were performed in triplicate, Z-VDVAD and Z-LEHD performed in singlicate. Representative of four donors. Error bars refer to mean + SD of triplicate samples.

Figure 5.13 - Survival of HCMV-infected DCs using tagged, untagged and Δ UL36 strains, in control conditions (left) or following treatment with Z-VAD (right). DCs were co-cultured with UL36-GFP, IE2-GFP or Δ UL36-GFP infected HFFF-His cells for 24hrs before separation of HFFFs and DCs. Z-VAD was added to the media of the DCs immediately after separation from HFFFs. The percentage of infected cells was calculated from live dendritic cells at each time point, by staining the DCs with a viability stain and analysing fluorescence using flow cytometry. Each sample was performed in triplicate. Error bars refer to mean + SD of triplicate samples.

Figure 5.14 – Survival of HCMV-infected DCs using tagged, untagged and Δ UL36 strains, following treatment with caspase inhibitors. DCs were co-cultured with UL36-GFP, IE2-GFP or Δ UL36-GFP infected HFFF-His cells for 24hrs before separation of HFFFs and DCs. Caspase inhibitors were added to the media of the DCs immediately after separation from HFFFs. The percentage of infected cells was calculated from live dendritic cells at each time point, by staining the DCs with a viability stain and analysing fluorescence using flow cytometry. Each sample was performed in triplicate, error bars refer to mean + SD of triplicate samples.

Figure 5.15 – Comparison of HCMV gene expression in HFFFs and DCs from whole cell lysate data; infected via the cell-free and cell-associated routes, respectively. A) Temporal expression profiles showing relative abundance of HCMV genes. B) Graph showing relative abundance of the late gene UL32 in DCs and HFFFs.

Figure 5.16 – Immediate early (IE1) and late gene (UL32) expression in dendritic cells co-cultured with Merlin-infected HFFFs, then the DCs separated from the HFFF. A) Immunofluorescence (IF) image taken 96hrs post co-culture, nuclei stained with DAPI, IE1 stained with anti- IE1-AF647, UL32 tagged with GFP in virus. B) IF data from each time point quantified in chart. Error bars refer to mean + SD of triplicate samples. *P < 0.05, ****P < 0.0001 by 1-way ANOVA.

Figure 5.17 – Histogram plots comparing gB expression DCs to positive control over a time course. DCs were co-cultured with UL36-GFP infected HFFF-His cells for 24hrs before separation of HFFFs and DCs. gB was stained for intracellularly and fluorescence was analysed by flow cytometry. HFFFs at 72hrs post-infection used as positive control for gB staining. “Mock” = DCs co-cultured with uninfected HFFFs. CMV -ve serum used as Fc block. Representative of two donors.

Figure 5.18 – Comparing cell-cell and cell-free infection rates of dendritic cells at 24hrs post-infection. Both Merlin (pAL2344) and TB40 (pAL2413) contained a UL36-P2A-GFP tag. DCs infected cell-free with Merlin at unknown MOI, or with TB40 at MOI 50. DCs infected cell-cell with Merlin were co-cultured with infected HFFF-His cells for 24hrs before separation of HFFFs and DCs. “Mock” = uninfected DCs not co-cultured with HFFFs. DCs were stained with a viability stain and live cells gated before analysing GFP fluorescence using flow cytometry.

Figure 5.19 – Modulation of APOBEC3A (A3A) and APOBEC3G (A3G) seen in the DC whole cell lysate proteomics dataset. DCs were co-cultured with UL36-RatCD2 infected HFFF-His cells for 24hrs before separation of HFFFs and DCs, and separation of infected and bystander DCs. DCs were lysed and the whole cell lysates analysed for protein abundance.

Figure 5.20 – Comparing gB expression in DCs with knocked down A3A to untreated DCs and HFFFs. QPCR used to measure gB copies per cell in each sample. Target cells A) DCs, and B) HFFFs were separated from HFFF-His cells at 24hrs post co-culture. Error bars refer to mean + SD of triplicate samples. ***P < 0.0001 by 1-way ANOVA.

Figure S.1 – Virion movement in RPE-1 cells. RPE-1 cells infected with UL32-GFP by co-culture with HFFFs. A) Images captured every 0.1 seconds. B) Video captured in real time. Follow this link for videos:
<https://photos.app.goo.gl/QAsvTYuDeGosSFNu5>

Figure S.2– Gating strategy showing poor viability of DCs at 96hrs post-infection with cell-free UL36-GFP (pAL2344).

List of Tables

Table 1.1 – Subfamilies and their genera in the family Herpesviridae, adapted from Davison et al².

Table 1.2 – HCMV gene family members and a summary of their functions^{16, 17, 18, 19, 20, 21, 22, 23, 24, 25, 26, 27}

Table 1.3 – Information on some strains of HCMV, including both laboratory and clinical strains.

Table 1.4 – List of anti-HCMV drugs that can be used for prophylaxis or treatment of CMV disease, the method of administration, and mechanism of action^{64, 77, 79, 81, 82}.

Table 1.5 – Some of the surface markers used for DC classification^{155, 158, 159}.

Table 2.1 – Tissue culture media and reagents used in this project.

Table 2.2 – List of cell lines used in this project.

Table 2.3 – MACS reagents used in this project.

Table 2.4 – List of siRNAs used in this project.

Table 2.5 – List of HCMV viruses used and/or made in this project.

Table 2.6 – List of antibodies used for immunofluorescence assays in this project.

Table 2.7 – List of antibodies used for flow cytometry in this project.

Table 2.8 – List of cell dyes used for flow cytometry in this project.

Table 2.9 – Reagents used for biotinylation of dendritic cell plasma membranes.

Table 2.10 – Standard PCR programme used in this project.

Table 2.11 - Phusion PCR programme used in this project.

Table 2.12 – Thermocycling programme, Comparative CT with Melt, used for qPCR in this project.

Table 2.13 – Primer Sequences used for qPCR and RT-PCR.

Table 2.14 – Reagents used for Western Blotting in this project.

Table 2.15 – Antibodies used for Western Blotting in this project.

Table 2.16 – List of buffers and solutions used in this project.

Table 2.17 – Information regarding vectors used for antibody cloning.

Table 2.18 – Sequences for heavy and light chains of anti-pentamer (2.18) and anti-gH (70.7) antibodies.

Table 2.19 – Primer sequences used for recombineering, En Passant and antibody cloning in this project.

Table 3.1 – Amino acid sequence for the linker used to tag genes with mCherry.

Table 3.2 – Settings used for optimisation of long-term fluorescence microscopy of HFFFs.

Table 4.1 – Targets chosen from list of proteomic hits from both data sets. PM = plasma membrane. WCL = whole cell lysate.

Table 4.2 – Summary of how each of the selected proteins was validated.

Table 4.3 – List of UL36-P2A-RatCD2 block deletion mutants engineered for proteomic analysis. Potential interactions with targets based on previous data ²⁴.

Table 4.4 – GRACy SNP analysis of the UL36-P2A-RatCD2 block deletion mutants.

Only mutations that were found in >10% of SNPs are noted h

Table 5.1 – Conditions tested during DC death investigations. Dendritic cells were co-cultured for 24hrs with HFFF-His cells infected with UL36-RatCD2 virus unless stated otherwise, before undergoing separation from the HFFFs, and then separation of infected and bystander DCs. DC death was measured by using flow cytometry to count the number of DCs before and after each step of the separation process and up to 72hrs post co-culture; and by staining the DCs with a viability stain. Each condition was tested with a minimum of two different donors.

Table 5.2 – List of specific caspase inhibitors used in this study.

Table 5.3 – Percentage reduction of A3A or GAPDH following siRNA knockdown in DCs. CT values and $2^{-(\Delta\Delta CT)}$ values using equations listed in Equation 5.1.

Abbreviations

<i>Abbreviation</i>	<i>Meaning</i>
<i>AC</i>	Assembly compartment
<i>ACV</i>	Acyclovir
<i>ADCC</i>	Antibody-dependent cellular cytotoxicity
<i>AF</i>	Alexa Fluor
<i>AIDS</i>	Acquired immune deficiency syndrome
<i>AIM2</i>	Absent in melanoma 2
<i>ALCAM</i>	Activated leukocyte cell adhesion molecule
<i>APC</i>	Antigen presenting cell
<i>A3A</i>	APOBEC3A
<i>A3G</i>	APOBEC3G
<i>BAC</i>	Bacterial artificial chromosome
<i>BDCA-2</i>	Blood DC antigen 2
<i>BFP</i>	Blue fluorescent protein
<i>BoHV6</i>	Bovine lymphotropic herpesvirus
<i>CASP10</i>	Caspase-10
<i>CCMV</i>	Chimpanzee cytomegalovirus
<i>cDC</i>	Conventional dendritic cell
<i>CDV</i>	Cidofovir
<i>CID</i>	Cytomegalic inclusion disease
<i>CLEC7A</i>	C-type lectin domain family 7 member A
<i>CLP</i>	Common lymphoid progenitor
<i>CMP</i>	Common myeloid progenitor
<i>CMV</i>	Cytomegalovirus
<i>CPE</i>	Cytopathogenic effect
<i>Cryo-SIM</i>	Cryo-structured illumination microscopy
<i>Cryo-SXT</i>	Cryo-soft X-ray tomography
<i>CTL</i>	Cytotoxic T lymphocyte
<i>DAVID</i>	Database for annotation, visualization and integrated discovery
<i>DC</i>	Dendritic cell
<i>DC-SIGN</i>	DC-specific ICAM-grabbing nonintegrin
<i>DMEM</i>	Dulbecco's modified eagle medium
<i>DMSO</i>	Dimethyl sulfoxide
<i>dNTPs</i>	Deoxynucleotides
Δ	Delta
<i>E</i>	Early
<i>EBV</i>	Epstein-Barr virus
<i>ECM</i>	Extracellular matrix
<i>EHV2</i>	Equid herpesvirus 2
<i>ElHV1/EEHV1</i>	Elephantid herpesvirus 1
<i>EL</i>	Early-late
<i>EM</i>	Electron microscopy
<i>ER</i>	Endoplasmic reticulum
<i>EYFP</i>	Enhanced yellow fluorescent protein
<i>Fab</i>	Antigen-binding fragment
<i>FACS</i>	Fluorescence-activating cell sorting
<i>FasL</i>	Fas ligand

<i>FcyR</i>	Fc gamma receptor
<i>FCS</i>	Foetal calf serum
<i>FMV</i>	Fomivirsen
<i>FOS</i>	Foscarnet
<i>GaHV2</i>	Gallid herpesvirus 2
<i>gB/D/H/L/M/N/O</i>	Glycoprotein B/D/H/L/M/N/O
<i>GCV</i>	Ganciclovir
<i>GFP</i>	Green fluorescent protein
<i>GMCMV</i>	Green monkey cytomegalovirus
<i>GM-CSF</i>	Granulocyte-macrophage colony-stimulating factor
<i>GPCMV</i>	Guinea pig cytomegalovirus
<i>GPCR</i>	G protein-coupled receptor
<i>GSDMD</i>	Gasdermin D
<i>GVHD</i>	Graft-versus-host disease
<i>HAART</i>	Highly active anti-retroviral treatment
<i>HCMV</i>	Human cytomegalovirus
<i>HDAC</i>	Histone deacetylase
<i>HEK293</i>	Human embryonic kidney 293 cells
<i>HEK293T</i>	Human embryonic kidney 293T cells
<i>HFFF</i>	Human foetal foreskin fibroblasts
<i>HHV-</i>	Human herpesvirus-1/3/4/5/6/8
<i>I/3/4/5/6/8</i>	
<i>His</i>	Histidine
<i>HIV</i>	Human immunodeficiency virus
<i>HLA-E</i>	Human leukocyte antigen E
<i>HSCT</i>	Haematopoietic stem cell transplant
<i>HSPG</i>	Heparan sulfate proteoglycan
<i>HSV</i>	Herpes simplex virus
<i>HTLV</i>	Human T-lymphotropic virus
<i>IAA</i>	Iodoacetamide
<i>ICAM3</i>	Intracellular adhesion molecule 3
<i>ICSL</i>	Inducible T-cell co-stimulator ligand
<i>IC₅₀</i>	IgG concentration needed to achieve 50% viral entry inhibition
<i>IE</i>	Immediate-early
<i>IF</i>	Immunofluorescence
<i>IFA</i>	Immunofluorescence assay
<i>IFN</i>	Interferon
<i>IgG</i>	Immunoglobulin G
<i>IL4/10</i>	Interleukin 4/10
<i>IMS</i>	Industrial methylated spirit
<i>iNOS</i>	Inducible nitric oxide synthase
<i>IPA</i>	Isopropanol
<i>IR</i>	Internal inverted repeat
<i>IRF3/7</i>	Interferon regulatory factor 3/7
<i>KSHV</i>	Kaposi's sarcoma-associated herpesvirus
<i>L</i>	Late
<i>LC</i>	Langerhans cell
<i>LAG3</i>	Lymphocyte activating gene 3
<i>LB</i>	Luria-Bertani

<i>LIR-1</i>	Leukocyte immunoglobulin-like receptor 1
<i>LPS</i>	Lipopolysaccharide
<i>MACS</i>	Magnetic-activated cell sorting
<i>MCMV</i>	Murine cytomegalovirus
<i>MCP</i>	Major capsid protein
<i>mCP</i>	Minor capsid protein
<i>mCPB</i>	Minor capsid protein binding protein
<i>MFI</i>	Median fluorescence intensity
<i>MHC-I/II</i>	Major histocompatibility complex class I/II
<i>MICA/B</i>	MHC-I related protein A/B
<i>MIE</i>	Major immediate early gene
<i>MIEP</i>	Major immediate early promoter
<i>miRNA</i>	MicroRNA
<i>moDCs</i>	Monocyte-derived dendritic cells
<i>MOI</i>	Multiplicity of infection
<i>MSHV</i>	<i>Miniopterus schreibersii</i> herpesvirus
<i>MuHV1</i>	Murid herpesvirus 1
<i>NEC</i>	Nuclear egress complex
<i>NFKB</i>	Nuclear factor kappa B
<i>NIEP</i>	Non-infectious enveloped particle
<i>NK</i>	Natural killer cell
<i>NKG2A/B/D</i>	Natural-killer group 2, member A/B/D
<i>NO</i>	Nitric oxide
<i>OD₆₀₀</i>	Optical density
<i>OMCMV</i>	Owl monkey cytomegalovirus
<i>ORF</i>	Open reading frame
<i>OSCAR</i>	Osteoclast-associated immunoglobulin-like receptor
<i>PAMP</i>	Pathogen-associated molecular pattern
<i>PBMC</i>	Peripheral blood mononuclear cells
<i>PBS</i>	Phosphate-buffered saline
<i>PCMV</i>	Porcine cytomegalovirus
<i>PCR</i>	Polymerase chain reaction
<i>pDC</i>	Plasmacytoid dendritic cell
<i>PDGFRα</i>	Platelet-derived growth factor receptor α
<i>PDL</i>	Poly-D-lysine
<i>PECAM1</i>	Platelet endothelial cell adhesion molecule
<i>PFA</i>	Paraformaldehyde
<i>PFU</i>	Plaque-forming units
<i>PI</i>	Protease inhibitor
<i>PM</i>	Plasma membrane
<i>PMNLs</i>	Polymorphonuclear lymphocytes
<i>pp65/150</i>	Phosphoprotein 65/150
<i>PRR</i>	Pattern recognition receptor
<i>PsSHV1</i>	Psittacid herpesvirus 1
<i>QPCR</i>	Quantitative polymerase chain reaction
<i>RCMV</i>	Rat cytomegalovirus
<i>RhCMV</i>	Rhesus cytomegalovirus
<i>RPE-1</i>	Retinal pigmented epithelial cells
<i>rpm</i>	Rotations per minute
<i>RPMI</i>	Roswell Park Memorial Institute medium

<i>SCIMP</i>	SLP adapter and CSK-interacting membrane protein
<i>SCP</i>	Smallest capsid protein
<i>SD</i>	Standard deviation
<i>SECTM1</i>	Secreted and transmembrane protein 1
<i>SEMA4A</i>	Semaphorin-4A
<i>SGV</i>	Salivary gland virus
<i>SLAM</i>	Self-ligand receptor of the signalling lymphocytic activation molecule
<i>SMCMV</i>	Squirrel monkey cytomegalovirus
<i>SPN</i>	Leukosialin
<i>TEM</i>	Transmission electron microscopy
<i>TER</i>	TAAB Embedding Resin
<i>tetR</i>	Tetracycline repressor
<i>TLR</i>	Toll-like receptor
<i>TMT</i>	Tandem mass tag
<i>TNF</i>	Tumour necrosis factor
<i>TNFα</i>	Tumour necrosis factor α
<i>TNFR1</i>	Tumour necrosis factor receptor 1
<i>TP</i>	Temporal protein
<i>TR</i>	Terminal inverted repeat
<i>TRIM21</i>	Tripartite motif containing-21
<i>TRI1</i>	Triplex subunit 1
<i>TRI2</i>	Triplex subunit 2
<i>TuHV</i>	Tupaiiid herpesvirus
<i>UL</i>	Unique long
<i>UL128L</i>	UL128 locus
<i>UPR</i>	Unfolded protein response
<i>Us</i>	Unique short
<i>vICA</i>	Viral inhibitor of caspase-8-induced apoptosis
<i>vIRA</i>	Viral inhibitor of RIP activation
<i>vMIA</i>	Viral mitochondria inhibitor of apoptosis
<i>WCL</i>	Whole cell lysate
<i>WHO</i>	World Health Organisation
<i>WT</i>	Wildtype

Chapter 1.

Introduction

1.1 Human Cytomegalovirus (HCMV)

Human cytomegalovirus, also known as Human herpesvirus-5 (HHV-5), a part of the *Herpesviridae* family, is the most common viral cause of congenital malformation, as well as being responsible for complications in immunocompromised individuals. HCMV infection is lifelong, and in immunocompetent people is usually asymptomatic; HCMV also has a worldwide seroprevalence. The global distribution of HCMV infection and the financial burden of treating those with complications of viral infection has led the WHO to designate the development of a vaccine as high priority.

1.1.1 Herpesviruses

Herpesviruses (also known as *Herpesviridae*) are a group of large DNA viruses that are able to infect a wide range of animals including primates, other mammals, birds, reptiles, fish, amphibians and invertebrates, with multiple species being able to infect the same host at any one time. Herpesviruses have a large, double-stranded DNA genome, enclosed in a spherical particle of around 200nm in diameter¹. The *Herpesviridae* family has recently been split into three families in the new order of *Herpesvirales*; these families are the *Herpesviridae* family, containing mammal, bird and reptile viruses; *Alloherpesviridae* family comprising of fish and amphibian viruses; and the *Malacoherpesviridae* family containing a bivalve virus².

The *Herpesviridae* family is then further classified into subfamilies *alpha*, *beta* and *gammaherpesvirinae*, which are summarised in Table 1.1. HCMV is of the subfamily *betaherpesvirinae*, this group of viruses infect a limited number of species and have comparatively slow replication cycles¹. The subfamily has been updated to comprise of the following genera: *Cytomegalovirus*, *Muromegalovirus*, *Roseolovirus*, and *Proboscivirus* (Figure 1.1); so far 20 species of viruses have been assigned to the *betaherpesvirus* subfamily³.

	<i>Subfamily</i>	<i>Genus</i>
<i>Alphaherpesvirinae</i>	<i>Simplexvirus</i>	(e.g. <i>Human herpesvirus 1</i> (HHV-1)/ <i>Herpes simplex virus 1</i> (HSV1))
	<i>Varicellovirus</i>	(e.g. <i>Human herpesvirus 3</i> (HHV-3)/ <i>Varicella-zoster virus</i>)
	<i>Mardivirus</i>	(e.g. <i>Gallid herpesvirus 2</i> (GaHV2)/ <i>Marek's disease virus type 1</i>)
	<i>Iltovirus</i>	(e.g. <i>Psittacid herpesvirus 1</i> (PsHV1)/ <i>Pacheco's disease virus</i>)
<i>Betaherpesvirinae</i>	<i>Cytomegalovirus</i>	(e.g. <i>Human herpesvirus 5</i> (HHV-5)/ <i>Human cytomegalovirus</i> (HCMV))
	<i>Muromegalovirus</i>	(e.g. <i>Murid herpesvirus 1</i> (MuHV1)/ <i>Murine cytomegalovirus</i> (MCMV))
	<i>Roseolovirus</i>	(e.g. <i>Human herpesvirus 6</i> (HHV-6))
	<i>Proboscivirus</i>	(e.g. <i>Elephantid herpesvirus 1</i> (ElHV1)/ <i>Elephant endotheliotropic herpesvirus</i>)
<i>Gammaherpesvirinae</i>	<i>Lymphocryptovirus</i>	(e.g. <i>Human herpesvirus 4</i> (HHV-4)/ <i>Epstein-Barr virus</i> (EBV))
	<i>Radinovirus</i>	(e.g. <i>Human herpesvirus 8</i> (HHV-8)/ <i>Kaposi's sarcoma-associated herpesvirus</i> (KSHV))
	<i>Macavirus</i>	(e.g. <i>Bovine herpesvirus 6</i> (BoHV6)/ <i>Bovine lymphotropic herpesvirus</i>)
	<i>Percavirus</i>	(e.g. <i>Equid herpesvirus 2</i> (EHV2)/ <i>Equine herpesvirus 2</i>)

Table 1.1 – Subfamilies and their genera in the family Herpesviridae, adapted from Davison et al².

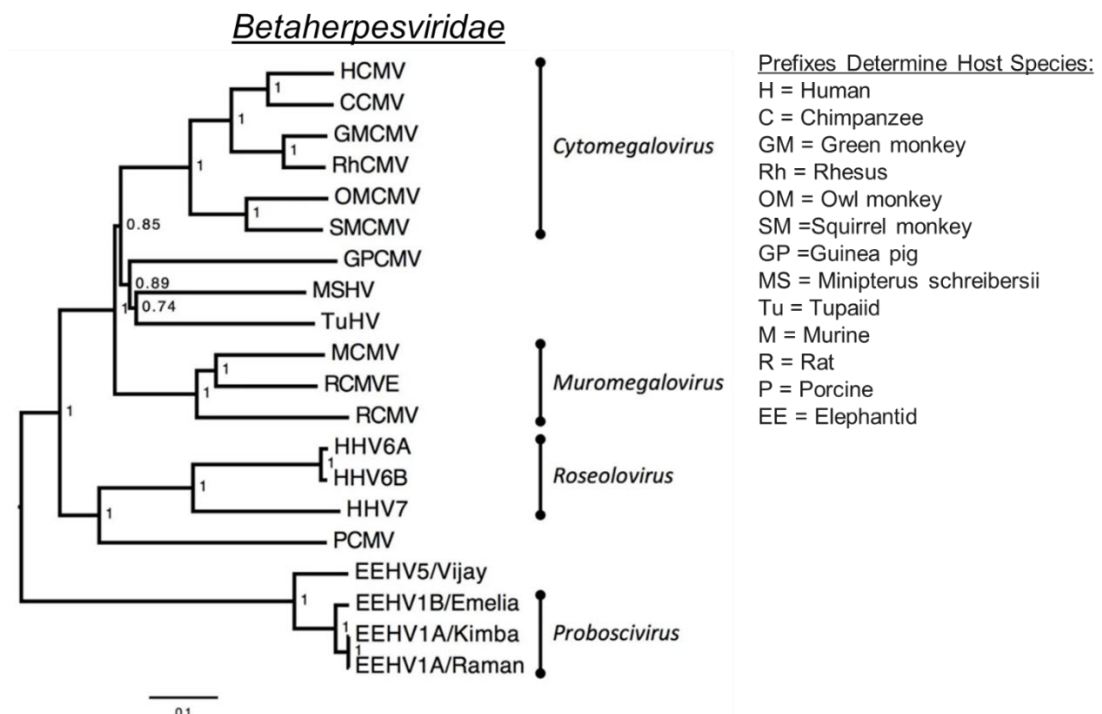


Figure 1.1 – Phylogenetic tree for the Betaherpesvirinae subfamily, adapted from Wilkie et al³. Based on concatenated amino acids of the core genes: U38, U39, U40, U41, U57, U60, U77 and U81.

1.1.2 Human Cytomegalovirus Genome

Herpesvirus genomes contain direct and inverted repeats, as well as lengths of unique regions (sometimes short and long regions). There are six different types of genome structures that have been recorded for herpesviruses (Figure 1.2). Human cytomegalovirus (HCMV) has a type E genome structure, this complicated genome structure is characteristic of *alphaherpesviruses* (especially *Simplexviruses*), although in the case of HCMV and chimpanzee cytomegalovirus (CCMV), their genomes evolved independently within the *betaherpesvirus* subfamily⁴.

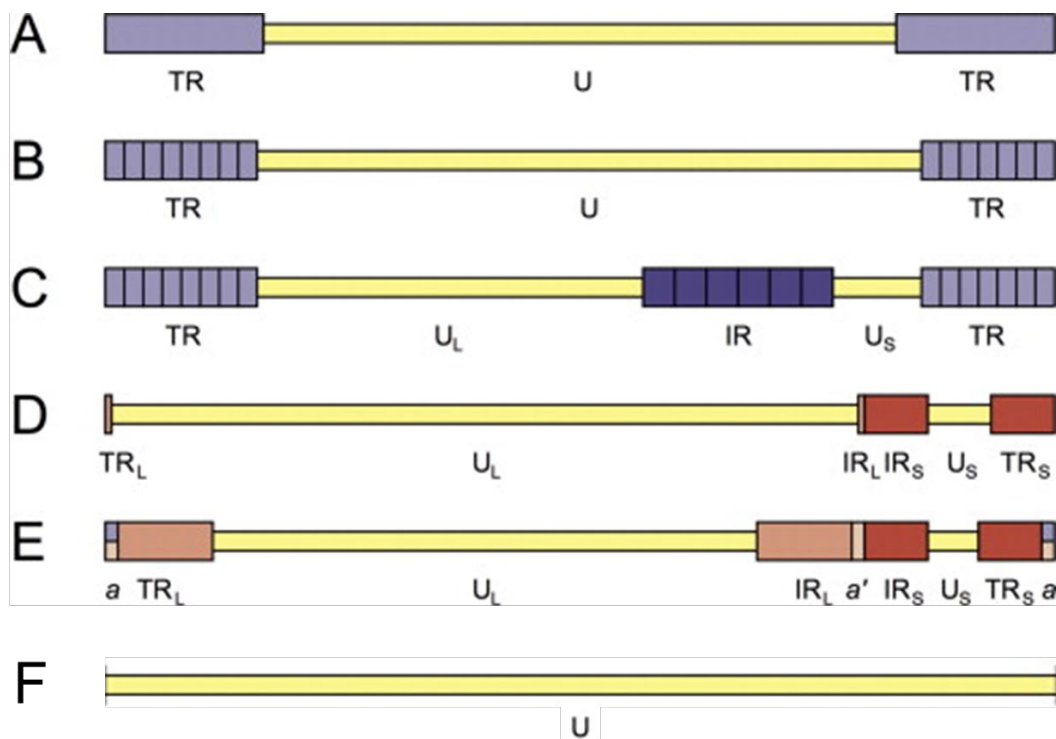


Figure 1.2 – Types of herpesvirus genome structure (not to scale), adapted from Davison¹⁻⁴. Only repeats shown in the same colour and shade within the same structure are identical, repeats with the same colour and shade in other structures are not necessarily related. Unique regions within the same structure are unrelated to each other. Type E structure: a copy of the direct repeat (a) at the genome termini is also present internally as an inverted copy (a'). Yellow = unique regions; blue = direct repeats; red = inverted repeats. TR/IR = terminal/internal inverted repeats; L/S = long/short.

HCMV has a linear genome of approximately 235,000bp in length⁵ (strain dependent), making it the largest known herpesvirus⁶. The genome (as previously mentioned) is type E – containing UL (unique long) and US (unique short) sequences, flanked by terminal (TR) and internal (IR) inverted repeats, with a single 3' unpaired base on each end⁷. The TR_L and TR_S regions consist of *a* and *b*, and *c* and *a* sequences, respectively; the IR_L to IR_S region consists of *b'a'c'* sequences, hence, the sequence of the type E genome is *ab*-UL-*b'a'c'*-US-*ca* – the prime specifies a sequence that is inverted^{5, 8, 9}.

There is much debate about the content of the HCMV genome, however the general understanding is wildtype HCMV encodes approximately 165-170 protein coding genes, 23 microRNAs (miRNAs), four long non-coding RNAs and two oriLyt RNAs (Figure 1.3 and Table 1.2)^{6, 10}.

The complete DNA sequence for AD169 (a heavily passaged strain) was the first to be published in 1990¹¹, and subsequent sequencing of low passage strains, including Merlin, and clinical isolates revealed that the AD169 genome actually contains multiple frameshift mutations and deletions affecting around 24 genes⁶ (dependent on stock). Akter et al. determined that disruption of the UL128 locus (UL128L) was also common in low-passage strains; specifically, disruptions of the UL128 gene (such as the single nucleotide substitution that results in a truncated form of the protein in the Merlin strain), frameshift mutations affecting UL131A, and deletions of both UL130 and UL131A¹². In addition to the UL128L disruptions in passaged strains, most were also found to contain mutations in the RL11 family⁶. Mutations of many of these genes is related to adaptation of HCMV to passage in human foetal foreskin fibroblasts (HFFFs), however systematic analysis of virus strain sequences over time in multiple cell types revealed that mutations are always selected when HCMV strains are passaged *in vitro*¹³, irrespective of the cell type used. Further work has shown that these mutations can be very subtle, and may not be easily detected by bioinformatic analysis. Examples of HCMV strains are found in Table 1.3, including major mutations in some commonly used laboratory strains and the source of isolation. Mutations are also common in circulating strains, a high-throughput analysis of clinical isolates found that only 23% had an ‘intact’ genome, and 15% of genes were found to have mutations, some of which are deleterious, including: RL5A, RL6, UL1 and UL9 of the RL11 family; UL111A, and UL150^{6, 14, 15}. Most of the genes that are mutated in clinical strains *in vivo* are hypervariable. Although a quarter of circulating

strains do not possess an ‘intact’ genome, the mutations that are found naturally in circulating strains are very different from those acquired following *in vitro* passage, thus it is important to differentiate the two situations.

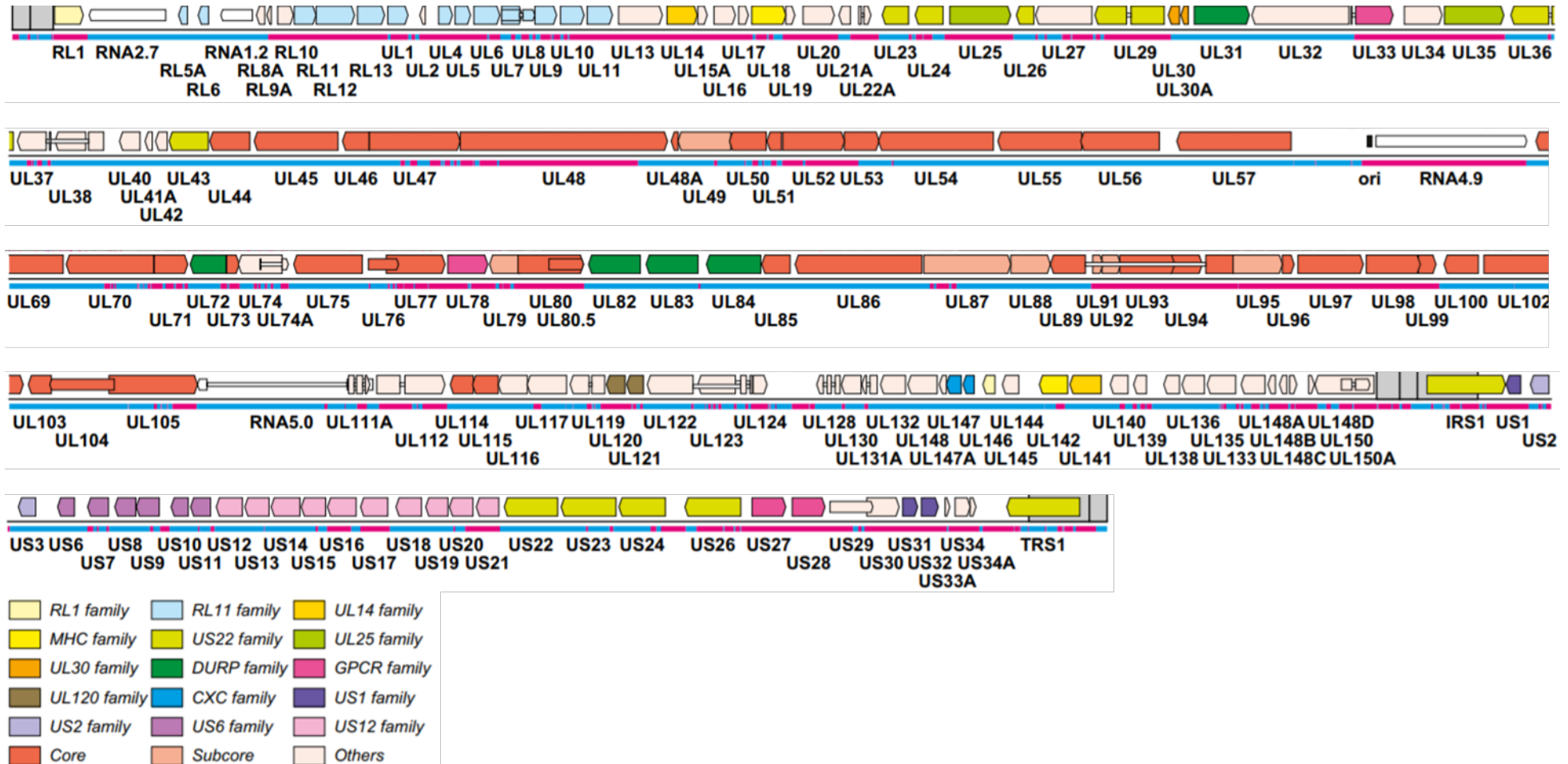


Figure 1.3 – The HCMV strain Merlin genome arrangement, adapted from Gatherer et al⁹. Inverted repeats (TR_L , IR_L , IR_S , TR_S) shown as grey blocks. Core genes are those conserved among α -, β -, and γ -herpesviruses; subcore genes are those conserved among β - and γ -herpesviruses; other genes grouped into gene families. UL72 is both a core gene and member of the DURP family.

<i>HCMV Gene Family</i>	<i>Family Members</i>	<i>Known Functions</i>
<i>RL1</i>	RL1, UL145	Potentially involved in blocking interferon α/β (IFN α/β) signalling (UL145)
<i>RL11</i>	RL5A, RL6, RL11, RL12, RL13, UL1, UL4, UL5, UL6, UL7, UL8, UL9, UL10, UL11	Immunomodulatory roles (UL10, UL11, UL7) and viral Fc γ receptors (RL11, RL12, RL13)
<i>UL14</i>	UL14, UL141	Natural killer (NK) cell evasion (UL141) and impairment of cell adhesion (UL14)
<i>UL18</i>	UL18, UL142	NK cell evasion
<i>UL25</i>	UL25, UL35	Tegument proteins and potentially involved in DNA damage and repair (UL35)
<i>UL30</i>	UL30, UL30A	Unknown
<i>UL82</i>	UL82, UL83, UL84, UL31, UL72	Tegument proteins involved in modulation of the cell cycle, gene expression, antiviral signalling and DNA replication (UL82, UL83, UL84)
<i>UL120</i>	UL120, UL121	Unknown
<i>UL146</i>	UL146, UL147	Chemokine homologues
<i>US1</i>	US1, US31, US32	Unknown
<i>US2</i>	US2, US3	Glycoproteins involved in blocking major histocompatibility complex-I (MHC-I) presentation
<i>US6</i>	US6, US7, US8, US9, US10, US11	Glycoproteins involved in blocking MHC-I presentation, although the function of US7 is unknown
<i>US12</i>	US12, US13, US14, US15, US16, US17, US18, US19, US20, US21	NK cell evasion and tropism (US16, US18, US20)
<i>US22</i>	US22, US23, US24, US26, UL23, UL24, UL28, UL29, UL36, UL43, TRS1, IRS1	Immunomodulation; UL36 is the viral inhibitor of caspase-8-induced apoptosis (vICA)
<i>GPCR</i>	UL33, UL78, US27, US28	G protein-coupled receptors (GPCRs); US28 manipulates multiple cellular pathways and is expressed during lytic and latent infection

Table 1.2 – HCMV gene family members and a summary of their functions^{16, 17, 18, 19, 20, 21, 22, 23, 24, 25, 26, 27}

<i>Strain</i>	<i>Passage Status</i>	<i>Notable Mutations</i>	<i>Isolated From</i>
<i>AD169</i>	High passage	Large deletion in UL/b' region (UL133-UL151) ²⁸ . Duplication of RL11, RL12, and part of RL13 ²³ . Mutations in RL13 and UL131A ^{23, 29} .	Adenoids of child ³⁰
<i>FIX (VR1814)</i>	Low passage	BAC clone is missing IRS1-US6, and RL12 and RL14 have been replaced by UL154 and UL153, respectively ³¹ . Mutated UL141 ³² .	Cervical swab of pregnant woman ^{33, 34}
<i>Merlin</i>	Low passage	Truncated UL128 ⁶ . Mutation in RL13 ³² .	Urine of congenitally infected infant ^{35, 36}
<i>TB40/E</i>	High passage	UL128L intact despite amino acid substitution in UL130, mutated UL141 ^{6, 37} . BAC clone is missing US1-US7 ³⁸ .	Throat wash of bone marrow transplant recipient ³⁹
<i>Toledo</i>	Low passage	Inversion of part of the UL/b' region ²⁸ . Disrupted UL128 ²⁹ .	Urine of congenitally infected infant ⁴⁰
<i>Towne</i>	High passage	13kbp deletion in UL/b' region ²⁸ . Large deletion in UL36 gene ⁴¹ .	Urine of congenitally infected infant ⁴²
<i>TR</i>	Low passage	BAC clone is missing US2-US5 ³¹ .	Ocular tissue of AIDS patient with retinitis ^{31, 43}
<i>W</i>	Unpassaged	Complete genome with intact UL128L ¹² .	Lung tissue of AIDS patient ²³
<i>3301</i>	Unpassaged	Complete genome with intact UL128L ¹² .	Urine of congenitally infected infant ²³

Table 1.3 – Information on some strains of HCMV, including both laboratory and clinical strains.

1.1.3 Discovery and Isolation

Cytomegalic cells with intranuclear inclusions were first described by Ribbet in 1881⁴⁴, however, these cells were initially believed to be as a result of a parasitic infection^{45, 46} and it wasn't until the 1920s that cells with intranuclear inclusions were linked to herpesviruses⁴⁷. The term 'cytomegalic inclusion disease' (CID) was first used by Wyatt *et al* in 1950 for the disease seen in congenitally infected infants, although its origin was unknown at the time⁴⁸. In 1953, the use of electron microscopy allowed Minder to visualise viral particles in the pancreatic cells of a child with CID⁴⁹, thus confirming the viral aetiology of the disease.

Human cytomegalovirus was isolated from human cells by Margaret Smith in the mid-1950s, who isolated the virus from a salivary gland and a kidney from two different patients, and determined that this salivary gland virus (SGV) was species specific^{44, 50}. Simultaneously, Rowe and Weller also isolated SGV from patients^{30, 51}, the latter naming the virus 'cytomegalovirus' (as the virus had been isolated from tissues other than the salivary glands) and discovering that there were differences between strains of the virus using serological testing^{52, 53}.

1.1.4 Seroprevalence Rates

HCMV has been detected in every human population that has been studied, although seroprevalence of HCMV (based on the presence of HCMV antibodies) varies depending on geographical location, socioeconomic status, and age.

In some parts of the world including East Asia, India, South America and Sub-Saharan Africa, seroprevalence in young children is greater than 90%, whereas children of the same age in northern Europe and North America have a rate of around 20% – although, in these areas, seroprevalence generally increases with age^{54, 55}.

With regards to the relationship between socioeconomic status and HCMV seroprevalence, lower/working class communities have higher rates of infection (up to 100% depending on country) when compared to middle class communities which have around 30-50% seroprevalence⁵⁶.

1.1.5 Congenital HCMV Infection

Congenital HCMV infection occurs when the pregnant mother either contracts a primary HCMV infection, becomes infected with a second strain, or during reactivation of a latent infection. Approximately 0.64% of infants worldwide are born CMV-positive⁵⁷; birth prevalence of congenital CMV in the UK is currently unknown as large-scale studies have not recently been performed, however a study conducted in London in the 1980s concluded that congenital CMV infection occurs in 0.33% of live-births⁵⁸ – this coincides with lower seroprevalence rates in women in industrialised countries. The results of congenital HCMV vary from defects of neurological development such as hearing loss, loss of sight and severe intellectual disabilities, to still-birth. Only 11% of CMV-positive live-born infants are symptomatic from birth, as reviewed by Kenneson in 2007⁵⁷.

1.1.6 Clinical Presentation in AIDS Patients and Transplant Recipients

Human cytomegalovirus is an opportunistic virus, and disease frequently manifests in patients with a compromised immune system, such as AIDS patients and transplant recipients (solid organ transplant (SOT) or haematopoietic stem cell transplant (HSCT)).

HCMV infection can cause disease in multiple organs including nephritis, hepatitis, encephalitis, colitis, pneumonia, splenomegaly, and retinitis⁵⁹. In patients suffering with AIDS, new disease (most commonly retinitis) caused by HCMV drops by up to 80% following highly active antiretroviral treatment (HAART)⁶⁰; those with AIDS-related HCMV end organ disease received anti-HCMV treatment such as ganciclovir⁶¹. However, some patients experience progression of end-organ disease after discontinuation of anti-HCMV therapy^{61, 62}.

HCMV disease in transplant recipients occurs following transmission from transplanted organ, reactivation within a CMV-positive recipient, or primary infection. The greatest risk of developing HCMV disease amongst SOT is for CMV seronegative patients that receive a CMV-positive organ, whilst for HSCT the highest risk is when a seropositive recipient receives a seronegative transplant; when both donor and recipient are CMV-negative, this carries the lowest risk^{63, 64} (Figure 1.4). HCMV disease usually presents itself 30-90 days post-transplantation (aided by

immunosuppressive treatment and the occurrence of graft-versus-host disease (GVHD)); symptoms include fever, malaise, leukopenia and others related to viral infection, but can also lead to pneumonia, gastrointestinal disease, hepatitis, fungal infections, and ultimately, graft rejection and death^{63, 65}.

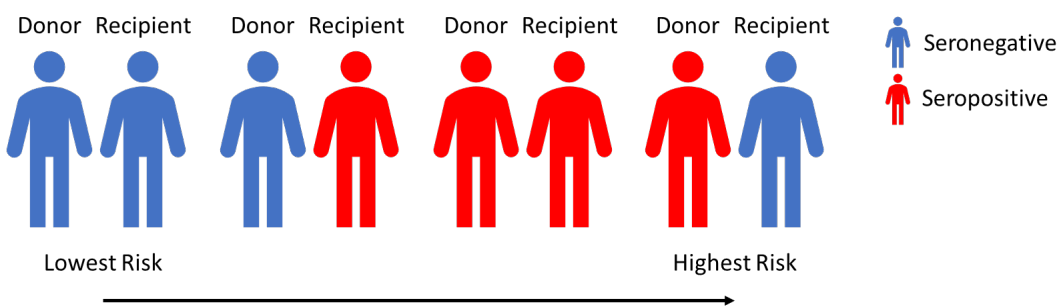


Figure 1.4 – Combinations of seropositive or seronegative donors and recipients and the risk of developing HCMV disease following solid organ transplantation.

1.1.7 Current Therapeutics and Vaccines

At the moment, there are no licensed vaccines for use against HCMV, despite the virus being in the most favourable category for a vaccine program⁶⁶. Attempts to generate a HCMV vaccine have so far focussed on either attenuated strains of the virus (modified virus vaccines), or delivery of viral subunits (individual antigen vaccines)⁶⁷.

Attenuated HCMV vaccines have been based upon the Towne⁴² and AD169⁶⁸ strains, both of which had been highly passaged in fibroblasts. While both vaccines were immunogenic in seronegative subjects, neither were able to boost antibody titres in seropositive subjects or prevent HCMV infection in renal transplant recipients^{67, 69}. Recently, another attenuated vaccine based on AD169 with an intact pentamer named V160 has been tested in clinical trials; in phase I trials it was deemed safe to use and was able to elicit cellular and humoral responses to levels comparable to those seen following natural HCMV infection⁷⁰. A phase II trial of the V160 vaccine, tested in seronegative women between the ages of 16-35 years old, was concluded in June 2021, however the results of that trial have not yet been published⁷¹.

A HCMV antigen vaccine comprised of recombinant gB and an oil in water adjuvant (MF59), was able to boost the immune response to the virus in seropositive women, 50% effective at preventing infection in seronegative women, and 50% effective at

preventing viraemia in SOT recipients^{72, 73, 74}. However this was not sufficient to progress development. It is now known that the majority of neutralising antibodies produced in response to HCMV infection target the pentameric complex rather than gB, potentially explaining this moderate efficacy⁷⁵.

A subunit vaccine tested in mice and non-human primates has produced promising neutralising antibody titres towards the pentameric complex; mRNA encoding the pentameric complex and gB encapsulated in a lipid nanoparticle developed by John et al., are delivered into the cell and then presented on the cell surface⁷⁶. When the pp65 antigen was included in the vaccine, along with a prime/boost regimen, the vaccine also induced a strong T cell response to pp65⁷⁶.

With vaccines against HCMV still undergoing testing, current treatments for infection involve anti-viral drugs, which can be used either for prophylaxis or pre-emptively to prevent CMV disease. The current marketed anti-virals approved for use for prophylaxis or treatment of CMV disease are listed in Table 1.4, with Ganciclovir being the most commonly used. However, there are drawbacks to these drugs, including significant toxicity, cost, the development of late-onset disease once treatment is discontinued, and mutations in the UL54 (DNA polymerase) and UL97 genes that lead to resistance^{77, 78, 79, 80}.

<i>Anti-Viral Drug</i>	<i>Method of Administration</i>	<i>Mechanism</i>		
<i>Acyclovir (ACV)</i>	Oral (prophylaxis only)	Inhibits viral synthesis	viral	DNA
<i>Cidofovir (CDV)</i>	Intravenous	Inhibits viral synthesis	viral	DNA
<i>Fomivirsen (FMV)</i>	Intraocular	Inhibits translation of early CMV proteins		
<i>Foscarnet (FOS)</i>	Intravenous	Inhibits viral DNA synthesis	viral	DNA
<i>Ganciclovir (GCV)</i>	Oral or intravenous	Inhibits viral DNA synthesis	viral	DNA
<i>Letermovir</i>	Oral or intravenous	Inhibits packaging of genomes into capsids		
<i>Valacyclovir (ACV prodrug)</i>	Oral	Inhibits viral DNA synthesis	viral	DNA
<i>Valganciclovir (GCV prodrug)</i>	Oral	Inhibits viral DNA synthesis	viral	DNA

Table 1.4 – List of anti-HCMV drugs that can be used for prophylaxis or treatment of CMV disease, the method of administration, and mechanism of action^{64, 77, 79, 81, 82}.

1.2 Virion Structure

The virions of herpesviruses are spherical and consist of four major components (from outer to innermost structure of virion): the envelope, tegument, capsid, and DNA core (Figure 1.5). The virion of HCMV is approximately 200-230nm in diameter¹⁰.

As well as infectious enveloped virions, HCMV also produces non-infectious enveloped particles and dense bodies during its life cycle, which are also released from infected cells (Figure 1.6). NIEPs resemble the mature virion structure, however they possess immature B-capsids and do not contain viral DNA^{83, 84}. Dense bodies on the other hand, can be far larger, ranging from 250-600nm in diameter, tend to be spherical, are composed predominantly of phosphoprotein 65 (pp65, UL83 gene product) and are enveloped but lack capsids and DNA cores^{83, 85}. Dense bodies and NIEPs can be produced in a larger quantity than infectious particles *in vitro*, sometimes constituting 99% of particles in a purified viral preparations when using passaged strains – for this reason it has been proposed that the purpose of these structures being produced by HCMV is as an immune evasion strategy, where the dense bodies and NIEPs overwhelm the immune response, allowing infectious virions to go on to infect new cells^{10, 84}.

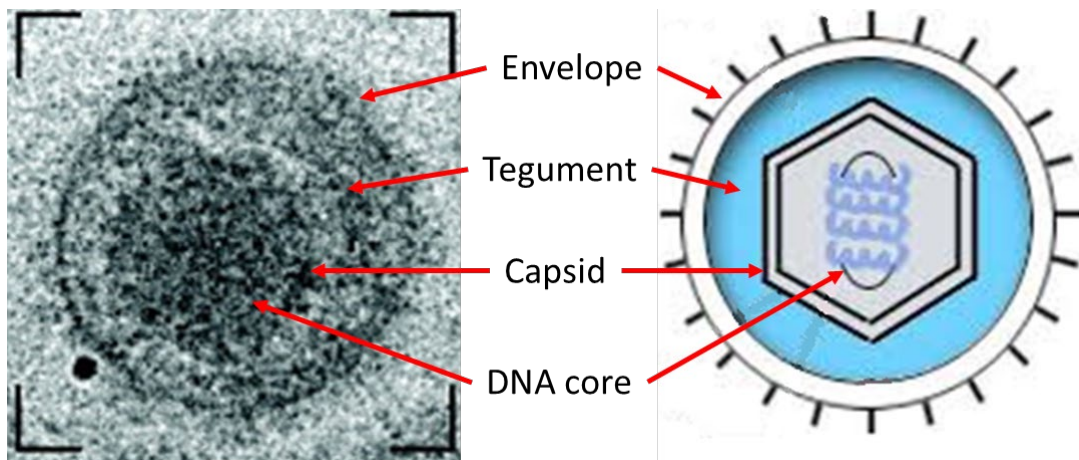


Figure 1.5 – The structure of a herpesvirus virion, adapted from a cryo-electron tomographic image of a HSV-1 virion⁸⁶. Black dot is a 10nm gold particle that was used as a fiducial marker.

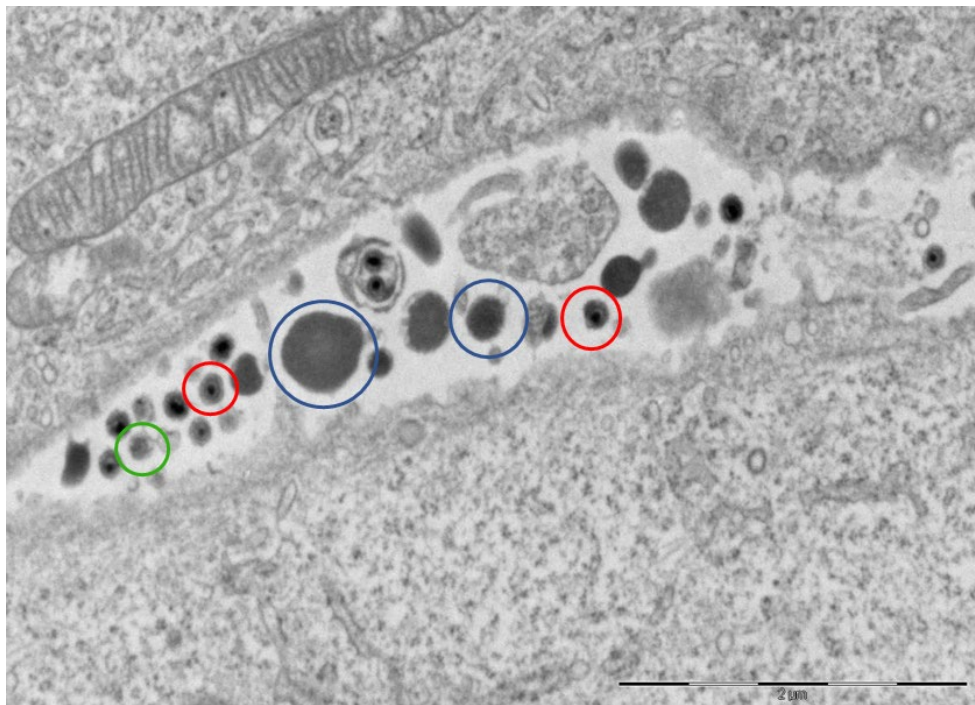


Figure 1.6 – Transmission electron microscopy (TEM) image of a cellular junction between an infected human foetal foreskin fibroblast (HFFF) and a dendritic cell (DC) taken by Chris Von Ruhland. Red circle = mature enveloped infectious virion; green circle = NIEP; blue circle = dense body. Bar represents 2μm.

1.2.1 Capsid

As previously mentioned, the double-stranded viral DNA densely packed inside the core of the HCMV particle is approximately 235kbp in length, and is protected by a 130nm icosahedral capsid¹⁰. The capsid is made up of four proteins: major capsid protein (MCP, UL86 gene product); triplex subunit 1/minor capsid protein (TRI1, UL46 gene product); triplex subunit 2/minor capsid protein binding protein (TRI2, mCBP, UL85 gene product); and the smallest capsid protein (SCP, UL48A gene product)^{10,87}. The portal complex is an additional component which allows for moving of DNA into and out of the capsid^{1,87}.

The T=16 icosahedral capsid is formed from 161 capsomeres (150 hexons and 11 pentons); the hexons and pentons are six and five copies of the MCP, respectively^{1,10,87}. Each copy of MCP in a hexon is joined externally to a SCP¹. The capsomeres are then joined together by triplexes consisting of TRI1 and TRI2¹.

HCMV produces A-, B- and C-capsids, the assembly process of which is shown in Figure 1.7. These were first described for HSV-1⁸⁸ and were later recovered from

AD169-infected cells⁸⁹. The procapsid, which is the first spherical structure formed as part of the capsid assembly process, is only transiently stable, it must undergo a structural transition into a stable polyhedral shape⁸⁴. Therefore, A-, B-, and C-capsids, all have the basic shell structure described above, however they differ in their packaging. A-capsids contain neither packaged viral DNA or any structural proteins, they are considered a “dead end” in the capsid assembly process^{83, 84, 90}. B-capsids contain some structural proteins (UL80 gene products), and are the capsid type that is within a non-infectious enveloped particle (NIEP); whereas C-capsids contain packaged DNA and are the precursor to mature virions^{10, 83}.

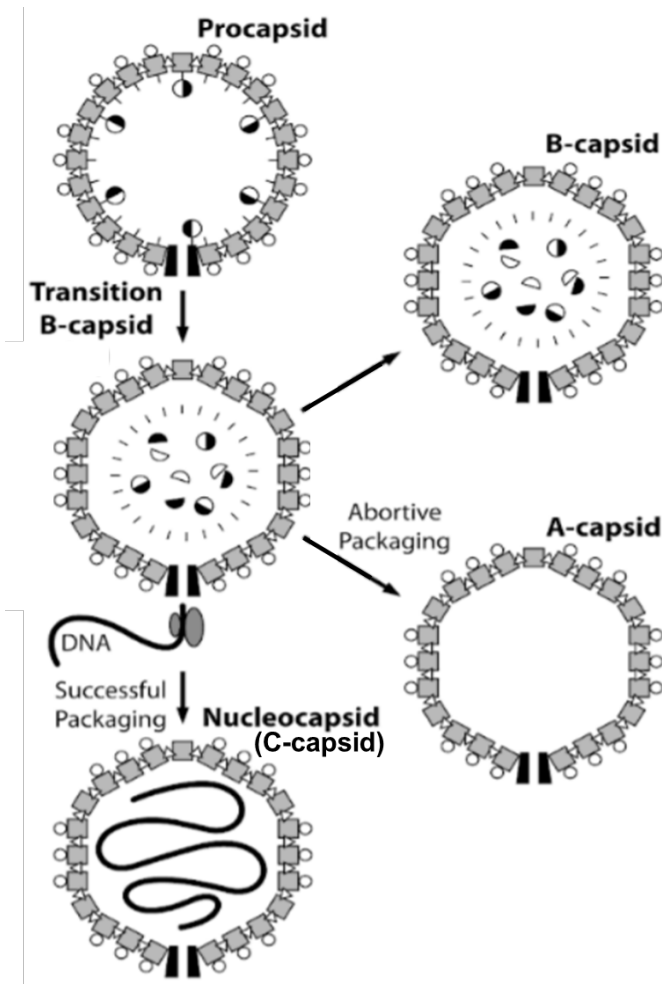


Figure 1.7 – Formation process of the three distinct types of capsids generated by HCMV, adapted from Reddehase et al⁹¹.

1.2.2 Tegument

Capsids are embedded in a layer of tegument, an amorphous phosphoprotein matrix, within the enveloped virion, tegument proteins also make up dense bodies. The tegument layer makes up around 50% of the virion in infectious particles⁹². There are 32 known tegument proteins, but the most abundant of which is pp65, also known as the lower matrix protein, and it is highly immunogenic^{10, 92}. pp65 is rapidly transported to the nucleus following infection with a mature HCMV virion, or take up of a dense body⁹³. From there, it modulates the host cell's response to infection, protecting immediate-early gene products from recognition by the immune system via phosphorylation, inhibiting host protein synthesis, dampening interferon responses, decreasing surface expression of major histocompatibility complex II (MHC-II), and other functions^{10, 94, 95, 96}.

The pp71 protein, encoded by UL82, is a tegument protein that is key in transcriptional activation. pp71 translocates to the nucleus after infection of fibroblasts⁹⁷ and epithelial cells⁹⁸ where it activates the major immediate early promoter (MIEP) during productive infection⁹⁹. In addition to its role in viral gene expression, pp71 disrupts antigen presentation to CD8 T cells, as it reduces expression of MHC class I (MHC-I) molecules on the cell surface¹⁰⁰.

Another notable tegument protein is pp150 (UL32 gene product), which plays a role in the maturation of HCMV virions in the late phase of infection; this protein was found to bind directly to capsids and is involved in stabilising C-capsids and transporting them through the nuclear pore to the cytoplasm for envelopment^{87, 101}. Without UL32, the virus is unable to grow¹⁶.

As such, the tegument layer is not only a structural component of the virion, but also plays a part in the maturation stage of the HCMV life cycle, and in immune evasion.

1.2.3 Envelope

The lipid bilayer envelope is the outermost layer of the virion, and is comprised of a combination of host and viral proteins. The lipid bilayer itself is formed from endoplasmic reticulum-Golgi intermediate compartment (ERGIC) and endosomal membranes, and is decorated with as many as 23 different viral glycoproteins¹⁰. These

glycoproteins are responsible for binding to and entering a host cell, and some have a role in evading the immune response.

Five of the glycoproteins found on the surface of a virion are considered essential proteins, as without which HCMV mutants are unable to grow, these are: glycoprotein B (gB, UL55 gene product); gH (UL75 gene product); gL (UL155 gene product); gM (UL100 gene product); and gN (UL73 gene product)¹⁶. A sixth glycoprotein, gO (UL74 gene product), is not absolutely essential for viral growth, but viruses lacking this protein observe a growth defect¹⁶.

1.2.3.1 In Vitro Adaptation

As mentioned above, when HCMV is grown *in vitro*, the genome undergoes modifications depending on the cell type the virus has been propagated in. These modifications affect not only cell tropism, but also viral growth (titre). Two of the earliest regions to be deleted/mutated *in vitro* are the RL13 gene and UL128L. RL13 is a highly glycosylated protein that, when repaired in a bacterial artificial chromosome (BAC)-derived virus, restricts HCMV replication in HFFFs and epithelial cells – even after a short time *in vitro*, RL13 mutants emerge yet again with enhanced growth properties¹⁰².

The UL128 locus, comprised of UL128, UL130 and UL131A, forms part of the pentameric complex which is essential for epithelial, endothelial and myeloid cell tropism – the UL128L is quickly mutated in some way (deletions, early stop codons etc.) when HCMV is passaged in fibroblasts, as the pentameric complex is not only dispensable for growth in HFFFs, but also inhibits virus growth. Further mutations can be selected after additional passage, often including UL141 along with additional genes between UL128-UL150 (the UL/b' region)¹⁰³.

Cloning of viral genomes into bacterial artificial chromosomes (E.coli) enabled the stable maintenance of genomes in E.coli, however early BACs were made from passaged strains, and therefore carried mutations previously acquired *in vitro*. When the Merlin strain was cloned into a BAC, it was repaired to a fully wildtype sequence, by reference to the sequence in the original clinical sample. When virus was isolated from the BAC, mutations were re-selected in both UL128 and RL13, in the same way as seen in clinical viruses. Both genes were therefore placed under the control of a

tetracycline repressor (tetR) response element, allowing selective repression of these genes in a fibroblast cell line expressing tetR, and therefore preventing the selection of mutations¹⁰². This remains the only way to produce virus *in vitro* expressing the complete repertoire of viral genes.

1.3 Life Cycle

The life cycle, or replication cycle, of human cytomegalovirus can either end in a lytic infection (Figure 1.8), where newly assembled virions are released and continue the life cycle by infecting new cells; or it can end in a latent/persistent infection, where the virus maintains low levels of essential gene expression until a trigger causes it to reactivate, and re-start the lytic infection cycle.

Both life cycles begin with HCMV entering the cell, and ultimately, will result in the egress of virions.

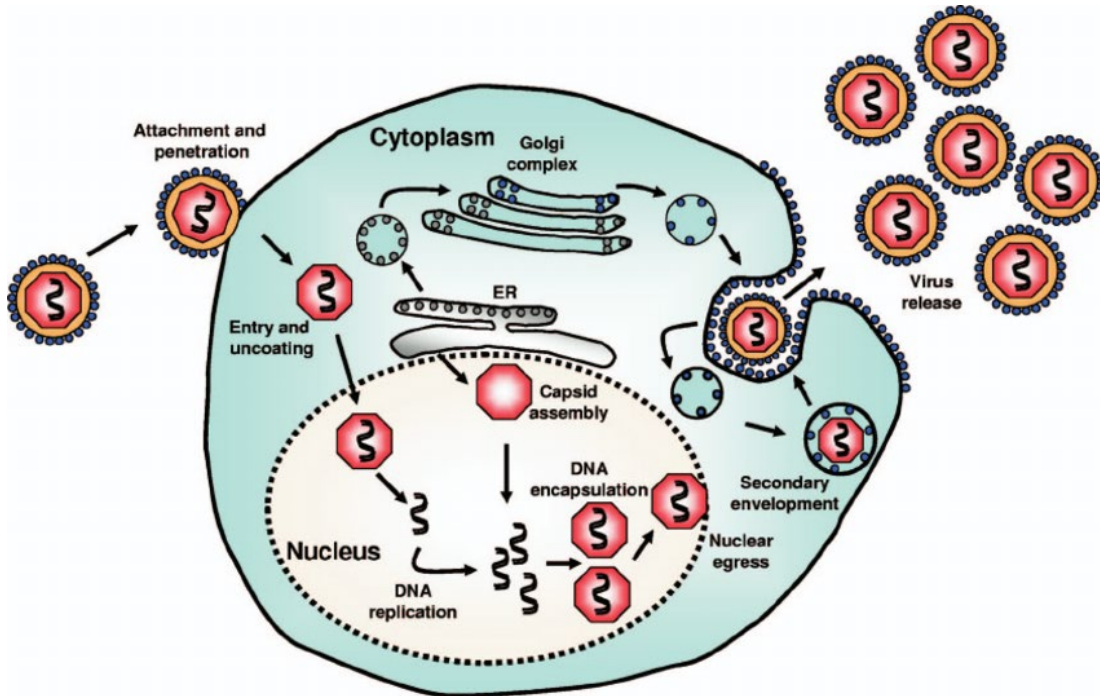


Figure 1.8 – Schematic showing the lytic lifecycle of HCMV in a host cell, from Crough et al.¹⁰⁴

1.3.1 Cell Entry

During a natural infection, HCMV usually enters the body via a mucosal surface following exposure to infected body fluids. After primary dissemination, virus can be

found in almost every organ in the body – although, mucosal epithelial cells, smooth muscle cells, connective tissue cells and endothelial cells are believed to be massive producers of infectious virions¹⁰⁵.

There are two methods of cell entry, cell-cell and cell-free infection, controlled in part by the pentameric and trimeric complexes (see below).

The entry process begins when glycoproteins on the surface of the HCMV virion interact with cellular receptors on the cell's membrane, also known as the binding step. Following binding, the viral envelope fuses with the cell membrane, either directly at the surface of the cell¹⁰⁶, or with the membrane of the endosome following endocytosis¹⁰. Either method results in the nucleocapsid being deposited into the cytoplasm of the cell.

1.3.1.1 Glycoproteins Required for Cell Entry

The glycoproteins gH and gL form the trimeric and pentameric complexes with gO and UL128L, respectively; these are required for cell entry and can dictate the tropism of a particular HCMV strain. gB, gM and gN, are also essential for viral infection and spread.

gB was initially thought to be required for tethering of the virion to the cell membrane, before a more stable attachment was made, as it binds to cell surface heparan sulfate proteoglycans (HSPGs) which are present on many different cell types¹⁰⁷. However, data published by Isaacson et al. actually suggest that gB is not vital for viral attachment, but it is vital for fusion of the viral and cellular membranes during cell entry¹⁰⁸. This glycoprotein forms a homodimer linked by disulphide bonds that is referred to as gCI^{109, 110}.

The gM glycoprotein forms a heterodimeric complex with gN (gCII), although the role for this complex is undefined. The gM/gN complex is known to bind to HSPGs, suggesting that this complex is involved in attachment, there is also a requirement of gN in order for gM to be transported through the secretory pathway, which indicates that the gM/gN complex is a major component of the virion envelope. Without it HCMV cannot successfully replicate^{109, 111}. In addition to this, HCMV infection results

in neutralising antibody response targeting gM/gN, these antibodies are able to restrict infectivity of AD169, TR and Toledo *in vitro*¹¹².

1.3.1.2 The Trimeric and Pentameric Complexes

The trimeric, gH/gL/gO (gCIII), and pentameric, gH/gL/UL128-131A, complexes are present on the virion envelope, and contribute to cell tropism of different strains. The trimeric complex is essential for cell-free spread in all cell types, as well as cell-cell spread in HFFFs, while the pentameric complex is utilised for cell-free and cell-associated spread in non-fibroblast cell types (mentioned above) – hence, the cell type in which a laboratory strain is propagated not only effects tropism, but also the method of viral spread.

The ratios of these complexes in the envelope varies between different strains, with Merlin having high pentamer and low trimer, while other strains are the other way round^{113, 114}. Since both complexes contain gH/gL, it is suggested that the gO isoform of Merlin is outcompeted by UL128-131A (UL128L) for binding of gH/gL, and therefore is less efficient at complexing with gH/gL than gO isotypes found in other strains such as AD169 and TB40/E¹¹⁴. In addition, TB40-BAC4 and FIX express lower levels of pentamer as a result of *in vitro* acquired single nucleotide mutations in UL128 and UL130, respectively (Table 1.3). As well as altering the ability of these viruses to spread by the cell-cell route, this also limits the selection of mutations in UL128L during propagation¹¹³.

Further investigation into gO expression by Merlin revealed that expression levels were in fact around 20-fold lower when compared to the TR strain¹¹⁵. These differences in complex ratios may offer an explanation as to why Merlin efficiently infects epithelial/endothelial cells/monocytes in a cell-cell context, where others infect more efficiently by the cell-free route.

1.3.1.3 Cell-Free Infection

For cell-free infection to occur, the virions released from an infected cell must diffuse in a 3-dimensional space and reach uninfected cells to initiate a new infectious cycle.

The efficiency of this method is dependent on the virions remaining stable and not facing any extracellular challenges¹¹⁶.

The trimeric complex not only determines cell tropism of HCMV strains, but is also associated with the cell-free infection method. The receptor predominantly used for infection of fibroblasts by HCMV is platelet-derived growth factor receptor α (PDGFR α), which is phosphorylated following interaction with gO, followed by fusion of the virion with the cell membrane^{117, 118}. However, cell-associated infection of HFFFs can also use the trimer and PDGFR α for entry¹¹⁹ – in a recent publication by Weiler et al., it was reported that recent clinical isolates have a pentamer^{high}/trimer^{high} phenotype, and the gO/PDGFR α interaction contributes to cell-associated infection in fibroblasts¹²⁰.

1.3.1.4 Cell-Associated Infection

Cell-associated infection can be a far more efficient method of infection than cell-free spread. In cell-free spread, virions are released into the extracellular matrix, seemingly at random, but in cell-cell spread, the virions can either be released in a directional or non-directional manner. Surface retention of virions by the infected cell accompanied by adhesion to a neighbouring cell, as seen in Figure 1.9A, is a non-directional method of cell-cell transfer which mitigates the problems of virion decay and delay seen in cell-free infections by increasing the local particle density and reducing the distance travelled by the virions¹¹⁶. However, efficiency of cell-associated infection can be increased further by polarising accumulation of viral particles on the cell surface at the site of the cell-cell contact (directional), depicted in Figure 1.9B¹¹⁶.

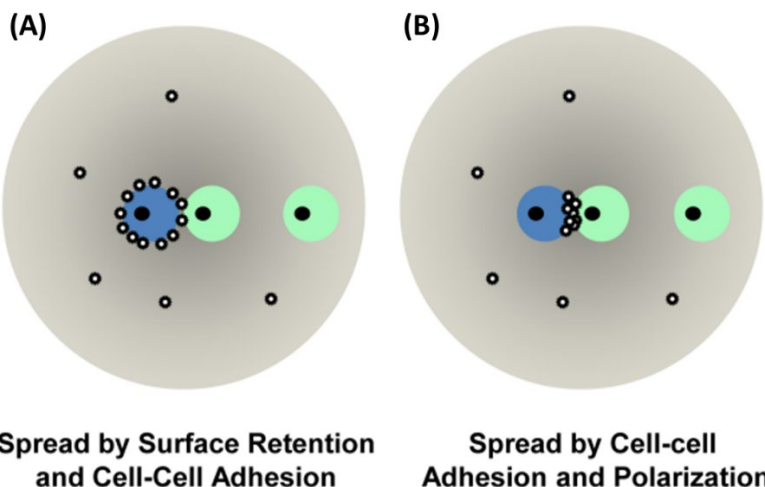


Figure 1.9 – Directional and non-directional cell-cell spread, adapted from Zhong et al¹¹⁶. This diagram shows the difference between: A) cell-associated infection via surface tension (non-directional); and B) polarisation (directional).

Recent clinical isolates of HCMV spread predominantly by cell-cell spread, and *in vivo*, cell-free virus is essentially impossible to isolate from the blood. Thus cell-cell spread is likely to play a major role in *in vivo* spread. Using the wildtype Merlin strain, it was found that high-level expression of the pentameric complex, and expression of RL13, resulted in loss of cell-free spread but efficient direct cell-cell transmission. This contrasts with passaged strains that lack these genes, and therefore utilise the cell-free route more extensively¹²¹. Transmission via the cell-cell route appears to be advantageous for concealment from the immune system, since it avoids the detrimental effects of neutralising antibodies, and enables the virus to more readily overcome interferon (IFN) and intrinsic cellular restriction factors^{121, 122} – although the actual mechanism of transfer is unknown.

There are several theories of the mechanism that have been suggested, including some that have been based on those used by retroviruses including human immunodeficiency virus (HIV) and human T-lymphotropic virus-1 (HTLV-1). Figure 1.10 shows diagrams of routes of cell-associated infection that have been seen in HTLV-1. The virological synapse is a protective niche, similar to an immunological synapse, that forms between two neighbouring cells; re-orientation of the microtubule-organising centre (MTOC) allows the transfer of virions directly to the uninfected cell while avoiding neutralising antibodies and other elements of the immune response¹²³. Cellular conduits are transient membrane extensions that reach out to neighbouring

uninfected cells, virions travel down these extensions and enter the uninfected cell when the membranes make contact¹²³. Newly synthesised virions may accumulate at the cell surface of the infected cell becoming associated with the extracellular matrix (ECM), forming extracellular viral assemblies; when these adhesive virions make contact with an uninfected cell then infection begins¹²³. Transient infection via dendritic cells (DCs), similar to a Trojan horse-style of infection, has been observed in HIV as well as HTLV-1; in this situation, DCs internalise virions but do not become infected, these virions can then be passed onto uninfected cells that come in to contact with the DC¹²³.

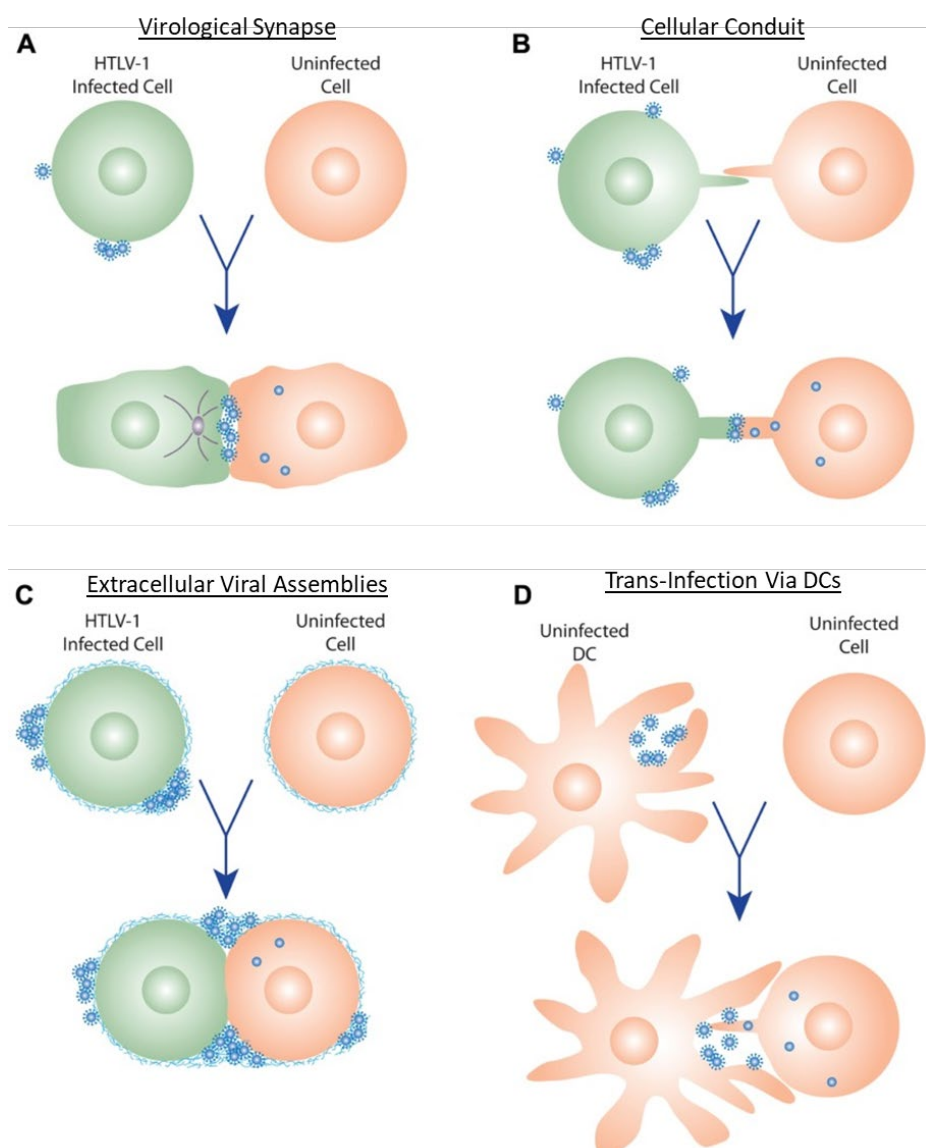


Figure 1.10 – Diagram of the potential mechanisms of transfer for cell-cell spread in HCMV, that have been observed in HTLV-1 (adapted from Pique et al¹²³).

What is known about the mechanism of cell-associated spread, and how it differs from cell-free spread, is that while trimer binding to PDGFR α is required for HCMV entry into fibroblasts by both the cell-free and cell-cell routes, this is not true for infection of epithelial, endothelial or myeloid cells¹²⁴. In these cell types, Trimer is still required to cell-free entry, by binding an unknown receptor, but is dispensable for cell-cell spread. However, pentamer is essential for both cell-free and cell-cell spread, by binding to either OR14I1 or NRP2.

Merlin has a pentamer^{high}/trimer^{low} phenotype, and this results in loss of cell-free infectivity, but highly efficient cell-cell infection of epithelial, endothelial and myeloid cells. Without the pentameric complex, HCMV is unable to infect these cells. However when UL128 is partially downregulated, this increases the amount of virus released into the supernatant; there is a certain level of UL128 that is necessary to restrict the virus to cell-associated spread¹²⁰. It is unclear whether this is directly due to pentamer levels, or because reductions in pentamer result in increases in trimer. However once cell-free infectivity increases, virus spread becomes much more susceptible to neutralising antibodies, and cannot form plaques in their presence. Interestingly, recent clinical isolates have been reported to express equally high levels of both complexes within the infected cell, although it was not determined whether this resulted in equally high levels in the virion. If true, this could suggest that clinical isolates can selectively alter expression of the pentamer to promote the release of cell-free virus into body fluids for dissemination, or that there are strain specific differences in complex levels in vivo.

1.3.2 Replication

1.3.2.1 Genome Replication

Nucleocapsids in the cytoplasm are transported to the nuclear pore via microtubules, where the HCMV genome is deposited into the nucleus and is then circularised^{1, 125}. Replication of the genome occurs using the rolling circle mechanism resulting in the production of long continuous DNA molecules containing multiple copies of the HCMV genome called concatemers, which is also seen in other herpesviruses^{90, 125, 126}.

During lytic infection, replication of the HCMV genome commences by 48hrs following infection of the cell. Expression of HCMV genes can be divided into four phases: immediate early (IE), early (E), early-late (EL) and late (L); this cascade was defined with the use of metabolic inhibitors such as cycloheximide and ganciclovir, which inhibit viral protein synthesis and DNA synthesis, respectively¹²⁷. Immediate early genes are expressed within 24hrs following infection and do not require the *de novo* expression of other viral or cellular genes; IE genes are responsible for counteracting innate immunity, and activating the Early genes required for DNA replication. The major IE gene (MIE) is spliced into several phosphoproteins, including IE1 and IE2, which play a major part in: regulating viral gene expression in the other phases; autoregulating IE expression; inhibiting epigenetic repression; and establishing areas within the nucleus for DNA synthesis to begin¹⁰.

1.3.2.2 Virion Assembly and Egress

Each HCMV genome is packaged into a preformed capsid when the short-arm of the concatemer is fed into the capsid via the portal-protein complex (UL104). Once one copy of the genome has entered, it is cleaved and the next short-arm of the concatemer can begin to be packaged^{83, 125}. These nucleocapsids are exported from the nucleus by the herpesvirus-conserved nuclear egress complex (NEC), becoming enveloped then de-enveloped at the nuclear membrane^{10, 83}.

Virion maturation occurs in the assembly compartment (AC) – a structure composed of reorganised Golgi among other organelles detected in cells 72-96hrs post-infection^{128, 129}. The enlarged “kidney bean” shaped nucleus which is characteristic of HCMV infection, is down to the connections formed between the AC and nucleus which permit budding of the capsids directly into the AC (Figure 1.11). The assembly compartment acts as a microtubule-organising centre (MTOC), actively transporting nucleocapsids along newly formed microtubules¹³⁰. As nucleocapsids pass through the assembly compartment, they become wrapped in the tegument proteins that have accumulated there. Tegumented capsids bud into cytoplasmic vesicles, obtaining their final envelope and maturing into infectious virions¹³¹. The cytoplasmic vesicles move towards and fuse with the cellular membrane, releasing infectious virions, dense bodies and NIEPs into the supernatant.

Following egress from the cell, HCMV can disseminate to other organs in the body, but can also be shed in the saliva, urine and other body fluids of the individual, potentially leading to infection of a new host¹⁰.

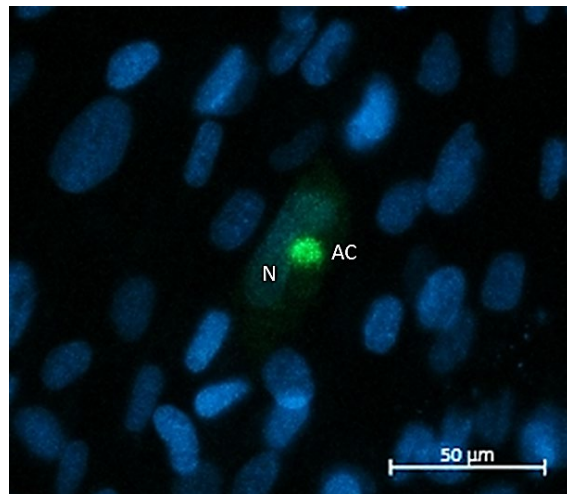


Figure 1.11 – The HCMV assembly complex in an infected fibroblast. HFFF were infected at an MOI 5 with a virus expressing GFP-tagged tegument protein UL32, 72hrs post-infection the cells were stained with Hoescht and imaged using a Zeiss microscope (Axio Observer Z1 with a XL Multi SI Incubator) and APOTOME. AC = assembly complex; N = nucleus; Scale bar = 50μm.

1.3.3 Latent Infection and Reactivation

The definition of latency is the presence of the viral genome in the absence of infectious virion production; a trait shared by all herpesviruses. Human cytomegalovirus establishes a lifelong infection in its host; the virus goes through cycles of latency and reactivation, suppressing its genes and therefore production of infectious viral particles, evading eradication by the host's immune system. Any reactivation within an immunocompetent host is typically well controlled, whereas reactivation in an immunocompromised host can lead to devastating disease, as described previously.

It was not until the development of highly sensitive PCR protocols that HCMV DNA was found in the peripheral leukocytes of healthy seropositive carriers, as less than 1 in 10,000 monocytes that carry HCMV DNA¹³². Viral DNA can also be found in CD34+ haematopoietic progenitor cells – these myeloid progenitors differentiate into monocytes, T cells, B cells and polymorphonuclear lymphocytes (PMNLs) – however, of these subsets, genomes have only been detected in monocytes¹³². HCMV is able to

become latent in monocytes by forcing CD34+ cells to differentiate into a type of monocyte that has an increased life span and higher levels of inducible nitric oxide synthase (iNOS) *in vitro*; production of nitric oxide (NO) allows the monocytes to suppress proliferation of CD4+ and CD8+ T cells¹³³. While HCMV DNA is detected in these cells, there is little or no IE gene expression; Epstein Barr virus has a designated latent origin of replication, but this is not thought to be the case for HCMV¹³⁴. What is known, is that the viral genome is controlled (at least in part) by cellular factors during latency, which recruit histone deacetylases (HDACs) to the major immediate-early promoter (MIEP), condensing the chromatin and silencing HCMV genes^{10, 132}. The virus is not transcriptionally silent during latency, however only a restricted set of genes are expressed; to date, LUNA (UL81-UL82 locus)¹³⁵, US28¹³⁶, UL111A¹³⁷, UL144¹³⁸, and UL138¹³⁹, have been detected. Latency-associated gene expression is dependent on the model used, and the genes listed here may be not all be expressed, but there may be a combination.

Reactivation of latent virus is a poorly understood mechanism, although there appears to be a correlation between differentiation of myeloid cells into macrophages and dendritic cells and re-entering the lytic life cycle. It has been observed by Reeves et al. that following differentiation of monocytes and CD34+ cells isolated from seropositive individuals into mature DCs, the MIEP becomes associated with acetylated histones and IE gene expression is detected – suggesting that cellular differentiation leads to chromatin remodelling around the MIEP, which triggers the lytic life cycle¹⁴⁰.

Reactivation may also be triggered by inflammation, particularly following increased levels of the inflammatory cytokine TNF α , which is associated with sepsis, graft rejection, and other inflammatory conditions. TNF α activates both the MIEP and NF κ B – NF κ B also mediates activation of the MIEP, creating an amplifying loop where reactivation of HCMV drives expression of inflammatory cytokines¹⁴¹.

1.4 Evasion of the Immune Response

HCMV infection triggers a response from both arms of the immune system – the innate and the adaptive. Although infection is controlled to some extent by a combination of these defences, neither is capable of eradicating HCMV from the host – the virus encodes a vast number of proteins whose sole function is subversion of the immune response, and these contribute to the virus' persistence in the body.

1.4.1 Innate Immunity

The innate immune system is the body's first defence against pathogens, it is fast-acting and comprises of physical barriers (skin) as well as neutrophils, natural killer (NK) cells, monocytes, macrophages and DCs. Innate immune cells use pattern recognition receptors (PRRs) to detect viral pathogen-associated molecular patterns (PAMPs); interaction with the PRR can trigger a cascade of events within the cell.

Professional antigen presenting cells (APCs), DCs and macrophages, bridge both arms of the immune response by processing and presenting viral antigens via the major histocompatibility complex (MHC) class I and II molecules to CD8⁺ and CD4⁺ T cells, respectively, and presenting intact antigen to B cells – antigen presentation as well as activation of interferon regulatory factor 3 (IRF3) and nuclear factor kappa B (NFκB), and production of type I interferon (IFN), pro-inflammatory cytokines and chemokines are triggered by engagement of the PRR depending on cell type^{142, 143, 144, 145}.

HCMV is able to subvert the innate immune response before viral transcription even begins, with proteins in the viral particle able to act immediately after fusion with the cell membrane. For example viral glycoproteins induce activation and nuclear accumulation of NFκB and IRF3, however, the virus is able to prevent full activation of the IFN pathway – the tegument protein pp65 is believed to have a role in this, but also IE2 is known to interfere with NFκB activation and therefore DNA binding^{144, 146}.

HCMV is known to encode several NK evasion genes, the cells that are believed to be the first to respond to infection. The virus downregulates MHC-I to prevent presentation of peptides to T-cells, however loss of MHC-I from the cell surface makes cells more susceptible to NK-mediated cell lysis – hence, HCMV encodes a MHC-I

homolog, UL18¹⁴⁴. This protein binds the inhibitory leukocyte immunoglobulin-like receptor 1 (LIR-1) on NK cells and blocks lysis, but only by LIR-1⁺ NKs¹⁴⁷. Another method of NK evasion that is employed by the UL142, UL148A, US18 and US20 gene products is inhibition via downregulation of MHC-I related protein A (MICA), a ligand for Natural-killer group 2, member D (NKG2D) which is an activating receptor expressed ubiquitously on NK cells^{148, 149}. The genes responsible for downregulating MICA achieve this by either sequestering the protein in the *cis*-Golgi, or by targeting it to the lysosome for degradation. Similarly, UL16 is responsible for retaining MHC-I related protein B (MICB)¹⁵⁰. Tomasec et al. identified UL141 as another NK evasion gene, it blocks surface expression of CD155, the ligand for the activating receptor CD226 expressed on NK cells³⁷. The same lab found that the UL40 gene product upregulates human leukocyte antigen E (HLA-E), a MHC-I molecule that interacts with NKG2A/B and conveys an inhibitory signal to the NK cell^{35, 151}. Despite all of the efforts to evade detection by NK cells, or perhaps because of these functions, infection induces dramatic NK cell alterations in the host¹⁴⁹.

1.4.2 Adaptive Immunity

As well as modulating the immediate response to infection, HCMV has evolved mechanisms to perturb the adaptive immune response. The adaptive immune response must be primed by elements of the innate immune response, takes several weeks to establish, and comes in to play when innate immunity has failed to clear infection. It is more specific than the innate system and has memory, so in the event of re-infection the reaction time should be faster. The two types of response are the cell-mediated immune response, and the humoral immune response.

The importance of T cell-mediated immunity is clear in those with AIDS and HSCT patients, where the severity of HCMV disease can be high; these patients have an impairment of their T cells. HCMV encodes genes that target the MHC class I and II complexes, which aid evasion of cytotoxic T cells. US2, US3, US6 and US11 block antigen presentation by MHC-I using several processes including ER retention, blocking peptide transport and targeting the complex for proteasomal degradation¹⁰. There are several genes that target the MHC class II molecule, inhibiting presentation to CD4⁺ T cells; the US2 gene is also responsible for degradation of MHC-II, the US3

gene binds to and causes mis-localisation of the complex, and finally pp65 directs newly synthesised MHC-II to perinuclear lysosomes for degradation¹⁵².

CD58, a ligand that is normally upregulated on infected cells, interacts with the CD2 molecule found on both T cells and NK cells. The viral UL148 leads to retention of CD58 in the endoplasmic reticulum (ER), consequently the infected cell avoids recognition by CD8⁺ cytotoxic T lymphocytes (CTLs), degranulation by NKs and antibody-dependent cellular cytotoxicity (ADCC) mediated by NK cells¹⁵³. Similarly to NK cells, T cell expansion is also noted during HCMV infection.

The humoral response to HCMV can alleviate symptoms of congenital disease, and the MF59 vaccine, which was designed to elicit neutralising antibodies, has been shown to have some effect in phase 2 studies as described above. The majority of neutralising antibodies that are produced target glycoproteins and envelope complexes of the virus, which suggests that the humoral response is likely to have an effect on transmission of the virus in cell-free secretions¹⁰. HCMV also encodes two receptors for the Fc domain of immunoglobulin G (IgG) (Fc γ Rs), glycoproteins 34 and 68, which antagonise antibody-dependent activation of cellular immunity¹⁵⁴.

1.4.3 Dendritic Cells

Dendritic cells link both arms of the immune response, they are APCs that induce activation and proliferation of T cells, and in some instances can initiate an antigen-specific antibody response by presenting antigens to naïve B cells¹⁵⁵. DCs are present in most tissues, initially in an immature form, but they mature following detection of PAMPs or changes in the homeostasis of their environment. Mature DCs migrate from peripheral tissues to secondary lymphoid tissues where they are able to interact with naïve T cells¹⁵⁶.

DCs have a high level of expression of MHC molecules and CD11c, but the presence/absence of other molecules on the cell surface categorises the cells into different subtypes, see Table 1.5. The main subtypes being conventional DCs (cDCs), plasmacytoid DCs (pDCs), and monocyte-derived DCs (moDCs). cDCs and pDCs were initially referred to as “myeloid” and “lymphoid” DCs, respectively, however it is now known that both subtypes are able to differentiate from common myeloid

progenitors (CMPs) and common lymphoid progenitors (CLPs) – the lineage origin of the subset does not alter the transcriptional profile of the DCs¹⁵⁷. MoDCs are differentiated *in vitro* by culturing CD14⁺ monocytes in the presence of interleukin-4 (IL-4) and granulocyte-macrophage colony-stimulating factor (GM-CSF) – these cells are more alike to cDCs, as they express toll-like receptor 2 (TLR2) and not blood DC antigen 2 (BDCA-2), but they are not as efficient at stimulating CD4⁺ T cells to proliferate¹⁵⁸.

Langerhans cells (LCs), another subtype of DC, are resident cells of the epidermis and epithelia; these cells have a distinct differentiation pathway from cDCs, pDCs and moDCs as their precursors migrated to the skin prior to differentiation¹⁵⁹.

<i>Dendritic Cell Subtype</i>	<i>Identifying Cell Surface Markers</i>
<i>Conventional DCs (cDCs)</i>	TLR2 ⁺ , BDCA-2 ⁻ , CD11b ⁺
<i>Plasmacytoid DCs (pDCs)</i>	TLR2 ⁻ , BDCA-2 ⁺ , CD11b ⁻
<i>Monocyte-derived DCs (moDCs)</i>	TLR2 ⁺ , BDCA-2 ⁻ , CD11b ⁺
<i>Langerhans cells (LCs)</i>	Langerin ⁺ , CD11c ^{low} , MHC-II ^{low}

Table 1.5 – Some of the surface markers used for DC classification^{156, 159, 160}.

Human cytomegalovirus has evolved many immune evasion strategies, with genes that specifically target NK cells, T cell activation and other elements of both arms of the immune response. So it is expected that as key coordinators of the immune response, and a site of reactivation of latent HCMV and also primary infection¹⁶¹, HCMV would encode DC modulation genes.

HCMV is believed to infect DCs by entering via the DC-specific ICAM-grabbing nonintegrin (DC-SIGN) on the cell surface, which is also utilised by HIV-1 and Ebola virus^{162, 163, 164}. In 2000, Riegler et al found that infection of DCs resulted in the full lytic lifecycle, where infectious viral particles were released into the supernatant from DCs from 5 days post-infection, although with delayed kinetics when compared to infection of HFFFs¹⁶⁵. Further to this, the same lab investigated the effect of productive infection; tumour necrosis factor α (TNF- α) secretion, which plays a role in stimulating T cell proliferation, increased following infection; interleukin 10 (IL-10) production, an anti-inflammatory cytokine which limits damage to the host during the response to a pathogen, was reduced; while MHC-I, MHC-II, CD40 and CD80

(co-stimulatory molecules) were downregulated on the cell-surface¹⁶⁶. The same pattern of immunomodulation was seen by Moutaftsi et al¹⁶⁷, demonstrating that HCMV is able to inhibit some DC functions, however cross-presentation by the bystander (uninfected) DCs is able to surpass the immune evasion techniques employed by the virus and generate antigen-specific T cell responses which control the infection in immunocompetent hosts^{168, 169}.

1.5 Aims

Cell-cell spread is the major mode of spread *in vivo*, and alters the ability of the immune system to control infection. However how it occurs is poorly understood. The Merlin strain accurately recapitulates this mode of spread, enabling us to characterise it in more detail. It also enables efficient infection of DCs with a virus expressing the full repertoire of HCMV genes; all previous studies have used cell-free infection with passaged virus strains, which may not modulate DC function in the same way as virus *in vivo*. This therefore provides an opportunity to understand how HCMV manipulates DCs to affect the induction of adaptive immunity. The aims of my thesis are therefore:

- To capture the transfer of virions in the context of cell-associated infection, the method of which is currently unknown.
- To determine key proteins expressed by DCs that could be instrumental to mounting a successful immune response to HCMV, but are modulated by the virus (either upregulated or downregulated).
- Finally, the ability of Merlin to undergo its full lytic cycle in dendritic cells will be questioned in the context of intrinsic antiviral mechanisms that may be employed by DCs.

This project will provide the first description of how HCMV intra-host spread may occur using a clinical isolate with an intact genome, and it will generate a detailed picture of how the virus modulates the host immune response to promote persistence. This information will contribute to the understanding of dissemination within the host and evasion of the immune response, which could be crucial for the development of therapeutics.

Chapter 2.

Methods and

Materials

2.1 Tissue Culture

All tissue culture in this project was carried out in a Class II biological safety hood using aseptic techniques. Tissue culture media and other reagents were warmed in a 37°C water bath before use, and sprayed with 70% IMS (industrial methylated spirit) before being placed into the hood.

<i>Abbreviation</i>	<i>Comment</i>
<i>Avicel</i>	20g Avicel RC-591 NF mixed into 1L dH ₂ O
<i>0% DMEM</i>	Dulbecco's modified eagle medium (DMEM, Sigma D5796)
<i>2% DMEM</i>	DMEM plus 2% (v/v) foetal calf serum (FCS, Sigma F9665)
<i>2X DMEM</i>	250ml sterile water, 100ml 10x MEM (Gibco 21430), 100ml FCS, 30ml sodium bicarbonate (Gibco 25080), 20ml Pen/Strep (Gibco 15070063), 10ml L-glutamine (Gibco 25030024)
<i>10% DMEM</i>	DMEM plus 10% (v/v) FCS
<i>DMSO</i>	Dimethyl sulfoxide (DMSO, Sigma D2650)
<i>Freezing Medium</i>	90% (v/v) FCS plus 10% (v/v) DMSO
<i>0.5% NP-40</i>	250µl NP40 (Calbiochem 492016) in 50ml PBS
<i>PBS</i>	Dulbecco's Phosphate-Buffered Saline (PBS, Sigma D8537)
<i>4% PFA</i>	500ml dH ₂ O, 5 PBS tablets (Oxoid BR0014G), 20g PFA, filtered
<i>0% RPMI</i>	Roswell Park Memorial Institute (RPMI) 1640 medium (Sigma R0883)
<i>10% RPMI</i>	RPMI plus 10% (v/v) FCS
<i>TrypLE</i>	1X TrypLE Express (Gibco 12605-010)
<i>Trypsin-EDTA</i>	1X Trypsin-EDTA solution (Sigma T3924)

Table 2.1 – Tissue culture media and reagents used in this project.

2.1.1 Cell Maintenance

Adherent cells were kept in a 37°C incubator with 5% CO₂, and maintained with 10% DMEM unless stated otherwise. When cells reached a confluence of 80-100%, they were passaged (at least once per week) – the cells were first washed with PBS, then treated with Trypsin-EDTA for 5 minutes on a rocker at 37°C. Flasks were tapped to encourage cells to come away from the flasks, and then trypsin was neutralised with 10% DMEM. The cells could then be plated for use in experiments, or split 1:3 or 1:6, depending on cell type, to continue passage.

Monocytes and dendritic cells were cultured in 10% RPMI in a 37°C incubator with 5% CO₂, the media was supplemented as described in 2.1.4.2.

2.1.2 Cell Counting

In order to plate cells for use in experiments, they were counted using a disposable counting chamber. After the trypsin had been neutralised, cells were pipetted to obtain a single cell suspension which was then pipetted into the chamber. The average count of 4 grids was used to calculate the average cell number per ml, by multiplying this number by 1×10^4 . Once the cell count was determined, the cells could either be plated in 10% DMEM, or the required number of cells centrifuged at 1500rpm for 3 minutes, and then resuspended in 0% DMEM before plating.

2.1.3 Long-Term Storage of Cell Lines

To avoid the use of high-passaged cell lines in experiments, cell lines were stored in liquid nitrogen tanks. When cells had been split, a portion of the cells were centrifuged at 1500rpm for 3 minutes, and resuspended in 1ml freezing medium (Table 2.1) per cryovial. Cryovials were frozen at a rate of $-1^\circ\text{C}/\text{minute}$ in a “Mr Freezy” pot (NALGENE 5100-0001) until they reached -80°C before being placed in liquid nitrogen.

<i>Cell line/Abbreviation</i>	<i>Comment</i>
<i>293T</i>	Highly transfectable derivative of human embryonic kidney 293 (HEK293) cells containing the SV40 T-antigen
<i>HFFF-TERT/ TERT</i>	hTERT-immortalized human foetal foreskin fibroblasts (HFFFs) ^{170, 171}
<i>HFFF-TERT LifeAct GFP/ LifeAct GFP HFFF</i>	hTERT-immortalized HFFFs expressing actin tagged cell with GFP
<i>HFFF-TERT LifeAct mCherry/ LifeAct mCherry HFFF</i>	hTERT-immortalized HFFFs expressing actin tagged cell with mCherry
<i>HFFF-TET/ TET</i>	hTERT-immortalized HFFFs expressing the tetracycline repressor ^{170, 171}
<i>3468HF-Retro2264 HFFF/mCherry HFFF/HFFF-His Primary HFFF RPE-1</i>	hTERT-immortalized HFFFs expressing 6xHis-tagged cell surface mCherry Low passage primary HFFFs Retinal pigmented epithelial cell line

Table 2.2 – List of cell lines used in this project.

2.1.4 Dendritic Cells

2.1.4.1 Purification of CD14+ Cells from Blood

Peripheral blood was obtained from three sources: buffy coats and apheresis cones (leukoreduction system chambers) from the Welsh Blood Service, and fresh blood was donated by healthy volunteers.

Apheresis cones were washed with PBS plus Heparin Sodium (1000U/ml, Wockhardt) to remove all cells, and topped up to 50ml. 50ml blood donated by volunteers was collected with Heparin. Buffy coats (approx. 50-60ml) were diluted 1/4 with PBS.

To obtain the peripheral blood mononuclear cells (PBMCs), the blood was layered over Histopaque (Sigma 10771) at a ratio of 2:1 (blood:Histopaque) and centrifuged at 2000rpm for 20 minutes with the brake off.

The PBMC layer was removed and washed in PBS, and then CD14+ monocytes were isolated by magnetic activated cell sorting (MACS) using CD14+ microbeads and LS columns, using 70 μ m pre-separation filters if necessary (Table 2.3) – by using the CD14+ microbeads, this allowed positive selection of the monocytes. The purity of the CD14+ sample was assessed by flow cytometry with a CD14 antibody (Table 2.7), staining for 15 minutes at 4°C. Purified CD14+ monocytes were seeded into un-treated cell culture plates.

MACS Reagents	Manufacturer	Cat No.
CD14 microbeads (human)	Miltenyi Biotec	130-050-201
IgG microbeads	Miltenyi Biotec	130-048-401
LS columns	Miltenyi Biotec	130-042-401
MACS Separation Buffer	Miltenyi Biotec	130-091-221
PE microbeads	Miltenyi Biotec	130-048-801
Pre-Separation Filters (70 μ m)	Miltenyi Biotec	130-095-823

Table 2.3 – MACS reagents used in this project.

2.1.4.2 Differentiation of CD14+ Cells into Dendritic Cells

The cells were differentiated into dendritic cells (DCs) by culturing for 6 days in RPMI supplemented with 10% FCS, IL-4 (100ng/ml, Peprotech) and GM-CSF (100ng/ml, Peprotech), and β -Mercaptoethanol (50nM, Gibco); media and supplement changes were carried out every 3 days, excluding β -Mercaptoethanol which was added on the

day of isolation only. The DCs were phenotyped 6 days following purification by staining with anti-CD14, CD1a and DC-SIGN antibodies (Table 2.7) and analysing by flow cytometry. Cells that were CD14-low, DC-SIGN-high and CD1a-high were considered dendritic cells and used in experiments.

2.1.4.3 Maturation of Dendritic Cells

Maturation of DCs was performed by treating the cells with either LPS (1 μ g/ml, Invitrogen) or TNF α (10ng/ml, Peprotech) for 24hrs prior to use in experiments. Maturation was confirmed by flow cytometry using the anti-CD83 and anti-CD86 antibodies found in Table 2.7.

2.1.5 Knock-down of Cellular Proteins using siRNA

To knockdown cellular proteins in primary DCs, the cells underwent two rounds of transfection on consecutive days before being harvested for validation by RT-PCR two days following the second transfection. The reaction mix consisted of 2 μ l HiPerfect transfection reagent (Qiagen 301704), 150nM siRNA (Table 2.4) and 45 μ l 0% RPMI, which was incubated for 15 minutes in a 96-well plate. After incubation, 100,000 DCs per 150 μ l 10% RPMI were added to the reaction mix for reverse transfection. This process was repeated for the second transfection. Volumes scaled up accordingly when required.

<i>Target</i>	<i>Manufacturer</i>	<i>Cat No.</i>
<i>AllStars Negative Control</i>	Qiagen	1027280
<i>APOBEC3A (Human)</i>	Horizon	L-017432-00-0005
<i>GAPDH (Human)</i>	Dharmacon	D-001830-01-05

Table 2.4 – List of siRNAs used in this project.

2.1.6 Lentivirus Transduction

To transduce HFFF-TERTs with a lentivirus, the protocol include two stages: lentivirus production, and HFFF-TERT transduction.

2.1.6.1 Lentivirus Production

293T cells were seeded into a 6 well plate at 1.1×10^6 cells per well in 2ml 10% DMEM, these cells were transfected 24hrs later. The transfection mix consisted of 1.337 μ g of each of the packaging plasmids (pMDL, pRSV-REV, pTAT, pVSVG; a gift from Dr. Mike Weekes), plus 1.337 μ g of LifeAct mCherry plasmid, LifeAct GFP plasmid (both LifeAct plasmids were gifted by Lopamudra Sadhu), or pHAGE GFP control, mixed by pipetting in a 5ml universal tube.

The transfection reagent, Genejuice, was warmed to room temperature and 31.5 μ l added to 1018.5 μ l 0% RPMI (without L-Glutamine). The solution was mixed by gently tapping the sides of the tube, and incubated for 5 minutes.

Following incubation, 525 μ l of the transfection reagent was added dropwise to 525 μ l plasmid DNA, mixed gently by tapping the side of the tube, and incubated for 30-40 minutes to allow formation of transfection complexes. During this incubation, the media on the 293Ts was replaced with 2ml fresh 10% DMEM.

Once the transfection complexes had formed, 150 μ l of the transfection mix was added dropwise to each well of the 6 well plate. After 72hrs, supernatants were harvested from the transfected 293Ts and centrifuged at 3000rpm for 15 minutes to remove cell debris. Supernatants were then filtered using 0.45 μ m low adsorption filters and stored at -80°C in 2ml aliquots.

2.1.6.2 Transduction of HFFF-TERT

HFFF-TERTs were seeded at 7×10^5 in a T25 with 10% DMEM. After 24hrs, the media was replaced with 2ml filtered lentivirus supernatant and 4ml fresh 10% DMEM. Fluorescence was detected by microscopy at 48hrs, and then fluorescent cells were sorted.

2.1.7 Cell Sorting

HFFF cells that required sorting based on fluorescence were harvested using Trypsin as described previously; the HFFFs were centrifuged at 1500rpm for 3 minutes, the supernatant was removed and the cells were resuspended in 200 μ l PBS before being placed into a FACS tube with a cap. All cell sorting was performed by Mrs Kelly

Miners, using a BD FACSaria. Following cell sorting, the HFFFs were cultured in 10% DMEM at 37°C in a 5% CO₂ incubator an appropriate-sized plate for the number of cells that were purified.

2.2 Virology

2.2.1 Generation of Viral Stocks

When growing stocks of HCMV, HFFFs were either infected at a low multiplicity of infection (MOI) with an existing viral stock, or transfected with a HCMV bacterial artificial chromosome (BAC).

2.2.1.1 Transfection Method

For transfection of HFFFs, 2 μ g HCMV BAC DNA was transfected into 1x10⁶ cells using the Amaxa Basic Nucleofector Kit for Primary Mammalian Fibroblasts (Lonza VPI-1002) according to manufacturer's guidelines. Transfected cells were seeded into a T25 flask with 10% DMEM, and were trypsinised and re-seeded weekly to encourage plaque spread. Supernatant was harvested (bled) every 2 days and frozen at -80°C once the flasks showed ~90% cytopathogenic effects (CPE), bleeds continued until the monolayer had died.

2.2.1.2 Growing Viral Stocks

When growing HCMV for viral stocks, 5 T150 flasks of HFFFs were infected either using MOI 0.03 of an existing stock, or the supernatant from a transfected T25 that had reached ~90% CPE. The flasks were maintained until ~90% CPE was reached, at which point the supernatant was harvested every 2 days and frozen at -80°C until the cells had died. Once completed, supernatants were thawed in a 37°C water bath and centrifuged at 1500rpm for 3 minutes to pellet any cells or debris. The supernatant was then pooled and centrifuged at 14,000rpm for 2hrs at 20°C. Following this, the viral pellet was resuspended in 5ml 10% DMEM, and clumps were disaggregated using a needle and 5ml syringe. Virus preps were aliquoted at 300 μ l and stored at -80°C.

Growing viral stocks in RPE-1 cells required a slightly different approach. HFFF-TERT cells were seeded into a T150 flask in 0% DMEM for 24 hrs before being infected with a MOI of 5 in 0% DMEM for 2hrs on a rocker at 37°C. Following incubation, the inoculate was removed and replaced with 0% DMEM for a further 24hrs until it was replaced with 10% DMEM. After 72hrs, the TERTs were trypsinised and divided equally between 5 T150 flasks of confluent RPE-1s. As the Merlin strain

spreads through the monolayer slowly in these cells, the flasks were trypsinised and reseeded weekly to encourage the spread of infection. As above, once ~90% CPE was observed, supernatants were harvested and concentrated.

All viruses from the Merlin backbone used in this study contained a wildtype (Tet repressed) UL128L, RL13 was either mutated or Tet repressed (Table 2.5).

<i>Laboratory Designation</i>	<i>CMV Backbone Strain</i>	<i>RL13</i>	<i>Modifications</i>
<i>pAL1778</i>	Merlin	Mutated	None
<i>pAL1938</i>	Merlin	Mutated	IE2-GFP fusion tagged
<i>pAL2270</i>	Merlin	Tet repressed	UL36-P2A-GFP tagged
<i>pAL2288</i>	Merlin	Tet repressed	ΔUL36-P2A-GFP tagged
<i>pAL2310</i>	Merlin	Tet repressed	UL36-P2A-Rat CD2 tagged
<i>pAL2343</i>	Merlin	Mutated	UL36-P2A-Rat CD2 tagged
<i>pAL2344</i>	Merlin	Mutated	UL36-P2A-GFP tagged
<i>pAL2413</i>	TB40/E-BAC 4	N/A	UL36-P2A-eGFP tagged
<i>pAL2422</i>	Merlin	Mutated	UL32-GFP tagged
<i>pAL2448</i>	Merlin	Mutated	UL32-GFP tagged, UL100-mCherry tagged
<i>pAL2479</i>	Merlin	Mutated	UL32-GFP tagged, UL100-mCherry tagged, UL36-P2A-mtag-BFP2 tagged
<i>pAL2544</i>	Merlin	Mutated	UL36-P2A-FLAG-Rat CD2 tagged
<i>pAL2545</i>	Merlin	Mutated	UL36-P2A-3xFLAG-RatCD2 tagged
<i>pAL2546</i>	Merlin	Mutated	UL36-P2A-3xHA-eGFP-GPI tagged
<i>pAL2547</i>	Merlin	Mutated	UL36-P2A-eGFP-3xFLAG tagged
<i>pAL2550</i>	Merlin	Mutated	UL36-P2A-3xHA-GFP tagged
<i>pAL2566</i>	Merlin	Mutated	UL32-GFP tagged, UL75-mCherry (terminus) tagged
<i>pAL2605</i>	Merlin	Mutated	UL32-GFP tagged, UL55-mCherry (terminus) tagged
<i>pAL2624</i>	Merlin	Mutated	UL32-GFP tagged, UL100-mCherry (external loop) tagged, ΔR54
<i>pAL2755</i>	Merlin	Mutated	UL36-P2A-GFP, UL144-P2A-mCherry
<i>pAL2756</i>	Merlin	Mutated	UL36-P2A-GFP, UL138-P2A-mCherry
<i>pAL2758</i>	Merlin	Mutated	UL32-GFP, UL36-P2A-mtag-BFP2 tagged
<i>pAL2759</i>	Merlin	Mutated	UL32-GFP, UL36-P2A-mtag-BFP2, UL100-mCherry (external loop) tagged, ΔR54

<i>pAL2773</i>	Merlin	Mutated	ΔUL22A-UL25, UL36-P2A-Rat CD2 tagged
<i>pAL2777</i>	Merlin	Mutated	UL32-GFP, UL36-P2A-mCherry
<i>pAL2827</i>	Merlin	Mutated	ΔUS12-US17, UL36-P2A-Rat CD2 tagged
<i>pAL2839</i>	Merlin	Mutated	ΔRL1-RL6, UL36-P2A-Rat CD2 tagged
<i>pAL2856</i>	Merlin	Mutated	ΔRL10-UL1, UL36-P2A-Rat CD2 tagged
<i>pAL2857</i>	Merlin	Mutated	ΔUL13-UL20, UL36-P2A-Rat CD2 tagged
<i>pAL2858</i>	Merlin	Mutated	ΔUS18-US22, UL36-P2A-Rat CD2 tagged
<i>pAL2906</i>	Merlin	Mutated	ΔUS29-US34A, UL36-P2A-Rat CD2 tagged
<i>pAL2907</i>	TB40-BACKl7- SE	N/A	UL32-eGFP, intact US2-US6 a gift from Dr. Christian Sinzger
<i>pAL2988</i>	Merlin	Tet repressed	US28-P2A-mCherry tagged
<i>pAL2993</i>	Merlin	Mutated	ΔUS18, UL36-P2A-Rat CD2 tagged
<i>pAL3032</i>	Merlin	Mutated	ΔUL2-UL11, UL36-P2A-Rat CD2 tagged
<i>pAL3050</i>	Merlin	Mutated	ΔUS20, UL36-P2A-Rat CD2 tagged
<i>pAL3060</i>	Merlin	Mutated	ΔUS16, UL36-P2A-Rat CD2 tagged
<i>pAL3068</i>	Merlin	Mutated	ΔUL148-UL140, UL36-P2A-Rat CD2 tagged
<i>pAL3080</i>	Merlin	Mutated	ΔUS16, ΔUS20, UL36-P2A-Rat CD2 tagged
<i>pAL3113</i>	Merlin	Mutated	ΔUS27-US28, UL36-P2A-Rat CD2 tagged
<i>pAL3114</i>	Merlin	Mutated	ΔUS1-US11, UL36-P2A-Rat CD2 tagged
<i>pAL3130</i>	Merlin	Mutated	ΔUL139-UL150, UL36-P2A-Rat CD2 tagged
<i>pAL3132</i>	Merlin	Mutated	ΔUS20, UL36-P2A-Rat CD2 tagged
<i>pAL3137</i>	Merlin	Mutated	ΔUS12-US21, UL36-P2A-Rat CD2 tagged
<i>pAL3186</i>	Merlin	Mutated	ΔUS18, ΔUS20, UL36-P2A-Rat CD2 tagged

Table 2.5 – List of HCMV viruses used and/or made in this project.

2.2.2 Titration of HCMV by Plaque Assay

HCMV viral stocks were titrated by plaque assay in primary HFFFs, the cells were seeded at 2.5×10^5 cells/well of a 6-well plate. The cells were infected 24hrs after

seeding, using 10-fold dilutions (10^{-4} , 10^{-5} , 10^{-6}) of the viral aliquot, 100 μ l inoculate was added to the cells in duplicate which were then rocked for 2hrs at 37°C. After 2hrs, the inoculate was removed and replaced with a 50:50 mixture of 2X DMEM and 2% Avicel (Table 2.1), and the cells placed back in the incubator. The HFFFs were left undisturbed for 2 weeks, at which point they were washed in PBS and the plaques counted – if the plaques were too small then the 2X DMEM/Avicel was replaced and the cells left for another week. The serial dilution with an appropriate number of plaques was counted in duplicate, which was used to calculate the titre in plaque-forming units (PFU) per ml: Plaques (in 100 μ l) x 10 x dilution factor.

2.2.3 Infecting Cell Lines with HCMV

To infect HFFFs with the “cell-free” method of infection, HFFFs are seeded in 0% DMEM for 24 hrs before being infected with a MOI of 5, unless stated otherwise, in 0% DMEM for 2hrs on a rocker at 37°C. Following incubation, the inoculate was removed and replaced with 0% DMEM for a further 24hrs until it was replaced with 10% DMEM.

2.2.4 Co-Cultures

2.2.4.1 *Infecting Cells by Co-Culture*

When performing co-cultures, infected mCherry HFFFs (HFFF-His) are co-cultured with either primary DCs, HF-TERT or RPE-1 cells (Table 2.2). The mCherry HFFFs were infected using the “cell-free” method described above, and the co-cultures were set up 72hrs post-infection; at this time point progeny virions are released and can infect neighbouring uninfected cells.

2.2.4.2 *Separating Different Cell Types from Co-Culture*

The mCherry HFFFs and target cells were separated 24hrs after co-culture, to ensure that all target cells were infected within a 24h window.

The mCherry HFFFs expressed a 6-His-tagged mCherry on the cell surface, this allowed the use of MACS to separate the different cell types from the co-culture. The

co-culture was harvested, either using Trypsin-EDTA, TrypLE, or harshly tapping the flask – the monolayer was also washed with PBS to remove any bound DCs. The cells were centrifuged and resuspended in 500 μ l MACS buffer, and stained with anti-His.H8 (1:250, Table 2.7) for 15 minutes at 4°C. After washing with MACS buffer and resuspending in 80 μ l/10x10⁶ cells, the samples were incubated with 20 μ l/10x10⁶ cells magnetic anti-IgG beads (Table 2.3) for 15 minutes at 4°C. The samples, after washing and resuspending in 500 μ l MACS buffer, were put through a LS column and magnet, which binds the positive cells (mCherry HFFFs), allowing the negative (target) cells to flow through. The columns were washed 3 times with 3ml MACS buffer, and the positive cells eluted from the column with 5ml MACS buffer. Purity was checked using flow cytometry.

For experiments where viruses expressing a UL36-P2A-RatCD2 (Table 2.5) were used, MACS was also used to separate the infected from uninfected target cells. The second separation took place immediately following the mCherry HFFF separation, except when DCs were used – these were given at least two hours rest in 10% RPMI + IL4 + GMCSF between separations. Cells were separated using the same protocol as above, but stained with anti-RatCD2-PE (1:250, Table 2.7), followed by 20 μ l/10x10⁶ cells magnetic anti-PE beads (Table 2.3). The flow through contained the uninfected cells, the retained contained the infected cells, purity was checked using flow cytometry.

2.2.5 HCMV Genome Delivery Assay

Cells were either co-cultured or infected with cell-free HCMV preparations for the genome delivery assay.

The co-cultures were set up as described above (2.2.4.1), using a Merlin virus expressing UL36-P2A-RatCD2 so that the infected cells could be purified.

For the cell-free infections, HFFFs were seeded into a T25 on Day 1, then infected at varying MOIs on Day 2. The infected and uninfected HFFFs were separated on Day 3 using MACS as with the co-cultured cells.

To eliminate virus bound to the surface of infected cells, they were incubated with 2mg/ml Proteinase K (Qiagen DNeasy Blood and Tissue kit 69504) for 1 hour at 4°C

before being washed in PBS. The DNA was extracted from the cells using Qiagen DNeasy Blood and Tissue Kit, concentration was determined using the NanoDrop ND-1000 spectrophotometer before using quantitative PCR to quantify the genomes per newly infected cell.

2.2.5.1 Extracting DNA from Nuclei

To extract DNA from the nuclei of cells, the cells are first washed with PBS and pelleted (1500rpm, 3minutes). All PBS was aspirated, and from this point on, all work was done on ice. The pellet was resuspended in 500µl Pierce IP lysis buffer (Thermo 87788) and transferred to an Eppendorf, before being placed on a rotating mixer at 4°C for 15 minutes. The Eppendorfs were then centrifuged at 13,000rpm for 15 minutes at 4°C. The pellet was resuspended in 500µl Pierce IP lysis buffer, and the process repeated. DNA was then extracted from the nuclei-containing pellet using the Qiagen DNeasy Blood and Tissue Kit as before.

2.2.6 Viral DNA Extraction for Sequencing

All newly generated HCMV viruses were sequenced by collaborators in Dr. Andrew Davison's group, Glasgow University. This was done to ensure no second site mutations had occurred in the HCMV genome during recombineering or transfection. Viral DNA was extracted from an aliquot that had been frozen at -80°C in 2.2.1.2, using the QIAMP MinElute Virus Spin Kit (Qiagen 57704) and protocol. DNA extracts were frozen at -20°C until ready to be shipped to Glasgow on dry ice, where Dr Andrew Davison performed high-throughput sequencing using the Illumina MiSeq System¹⁰³.

2.3 Microscopy

2.3.1 Live Cell Imaging

All live cell imaging was performed using a Zeiss microscope (Axio Observer Z1 with a XL Multi S1 Incubator) and Zen2 Pro Software. The live cell imaging was done using both fibroblasts and epithelial cells. The fibroblasts were seeded into a glass-bottomed 96-well plate (Ibidi 89626) and infected with a MOI of 0.2 as described in 2.2.3 – a low MOI was used to ensure single cells were infected so that plaque formation could be visualised. To infect epithelial cells, RPE-1s were seeded into a glass-bottomed 96-well plate with infected fibroblasts (10:1 ratio).

The plate was imaged with the 40X oil lens for more detailed images, the optimum settings for long-term live cell imaging were 2x2 binning, 50% power, 20ms exposure, taken every 30 minutes with a Z-stack to obtain information from several planes.

2.3.2 Transmission Electron Microscopy

Transmission electron microscopy (TEM) was performed by Dr. Chris Von Ruhland at Central Biotechnology Services, Cardiff University.

HFFFs were seeded onto Thermonox coverslips in a 12-well plate then infected with virus (Table 2.5). DCs were co-cultured with the HFFFs (2:1) for 2, 4, 6 and 8hrs, before unattached DCs were washed away with 0% DMEM, and the coverslips were fixed using 1% Glutaraldehyde in 0% DMEM for 1hr at room temperature, fixative was then replaced with PBS. Dr. Chris Von Ruhland prepared, cut and imaged the sections using the following protocol: coverslips were treated with 1% glutaraldehyde in 300mOsM PBS for 1hr, followed by 2% osmium tetroxide in PBS for 1hr. After washing for 5 minutes in water three times, coverslips were left for an hour in 2% uranyl acetate in H₂O, followed by three further 5 minute washes in water. The next step involved washing the coverslips in increasing concentrations of isopropanol (IPA), each for 15 minutes: 50% IPA in H₂O, 70% IPA, 90% IPA, 2 x IPA. Lastly, samples were treated with 50% TAAB Embedding Resin (TER) (TAAB Laboratories Equipment Ltd. UK) in IPA for 30 minutes, followed by four 1hr incubations in TER.

Samples were placed cell-side down across the rim of TER-filled embedding capsules and cured at 60°C overnight. Coverslips were removed by plunging pre-cooled (-35°C)

samples into liquid nitrogen and then transferring into hot (approximately 60°C) water, leaving the cells embedded on the surface of the resulting block. Pieces of block surface were sawn out and attached to blank resin blocks with epoxy resin for subsequent sectioning. Semithin (0.35µm thick) sections were cut on an Ultracut E ultramicrotome, stained with toluidine blue, and examined and imaged with an Olympus BX51 research light microscope (Olympus Optical Co. (U.K.) Ltd, London, U.K) fitted with a Zeiss Axiocam and Axiovision software (Carl Zeiss Vision GmbH, Hallbergmoos, Germany).

Representative areas of cells were selected, and thin (100nm thick) sections cut and collected onto 300 mesh copper grids. Sections were stained with lead citrate and examined in a Philips CM12 TEM (FEI U. K. Ltd. UK) at 80kV and images captured with a Megaview III camera and AnalySIS software (Soft Imaging System GmbH, Germany).

To differentiate between the HFFFs and DCs, the DCs were stained with CFDA: DCs were centrifuged at 1500rpm for 3 mins to remove media, and washed in PBS. Cells were resuspended in CFDA (Table 2.8) and incubated for 15 minutes at 37°C before being washed in 10% RPMI and co-cultured with HFFFs.

2.3.3 Immunofluorescence Assay

DCs (infected, bystanders and uninfected) were seeded into a glass-bottom 96-well plate which had been pre-treated with poly-D-lysine hydrobromide (PDL, Sigma P6407) for 1-24hrs to ensure that DCs attached to the plate. DCs were fixed with 4% PFA (Table 2.1) for 15 minutes, washed, and permeabilised with 0.5% NP-40 (Table 2.1) for a further 15 minutes before being washed then stained with primary and secondary antibodies (Table 2.6) for 30 minutes at 37°C with PBS washes between each step. Cells were stained with DAPI (300nM, Invitrogen) before being visualised using the Zeiss microscope with a 40X oil lens.

<i>Antibody Target</i>	<i>Species</i>	<i>Fluorochrome</i>	<i>Dilution</i>	<i>Manufacturer</i>	<i>Cat#</i>
<i>IE1</i>	Mouse	Unconjugated	1:100	Millipore	Mab810R
<i>IRF7</i>	Rabbit	Unconjugated	1:100	Novus Biologicals	NBP2- 38678
<i>Mouse</i>	Goat	AF647	1:500	Invitrogen	A21242
<i>Rabbit</i>	Goat	AF488	1:500	Invitrogen	A11070

Table 2.6 – List of antibodies used for immunofluorescence assays in this project.

2.4 Flow Cytometry

2.4.1 Surface Staining for Flow Cytometry

Cells were first washed in PBS before being stained with the primary antibody (Table 2.7) for 15 minutes at 4°C; if the antibody was conjugated to a fluorophore then cells were washed in PBS after incubation before being fixed with 4% PFA and analysed with either BD Accuri C6 or Attune Nxt Flow Cytometer. Unconjugated antibodies were washed and incubated with the secondary antibody for 15 minutes at 4°C before being washed, fixed and analysed.

2.4.2 Intracellular Staining for Flow Cytometry

Intracellular staining for flow cytometry was performed using the BD CytoPerm/CytoFix kit (554722), cells were stained in U-bottom 96-well plates, according to protocol. Antibodies used for intracellular staining can be found in Table 2.7, any viability dyes (Table 2.8) used were added to the cells prior to fixation with the BD CytoPerm/CytoFix solution.

Antibody Target	Species	Fluorochrome	Dilution	Manufacturer	Cat No.
<i>Caspase 10</i>	Rabbit	Unconjugated	1:100	Abcam	AB177475
<i>CD1a</i>	Mouse	FITC	1:100	BD Pharmingen	555806
<i>CD14</i>	Mouse	PECy7	1:100	eBioscience DX	9025-0149-120
<i>CD166 (ALCAM)</i>	Mouse	PerCP-eFluor 710	1:100	eBioscience	46-1668-41
<i>CD166 (ALCAM)</i>	Mouse	PECy7	1:100	Biolegend	343911
<i>CD223 (LAG3)</i>	Mouse	PerCPeFluor 710	1:100	eBioscience	46-2239-41
<i>CD275 (ICOSL)</i>	Mouse	APC	1:100	Miltenyi Biotec	130-098-738
<i>CD31 (PECAMI)</i>	Mouse	APC	1:100	eBioscience	17-0319-42
<i>CD369 (Dectin-1)</i>	Mouse	PerCP-eFluor 710	1:100	eBioscience	46-9856-41
<i>CD43 (Leukosialin)</i>	Mouse	APC	1:100	eBioscience	17-0439-42
<i>CD83</i>	Mouse	APC	1:100	BD Biosciences	561960
<i>CD84</i>	Mouse	BV421	1:100	BD Biosciences	566094

<i>CD86</i>	Mouse	PE	1:100	Miltenyi Biotec	130-114-098
<i>c-Met</i>	Mouse	Alexa Fluor (AF) 647	1:100	BD Biosciences	566014
<i>DC-SIGN</i>	Mouse	PE	1:100	BD Biosciences	551265
<i>FLAG</i>	Mouse	Unconjugated	1:200	Cell Signalling Technology	81468
<i>gB</i>	Mouse	Unconjugated	1:100	Abcam	ab6499
<i>HA</i>	Mouse	Unconjugated	1:500	Invitrogen	32-6700
<i>His.H8</i>	Mouse	Unconjugated	1:200	Invitrogen	MA1-21315
<i>ICAM3</i>	Mouse	FITC	1:100	Santa Cruz Biotechnologies	sc-53338-FITC
<i>IE1</i>	Mouse	Unconjugated	1:100	Millipore	Mab810R
<i>Mouse IgG</i>	Goat	AF647	1:500	Invitrogen	A21242
<i>Mouse IgM</i>	Goat	AF647	1:500	Life Technologies	A21238
<i>OSCAR</i>	Mouse	APC	1:100	Miltenyi Biotec	130-119-573
<i>PDGFRα</i>	Mouse	Unconjugated	1:200	BD Biosciences	556001
<i>Rat CD2</i>	Mouse	PE	1:250	Biolegend	201305
<i>SCIMP</i>	Mouse	AF647	1:100	Biolegend	367903
<i>SECTM1</i>	Mouse	Unconjugated	1:100	Proteintech	60281-1-IG
<i>SEMA4A</i>	Mouse	PerCP-eFluor 710	1:100	eBioscience	46-9753-41

Table 2.7 – List of antibodies used for flow cytometry in this project.

	<i>Stain</i>	<i>Dilution</i>	<i>Manufacturer</i>	<i>Cat No.</i>
<i>CellTrace Far Red DDAO-SE</i>		1:2500	Thermofisher	C34553
<i>CFDA eFluor 450</i>		1:50,000	Molecular Probes	V-12883
<i>LIVE/DEAD™ Fixable Aqua Viability eFluor 660</i>		1:1000	eBioscience	65-0842-85
		1:1000	Invitrogen	L34965
		1:1000	Invitrogen	65-0864-14

Table 2.8 – List of cell dyes used for flow cytometry in this project.

2.5 Proteomics

2.5.1 Biotinylation of Dendritic Cell Plasma Membrane

Biotinylation of the DCs was performed using a two-step method where oxidation and aminoxy-biotinylation are carried out separately.

After separation, the DCs were pelleted by centrifuging at 500g for 5 minutes. The pellet was resuspended in 1ml PBS and layered over 3ml Histopaque in a 15ml Falcon then centrifuged at 2000rpm for 20 minutes with the brake off. DCs were then removed from the interface, washed in PBS and pelleted again.

The DC pellet was resuspended in 3ml 10X Sodium Periodate and incubated on a falcon roller at 4°C for 20 minutes. The periodate was quenched using 600μl 5X Glycerol, cells were then pelleted and washed twice in ice-cold PBS pH 7.4. The biotinylation mix was made up within 10 minutes before being added to the DCs. This consisted of 30ml ice-cold PBS pH 6.7, 33.3μl aminoxy-biotin (1000X) and 30.7μl Aniline, which was vortexed, then 1.7ml filtered FCS was added – the mix was kept on ice. All PBS was aspirated from the pellet before addition of 3ml biotinylation mix. The cells were incubated at 4°C on a falcon roller for a further 30 minutes.

During this time, 10μl protease inhibitor (PI) was added to 10ml 1% lysis buffer, and 10 minutes before the end of incubation, 100X Iodoacetamide (IAA) solution was made and 100ul added to 10ml lysis buffer with the protease inhibitor (lysis buffer/PI/IAA).

After biotinylation, the DCs were centrifuged, and washed twice in ice-cold PBS pH 7.4. Once the PBS had been aspirated, the cells were lysed in 1ml Lysis buffer/PI/IAA and transferred to an Eppendorf tube which was kept on ice for 30 minutes. Samples were then centrifuged for 5 minutes at 13,000g, 4°C. The supernatant was transferred to a fresh Eppendorf, and centrifuged a further two times – transferring supernatant to a fresh Eppendorf between each spin. The lysates were snap frozen in an ethanol/dry ice bath and stored at -80°C.

<i>Abbreviation</i>	<i>Comment</i>
<i>Aminooxy-biotin (1000X)</i>	100µl DMSO and 5mg Aminooxy-biotin (BIOTIUM 90113).
<i>Aniline</i>	Aniline (Sigma 242284)
<i>Filtered FCS</i>	FCS (Table 2.1) filtered through .45µm syringe filter.
<i>1M Glycerol</i>	3.684g Glycerol (Fisher Chemical G/0650/17) and 40ml PBS pH 7.4.
<i>5X Glycerol</i>	50µl 1M Glycerol and 10ml PBS pH 7.4 – kept on ice.
<i>100X Iodoacetamide solution</i>	10-30mg Iodoacetamide (Sigma I6725) and 108-324µl Lysis buffer plus protease inhibitor (multiply weight by 10.8).
<i>1% Lysis buffer</i>	500µl 1M Tris-HCl, 25ml 2% Triton, 7.5ml 5M NaCl (), 17ml ultra-pure H ₂ O (Sigma W4502).
<i>PBS pH 6.7</i>	500ml PBS pH 7.4 and 1.1ml HCl, ice-cold.
<i>PBS pH 7.4</i>	PBS with Ca/Mg (Sigma D8662), ice-cold.
<i>Protease inhibitor</i>	Protease inhibitor cocktailP8340-1ML (Sigma P8340)
<i>10X Sodium Periodate</i>	25-40mg Sodium meta-Periodate (Thermo 20504) and 11.75-18.8ml PBS pH 7.4 (multiply weight by 0.47) – kept on ice.
<i>2% Triton X-100</i>	10% Surfact-Amps X-100 (Thermo 28314) and 40ml ultra-pure H ₂ O.

Table 2.9 – Reagents used for biotinylation of dendritic cell plasma membranes.

2.5.2 Single Shot and Fractionation of Samples

The frozen samples were shipped on dry ice to University of Cambridge, to our collaborators Dr Michael Weekes and Dr Lior Soday. The samples are then digested into peptides and labelled with 10-plex tandem mass tag (TMT) reagents, before being mixed together and analysed by mass spectrometry. The combination of 10-plex TMT reagents and the ‘MS3’ method of analysis on an Orbitrp Fusion MS, enables accurate comparative quantitation to be performed between samples that are mixed together in a single run on the MS. Samples were initially run as an unfractionated single shot, to ensure similar peptide loading across each TMT channel and avoid excessive electronic normalisation, before HpRP fractionation of the samples^{172 173}.

2.6 Polymerase Chain Reaction (PCR)

2.6.1 Standard PCR

Standard PCR reactions for the generation of templates for use in recombineering, antibody cloning and for checking the presence of a gene in a BAC or cell line were set up as 50 μ l reactions in thin walled PCR tubes (Grenier Bio-One 682201). Forward and reverse primers were diluted to 100nM with dH₂O prior to addition to reaction mix to reduce the occurrence of primer dimers and improve efficiency of the reaction. For the generation of recombineering templates, the reactions consisted of 1 μ l vial 1 (Enzyme mix; Expand High Fidelity PCR System, Sigma 11732650001), 5 μ l of vial 2 (10X Buffer with 15mM MgCl₂), 1.5 μ l DMSO, 1 μ l dNTPs (10mM; NEB N0447L), 1 μ M each of the forward and reverse primers, 1 μ l of template (i.e. recombineering cassette) and 38.5 μ l dH₂O.

For preparing inserts to be used in antibody cloning, the reactions consisted of 0.5 μ l Phusion DNA polymerase (Phusion High-Fidelity DNA Polymerase kit, NEB M0530), 10 μ l Phusion HF buffer, 1 μ M each of the forward and reverse primers, 1 μ l template (i.e. GeneArt Strings DNA Fragments), 1.5 μ l DMSO and 35 μ l dH₂O.

For other reactions, this consisted of 0.25 μ l Taq polymerase (Taq DNA Polymerase kit, Invitrogen 18038-042) 5 μ l 10X PCR buffer, 1.5 μ l MgCl, 1.5 μ l DMSO, 1 μ M each of the forward and reverse primers, 1 μ l of template (i.e. BAC DNA or cellular DNA), 1 μ l dNTPs, and 37.75 μ l dH₂O. The reactions were amplified using the programmes found in Table 2.10 and Table 2.11, the annealing temperature and/or extension time was adjusted if necessary.

Standard Programme Stages	Temperature (°C)	Time	Cycles
<i>Pre-Heating</i>	99	-	-
<i>Initial Denaturation</i>	94	2 min	1
<i>Denaturation</i>	94	15s	34
<i>Annealing</i>	55	30s	
<i>Extension</i>	72	1.5 min	
<i>Final Extension</i>	72	15 min	1
<i>Hold</i>	4	∞	-

Table 2.10 – Standard PCR programme used in this project.

<i>Phusion Programme Stages</i>	<i>Temperature (°C)</i>	<i>Time</i>	<i>Cycles</i>
<i>Pre-Heating</i>	99	-	-
<i>Initial Denaturation</i>	98	30s	1
<i>Denaturation</i>	98	10s	34
<i>Annealing</i>	60	30s	
<i>Extension</i>	72	3 min	
<i>Final Extension</i>	72	12 min	1
<i>Hold</i>	4	∞	-

Table 2.11 - Phusion PCR programme used in this project.

2.6.2 Quantitative Polymerase Chain Reaction (qPCR)

The standards used for qPCR experiment were a series of 10-Fold dilutions of DNA from plasmids containing gB and GAPDH, generated in 2.8.3. Reaction mixes for qPCR were made up to 20µl - 10µl SYBR Green (BioRad 1708882), 0.4µl of each of the forward and reverse primers (Table 2.13), 100ng DNA diluted in Ultrapure distilled water (Invitrogen 10977-035), and made up to 20µl with Ultrapure water. Each sample was added to an Applied Biosystems™ MicroAmp™ EnduraPlate™ Optical 96-Well Clear Reaction Plate (Thermo Fisher 4483354) in triplicate for each reaction, the plate was sealed, vortexed and centrifuged briefly before being placed into a QuantStudio 3 Real-Time qPCR System machine. The thermocycling programme, Comparative Ct with Melt, is found in Table 2.12. Once the programme was complete, the data was analysed using ThermoFisher Standard Curve software.

<i>Stage</i>	<i>Temperature (°C)</i>	<i>Time</i>	<i>Data Collection</i>	<i>Cycles</i>
<i>Stage 1</i>	50	2 min		1
	95	10 min		
<i>Stage 2</i>	95	15s		40
	60	1 min	✓	
<i>Melt Curve</i>	95	15s		-
	60	1 min		
	95	15s	✓	

Table 2.12 – Thermocycling programme, Comparative CT with Melt, used for qPCR in this project.

2.6.3 RT-PCR

RNA was isolated from cells using the RNeasy Plus Mini kit (Qiagen 74134), samples were stored at -80°C.

SuperScript IV Reverse Transcriptase kit (Invitrogen 18090050) was used for reverse transcription of the RNA to cDNA. The 20 μ l reaction mix was set up using the RT-PCR primers found in Table 2.13, and incubated with the RNA as outlined in the manufacturer's protocol. Samples were stored at -20°C unless used immediately for a qPCR reaction.

<i>Project</i>	<i>Target</i>	<i>Sequence</i>
<i>qPCR</i>	GAPDH	F CCTCTGACTTCAACAGCGACAC R TGTCATACCAGGAAATGAGCTTGA
	gB	F CTGCGTGATATAACGTGAAGG R ACTGCACGTACGAGCTGTTGG
<i>RT-PCR</i>	APOBEC3A	F TGGCATTGGAAGGCATAAGAC R TTAGCCTGGTTGTAGAAAGC

Table 2.13 – Primer Sequences used for *qPCR* and *RT-PCR*.

2.7 Western Blotting

To perform a Western Blot, cells were first washed with PBS and then lysed with NuPAGE lysis buffer. The cells were rocked at 37°C for a few minutes before a cell scraper was used to collect cells which were then transferred to an Eppendorf tube. Samples were then boiled at 100°C for 10 minutes, and either used immediately or stored at -20°C.

A 10% pre-cast BioRad gel (5678084) was placed into a BioRad system tank with 500ml running buffer. A pre-stained protein ladder was used as a reference for band size (Novex, Invitrogen 57318). Depending on the number of cells lysed, 10-35µl of sample was loaded to each well. The gel was run at 150V for 1 hour.

Once the gel had finished, it was transferred to PVDF membrane (Amersham RPNF L/02/10), which had been activated with 100% methanol, and pre-soaked in 2X transfer buffer, this was done at 20V for 1 hour.

Blocking buffer was added to the PVDF membrane, and rocked for 1 hour at room temperature. The membrane was then stained with the primary antibody in blocking buffer, and rocked for 1 hour at room temperature. After primary antibody staining, the membrane was washed three times with PBST for 5 minutes on the rocker. After washing, the secondary antibody was added in blocking buffer, and again, the membrane was rocked for 1 hour at room temperature before being washed three times with PBST.

To image the Western Blot, SuperSignal West Pico PLUS Chemiluminescent Substrate (Thermo Scientific 34578) was added according to manufacturer's instructions, and the blot imaged with a GeneSys GelDoc (Syngene).

Reagent	Comments
Blocking Buffer	PBST and 5% dried milk powder
Running Buffer	TGS buffer and dH ₂ O
NuPAGE Lysis Buffer	25% 4X NuPAGE LDS buffer (NP0008), 10% DTT (Invitrogen Y00147), in dH ₂ O
PBST	1L dH ₂ O, 10 PBS tablets, 0.1% Tween (Merck 822184)
Stripping Buffer	Restore stripping buffer (Thermo, 21063)
2X Transfer Buffer	50ml 20X NuPAGE transfer buffer (NP0006-1), 50ml methanol, 400ml dH ₂ O

Table 2.14 – Reagents used for Western Blotting in this project.

<i>Target</i>	<i>Species</i>	<i>Dilution</i>	<i>Manufacturer</i>	<i>Cat. No</i>
<i>Actin</i>	Rabbit	1 :5000	Sigma Aldrich	A2066
<i>APOBEC3A</i>	Rabbit	1 :1000	Sigma Aldrich	SAB4500753
<i>APOBEC3G</i>	Rabbit	1 :1000	NIH AIDS Reagent Program	10082
<i>anti-serum</i>				
<i>Anti-Rabbit HRP</i>	Goat	1 :5000	BioRad	170- 6515

Table 2.15 – Antibodies used for Western Blotting in this project.

2.8 Molecular Biology

2.8.1 Buffers and Solutions

Solutions	Comment
<i>0.7% Agarose Gel</i>	1X TAE, 0.7% (w/v) agarose (Geneflow A4-0700), 1:2000 Midori Green (Nippon Genetics MG04)
<i>2% Agarose Gel</i>	1X TAE, 2% (w/v) agarose, 1:2000 Midori Green
<i>Ampicillin</i>	100mg/ml stock solution. Ampicillin sodium (Duchefa Biochemie A0104.0025) in dH ₂ O
<i>Chloramphenicol</i>	12.5mg/ml stock solution, Chloramphenicol (Boehringer 634 433) in 100% ethanol
<i>IPTG</i>	100mM stock solution. IPTG (Melford Biolaboratories MB1008) in dH ₂ O
<i>10% Glycerol</i>	dH ₂ O plus 10% (v/v) Glycerol
<i>Kanamycin</i>	15mg/ml stock solution. Kanamycin (Melford Biolaboratories K22000-10.0) in dH ₂ O
<i>L-Arabinose</i>	L-Arabinose powder (Sigma A3256)
<i>LB agar</i>	1L LB broth plus 7.5g Agar powder (VWR 20767.232)
<i>LB broth</i>	1L dH ₂ O plus 20g LB broth low salt (Duchefa Biochemie L1703.0500)
<i>Streptomycin</i>	200mg/ml stock solution. Streptomycin sulphate (Melford Biolaboratories S0148) in dH ₂ O
<i>1X TAE</i>	50X TAE (National Diagnostics B9-0030) diluted in dH ₂ O
<i>X-GAL</i>	40mg/ml stock solution. X-GAL (Melford Biolaboratories MB1001) in 100% DMSO

Table 2.16 – List of buffers and solutions used in this project.

2.8.2 Purification of DNA

Purification of DNA (from PCR products) used two methods: gel purification and solution purification.

2.8.2.1 Purification of DNA from Agarose Gel Slices

PCR products that had been run on a 0.7% agarose gel and found to have non-specific bands present were gel purified. The gel was placed on a transilluminator and the correct band cut out using a scalpel. DNA was extracted from the gel slice using FastGene Gel/PCR Extraction Kit (Nippon Genetics FG-91302) according to gel extraction manual.

2.8.2.2 Purification of DNA from PCR Products

For PCR products that had only the correct band, the PCR extraction manual of the FastGene Gel/PCR Extraction Kit was followed.

2.8.3 TOPO TA Cloning

TOPO TA Cloning was used to insert human GAPDH and HCMV gB genes into plasmids for use as standards in qPCR experiments.

2.8.3.1 Generating PCR Products for Insertion into Plasmid

Standard PCR was used to amplify gB from BAC DNA and GAPDH from cellular DNA using the primers in Table 2.13. The PCR products were run on a 2% agarose gel, as the genes are small, and purified accordingly (2.8.2).

2.8.3.2 TOPO TA Cloning Reaction

TOPO® TA Cloning® Kit for Sequencing, containing DH5 α ™ -T1R One Shot® Chemically Competent cells (Invitrogen K4595-01) was used to insert the PCR products into the pCRT™4-TOPO® plasmid. The cloning reaction was set up according to manufacturer's guidelines, then the competent bacteria transformed using the One Shot® chemical transformation protocol. Positive clones were selected for using LB plates containing 50 μ g/ml Kanamycin – plasmid DNA was extracted from the positive clones by minipreparation (2.8.7), and the DNA then sequenced (2.8.9).

2.8.4 Antibody Cloning

Antibody cloning was used in order to produce the potent neutralising antibodies used in the genome delivery assays, as Merck discontinued production.

2.8.4.1 Linearising the Vector

To linearise the vector, 3 μ g of the vector was cut using 1 μ l of the relevant restriction enzymes, 2 μ l of the relevant buffer (Table 2.17), and topped up to 20 μ l with ddH₂O.

The reactions were incubated at 37°C for 4 hours. To prevent the vectors recircularising, 2µl Antarctic phosphatase buffer and 1µl Antarctic phosphatase were added to the reactions and incubated at 37°C for 30 minutes, followed by 80°C for 2 minutes to inactivate the enzyme.

Vectors were gel purified as described in 2.8.2.1.

2.8.4.2 Antibody Chains

The heavy and light chain sequences (Table 2.18) for both the human anti-pentamer (2.18) and the rabbit anti-gH (70.7) were obtained from a patent published by Fu et al¹⁷⁴. The sequences were generated as either GeneArt Strings DNA fragments or GeneSyn cloned fragments (Thermofisher), before Phusion PCR was used to create the templates for ligation with the vectors (2.6.1). The PCR products were then gel purified.

2.8.4.3 Ligation of Antibody Chains and Vector

For ligation of the vectors and antibody chains, 100ng vector was combined with the insert to give a 1:3 molar ratio (New England Biolabs cloning calculator was used to calculate this), although the insert was left out for negative controls. The reaction was topped up to 5µl with ddH₂O, before the addition of 5µl NEBuilder® HiFi DNA Assembly Master Mix (NEB E2621S). Reactions were incubated at 50°C for 15 minutes.

2.8.4.4 Transformation of Stellar Competent Cells

The ligated vectors and antibody chains were used to transform Stellar competent cells. The cells were thawed in an ice bath, gently mixed with a Gilson pipette, then 50µl of the cells were transferred to a 15ml Falcon tube. After 1µl of the cloning reaction was added, the cells were placed on ice for 30 minutes, then heat shocked at 42°C for exactly 45 seconds and returned to the ice for 1-2 minutes. SOC medium which had been warmed to 37°C was added to bring the total volume in the tube to 500µl. The cells were then incubated in a 37°C shaking incubator for 1 hour before

plating on selective medium and incubating at 37°C (see Table 2.17 for antibiotics used).

Plasmid DNA was extracted from positive colonies and sequenced (2.8.7 & 2.8.9).

<i>Vector</i>	<i>Selection Marker</i>	<i>Restriction Enzymes</i>	<i>Digest Buffer</i>	<i>Comments</i>
<i>Human IgG kappa chain (pAL2642)</i>	Ampicillin	Agel and BsiWI	NEB 2.1	Encodes constant domain for cloning kappa chain of human IgG.
<i>Human IgG heavy chain (pAL2644)</i>	Ampicillin	Agel and Sall	NEB 3.1	Encodes constant domain for cloning heavy chain of human IgG.
<i>pVin2.0-rabbit IgG (pAL3167)</i>	Kanamycin and Neomycin	BsiWI	NEB 3.1	Encodes constant domains for cloning heavy and light chains of rabbit IgG. This vector was gifted by Lauri Peil at Icosagen Cell Factory.

Table 2.17 – Information regarding vectors used for antibody cloning.

<i>Antibody Chain</i>	<i>DNA Sequence</i>
<i>2.18 heavy chain</i>	GAGGTGCA GCTGGTGGAGTCTGGAGGAGGACTGGTGAGCCAGGAGGCTCCCTGAGGGCTGTCTTGC CCGCCAGCGGCTTCTCCTTTCTGACCA CGATATGGACTGGGTGCGCCAGGGCACCTGGC AAGG GGCCTGGAGTGGGTGGGCCGGAGCAGAAAACAAGGATTACAGCTCACCACAGAGTATGCAGCCTCCGTGAGGGCCGCTTCACCATCTC TGGGACGATAGCAAGAACTCCCTGTACCTGCA GATGAACAGCCTGAAGACCGAGGACACAGCCGTGACTATTGTGCCAGAGGCC CCAACACTCTGATAGAACGGCTACTATGGCGGACATTGACATCTGGGCCAGGGCACATGGT GACAGT GTCTAGC
<i>2.18 light chain</i>	GACATCCAGATGACACAGTCTCTAGCTCGTGAGCGCCTCCGTGGGCGATAGGGT GACCATCACATGCAGAGCCTCCAGGGCATCTCTAGCTGGCTGGCTGGTATCAGCAGAAGCCCGCAAGG CCCCTAAGCTGCTGATCTATGACGCCCTCACCTGGAGAGCGCGTGCCTCCCGGTTCTCGCAGCGCTCCGGCAGACACTTACCC TGACAATCTCTCTGCA CGCCAGAGGATTGCGCACCT
<i>70.7 heavy chain</i>	CAAAGCGTAGAAAGAGTCGCCGGGAGACTCGTGACGCCGGACTCCGTAACACTAACCTGTACCGCCAGTGGATTCTCTCTAGTTACATGATTGGGTACGCCAAGCACCTGGGAAAGG TTTATGGATCGGCTATATTAAATTATAACAACAACTCCGTACTATGCCACGTGGGCCAAGGGTCGATTACGATATCAGGACTTCAACA ACTGTGCGTAAAGATTACAAGCCAACGACTGAAGATT AGCTACCTACTCTGCCGCGAGCGGCAGGTAACTATTATGTAGGCGCCTAAACCTATGGGTCCGGGACCCCTGGTCACTATATCAAGC
<i>70.7 light chain</i>	GAACGAGATATGACTCAGACGCCGCTAGCGTTGAAGTCGCTGTGGCGGAAC TGTACGATAAAATGCAAGCATCTCAGGCTATCGGGAACCTTTGGCGTGGTATCA ACAAAAGCCAGGTCAAAGGCCAAGCTCTCATTTACGACCGCTGACGCCCTGGCGTCCGGAGTCGTTAAGGGATCTGGCTCAGGACTGAGTTCAACTAAC TATCTCCGGTGTACAATGCGCCATGCGGCAGTACTATTGCCAACAGGCTATATGACTAATGTGGAGAACGCATTGGGGTGGCACCGAGGTGGTAAAAA

Table 2.18 – Sequences for heavy and light chains of anti-pentamer (2.18) and anti-gH (70.7) antibodies.

2.8.5 Recombineering

Recombineering of BAC-derived viruses has previously been described by Stanton et al¹⁰². Primers used for the generation of recombineering templates and sequencing (Table 2.19) were designed using CLC Main Workbench 8.1 (Qiagen Bioinformatics), and synthesised by Eurofins.

2.8.5.1 Selection Cassettes

The RPSL cassette used for BAC-derived viruses contained either Kanamycin or Ampicillin resistance genes and Streptomycin susceptibility genes to allow for positive and negative selection of transformed colonies, and also a lacZ gene for blue/white selection. The BAC contains a Chloramphenicol resistance gene to ensure the growth of only BAC-containing bacteria.

2.8.5.2 Preparation of Competent Bacteria

The *E. coli* strain SW102 bacteria were grown overnight in LB containing 15µg/ml Chloramphenicol in a shaking incubator at 32°C. The bacteria were then grown to competency the following day in LB without antibiotics at 32°C in a shaking incubator, until they reached an optical density (OD₆₀₀) of 0.6. The lambda red proteins were then induced by incubating the bacteria in a 42°C water bath for 15 minutes. From this point on all steps were performed on ice/at 0°C.

2.8.5.3 Transformation of Competent Bacteria

The induced bacteria were centrifuged at 4000rpm, 0°C for 5 minutes, and washed twice with ice-cold dH₂O, and resuspended in the leftover water from pouring off the supernatant. A small aliquot of bacteria was then transformed. During the first round of recombineering, the bacteria were transformed with the RPSL cassette containing arms of homology for the region of interest. In the second round of recombineering, either an oligonucleotide to remove the region of interest, or a tag containing the arms of homology (mCherry, GFP etc.) was used. The aliquot of bacteria + DNA was added to a 2mm electroporation cuvette (Geneflow E6-0060) and electroporated with a BioRad MicroPulser, program EC3.

Transformed bacteria were recovered for 1-3 hours (depending on recombineering round) in LB broth before spreading on selective LB agar plates.

2.8.5.4 Positive and Negative Selection of Transformants

Bacteria transformed with the RPSL cassette were spread on LB agar plates containing 80 μ g/ml X-GAL and 200 μ M IPTG for blue/white selection of lacZ-containing colonies, where positive colonies appeared blue. The plates also contained 12.5 μ g/ml Chloramphenicol and either 15 μ g/ml Kanamycin or 50 μ g/ml Ampicillin, to ensure only bacteria transformed with a BAC containing the RPSL cassette grew.

Bacteria transformed in the second round of recombineering were spread on LB agar plates with X-GAL, IPTG, Chloramphenicol and 1200 μ g/ml Streptomycin to ensure that any bacteria still containing the RPSL cassette had limited growth – positive (RPSL-) colonies appeared white.

2.8.6 En Passant Mutagenesis

En Passant mutagenesis of BAC-derived viruses has previously been described by Tischer et al¹⁷⁵, using the GS1783 strain of *E. coli*.

2.8.6.1 Selection Cassettes

The *En Passant* cassette contains an *I-SceI* restriction site and kanamycin resistance gene for both positive and negative selection of colonies during the first and second rounds. During the first round, kanamycin resistant colonies are positive, in the second round kanamycin sensitive colonies are positive.

2.8.6.2 Transformation of GS1783 Bacteria with a BAC

“Empty” GS1783 bacteria were grown overnight in LB broth in a shaking incubator at 32°C. As in 2.8.5.2, the bacteria were grown to competency, centrifuged and washed, and then electroporated with the desired BAC DNA (2.8.7, 2.8.11). Selection for transformed GS1783 bacteria involved streaking for single colonies on LB agar

containing 30 μ g/ml Chloramphenicol. Minipreparation of the BAC DNA allowed confirmation of transformation using restriction digest, standard PCR and sequencing.

2.8.6.3 Preparation of Competent Bacteria

GS1783 bacteria containing the required HCMV BAC were grown overnight in LB broth plus 30 μ g/ml Chloramphenicol at 32°C in a shaking incubator. During the first round, the bacteria were grown to competency and induced as previously described in 2.8.5.2.

2.8.6.4 Transformation of Competent Bacteria

Following induction of the lambda red proteins, the culture was placed in an ice bath for 20 minutes. The bacteria were centrifuged and washed twice with ice-cold 10% glycerol. The pellet was resuspended in the leftover 10% glycerol after pouring off the supernatant. A small aliquot of bacteria was transformed using the *En Passant* cassette containing arms of homology for the region of interest; where a gene/tag was being inserted, the bacteria were transformed with the gene/tag containing the *En Passant* cassette and arms of homology. The bacteria + DNA were electroporated as before (2.8.5.3) and recovered for 1 hour before being spread on a LB agar plate containing 30 μ g/ml chloramphenicol and 30 μ g/ml kanamycin.

2.8.6.5 Resolution of Co-Integrates

Transformed bacteria were grown overnight in LB broth plus 30 μ g/ml Chloramphenicol at 32°C in a shaking incubator. The bacteria were inoculated into 1ml LB plus 30 μ g/ml chloramphenicol and placed in a shaking incubator at 32°C for 2 hours. LB broth plus chloramphenicol and 2% L-arabinose was then added, the bacteria were incubated for another hour before being placed into a 42°C water bath for 30 minutes. The culture was returned to the 32°C shaking incubator for a further 2 hours. The OD₆₀₀ of the culture was measured, and the bacteria diluted and spread on a LB agar plate containing 30 μ g/ml chloramphenicol and 1% L-arabinose.

2.8.6.6 Positive and Negative Selection of Transformants

LB agar plates plus chloramphenicol and kanamycin were used for positive selection of *I-SceI*-containing *E. coli* following the first round of *En Passant* mutagenesis – these colonies were taken forward to the second round. After the second round, colonies that had grown on the chloramphenicol and L-arabinose plates were checked for kanamycin sensitivity; this was done by picking a colony and spreading it on one LB agar plate containing chloramphenicol, and another containing kanamycin. Only kanamycin sensitive colonies were sequenced (2.8.9).

2.8.7 Minipreparation of BAC DNA

A universal containing 5ml LB broth plus chloramphenicol (and other antibiotic if necessary) was inoculated with either a loop scrape from a glycerol stock (2.9.9) or a colony picked from a LB agar plate (2.8.3, 2.8.5, 2.8.6), and incubated overnight in a shaking incubator at 32°C. A 500µl aliquot of the inoculated colony was stored at 4°C, the rest of the culture was centrifuged at 4000rpm for 5 minutes at 4°C and the BAC DNA extracted using QIAprep Spin Mini Prep kit (Qiagen 27106). Minipreparations of BAC DNA were stored at 4°C.

2.8.8 Restriction Digest

A restriction digest was used as a preliminary check of BAC DNA from 2.8.7, 8µl of BAC DNA was incubated with HinDIII (NEB R0104L) and 2.1 Buffer (NEB B7202S) for one hour at 37°C. The digests were then stained with DNA loading buffer and run on an electrophoresis gel alongside HighRanger Plus ladder (NORGEN 12000), to check the banding pattern.

2.8.9 Sequencing

If the banding pattern of the restriction digest appeared normal, the BAC DNA was used as a template for a standard PCR (2.6.1), using sequencing primers that bind outside of the region of interest. The PCR products were stained with DNA loading buffer and run on an electrophoresis gel, as with the restriction digests. The DNA ladder was used to check the size of the PCR product – if this was correct, the next

steps depended on whether the DNA came from a first or second round recombineering colony. If the colony was from the first round, a glycerol stock was made of the corresponding aliquot from 2.8.7. If the colony was from the second round, the PCR product was either solution or gel purified (depending on the presence of non-specific bands) as described in 2.8.2, and sequenced by Eurofins using the Eurofins Mix2Seq overnight kit and the sequencing primers.

Sequencing of BAC DNA was checked using CLC Main Workbench 8.1, where returned sequences were assembled to the predicted sequence – glycerol stocks were made of correct clones and the BAC DNA extracted on a larger scale (2.8.11).

2.8.10 Generation of Glycerol Stocks

Once a colony had been checked and confirmed by sequencing, it was then given a laboratory designation – “pAL” number – and a glycerol stock was created. Glycerol was mixed with the aliquot from 2.8.7 (15%:85%) and stored at -80°C.

2.8.11 Maxipreparation BAC DNA

Maxipreparation of BAC DNA similar to minipreparation, where BAC DNA is extracted from *E. coli* and purified, but on a much larger scale. A universal containing 5ml LB broth plus chloramphenicol was inoculated with the required BAC in the morning, allowed to grow throughout the day, and then added to a 1L conical flask containing 250ml LB broth plus chloramphenicol. The culture was incubated overnight at 32°C in a shaking incubator.

The following day, the culture was harvested by centrifuging in a 250ml pot for 15 minutes at 15,000rpm at 4°C. NucleoBond Xtra Maxi kit (Machery Nagel 12748412) was used for the maxipreparation according to manufacturer’s instructions. The BAC DNA was then quantified using the NanoDrop and could be transfected into fibroblasts (2.2.1.1). Maxipreparations of BAC DNA were stored at -20°C.

2.9 Statistical Analysis

GraphPad Prism 8 software (GraphPad Software, Inc., CA, USA) was used for all statistical analyses. Data sets with multiple samples were analysed by either one-way ANOVA or two-way ANOVA tests with Tukey's post-hoc analysis. All data was plotted as mean \pm standard deviation (SD) unless otherwise stated. Differences were considered and displayed as significant in figures and tables as follows; * $p < 0.05$; ** $p < 0.01$; *** $p < 0.001$ and **** $p < 0.0001$.

2.10 Primer Sequences

<i>Purpose</i>	<i>Primer</i>	<i>Sequence</i>
<i>Tag gB with mCherry</i>	Insert rpsl after gB (forward)	CCCAACCTACTAGACCGACTGCGACATCGCAAAAACGGCTACCGACAC TTGAAAGACTCTGACGAAGAAGAGAACGTCCCTGTGACGGAAGATCAC TTCG
	Insert rpsl after gB (reverse)	ATATCCAGTTAACCCGTATATCACAAGTCTGTGTCACTTTTTTT GTCTGTTTTTTCTCCTGGTTCACTGAGGTTCTATGGCTCTG
	Replace rpsl with mCherry (forward)	AGAAGCCAACCTACTAGACCGACTGCGACATCGCAAAAACGGCTACC GACACTGAAAGACTCTGACGAAGAAGAGAACGTGGCTCTGGTGGAA GCGG
	Replace rpsl with mCherry (reverse)	AGATATCCAGTTAACCCGTATATCACAAGTCTGTGTCACTTTTT TTGTCTGTTTTTTCTCCTGGTTCAATTACTGTACAGCTCGTCC
	Sequence gB (forward)	GATGCTTCTGGCCCTGG
	Sequence gB (reverse)	GCCGCCGCTCAGATAC
	Insert rpsl after gH (forward)	CGTCTCCTCATGATGTCCGTCTACGCGCTATCGGCCATCATGGCATA TCTGCTCTACCGCATGCTCAAGACATGCCGTGACGGAAGATCACTC G
	Insert rpsl after gH (reverse)	GTACCGTTTAGAAGGTTTGTGCGAATGTCTTAACCTCTGTCCCTT TTTCATAAAACTGTCAGGTCTACAATCACTGAGGTTCTATGGCTCTG
	Replace rpsl with mCherry (forward)	AGTCGTCTCCTCATGATGTCCGTCTACGCGCTATCGGCCATCATGGC ATCTATGCTCTACCGCATGCTCAAGACATGCGGCTCTGGTGGAAAGCG GA
	Replace rpsl with mCherry (reverse)	GGCCCGTACCGTTTAGAAGGTTTGTGCGAATGTCTTAACCTCTGT CCCTTTTCATAAAACTGTCAGGTCTACAATCACTGTACAGCTCGTCC
<i>Tag gH with mCherry</i>	Sequence gH (forward)	AAGTGGTGGTCTCATCTCCG
	Sequence gH (reverse)	ACCTCACGCATATAGTATCATCA

<i>Tag UL36 with P2A-BFP</i>	Insert I-SceI into BFP (forward)	CCACACAGGATACAAGTCTGCAGGACGGCTGCCTGATCTACAAACGTGA AGATCCGGGGCGTGAACTTCACTAGGGATAACAGGGTAATGGCCTGGT GATG
	Insert I-SceI into BFP (reverse)	GCATCACGGGGCCGTTGCTGGTGAAGTTCACGCCCGGATCTTCACGTT GTAGATCAGGCAGCCGTCCGTCAAGAAGAACCTCGTCAAGAAGGCGATA GAA
	Sequence BFP (forward)	ACCTTCATCAATCACACCC
	Sequence BFP (reverse)	CCATATCGTTCTGCCTTCC
	Insert P2A-BFP plus I-SceI after UL36 (forward)	ACGTCGGTCGACGGCA
	Insert P2A-BFP plus I-SceI after UL36 (reverse)	GGTTATATAAAAATGCTGTGTTA
<i>Remove RL1-RL6</i>	Sequence UL36 (forward)	CTTTATTGACCAGCGGAGTACA
	Sequence UL36 (reverse)	CACTTGAACTCTTACCGCT
	Replace RL1-RL6 with rpsl (forward)	CCCGATGGAAAACCGTCTTCTATCATCAACTGTGGTAAGATTCGACCC TGCAG GGT ATT CAG TTT CCT CAT ATC CAT CCT GTG ACG GAA GAT CAC TTC G
	Replace RL1-RL6 with rpsl (reverse)	CGGTCCAGTCACATTTTGGTGGGTGGGGGTACTAAAAAGTATTAA ATATT GGG GTT TAA TGA TAA AAT CCA GGT TCT GAG GTT CTT ATG GCT CTT G
	Sequence RL1-RL6 (forward)	ATGGCGAGCTGTTGCGT
	Sequence RL1-RL6 (reverse)	GTG GCT GGT ACA TAA GCT GG
<i>Remove RL10-UL1</i>	Oligo to remove rpsl	GCTCGCCTATTAACCTCCACCCACTACAAACACACACATGCCGCACAAT CAGCT AGG CAC GCT ATA AGT ACC CCC CCC CCA CAA TGG AAT GTT GCC AAA C
	Replace RL10-UL1 with rpsl (forward)	CAGGACGCTGAACAGCTGCGGACGGACCTGGATACGGAACCTCTGTTG TTGACG GTG GAC GGA GAT TTG GAA TAA AAG CCT GTG ACG GAA GAT CAC TTC G

	Replace RL10-UL1 with rpsl (reverse)	ATACAATGTAGAAGGTCAGGATTATATACCGTTGTCGATACGTGAA GTTGT TGC GTT TTT GAC GGT CAA CAC GCA TCT GAG GTT CTT ATG GCT CTT G
	Sequence RL10-UL1 (forward)	GCGCGAAAAGACAGGGAGA
	Sequence RL10-UL1 (reverse)	ACG GAG TAG GAA TAC AAT GAC G
	Oligo to remove rpsl	GTGCGGGAAAGGATTGACGTGTGCGGTGCTGTGGAACACGGTGTAA TTCACAAAGTACCAACGCTAATTATTAGGGTACATTGTACTACTTG T
Remove UL2-UL11	Replace UL2-UL11 with rpsl (forward)	TCTATGATAACGTAATTCAAATAAAGTACAGGTTCTAGTGACATGTTA TCATA AAA CAT AGA TTT TTC TAC GTG TTT CCT GTG ACG GAA GAT CAC TTC G
	Replace UL2-UL11 with rpsl (reverse)	ACTGTTAGGGGTGGTGGATTGGACTGGGTGTTATGATGGTA GTGCT TAT CGT CGT CTT CTT GGC GGT GGT GCT GAG GTT CTT ATG GCT CTT G
	Sequence UL2-UL11 (forward)	TAT TTG CAT CAT GTG CCT CAT
	Sequence UL2-UL11 (reverse)	GGAGTTGGCGTTCACAG
	Oligo to remove rpsl	CAGGTTCTAGTGACATGTTATCATAAACATAGATTTCTACGTGTT CACC ACC GCC AAG AAG ACG ACG ATA AGC ACT ACC CAT CAT AAA CAC CCC A
Remove UL13- UL20	Replace UL13-UL20 with rpsl (forward)	ATCCAAGGGGGCTTCCAAAGCCGACGTCCCTGATTCCCTCATAAAGC TGGTGTGCTCAAGTTCAAGTGTAGATTATGGAAAATATGTAGTCGT CAC TTC G
	Replace UL13-UL20 with rpsl (reverse)	TATCTTGTGCTCAAGTTCAAGTGTAGATTATGGAAAATATGTAGTCGT ACCG CTT GGG GCT CAG AGT CCA AAG TTC GCT GAG GTT CTT ATG GCT CTT G
	Sequence UL13-UL20 (forward)	GCG TAG GAA ATG ATT GCA TGA
	Sequence UL13-UL20 (reverse)	TACCCGGTTTGCTCCCT

	Oligo to remove rpsl	CCCTGATTCCCTTCATAAAGCTGTTGACCGGCCCTAGAAAGACCAAGAG CCGAA CTT TGG ACT CTG AGC CCC AAG CGG TAC GAA CTA CAT ATT TTC CAT A
Remove UL22A-UL25	Replace UL22A-UL25 with rpsl (forward)	CGAGATGTCGTCACCCAAGGTATTAACGGCACACAGCCAGACCGCTTC GTCAG CAG CGA CGC CGA CAA GAC CTC AGC CCT GTG ACG GAA GAT CAC TTC G
	Replace UL22A-UL25 with rpsl (reverse)	ACATAAAAAAAAACACACATACTTCCTGTGACTTCTATCATAA ACTGT TCC GCC CTG CTG TTT CGT CCC ACC ACT GAG GTT CTT ATG GCT CTT G
	Sequence UL22A-UL25 (forward)	GCG ACG GTG ACA GTG GAT
	Sequence UL22A-UL25 (reverse)	CGGAGAACAGAGGACGA
	Oligo to remove rpsl	GGCACACAGCCAGACCGCTTCGTCAGCAGCGACGCCACAAGACCTCA GCTGGT GGG ACG AAA CAG CAG GGC GGA ACA GTT TAT GAT AGA AAG TCA CAG G
Remove UL139-UL150	Replace UL139-UL150 with I-SCeI (forward)	TGACGTCTCAGGCTTCCGAAACCGCGTCAAGTTCAACGTTGGTTTCGG TTTAGCCTGCGAGCTGTATGCAGCGTTGCGTTAGGGATAACAGGGTAAT CG
	Replace UL139-UL150 with I-SCeI (reverse)	CCGCTACTCTTATTAACGTCTTCATCCCCCGCTTCTACACGCAACGCT GCATACAGCTCGCAGGCTAAACCGAAACCAGCCAGTGTACAACCAAT TA
	Sequence UL139-UL150 (forward)	GGTGGTAGTGCCGTTAGT
	Sequence UL139-UL150 (reverse)	TGTTTCTGCGGTGTTGT
	Replace UL148-UL140 with I-SCeI (forward)	ATAGCGCGGTGACGTACGCCGGGGCTTAGAATCTCCACCTGTAAGG CGACAAGTCTGAAGAGATGAGTAGGGATAACAGGGTAATCGATTATT CAA

	Replace UL148-UL140 with I-SCeI (reverse)	CCTCAACTGTTCTGATGAGCACCCGCCTCATCTCTCAGACTTGTC GCCTTACAGGTGGAGATTCTGCCAGTGTACAACCAATTAAACCAATTCT G
	Sequence UL148-UL140 (forward)	TGGCGACGTGGATTCTT
	Sequence UL148-UL140 (reverse)	AACTTGACGCGGTTTCGG
Remove US1-US11	Replace US1-US11 with rpsl (forward)	ACCTCCGCGGCCGAAAAAAATGTCAAACACACGCCCTACCACGTTCAT CATTGAAAGTCTCTCCAGTCCCTATGTTGCCTGTGACGGAAGATCACTT CG
	Replace US1-US11 with rpsl (reverse)	CGTGCAAGACTACATGCTATAAGATAGCCTTACAGCTTGAGTCTAGA CAGGGGAACAGCCTCCCTGTAAGACAGACTGAGGTTCTATGGCTCT TG
	Sequence US1-US11 (forward)	GGCCCATCTCTCGCAAAA
	Sequence US1-US11 (reverse)	CATCTGGTATCCAAACTACGCC
	Oligo to remove rpsl	CACGCCCTCACCACGTTCATCATTGAAAGTCTCTCCAGTCCCTATGTTG TCTGTCTTACAAGGGAAAGGCTGTTCCCTGTCTAGACTCAAAAGCTGTA A
Remove US12-US17	Replace US12-US17 with rpsl (forward)	AGCAGCATAGCGGTGCGCAGCAGGTCGCCGTCCGTAGCAATTGAC GGTGAG CGA TAA AGC ACC GTT AAT GTG TCG CCT GTG ACG GAA GAT CAC TTC G
	Replace US12-US17 with rpsl (reverse)	ACGCCGTGTGGGAATGACGGTGATTATATTACACTCTATAAACGGTTCT CATAC GCG CCT TTT GAT AGC CAC CGC CGT CCT GAG GTT CTT ATG GCT CTT G
	Sequence US12-US17 (forward)	GGA CAG TAC GAC AGA TTA GGT GAT AG
	Sequence US12-US17 (reverse)	AGACAGACAGAACACCGCA
	Oligo to remove rpsl	CGTCCGTGTAGCAATTGACGGTGAGCGATAAAGCACCGTTAATGTGTC GGACG GCG GTG GCT ATC AAA AGG CGC GTA TGA GAA CCG TTT ATA GAG TGT A

Remove US16 ¹⁴⁸	Replace US16 with I-SceI (forward)	CGTGGCATAAGAACGTGACGGACGAAAAGGACCTGCTGCGAAAAGTGG CCGGCGAAGATAGACAGCCGGAGGCTATGATAGGGATAACAGGGTA ATCG
	Replace US16 with I-SceI (reverse)	CTAAAAGTCCCCCACGGATCTCGCGTCTAGACGCGCGGTATATAGC CTCCGGCTGTCTATCTTCGCCGGCCACTTTGCCAGTGTACAAACCAATT A
	Sequence US16 (forward)	TCTGGAAACGGCTGCTCT
	Sequence US16 (reverse)	GGCCGCCAAACATCTAAA
	Replace US18 with rpsl (forward)	GGGAGGTTCATCGTCTGTCTAGAGGGAAAGGTGGGAACGTCTAACG GAGCGGGAGCGTGTCACTCCCCCATCTTCCTGTGACGGAAGATCACT TCG
	Replace US18 with rpsl (reverse)	CGGCCACGTCTGGGTGCAGCAGTACGCCGAGAAACACGGCGGACGCAT CGACGGCGTGAGTCTCCTCAGCTTGTAACTGAGGTTCTTATGGCTCT TG
	Sequence US18 (forward)	AGAGTGTAAATATAATCACCG
Remove US18 ¹⁴⁸	Sequence US18 (reverse)	CTCTATGTCGAAAATGTGGC
	Oligo to remove rpsl	AAGGTGGGAACGTCTAACCGAGCGAGCGGGAGCGTGTCACTCCCCATCTT TGCTGCCGCTTACGACCCTGTGCGGTCTAAGGTAGGCGTCATGAAACA GT
	Replace US18-US22 with rpsl (forward)	CCATACGGTGAACCTTTGAACCACTCGAGAGCCTCCATGCGGGAGAGC AGCAG CGC GTT AGC CTC CTG CGC CTG CAT CCT GTG ACG GAA GAT CAC TTC G
	Replace US18-US22 with rpsl (reverse)	ACCGTGCCCCACTCGCTCGCTTGTATAAGAGAAGGGTAGGTGCGCCG CAGCG GCT TTG TGC CGA GAC CGT CGC CAC CCT GAG GTT CTT ATG GCT CTT G
	Sequence US18-US22 (forward)	AGA CTC ACG CCG TCG ATG C
	Sequence US18-US22 (reverse)	CGGAGTGGGTCAAGAGTT

	Oligo to remove rpsl	CGCTGTTTAGACAACGTTCCACGCTGGTAGATGAGATCCAGGGTCTC GGCCG GCA AAG CCG TCT CGA CAG CGA GTC GGA TAA AGC GCG CTG CGC GAA A
Remove US20 ¹⁴⁸	Replace US20 with rpsl (forward)	ACGGTCCATTCTAGCGGGACGACATGAAGCATGGCGACAAGCGCGGCT GCTGTAAAACGGCGCGGTTTATAGGCACCTGTGACGGAAGATCACT TCG
	Replace US20 with rpsl (reverse)	CCGTTGGATTAGTCTTCGGACGGCGCGCCTTGGACAACGGGACTTG ACAGCCGCCAGTACGACGGGAAGTCCTAACTGAGGTTCTTATGGCTCT TG
	Sequence US20 (forward)	CATTCTAGCGGGACGACA
	Sequence US20 (reverse)	CCCCAGTCGTCTCCTAACATC
	Oligo to remove rpsl	GCATGGCGACAAGCGCGCTGCTGTGAAAACGGCGCGGTTTATAGG CAGGTGGCGACGGTCTCGGCACAAAGCCGCTGCGCGCACCTACCCTC TCT
Remove US27- US28	Replace US27-US28 with rpsl (forward)	AGGAACCTGGGTGCTTAGACAACTAACGTGTAATGCTTTTACAGGACC GTTCA ACA GGT GAT ACT ACC TGC AAG GTA CCT GTG ACG GAA GAT CAC TTC G
	Replace US27-US28 with rpsl (reverse)	ATGGTGCTCGCCGAATTGTTAATTAGGATCCATAACTCGTATAATG TATGCTATACGAAGTTATAGCGCTTTTACTGAGGTTCTTATGGCTCT G
	Sequence US27-US28 (forward)	GTT GGC AGC TCC GGT CTG
	Sequence US27-US28 (reverse)	CCACACCCTAACTGACAC
	Oligo to remove rpsl	TGTAATGCTTTTACAGGACC GTCAACAGGTGATACTACCTGCAAGGT ATAAAAAAAGCGCTATAACTCGTATAGCATACATTATACGAAGTTATGG AT
Remove US29- US34A	Replace US29-US34A with rpsl (forward)	CACGACCATTCCGTGCATTAGCGAACCGGAAAAGTTATGGGGAAA AAGACGTAGGAAAGGATCATGTAGAAAAACCTGTGACGGAAGATCAC TTCG

<i>Insert 2.18 IgG chains into vector</i>	Replace US29-US34A with rpsl (reverse)	TTAGTCACACATCGGCATCTTGTCAATAAGACGCACGCCGCCGTGACC CATAC CGC AGC TCG GAC CCA CCG CCC CAA GCT GAG GTT CTT ATG GCT CTT G
	Sequence US29-US34A (forward)	CTATGACCATGATTACGCCAAG
	Sequence US29-US34A (reverse)	TTCATCCCCACATCCAC
	Oligo to remove rpsl	CGGAAAAGTTATGGGGAAAAAGACGTAGGAAAGGATCATGTAGAAAA ACCTTGGGGCGGTGGTCCGAGCTGCGGTATGGGTACGGCACGGCGGTGC GTCT
	Insert 2.18 heavy chain (forward)	ATCCTTTCTAGTAGCAACTGCAACCGGTGTACATTCTGAGGTGCAGC TGGTGAA
	Insert 2.18 heavy chain (reverse)	GGAAGACCGATGGGCCTTGGTCGACGCAGATGACACGGTGACCATG
	Insert 2.18 light chain (forward)	ATCCTTTCTAGTAGCAACTGCAACCGGTGTACATTCTGACATCCAGAT GACCCAGTC
	Insert 2.18 light chain (reverse)	AAGACAGATGGTGCAGCCACCGTACGTTGATYTCCACCTGGTC
	Sequence IgG chain	GCTTCGTTAGAACGCGGCTAC
	Insert 70.7 heavy chain (forward)	GGGAAACACGGAAGGAGCCTGGGCTGGCGCTTGATATAGTGACCAG GG
<i>Insert 70.7 IgG chains into vector</i>	Insert 70.7 heavy chain (reverse)	TGTTCTTCTGTCCGTGACCACAGGCGTCCACAGCCAAGCGTAGAAGA GTCGCG
	Insert 70.7 light chain (forward)	CTCGTGCTCACCCCTCAAGGGAGTCCAGTGCACGAGATATGACTCAGA C
	Insert 70.7 light chain (reverse)	GATCAGCACGGTGGGGGCCACAGGGCCCTTTTACCAACACCTCGGTG C
	Sequence 70.7 heavy chain	ATGGAGTGGTCTGGGTGTT
	Sequence 70.7 light chain	TGAACCTCGGACTGCGCCTG

Table 2.19 – Primer sequences used for recombineering, En Passant and antibody cloning in this project.

Chapter 3.

Mechanisms of

Cell-Cell

Transmission of

the Merlin Strain

One of the many challenges for HCMV research is that the virus mutates rapidly in the lab, becoming phenotypically different to clinical strains. For example, lab-adapted strains that have been heavily passaged in fibroblasts (HFFFs) possess mutations in the UL128L and RL13 gene, therefore disseminating predominantly via the cell-free method in vitro, and are also unable to infect epithelial, endothelial and myeloid cells^{113, 118, 176}.

The Merlin strain has had its genome repaired so that it mimics clinical HCMV strains, and not only infects almost exclusively by direct cell-cell contact, but is also able to infect a wider range of clinically relevant cell types¹⁰². It has been shown that cell-cell transfer of Merlin is >1,750-fold more efficient than cell-free infection, as well as being more resistant to innate and intrinsic antiviral mechanisms, and to neutralizing antibodies^{121, 122, 177}. However, the mechanism of cell-cell transfer is unknown.

The mechanisms of cell-cell transfer in other viruses, such as HIV^{178, 179} and HTLV-1¹²³ have been well documented, and are the basis for several theories for HCMV. One mechanism in particular, is the virological synapse – this is a cellular junction formed between an uninfected and infected cell, similar to an immunological synapse. Here, the virus is safely transferred in a protective niche without exposure to elements of the immune system.

Another theory of HCMV cell-cell transfer was published by Gerna et al¹⁸⁰. This suggests that microfusions form in the membranes of adjacent cells, allowing the virions (usually non-enveloped) to pass through into uninfected cells. The laboratory strains used in this study have large deletions in the genome, and so this theory needs to be tested using the wildtype strain Merlin.

We therefore aimed to visualise cell-cell transfer directly by using fluorescently tagged Merlin, using long-term imaging to track both entry and egress of HCMV in HFFFs, and potentially to see plaque formation. To complement live cell imaging, we aimed to determine the method HCMV uses to infect neighbouring cells by using both electron microscopy and soft x-ray tomography, and to quantify the effect of potent neutralising antibodies on the delivery of HCMV genomes following cell-cell and cell-free infection.

3.1 Visualising Cell-Cell Transfer

3.1.1 The Generation of Fluorescent Viruses

To enable the visualisation of cell-cell transfer of Merlin, recombineering was used to generate viruses in which the virion was directly tagged with multiple fluorescent proteins. Previously, using passaged HCMV strains, the inner tegument protein UL32 has been fused to eGFP, permitting tracking of individual virions¹⁸¹. This work has been extended by also tagging the envelope protein gM with mCherry¹⁸². Combining the two generated a virus in which fusion of the virion envelope could be visualised, as loss of the mCherry signal, but retention of the eGFP signal. We applied the same technology to Merlin, while also adding a BFP tag linked to UL36 with a P2A self-cleaving peptide. The BFP does not become a component of the virion, but provides an IE-expressed marker of infection.

3.1.1.1 *UL32-GFP/UL36-P2A-BFP/gM-(linker)mCherry*

The UL32-GFP/UL36-P2A-BFP/gM-(linker)mCherry genome (pAL2479) had been generated by an undergraduate student before the start of this project (based on the work of Sampaio et al.^{181, 182}). Following maxiprep of the BAC DNA, HFFFs were transfected. At 5 weeks post-transfection, supernatant was used to infect fresh HFFFs cell-free (MOI unknown). These cells were imaged 72 hours later (Figure 3.1). Clear problems were evident with this virus. It grew extremely poorly, failing to reach 100% infection of a T25 flask even after 5 weeks. Furthermore, although the gM-(linker)mCherry localised to the expected site of the assembly compartment, unlike UL32-eGFP, it was also unexpectedly found in large punctate structures throughout the cytoplasm. Given these two observations, it seemed likely that the mCherry tag affected the function of gM, as viruses tagged with UL32-GFP or UL36-P2A-GFP/mCherry individually show no growth issues. Thus this virus was abandoned and other potential glycoprotein-fluorescent fusions investigated.

<i>Linker Amino Acid Sequence</i>
<i>For mCherry Gly Ser Gly Gly Ser Gly Gly Ser Gly</i>

Table 3.1 – Amino acid sequence for the linker used to tag genes with mCherry.

pAL2479

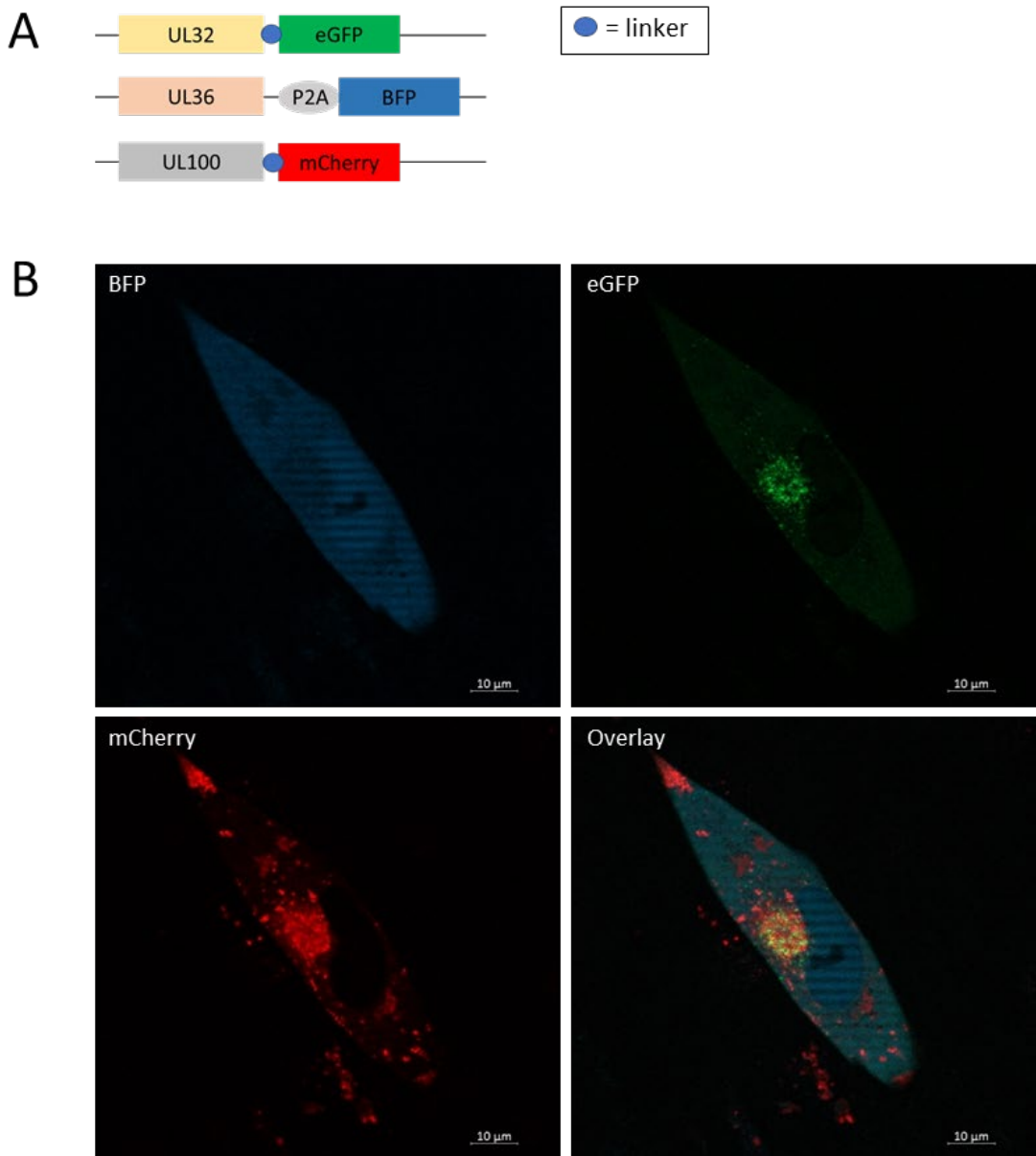


Figure 3.1 – UL32-GFP/UL36-P2A-BFP/gM-(linker)mCherry virus. A) Schematic of pAL2479 construct. UL100 = gM. B) HFFF were infected with the supernatant from pAL2479-infected fibroblasts (MOI unknown), 72hrs post-infection the cells were imaged using a Zeiss microscope (Axio Observer Z1 with a XL Multi SI Incubator) and APOTOME. Panels show fluorescence of individual markers and an overlay of all three. Scale bar = 10μm.

3.1.1.2 UL32-GFP, gB-mCherry and UL32-GFP, gH-mCherry

Given that individually tagging the tegument (UL32) and tagging UL36 as a marker of infection, has worked previously with Merlin, we investigated alternative ways to tag the virion envelope. Previous work with Herpes Simplex Virus (HSV) has

successfully tagged the C-terminus of gB, gD and gH envelope proteins with enhanced yellow fluorescent protein (EYFP)¹⁸³, seemingly without consequences. As there is homology between gB and gH glycoproteins found in HSV and HCMV, recombineering was used to tag these proteins with mCherry.

Transfection of UL32-GFP/gH-mCherry (pAL2566) and UL32-GFP/gB-mCherry (pAL2605) BAC DNA (Figure 3.2), showed serious problems. The gH-mCherry virus failed to successfully form plaques in the HFFF monolayer following transfection, which suggests that placing a tag on the C-terminus of this protein in HCMV has major effects on both cell-free and cell-cell infection. The gB-mCherry virus had both growth and localisation issues, similar to the gM-mCherry virus. Figure 3.3A shows one of the plaques that formed following transfection of HFFFs with BAC DNA – we expected to see both UL32 and gB localised to the virion assembly complex (indicated in Figure 3.3B), however, these proteins were also distributed throughout the cell in most cells within the plaque, which was unexpected. The cells were trypsinised and re-seeded once per week to encourage spread of the virus, however, the infected cells died before 100% CPE was reached, indicating some growth issues.

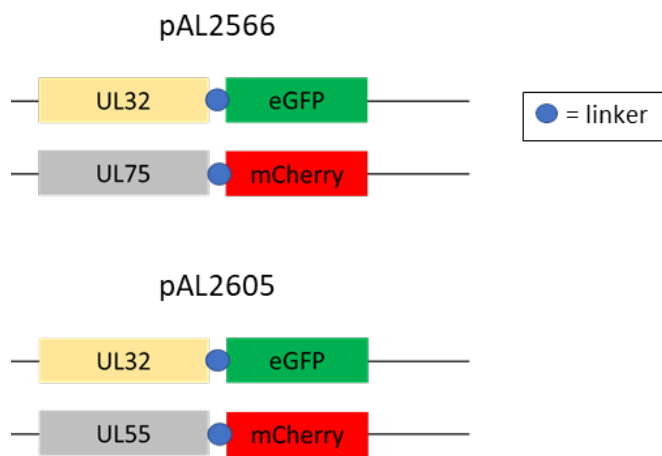


Figure 3.2 – Schematic of pAL2566 (top) and pAL2605 (bottom) constructs. UL75 = gH; UL55 = gB.

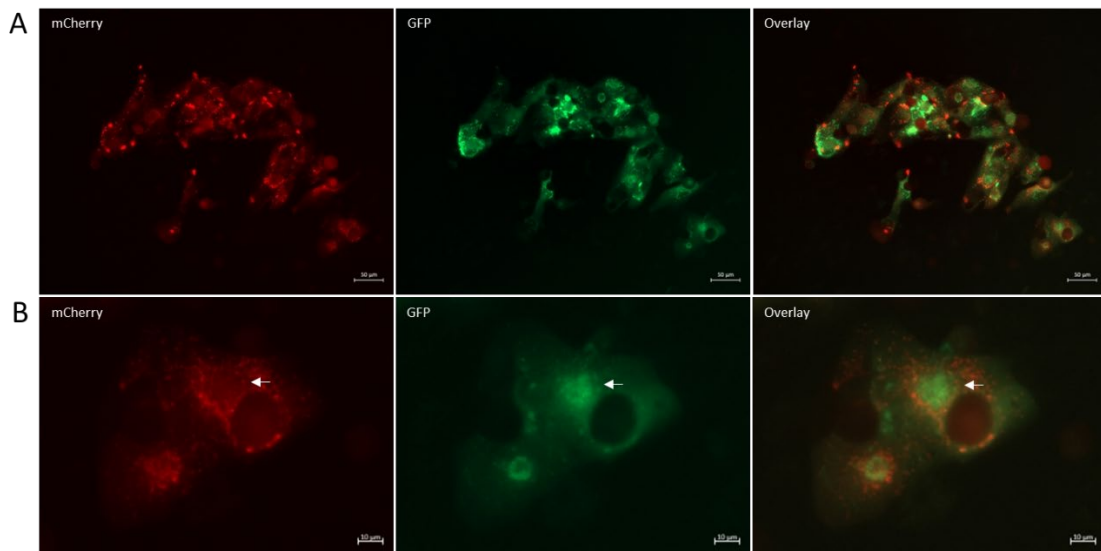


Figure 3.3– UL32-GFP/gB-mCherry virus in HFFFs imaged using a Zeiss microscope 19 days post-transfection. A) One of three plaques. Scale bar = 50µm. B) Two cells within the plaque, white arrow indicates the virion assembly complex. Scale bar = 10µm.

3.1.1.3 UL32-GFP/UL36-P2A-BFP/gM-mCherry-gM

As previous attempts at tagging HCMV envelope glycoproteins had been unsuccessful, the UL32-GFP/gM (external loop)-mCherry virus¹⁸² (pAL2624, Figure 3.4A), where mCherry is inserted after the first transmembrane loop of gM, was gifted by Dr. Christian Sinzger – his lab had found that this enabled successful recovery of a virus in which the envelope was fluorescently tagged, although it was noted that this virus experienced a 1-log reduction in titre. The BFP tag was inserted after UL36, using a P2A linker, using *En Passant* mutagenesis to generate UL32-GFP/UL36-P2A-BFP/gM-mCherry-gM (pAL2759) – see Figure 3.4B for construct.

This virus was successfully recovered in culture, however the titre obtained was very poor, leading to the conclusion that the presence of three fluorescent tags severely impacts the growth of HCMV, irrespective of where they are located.

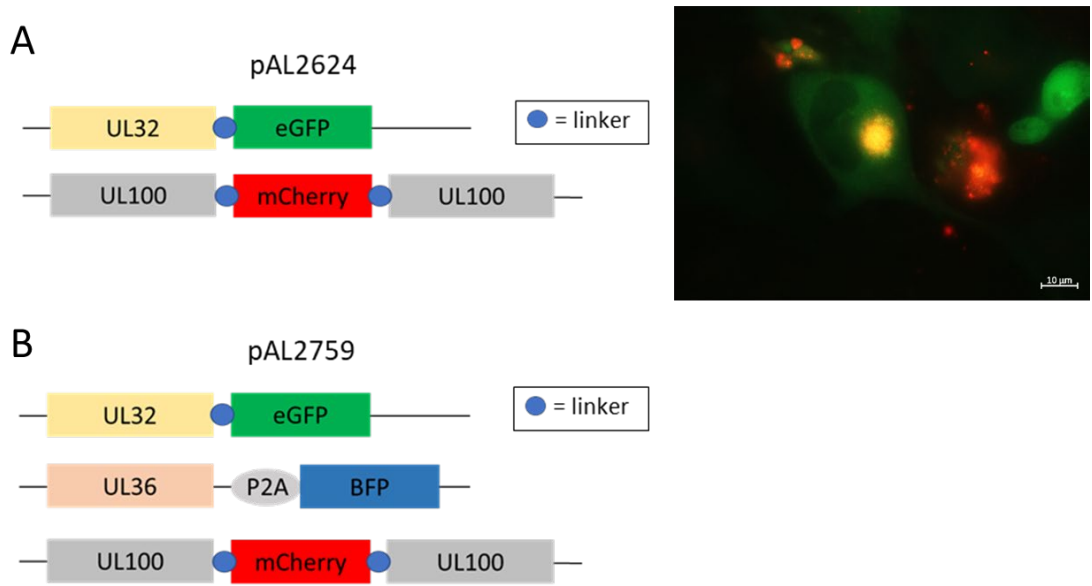


Figure 3.4 – UL32-GFP/UL36-P2A-BFP/gM-mCherry-gM virus. A) Schematic of pAL2624, and image of HFFF infected with pAL2624 taken with Zeiss microscope. B) Schematic of pAL2759 construct. Scale bar = 10 μ m.

3.1.2 Cell-Cell Transmission in Live Cells

3.1.2.1 Optimisation of Long-Term Fluorescence Microscopy

When imaging cells with fluorescence for long periods of time, care must be taken not to cause bleaching or phototoxicity to the cells. Therefore, troubleshooting of different settings on the Zeiss microscope was performed in order to minimise stress to the cells. As virus transfer could occur in any Z-plane, images were captured from multiple Z-planes – this in turn exposes the cells to more light and potentially results in more toxicity. Table 3.2 shows the combination of settings tried with fibroblasts infected with the UL32-GFP virus (pAL2422).

Most settings caused cell death to a certain extent – where the majority of infected cells in a plaque underwent apoptosis (Figure 3.5). Cell death could be reduced by reducing light power (and therefore intensity), but still occurred relatively quickly. Given that this was using a single coloured virus, the problem would likely be more acute with a virus containing multiple fluorescent tags. To determine whether the cells are generally sensitive, or whether infection makes them more sensitive to phototoxicity, imaging was performed using a Hoechst stain (10ng/ml) on HFFFs infected with UL32-GFP at MOI 0.02 to determine whether uninfected cells are equally susceptible to phototoxicity – the low MOI ensured that there was both

infected and uninfected cells to image in the well. Figure 3.6 shows that both infected and uninfected cells are susceptible to phototoxicity over a prolonged period, and as can be seen in Figure 3.6B, it was not a result of the Hoechst stain as only the imaged cells in the well died. It is possible that the more channels used during imaging increases the risk of phototoxicity to the cells.

As HFFFs appeared to be particularly sensitive to repeated exposure to fluorescent light, which was exacerbated by dual-fluorescence imaging, imaging was then attempted in RPE-1 cells.

Binning	Exposure (ms)	Power (%)	Frequency	No. of Images	Comments
3x3	10	100	30 mins	7	Out of focus
3x3	10	50	30 mins	30	Appears healthy
2x2	20	50	30 mins	30	Some apoptosis after 10hrs
1x1	30	50	30 mins	96	Apoptosis after 16hrs
1x1	40	25	30 mins	127	Apoptosis after 40hrs
1x1	50	15	30 mins	37	Bleaching after 4hrs

Table 3.2 – Settings used for optimisation of long-term fluorescence microscopy of HFFFs.

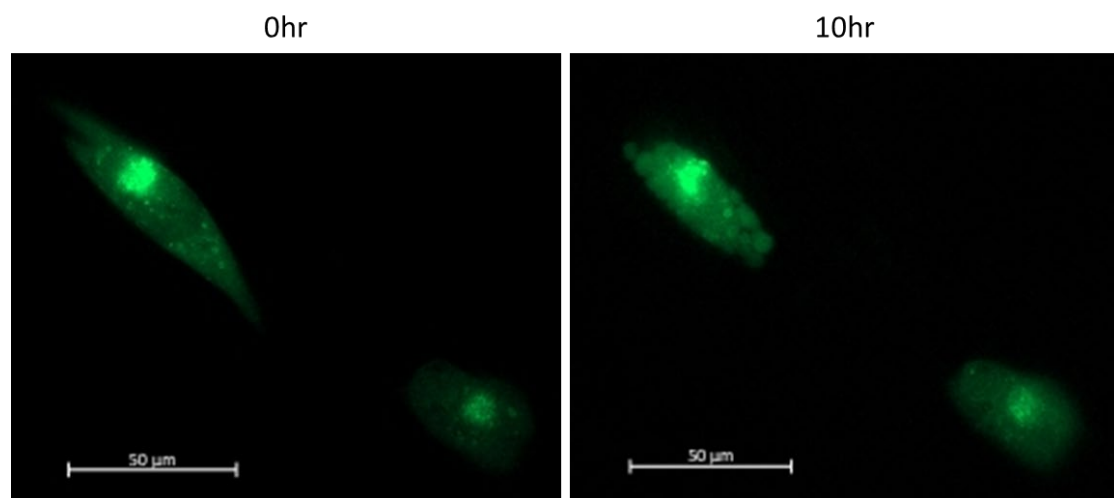


Figure 3.5 – HFFFs imaged using 2x2 binning, 20ms exposure, 50% power, every 30 mins. In the second image, taken 10 hours after the first, the cell on the left, which appeared healthy at 0hrs, can be seen breaking up into fragments, indicative of apoptosis, while the cell on the right remains intact. Scale bar = 50μm.

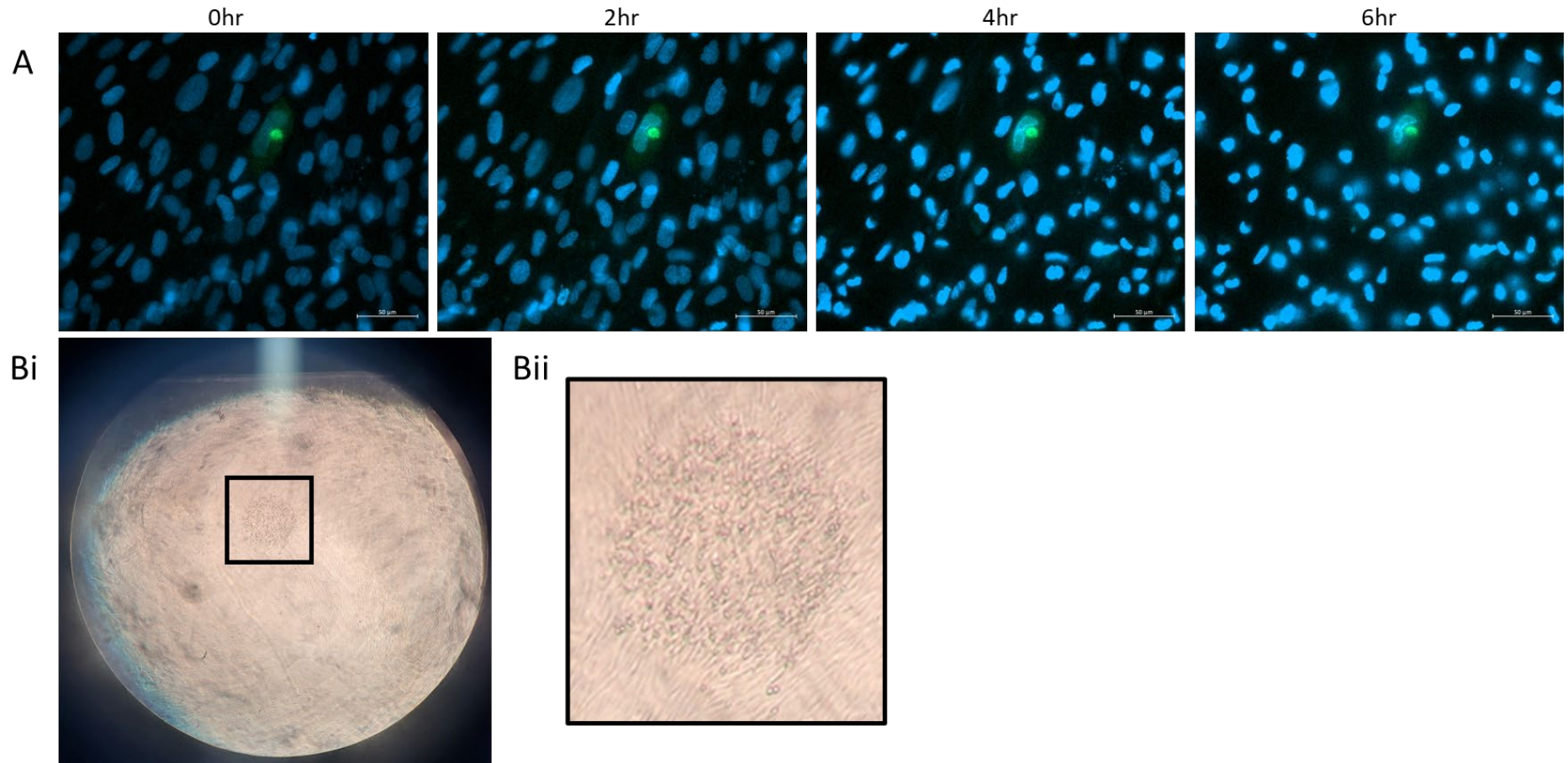


Figure 3.6 – HFFFs infected with UL32-GFP then stained with Hoescht (10ng/ml) and imaged using 1x1 binning, 30ms exposure, 25% power, every 30 minutes. A) Images that were taken at 0hr, 2hr, 4hr and 6hr time points selected. Scale bar = 50 μ m. B) Phase contrast image of the well after imaging. Bii) Higher magnification of the area highlighted by the black box in Bi.

3.1.2.2 Fluorescent Imaging in RPE-1s

To determine if fibroblasts have a particular sensitivity to phototoxicity, RPE-1 cells were imaged as a comparison. RPE-1 cells were co-cultured with UL32-GFP/gM-mCherry (pAL2624) infected HFFFs (1 HFFF:10 RPE-1s), and imaged every 30 minutes for 48 hours. In the time course shown in Figure 3.7, cell death is seen in the cells that have an assembly complex (they are in the late stage of infection), it is unclear whether viral lysis is killing these cells or if it was due to the phototoxicity, however, the white box indicates a cell that forms an assembly complex during imaging, which remains healthy at 48hrs. If the UL32-GFP/UL36-BFP/gM-mCherry virus had obtained a good titre, it would have been easy to establish what stage of infection the cell was in at the beginning of the time course – UL36-BFP would have indicated if the cell was already infected, and whether any cells surrounding the plaque became infected.

As the RPE-1 cells appeared to be less sensitive than the HFFFs to phototoxicity, these cells were used for long-term fluorescence microscopy. While imaging the infected RPE-1s, two other phenomena were noticed: virion movement can be observed in real time (Figure S.1), and some infected RPE-1s form membrane extensions which could be a method of transmission.

HTLV-1 has been known to form transient membrane extensions/cellular conduits to infect neighbouring cells, as reviewed by Pique and Jones¹²³. Figure 3.8 shows structures that are formed by RPE-1 following infection with UL32-GFP and UL32-GFP/gM-mCherry viruses, virion movement was observed in these extensions, but without the use of a UL36-tagged virus, it was not possible to determine whether these structures were a route of transmission within the scope of this project.

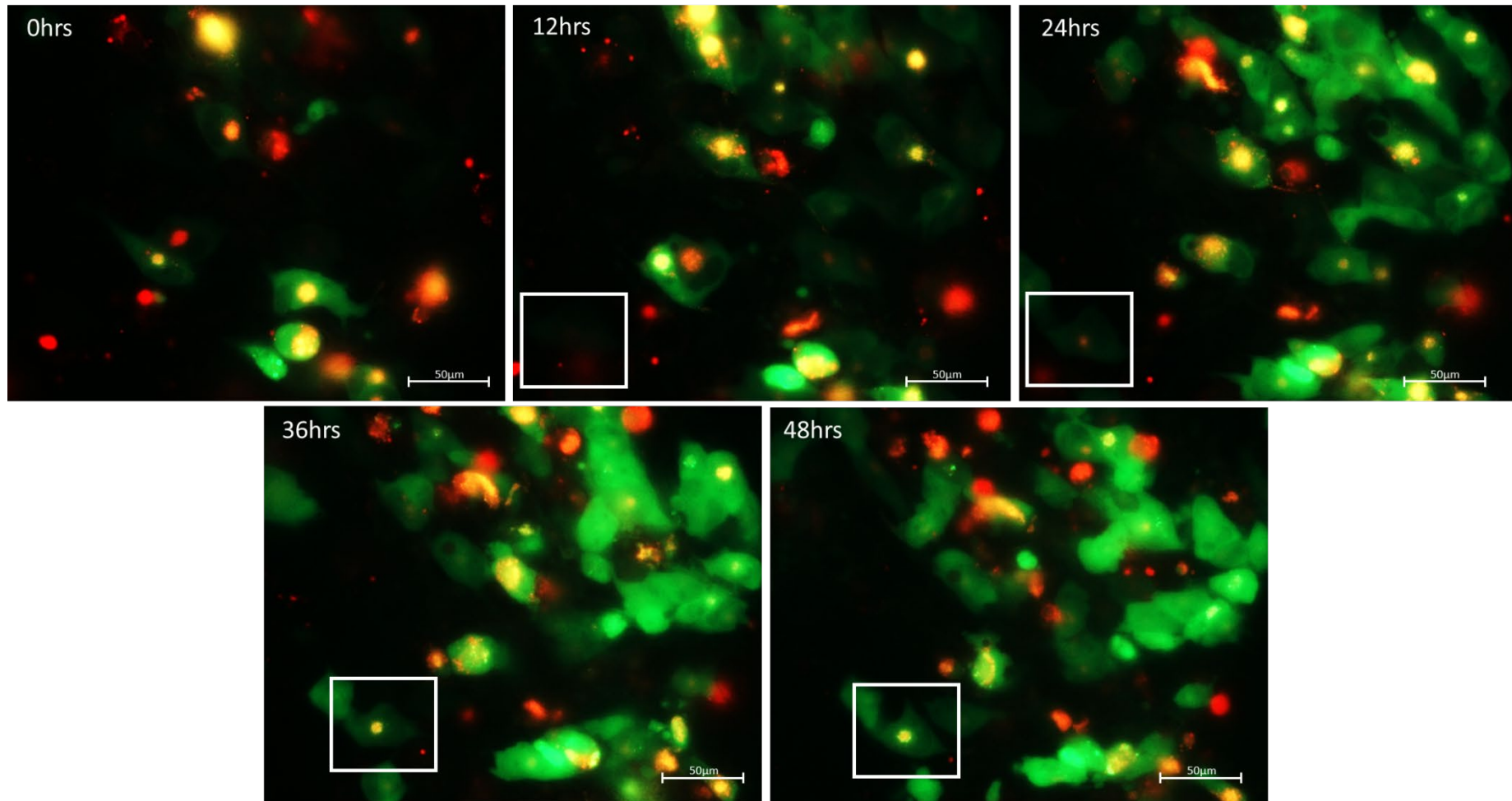


Figure 3.7 – RPE-1 cells infected with UL32-GFP/gM-mCherry (pAL2624) imaged every 30 minutes for 48hrs. White boxes indicate a cell forming an assembly complex during the time course. Scale bar = 50μm.

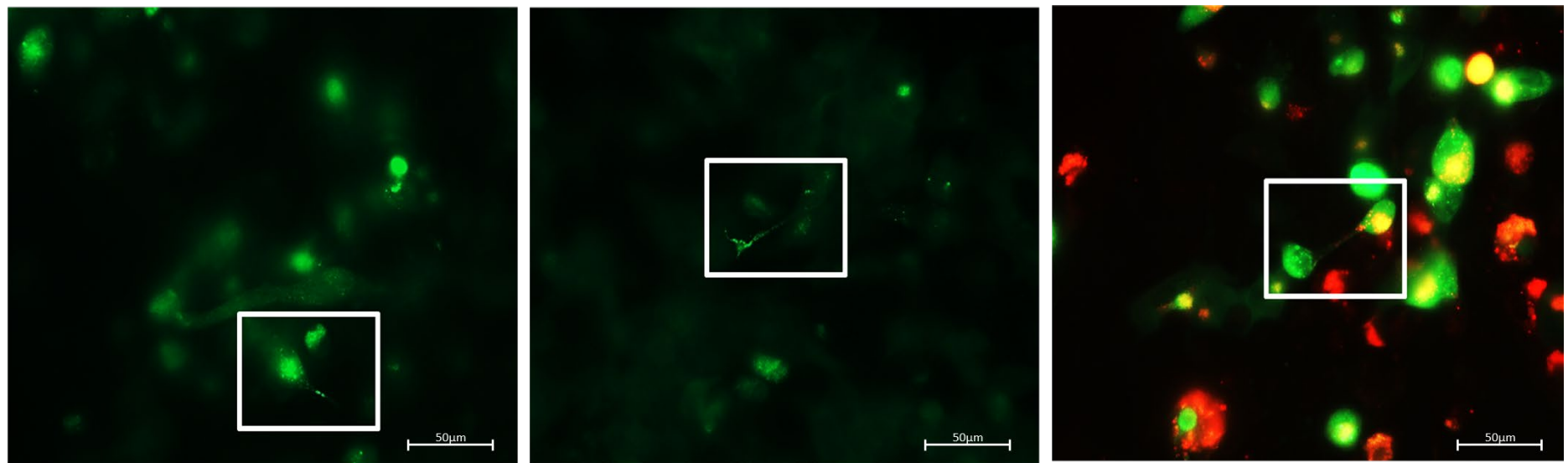


Figure 3.8 – Structures formed by infected RPE-1 cells. Left and middle images, UL32-GFP; right image, UL32-GFP/gM-mCherry. Scale bar = 50μm.

3.1.3 Formation of a “Virological Synapse”

3.1.3.1 Transmission Electron Microscopy

As previously mentioned, both HIV and HTLV-1 use a structure termed a “virological synapse” when infecting neighbouring cells by cell-associated spread^{123, 178}. To investigate whether this is also true for HCMV, electron microscopy was performed on dendritic cells and HFFFs; DCs were used as they are smaller than HFFFs and epithelial cells, and they are also mobile and able to crawl over the adhered HFFFs in a well to form conjugates. The DCs were co-cultured with Merlin-infected HFFFs – HFFFs were infected with Merlin for 72hrs prior to co-culture with DCs, to ensure HCMV virions were being produced. Cells were fixed in 1% glutaraldehyde at 2, 4, 6 and 8hrs post co-culture. Sections were cut and imaged using transmission electron microscopy (TEM) by Chris Von Ruhland.

Figure 3.9A shows a niche that has formed between the fibroblast on the right and the DC in the middle. By using a higher magnification (Figure 3.9B), we can see mature virions (red circle), and dense bodies (black circle) - these are produced during the normal life cycle of the virus – and appear to be concentrated at the cell-cell junction. The structure formed between the two cells may be a virological synapse.

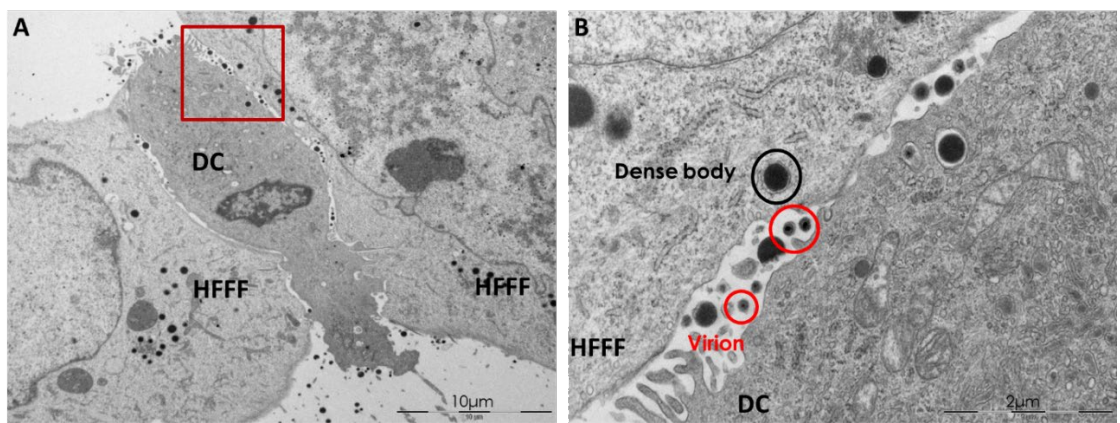


Figure 3.9 – Electron microscopy image taken by Chris Von Ruhland, showing structure formed between HFFF and DC at 6hrs post co-culture. A) Lower magnification showing structure formed between the membranes of adjacent HFFF (right) and DC (centre). Scale bar = 10μm. B) Higher magnification of the area highlighted by the red square, shows HCMV particles between the two cells; DC right; HFFF left. Red circle = mature virion; black circle = dense body. Scale bar = 2μm.

3.1.3.2 Cryo-Soft X-Ray Tomography

To complement the TEM images, a collaboration with Diamond Light Source Ltd was set up to use cryo-soft X-ray tomography (cryo-SXT) to provide 3D images of the cellular ultrastructure. This method allows high resolution imaging of thick sections including whole cells¹⁸⁴. To prepare samples for cryo-SXT, primary immature dendritic cells were prepared and transported to Dr Maria Harkiolaki at Diamond Light Source; once there, the DCs were placed into co-culture with HCMV-infected HFFFs for up to 24hrs. The virus used expressed a UL32-GFP protein (pAL2422), to provide an indication of infection and also to allow easier identification of virions when tomograms were processed. After preliminary experiments, we discovered that it was difficult to securely identify healthy infected HFFF by CryoEM. We therefore generated HFFFs expressing either LifeAct mCherry or LifeAct GFP using lentivirus transduction. As a result the actin filaments in these cells are tagged with fluorescent proteins (Figure 3.10). This enabled easier identification of infected HFFFs by cryo-SIM, and (it was hoped) would simplify the construction of tomograms following cryo-X-Ray tomography.

The LifeAct HFFFs were first seeded onto 3.05 mm gold TEM grids coated with a carbon substrate. Once the DCs had been received by Harkiolaki's group, they were stained using Hoescht and then co-cultured with the HFFFs. After co-culturing for up to 24hrs, the grids were washed gently with PBS to remove any unattached DCs, before being cryo-preserved using plunge freezing. Following preservation of the samples, the grids were "pre-mapped" using cryo-light microscopy to identify areas of interest, in particular areas where a HFFF and DC could be seen in close proximity. Once an area of interest was found, cryo-structured illumination microscopy (cryo-SIM) was used to generate stacks of high resolution images and provide a 3D map of the intracellular location of fluorophores – this fluorescence data could be used when processing tomograms. The Cryo-SXT data was collected by placing the grids into an X-ray microscope and a tilt series collected from $\pm 65^\circ$. Following collection, the tilt series is aligned and the 3D reconstruction can be made.

Due to the COVID19 pandemic, all work at Diamond had to be carried out remotely, with Diamond staff preparing all samples following remote instructions. This posed a number of technical challenges. These problems were further compounded following the breakdown of sample loader on the X-ray microscope. Nevertheless, we

discovered that although the Lifeact staining was useful to differentiate HFFF and DC with cryo-SIM, it was insufficient to enable reconstruction of tomograms. We therefore included an additional stain (far red mitotracker) to assist with this process. Together, the combination of Lifeact expressing HFFF, UL32-GFP virus, Hoescht labelled DCs, and far-red mitotracker, enabled us to demonstrate that our cells are compatible with cryo-Xray tomography, and it is possible to successfully image infected HFFFs in contact with DCs. Figure 3.11 shows a fibroblast surrounded by DCs at 3hrs post co-culture that was selected for cryo-SXT. Once the stage on the X-ray microscope has been fixed, we hope that this will enable successful imaging and reconstruction through the complete depth of cell-cell interfaces at high resolution.

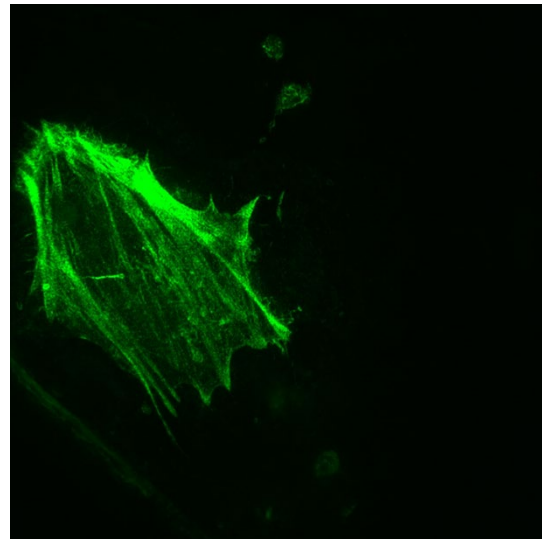


Figure 3.10 – Image of a LifeAct GFP HFFF cell taken during pre-mapping at Diamond Light Source.

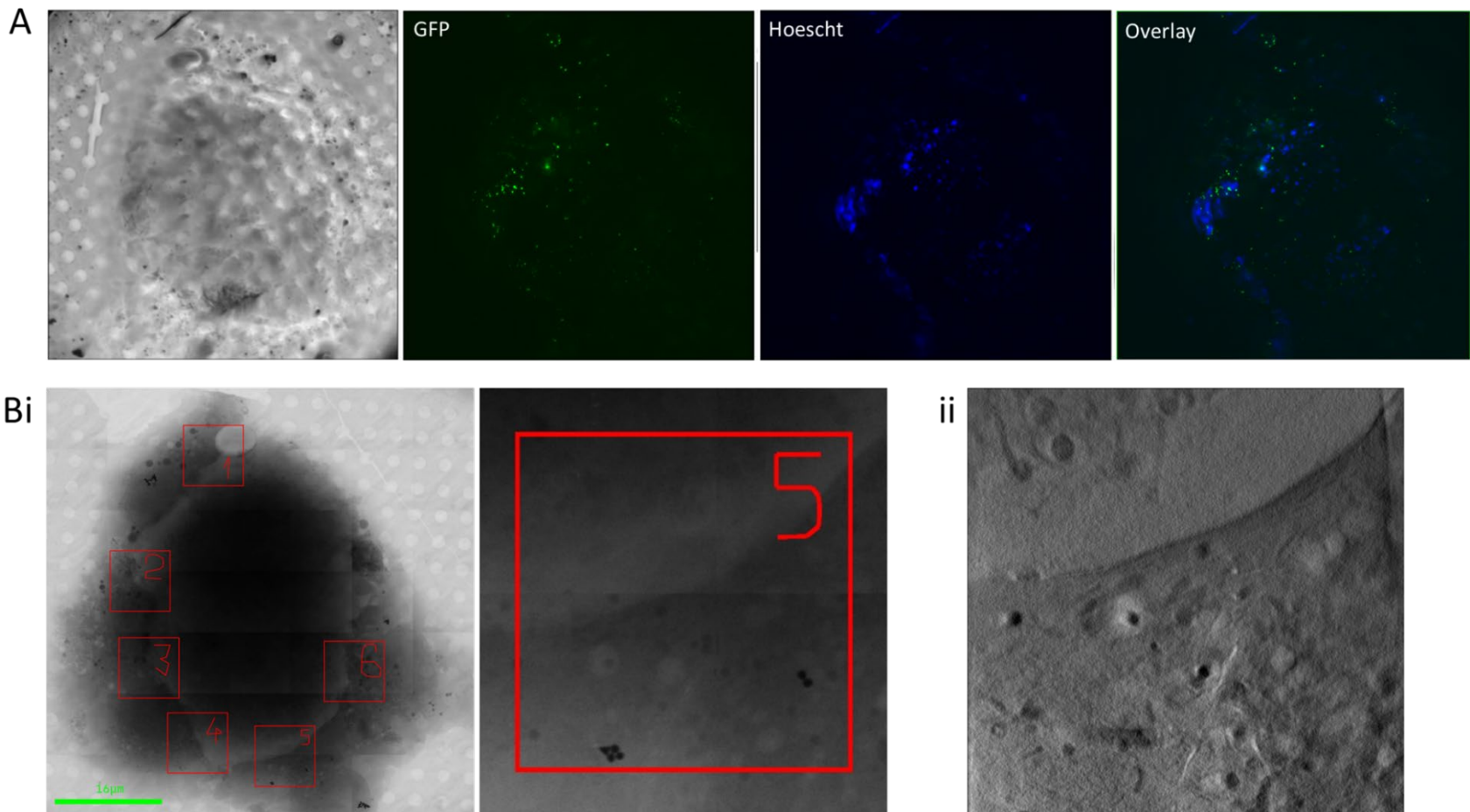


Figure 3.11 – Cryo-SXT imaging progression of DCs co-cultured with HFFFs. Non-fluorescent HFFF cells infected with UL32-GFP HCMV were co-cultured with DCs for 3hrs, DCs were stained with Hoescht prior to co-culture. A) Close up brightfield and fluorescence images taken during pre-mapping. Bi) X-ray mosaic of the area identified in A (bar = 16 μ m). Bii) A single field or view X-ray projection of area 5 in Bi. Data collected at B24 by Maria Harkiolaki and colleagues.

3.2 Quantifying Cell-Cell Transfer

3.2.1 Delivery of Viral Genomes Following Cell-Cell or Cell-Free Infection

In other viruses, such as HIV & HTLV, cell-cell spread has been shown to deliver a very high number of virions to neighbouring cells. To determine whether the same is true for HCMV, HFFFs infected via cell-free or cell-cell route were lysed 24hr post-infection, and QPCR was used to quantify the number of gB copies, and therefore number of genomes, present in the infected cells – this would be able to show if there is indeed any difference between the viral load delivered via both routes of infection.

Uninfected HFFFs were co-cultured with infected HFFFs for 24hrs. The initially infected HFFF expressed 6-His-tagged mCherry on their cell surface (HFFF-His), while the virus expressed a truncated RatCD2 from a P2A linker after UL36. As a result, infected cells expressed RatCD2 on the cell surface. During the 24hrs of co-culture, virus transferred from the HFFF-His, to the HFFF. MACS was then used to enrich the newly-infected HFFF population away from HFFF-His (Figure 3.12), while RatCD2 expression was used to purify infected cells away from uninfected ones. The DNA was then extracted from the newly infected cells to quantify the genomes delivered during the 24hr co-culture.

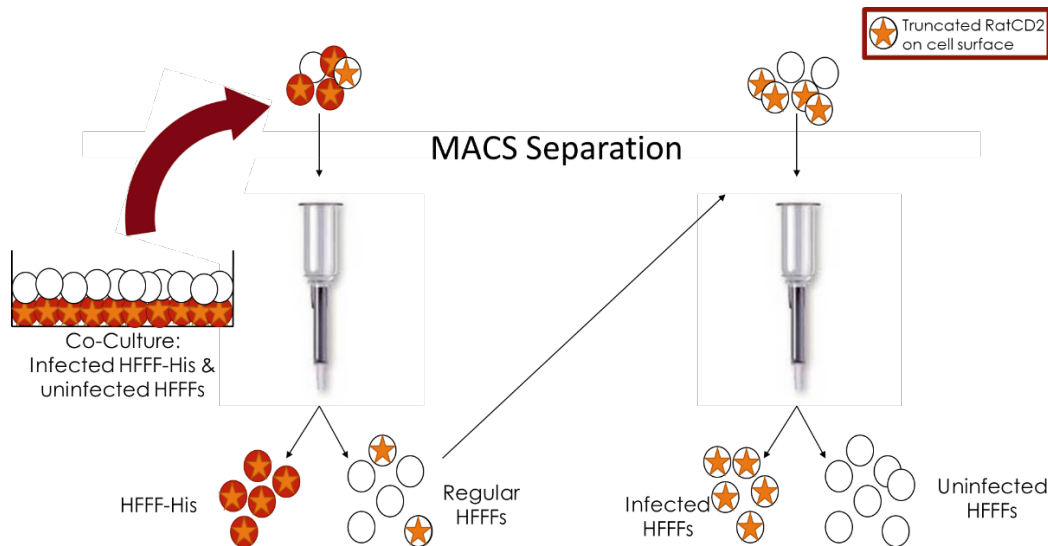
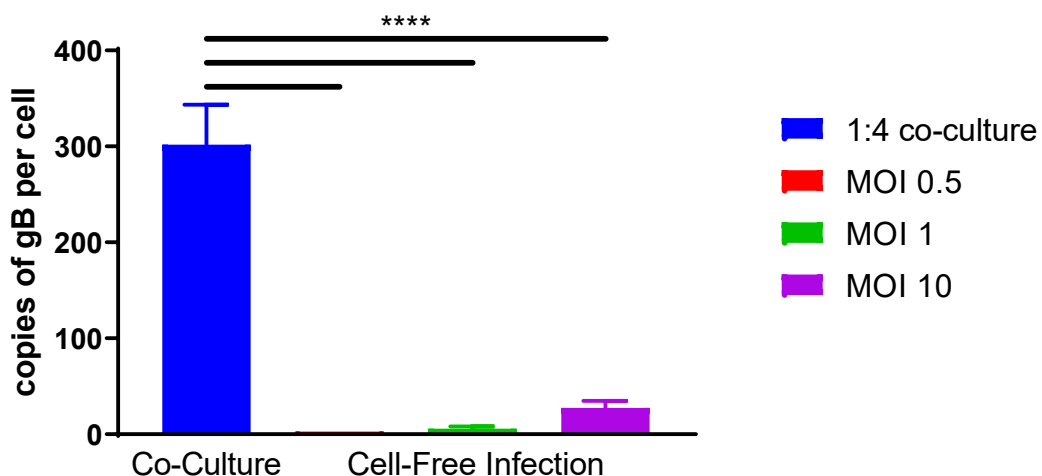


Figure 3.12 – Magnetic-activated cell sorting (MACS) of newly-infected HFFFs. Negative enrichment of mCherry-negative HFFFs, followed by enrichment of RatCD2-positive (infected) HFFFs.

By using QPCR of both a cellular gene (GAPDH) and the viral genome (gB), the number of genomes delivered to fibroblasts following cell-cell and cell-free infections was quantified. Cell-free infection at MOI 10 delivers 20-30 genomes per cell, however, infection by co-culture delivers >300 genomes per cell (Figure 3.13) – equivalent to a very high MOI infection, demonstrating that cell-associated HCMV infection is far more efficient than cell-free and in line with the literature for other viruses¹¹⁶.

The formation of a virological synapse and the delivery of such a high number of genomes, could explain how cell-cell transmission is more resistant to multiple arms of immunity.



*Figure 3.13 – Genome delivery following co-culture or cell-free infection measured by gB copies per cell. HFFFs were infected with a UL36-P2A-RatCD2 virus for 24hrs either cell-free at a range of MOIs or by co-culture (four uninfected HFFFs per infected HFFF). Newly infected HFFFs were purified using MACS, DNA was extracted from the cells and gB and GAPDH quantified using QPCR. Results are representative of 3 independent experiments. Error bars refer to mean + SD of triplicate samples. ***P < 0.0001, by 1-way ANOVA.*

3.2.2 Potent Neutralising Antibodies

Neutralising antibodies effectively reduce cell-free infection, although HCMV is able to evade naturally occurring polyclonal antibody responses by infecting neighbouring cells by direct cell-cell contact^{121, 122}. Polyclonal antibodies could weakly inhibit at very high concentrations, suggesting that antibodies may inhibit cell-cell spread if they can be delivered in sufficient amounts. Merck developed two antibodies against gH/gL

and the pentamer that are active against cell free virus at extremely low concentrations; the IgG concentration needed to achieve 50% viral entry inhibition (IC_{50}) was 0.9ng/ml for the anti-pentamer¹⁸⁵ and 21ng/ml for anti-gH/gL¹⁸⁶. We therefore tested whether these potent antibodies had any effects on reducing cell-cell spread of Merlin^{185, 187}. To assess this, infected HFFFs (HFFF-His) were co-cultured with RPE-1 cells for 24hrs with or without treatment with either of the antibodies. Antibodies were added before co-culture, and maintained throughout. Figure 3.14 demonstrates that these potent neutralising antibodies significantly reduce infection rates following cell-cell transfer, but do not abrogate it completely. This led us to perform QPCR (Figure 3.15) to determine whether, in cells that are infected, the number of virions being delivered are reduced by neutralising antibody.

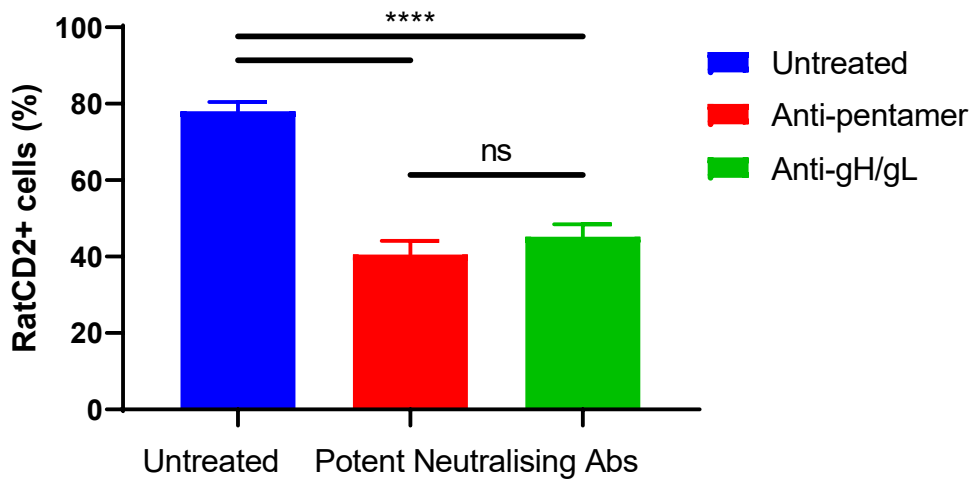


*Figure 3.14 - Treatment with potent neutralising antibodies reduces infection rates following cell-cell transfer. RPE-1 cells were infected for 24hrs with a UL36-P2A-RatCD2 virus by co-culture with HFFF-His cells. 200 μ g/ml antibody added at the same time as the co-culture. RPE-1 cells purified from HFFF-His cells 24hrs post co-culture using MACS, and analysed using flow cytometry. Results are representative of 2 independent experiments. Error bars refer to mean + SD of triplicate samples. ***P < 0.0001, by 1-way ANOVA.*

Following the same purification protocol from Figure 3.12, DNA was extracted from the pure population of newly-infected RPE-1 cells, and QPCR of gB copies in these cells revealed that treatment with the potent neutralising antibodies appears to increase the number of genomes delivered to these cells (Figure 3.15). There are several explanations for this: either the antibodies are coating the virus particles and driving

increased internalisation of the virions which are then trapped in endosomes, unable to reach the nucleus and therefore not causing a productive infection of the epithelial cells; or, the antibodies are blocking only a proportion of entry events so the infection rate is reduced, while the cells that do become infected receive a higher number of genomes.

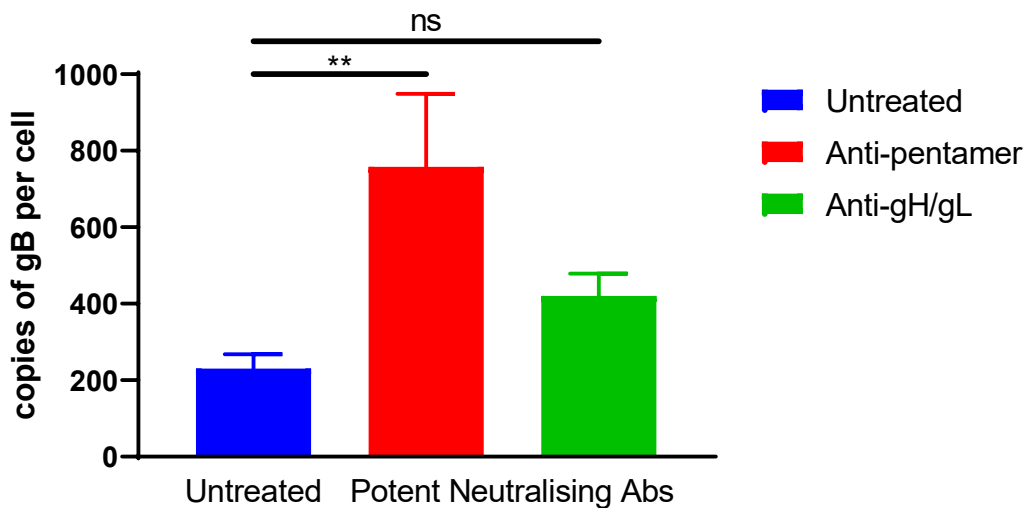
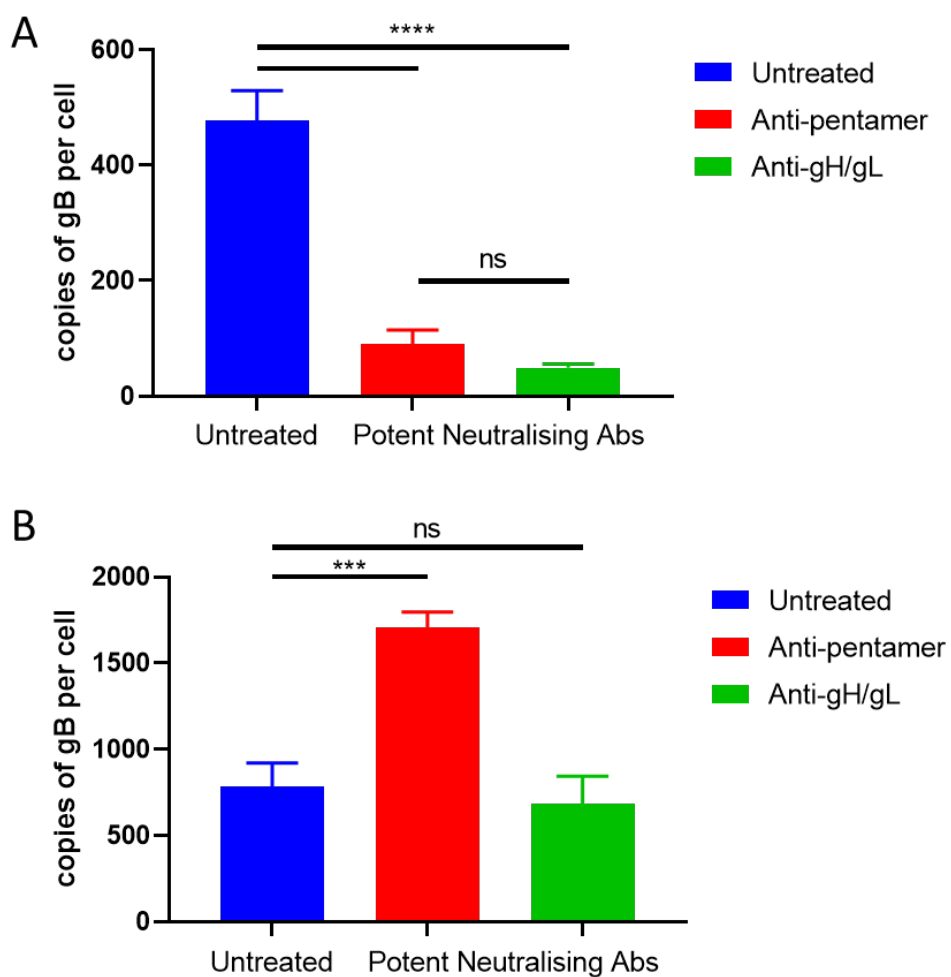


Figure 3.15 – Genome delivery following co-culture +/- treatment with potent neutralising antibodies. RPE-1 cells were infected for 24hrs with a UL36-P2A-RatCD2 virus by co-culture with HFFF-His cells. 200 μ g/ml antibody added at the same time as the co-culture. Newly infected RPE-1s were purified using MACS, DNA was extracted from the cells and gB and GAPDH quantified using QPCR. Results are representative of 2 independent experiments. Error bars refer to mean + SD of triplicate samples. **P < 0.01, by 1-way ANOVA.

To determine if the virions are being sequestered in endosomes, DNA was extracted from the nuclei of the RPE-1 cells – this was done by treating the cells with NP-40 Lysis Buffer, pelleting nuclei, and then extracting DNA. The first attempt at measuring genome delivery to the nucleus of epithelial cells showed a reduction in genome numbers when cells are treated with potent neutralising antibodies. This would indicate that potent neutralising antibodies are capable of partially inhibiting cell-cell spread, and reducing the number of genomes delivered in those cells that are successfully infected (Figure 3.16A). The experiment was repeated to prove that the data was reproducible, however, the data in Figure 3.16B was more similar to that seen previously from the whole cell (Figure 3.15) and suggested that the virions were

actually able to reach the nucleus despite the presence of neutralising antibodies, and in the presence of anti-pentamer, uptake could possibly be enhanced.

Unfortunately the potent neutralising antibodies were discontinued by Merck before a repeat could be done, I found the sequences of the antibodies in a patent, and began to clone these sequences in order to produce them myself using the antibody cloning techniques described in methods; unfortunately, it was not possible to complete production within the time scale of the project.



*Figure 3.16 – Genome delivery to nucleus following co-culture +/- treatment with potent neutralising antibodies. RPE-1 cells were infected for 24hrs with a UL36-P2A-RatCD2 virus by co-culture with HFFF-His cells. 200µg/ml antibody added at the same time as the co-culture. Newly infected RPE-1s were purified using MACS, DNA was extracted from the nuclei and gB and GAPDH quantified using QPCR. A and B represent two independent experiments. Error bars refer to mean + SD of triplicate samples. ****P < 0.0001, ***P < 0.001, by 1-way ANOVA.*

3.3 HCMV Superinfection

Cudini et al determined that the relatively high nucleotide diversity of HCMV seen in immunocompromised children was as a result of genetically distinct HCMV strains superinfecting and recombining within the host¹⁸⁸. It was also shown by Baldanti et al that AIDS patients can become infected by multiple unrelated strains of HCMV during their lifetime but during this study, immunocompetent mothers and their congenitally infected infants carried single strains¹⁸⁹. Hence, it is likely that multiple HCMV strains superinfect immunocompromised patients and recombine within the host to produce genetically distinct strains.

As recombination requires multiple genomes to infect the same cell, and cell-cell spread delivers more genome per cell, it is possible that infection via the cell-cell route could potentially lead to greater rates of recombination if more than one strain were to be present. To evaluate this *in vitro*, a virus containing a UL36-P2A-GFP tag (pAL2270) and a second virus with a US28-P2A-mCherry tag (pAL2988) were used to superinfect HFFFs. By using these two different fluorescent tags, flow cytometry could be used to identify double positive cells, and hence measure the rate of superinfection; the tags are at opposite ends of the viral genome, so in the event of recombination between the two viruses it is likely that new virions will express both GFP and mCherry.

3.3.1 The Ability of HCMV to Superinfect Cells Over Time

3.3.1.1 PDGFR α Expression Time Course

Platelet-derived growth factor receptor α (PDGFR α) is expressed on fibroblasts, and is the predominant receptor for cell-free HCMV entry in this cell type^{117, 119, 190}. To determine whether PDGFR α is downregulated from the cell surface following cell-free infection, HFFFs were infected and flow cytometry was used to measure surface expression of PDGFR α at 24hr intervals for 72hrs (Figure 3.17). The median fluorescence intensity (MFI) of PDGFR α decreases over time on the surface of infected cells, this suggests that the receptor is internalised either during or shortly after the virions enter the cell, from this data we predicted that it would become increasingly difficult to superinfect HFFFs once an initial infection has already been established.

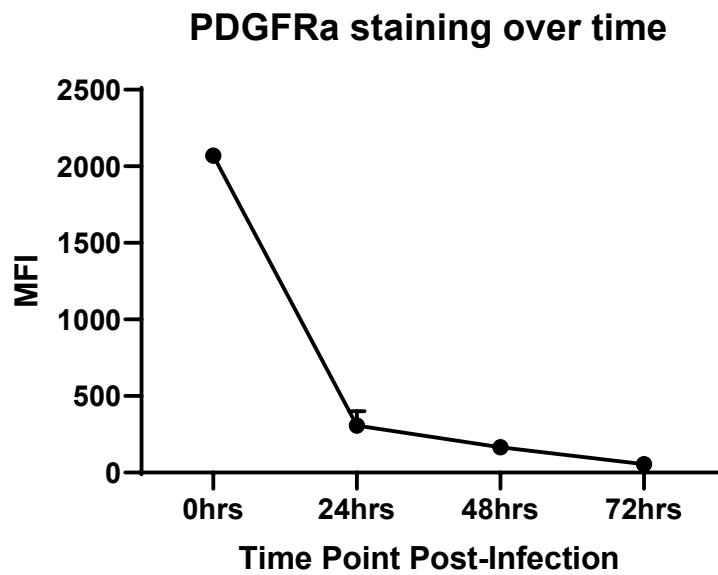


Figure 3.17 – Median fluorescence intensity (MFI) of PDGFR α on HCMV-infected HFFFs. HFFFs were infected with UL36-GFP Merlin at MOI 5 for 24hr in duplicate. Cells were harvested at 24hr intervals and surface stained with a primary anti- PDGFR α antibody and secondary anti-mouse AF647 antibody before fixing. The MFI of PDGFR α was calculated. Error bars refer to mean + SD of duplicate samples.

3.3.1.2 Superinfection Time Course

Before performing superinfection experiments, a time course was done to measure the intensity of the fluorescent tags over time. pAL2270 has a UL36-GFP tag, which was expected to be present in infected cells from 24 hours post-infection; whereas pAL2988 has a US28-mCherry tag, a protein which is abundant in the cell from 48 hours post-infection. Figure 3.18 shows the expression time course of both viruses. Despite not all cells being infected by UL36-GFP (Figure 3.18A), it is clear that GFP is present in the cell from 24 hours post-infection. In Figure 3.18B, the intensity of the mCherry in the US28-mCherry-infected cells increases over time, hence any superinfection work would best be analysed 72hrs post US28-mCherry infection, to ensure that infected cells are distinguishable from mock.

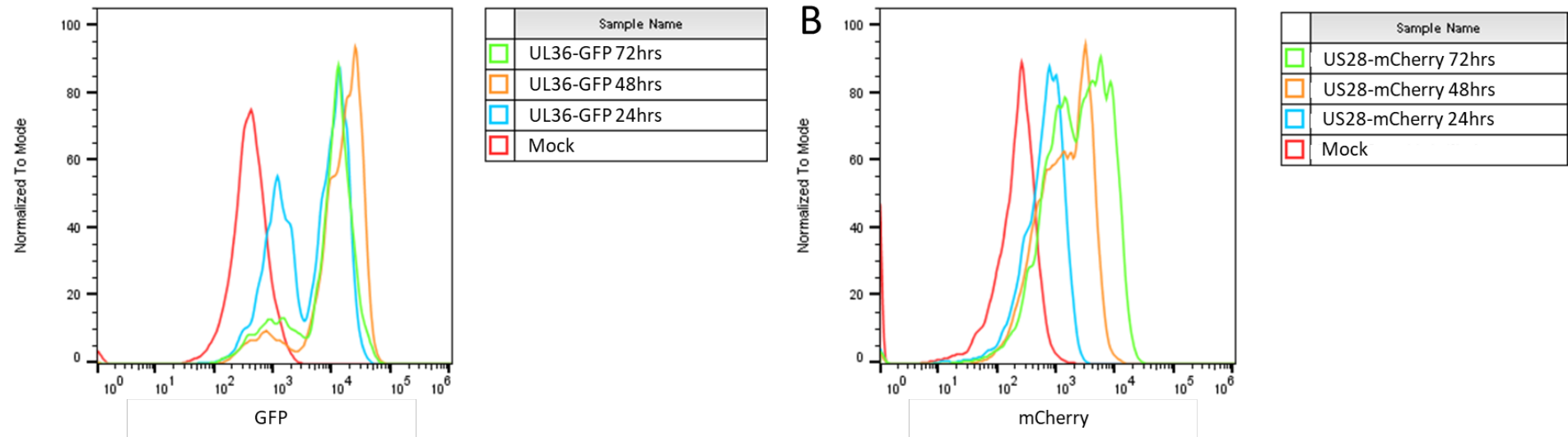
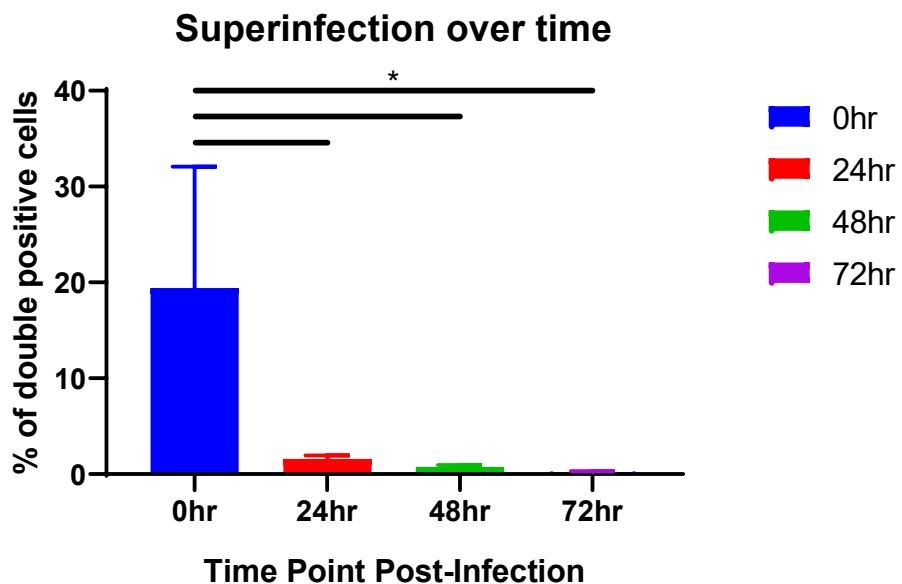


Figure 3.18 – Fluorescent tag expression time course. HFFFs were infected at an MOI 5 for 24hrs with either UL36-GFP Merlin (*pAL2270*) or US28-mCherry Merlin (*pAL2988*). Cells were harvested at 24hr intervals and fluorescence analysed by flow cytometry. A) Time course of UL36-GFP expressed in *pAL2270*-infected cells. B) Time course of US28-mCherry expressed in *pAL2988*-infected cells. Mock cells are uninfected HFFFs.

Superinfection was first investigated in the context of cell-free infections. HFFFs were infected with US28-mCherry and then with UL36-GFP either at the same time, or 24, 48 or 72hrs following the first infection. Figure 3.19 shows that the ability of HCMV to co-infect at 0hrs is higher than its ability to superinfect at 24hrs or later, which mirrors what was seen with the PDGFR α expression data. From these data it was concluded that superinfection via the cell-free route is extremely difficult in a cell where an infection has already been established.



*Figure 3.19 – Percentage of cells expressing GFP and mCherry at 96hrs post-US28-mCherry infection. HFFFs infected at MOI 5 for 24hrs with US28-mCherry (pAL2988), these cells were also infected with UL36-GFP (pAL2270) at MOI 5 either at the same time or at 24hr intervals following US28-mCherry infection. Cells were harvested and analysed by flow cytometry at 96hrs post US28-mCherry infection. Error bars refer to mean + SD of triplicate samples. *P < 0.05 by 1-way ANOVA.*

3.3.2 Superinfection via Cell-Cell vs Cell-Free Transmission

As infection by cell-cell contact delivers a far greater number of virions to uninfected cells, it was hypothesised that a co-culture system may be able to overcome the reduction in cell surface PDGFR α , and therefore make superinfection possible. HFFFs were infected with either UL36-GFP or US28-mCherry, and co-cultured 72hrs post-infection. Samples were taken for flow cytometry 24hrs post co-culture, and analysed to determine whether cells previously infected with the mCherry expressing virus, became superinfected with virus expressing the GFP tag. Surprisingly, co-culture did

not improve the rate of superinfection of HFFFs (Figure 3.20A) – suggesting that the PDGRF α reduction on the cell surface at 72hrs post-infection is sufficient to prevent cell-cell infection.

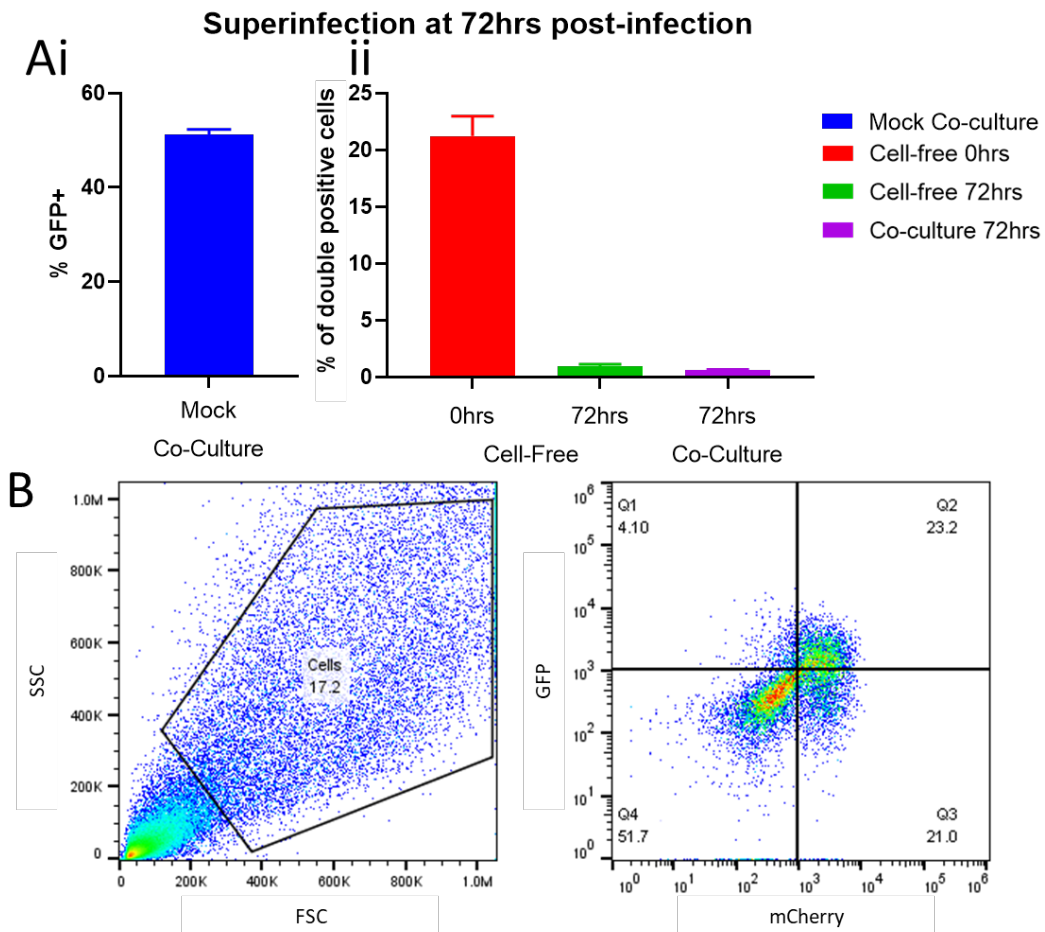


Figure 3.20 – Infecting HFFFs using a co-culture system does not increase the percentage of cells that become superinfected. HFFFs infected with US28-mCherry Merlin at MOI 5, then either infected cell-free with UL36-GFP Merlin immediately or 72hrs later, or co-cultured with UL36-GFP-infected HFFFs at 72hrs post-infected. Ai) Percentage of cells expressing GFP, mock is uninfected HFFFs co-cultured with infected HFFF-His cells (UL36-GFP); ii) percentage of cells expressing both GFP and mCherry following cell-free and cell-cell infection. B) Gating strategy for identifying double positive cells in the co-culture. Error bars refer to mean + SD of triplicate samples.

To test whether the cells are more susceptible to superinfection by co-culture when they are in the earlier stages of infection, HFFFs were infected with US28-mCherry, and stained with a violet dye to ensure we were able to determine which cells were originally infected with US28-mCherry. Then, these cells were co-cultured 24hrs later with late stage UL36-GFP infected cells (72hrs post-infection), and analysed 72hrs

post co-culture – this was due to the results of Figure 3.18B, where the intensity of the mCherry is highest at 72hrs. There was a slight improvement in the number of cells superinfected, which is shown as the percentage of US28-mCherry-infected cells that are GFP positive (Figure 3.21), however, infection was still heavily restricted in the US28-mCherry-infected cells when compared to mock (gating strategy shown in Figure 3.22). An alternative explanation was that superinfection was occurring, but UL36-GFP gene expression was suppressed. If this was the case, GFP would not be seen in the HFFFs, but recombination could still occur.

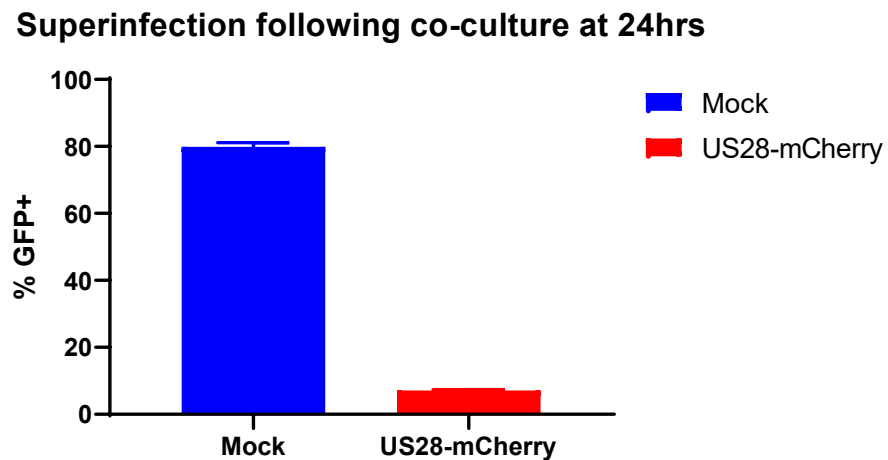


Figure 3.21 – Percentage of cells expressing GFP 72hrs post co-culture. HFFFs were infected with US28-mCherry (pAL2988) with MOI 5 for 24hrs before being stained with a violet dye and co-cultured with late stage UL36-GFP-infected cells (72hrs post-infection) and analysed by flow cytometry 72hrs post co-culture to determine the percentage of mCherry⁺ or mock cells that obtained GFP fluorescence during the co-culture. Mock cells were uninfected cells co-cultured with late stage UL36-GFP infected HFFFs. Error bars refer to mean + SD of triplicate samples.

When analysing the data for the cell-free and co-culture superinfection experiments, it was apparent that cells in a co-infection did not express UL36-GFP to the same magnitude as those infected by UL36-GFP alone. As can be seen in Figure 3.23, when analysed either as a quadrant or as a histogram, the intensity of GFP in co-infected cells remains below the intensity of UL36-GFP-infected cells, but above mock cells (Figure 3.23A and B). It is possible therefore that superinfection rates following co-infection or co-culture are higher than shown by flow cytometry, and in fact the UL36-GFP is being suppressed and the untagged UL36 from US28-mCherry is preferentially

expressed. To determine this, QPCR could be used to measure the copies of GFP and mCherry in superinfected cells.

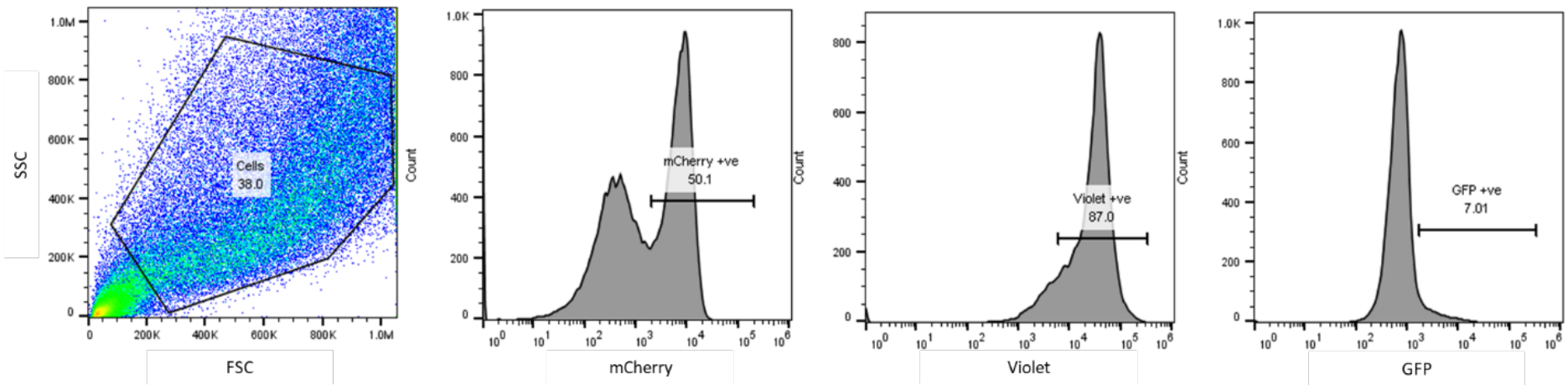


Figure 3.22 – Gating strategy to identify US28-mCherry (pAL2988)-infected cells that became GFP+ following co-culture with UL36-GFP (pAL2270)-infected cells. HFFs were infected with US28-mCherry (pAL2988) with MOI 5 for 24hrs before being stained with a violet dye and co-cultured with late stage UL36-GFP-infected cells (72hrs post-infection) and analysed by flow cytometry 72hrs post co-culture.

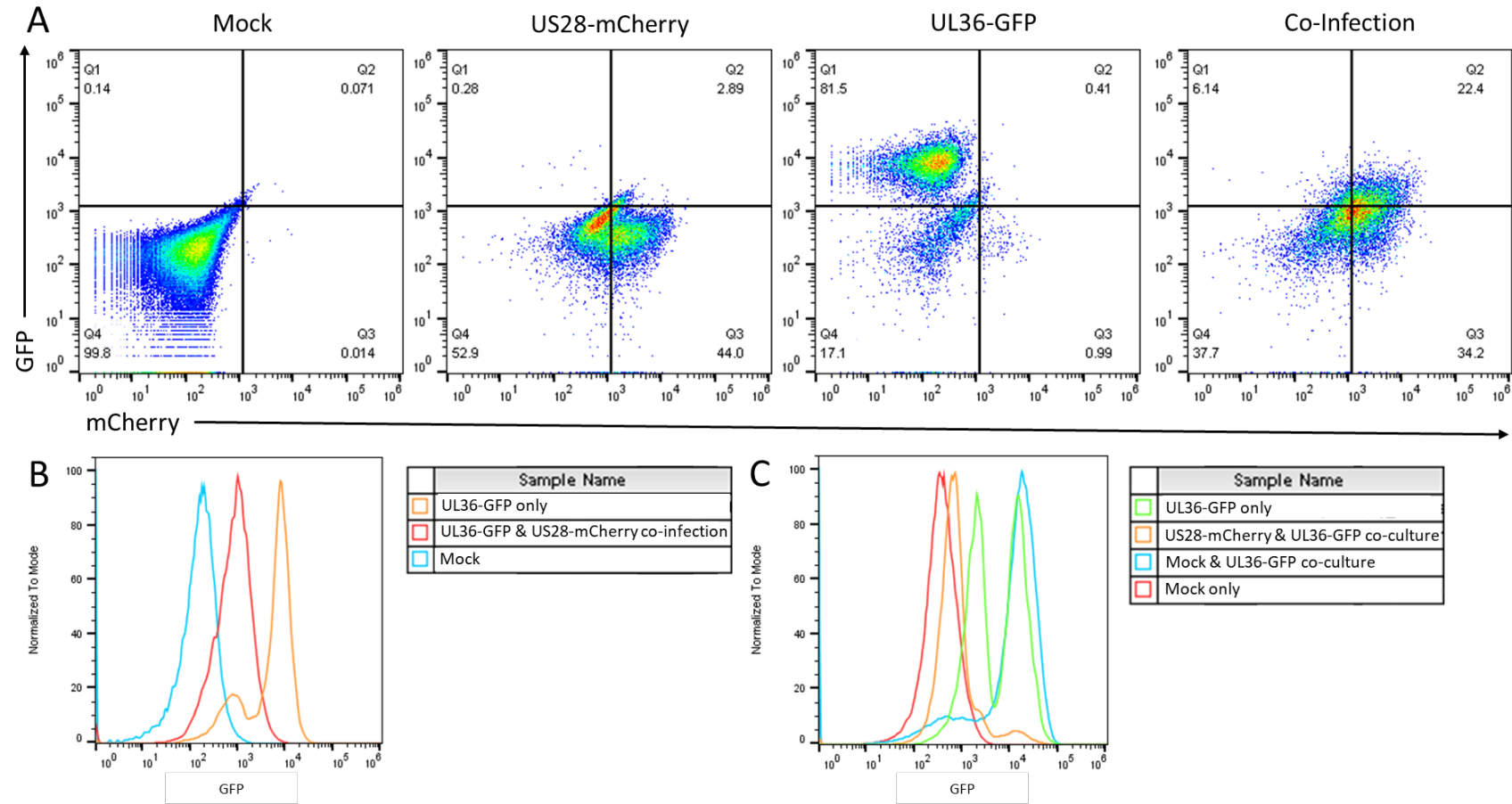


Figure 3.23 – Co-infection reduces the intensity of UL36-GFP. HFFFs were infected with either US28-mCherry Merlin, UL36-GFP Merlin, or both for 24hrs at MOI 5 before being analysed by flow cytometry at 72hrs post-infection. A) GFP and mCherry intensity for mock (uninfected), US28-mCherry, UL36-GFP and cells co-infected with both viruses at 0hrs (cell-free). B) Histogram demonstrating a “middle intensity” peak for cells co-infected at 0hrs, compared to mock and UL36-GFP-infected cells. C) Histogram demonstrating GFP intensity in cells superinfected at 24hrs post-infection.

3.3.3 Recombination Following Superinfection

If cells were potentially superinfected, but not expressing the fluorescent tag, then recombination could still occur. To determine if this was the case, supernatant from the previous experiment (Figure 3.21) was used to infect primary fibroblasts, which were then overlayed with 2X DMEM/2% Avicel and left for two weeks to allow plaques to develop. The wells were washed with PBS and imaged using the Zeiss microscope (Figure 3.24A). From this, the number of GFP⁺, mCherry⁺, and mCherry⁺GFP⁺ plaques was determined and summarised in the graph shown in Figure 3.24B. It was evident from the microscopy images that there were far more mCherry⁺ plaques than GFP⁺; this may be because the UL36-GFP-infected cells were at 72hrs post-infection at the time of co-culture, and hence were at 144hrs post-infection at the time of supernatant collection – it is probable that these cells may have died and stopped producing virions at this time point. It was also evident that recombination between the two viruses was very inefficient, only 10% of GFP⁺ cells were also mCherry⁺ (17 of 177 GFP⁺ cells), suggesting that the large majority of virions produced during the superinfection experiment carried a single fluorescent tag. For the 10% of cells that were double positive, it would be necessary to plaque purify and sequence the viruses in order to state whether recombination or superinfection has occurred.

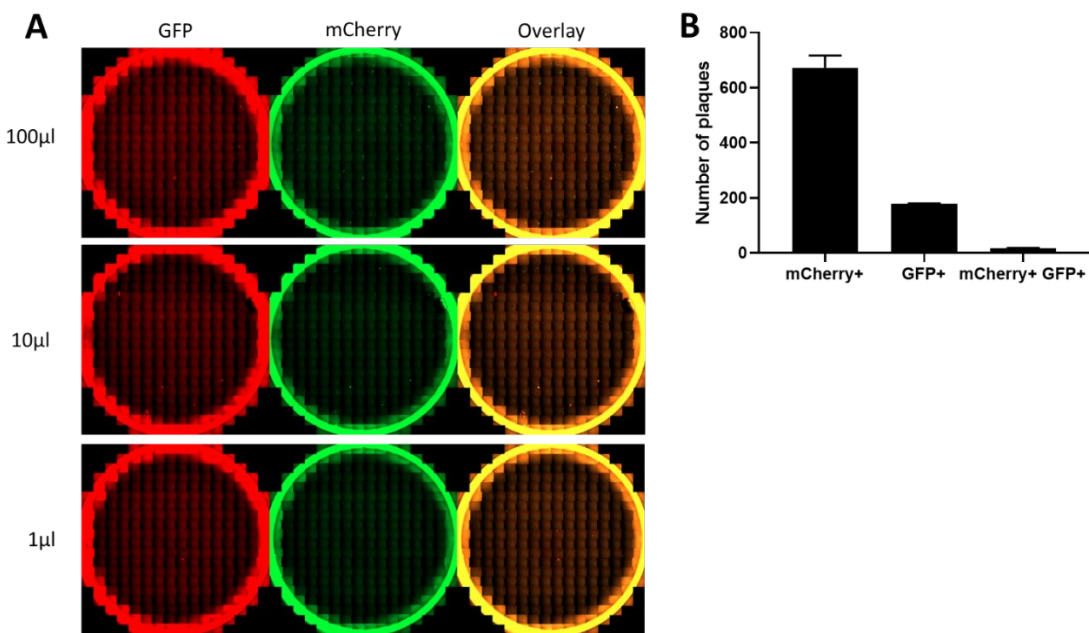


Figure 3.24 – Primary HFFFs infected with supernatant from superinfected HFFFs to determine if recombination occurred. Primary HFFFs infected with varying quantities of supernatants for 24hrs before being overlayed with 2X DMEM/2% Avicel. A) Cells were imaged with Zeiss microscope two weeks after infection, each dilution represents two replicates. B) Plaques counted in 100 μ l wells. Error bars refer to mean + SD of triplicate samples.

3.4 Summary

The data in this chapter have shown that there is a limit to the number of fluorescent tags that can be incorporated into the HCMV virion without creating major growth issues. It has also been shown that long-term fluorescence is best performed in RPE-1 cells, and that this requires a virus containing multiple fluorescent tags to provide any conclusive results regarding cell entry to egress. Further to this, the most likely mechanism used in cell-cell infection is the virological synapse, which forms between the infected cell and a neighbouring uninfected cell. Cell-cell transfer delivers a very high number of genomes to neighbouring cells, is resistant to most neutralising antibodies produced following natural infection, but can be reduced by potent neutralising antibodies targeting the pentamer and gH/gL. In addition to this, cell-cell infection doesn't appear to be able to overcome downregulation of PDGFR α on the surface of HFFFs to superinfect these cells *in vitro* – and there appeared to be very little recombined virions released into the supernatant.

Chapter 4.

HCMV

Manipulation of

Dendritic Cells

Following Cell-

Cell Transfer

HCMV causes a life-long infection and is never cleared by the immune system. Previous work on NK and T cells has demonstrated that HCMV encodes proteins that inhibit activation of these cells and modulates the immune response to infection^{24, 148, 191}. Since clinical strains also infect dendritic cells (DCs), and these cells play a major role in the generation of an adaptive immune response, it is likely that HCMV also manipulates DCs in a way that contributes to its persistence in the host. Having established techniques to infect a wide range of cell types with a HCMV strain expressing the complete repertoire of HCMV gene functions, through cell-cell spread, we were therefore able to ask questions about what happens post-infection, in DCs.

To do this, we used multiplexed quantitative proteomics. This is an extremely powerful tool because it enables precise quantitation of the entire proteome under multiple different conditions. Weekes et al. used this approach to investigate the effect of HCMV infection in fibroblasts (HFFFs), and provided an in-depth profile of HCMV protein expression and proteins that are vital to host antiviral mechanisms¹⁷². We now advanced this approach into DCs by generating whole cell lysates and plasma membrane preparations of primary immature DCs infected with HCMV via the cell-cell route, and analysing for protein abundance; processing both samples presented a picture of what happens to the cell overall, and what happens to the all-important cell membrane of the DCs following infection.

The results showed that HCMV influenced multiple proteins (targets) involved in DC function, suggesting that viral manipulation of DCs has evolved in an attempt to limit detection of HCMV, and therefore the induction of an adaptive immune response in the host. The use of multiple ‘block deletion’ mutants provides insight into the HCMV gene families likely to be responsible for modulating each of the identified target proteins.

4.1 Preparation of Samples for Proteomic Analysis

4.1.1 Obtaining Pure Populations of HCMV-Infected DCs

PBMC were isolated from buffy coats, then CD14⁺ monocytes enriched by magnetic activated cell sorting (MACS) before being differentiated into DCs with IL4 and GMCSF. DCs were phenotyped (CD14^{low}, CD1a^{high}, DC-SIGN^{high}) and co-cultured with HCMV infected HFFFs for 24hrs, during which time HCMV infected the DCs by direct cell-cell contact. This resulted in a mixed population of infected HFFFs, and infected and uninfected DCs. For many experiments, it was necessary to have pure populations of cells. Therefore the fibroblasts were engineered to express a 6-His-tagged mCherry on their cell surface (HFFF-His), which allowed purification of the DCs away from HFFFs, by negative selection using MACS. This was performed at 24h post co-culture, since this resulted in a significant percentage of infected DCs, without the infected cells being at widely differing stages of the viral life cycle. The virus used in these experiments expressed RatCD2 on the cell surface (with a truncated cytoplasmic tail, so it couldn't signal), allowing MACS separation to be used to separate infected and bystander DCs (Figure 4.1). Cells were rested for at least 2hrs in supplemented RPMI in between the two separations (i.e. separation from HFFFs, and separation of infected and bystander DCs), because in preliminary experiments the size and granularity of DCs was altered, indicative of cell death, when separations were performed immediately after each other (Figure 4.2) – it is possible that the difference seen between Figure 4.2A&B may be as a result of donor variation, however, as resting the DCs alleviated cell death, this was done for all further experiments.

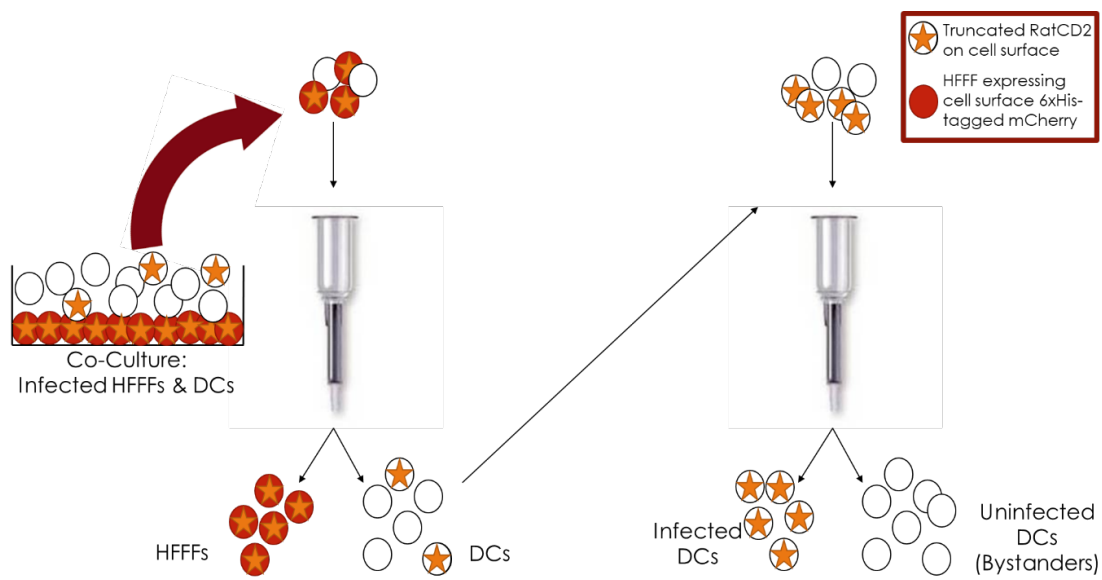


Figure 4.1 – Use of MACS to separate fibroblasts from DCs, then infected from uninfected DCs.

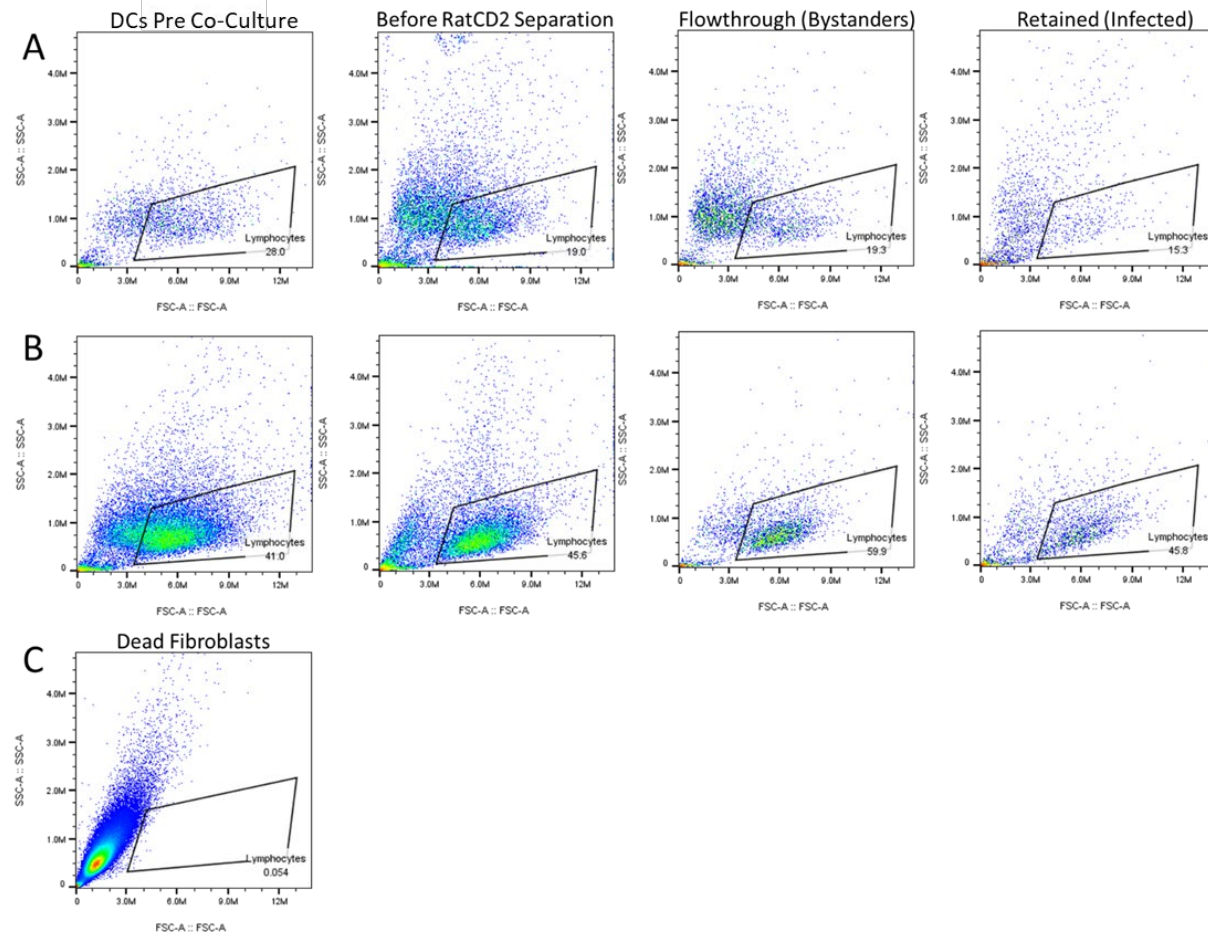


Figure 4.2 – Dot plots showing the benefit of resting the DCs between separations. DCs that have undergone two separations immediately after each other show a significant shift in FSC/SSC (A), compared to those that are rested for 4hr between separations (B). C) HFFFs killed by washing in 100% ethanol, demonstrating that dead cells shift to the left on FSC.

4.1.2 Optimisation of Separation Protocols

4.1.2.1 Separating Dendritic Cells from Fibroblasts

During multiple uses of the His-tagged mCherry expressing HFFFs, it became apparent that over multiple passages in cell culture, two populations emerged in the cell line: a mCherry-high and a mCherry-low, which were not present in early passage cells of the same line (Figure 4.3A). When these cells were used in co-cultures, it was not possible to separate the mCherry-low from non-mCherry cells by MACS (Figure 4.3B), whether these were DCs or HFFFs. This was presumably because the lower expression levels of mCherry in this population resulted in less antibody binding, which impaired retention in the magnetic field of the MACS column.

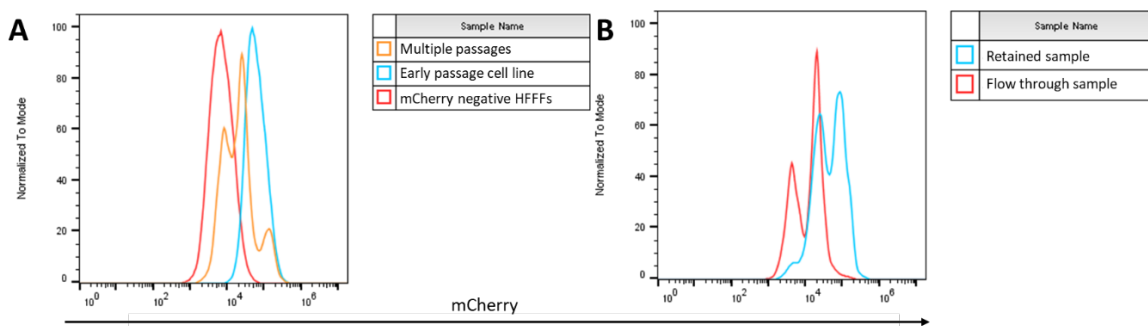


Figure 4.3 – Flow cytometric analysis of mCherry expression in HIS-tagged mCherry expressing HFFF cell line. A) Comparing expression in an early passage cell line to the same cell line after multiple passages. B) Analysis following MACS of multiple passage cell line co-cultured with regular HFFFs.

To address this issue, the mCherry-high and -low populations were purified by cell sorting by Mrs Kelly Miners (Figure 4.4). Following sorting, the expression of mCherry and binding of anti-His antibody was compared to the early passage cells and HFFFs lacking mCherry (Figure 4.5), demonstrating that the high and low expressing populations had been isolated to >95% purity. The mCherry-high population was used

in future co-culture experiments, and further problems with purifying mCherry expressing cells were not observed.

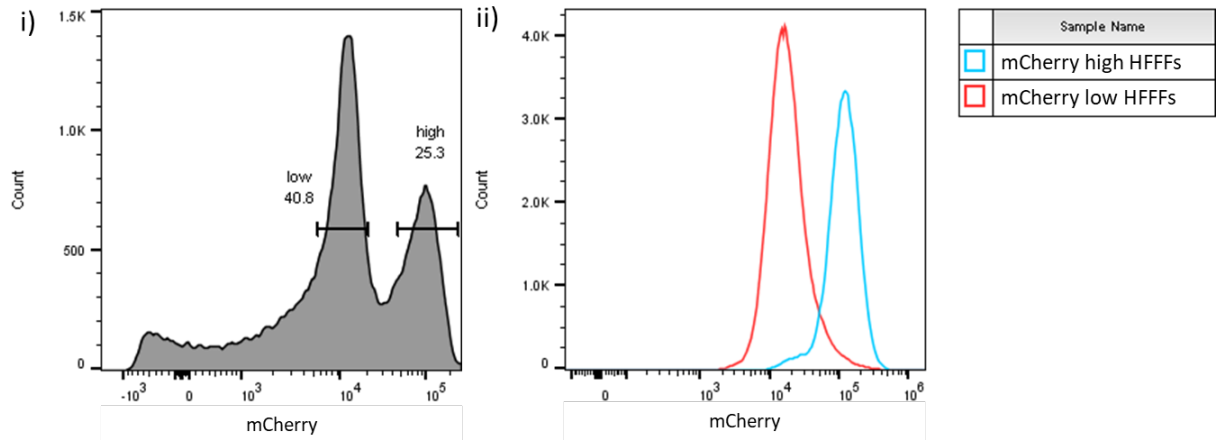


Figure 4.4 – Sort report of mCherry high- and low-expressing cells by Mrs Kelly Miners. HFFF-His cells that were shown to have two mCherry peaks were harvested and sorted using a BD FACSaria to purify each population within the cell culture. i) Pre-sorted sample. ii) Post-sorting, mCherry high and mCherry low samples.

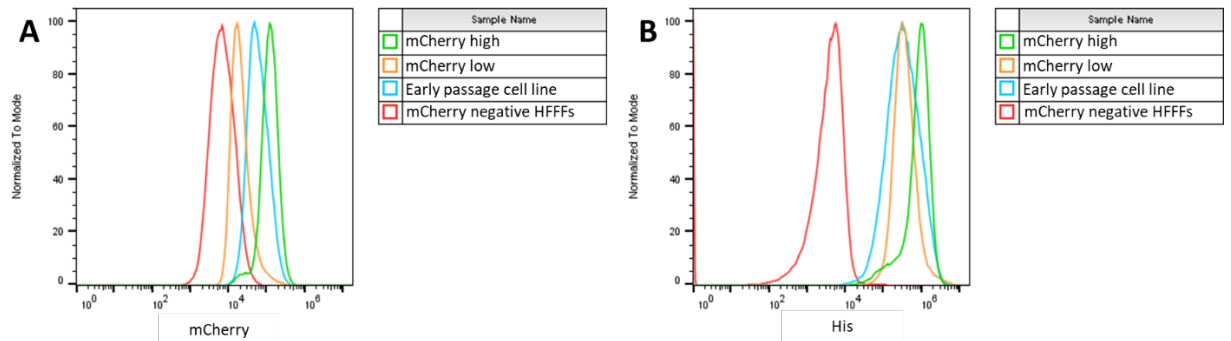


Figure 4.5 – Flow cytometric analysis comparing mCherry expression (A) and anti-His antibody binding (B) expression in different cell lines. Following purification of the mCherry high and mCherry low-expressing cells, these cell lines along with an early passage of the parental line and non-mCherry expressing HFFFs were stained with an anti-His and anti-Mouse AF647 and analysed by flow cytometry.

4.1.2.2 Purifying Infected Dendritic Cells

The virus used contained the coding sequence for RatCD2, expressed by fusion with a P2A sequence after UL36. Previous work demonstrated that fusing tags via a P2A linker to UL36 did not impact its anti-apoptotic functions but provided for immediate early tag expression¹⁹². RatCD2 was expressed on the cell surface, allowing MACS separation by first staining with Anti-RatCD2-PE antibody, and then with anti-PE

beads. This process resulted in >90% pure infected population, however, the cells can be in the MACS buffer for an extended period of time, which could reduce the viability of the dendritic cells (Figure 4.2).

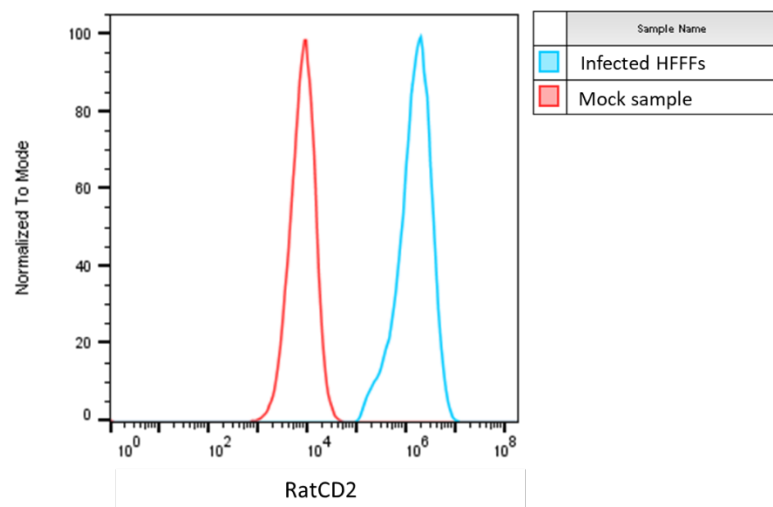


Figure 4.6 – Expression of RatCD2 on the surface of UL36-RatCD2 infected HFFFs.

Although separation with RatCD2 worked well (Figure 4.11), it required two separate incubation steps (one with the anti-RatCD2-PE antibody, and one with the anti-PE beads), with washes in between. Magnetic beads are available that are directly conjugated to antibodies that bind to epitope tags (e.g. HA or FLAG). Use of these would require only one staining step. Viruses were therefore constructed that expressed proteins containing HA or Flag epitope tags on the cell surface. Flow cytometry showed that although anti-tag antibodies bound to these proteins on the cell surface, the level of binding wasn't sufficient to permit reliable MACS sorting (not shown). Five additional constructs were therefore made in which multiple copies of the epitope tags were inserted (Figure 4.7). Three of the constructs also contained GFP, which would allow simpler detection of the infected cells without the requirement for an antibody.

To test these constructs, HFFFs were infected using supernatant from transfected HFFFs, at low MOI, then stained and analysed by flow cytometry 24hrs post-infection. Figure 4.8 shows that three viruses failed to bind the anti-tag antibodies, and two of the GFP-expressing viruses did not show GFP expression. Only two of the viruses,

UL36-P2A-FLAG-RatCD2 and UL36-P2A-3xHA-eGFP-GPI, showed successful binding of the anti-epitope tag antibody on the cell surface, however as can be seen in Figure 4.8A & Cii, the level of antibody binding was not improved compared to the original UL36-RatCD2 virus (Figure 4.8F), so the decision was made to continue using the original in future experiments.

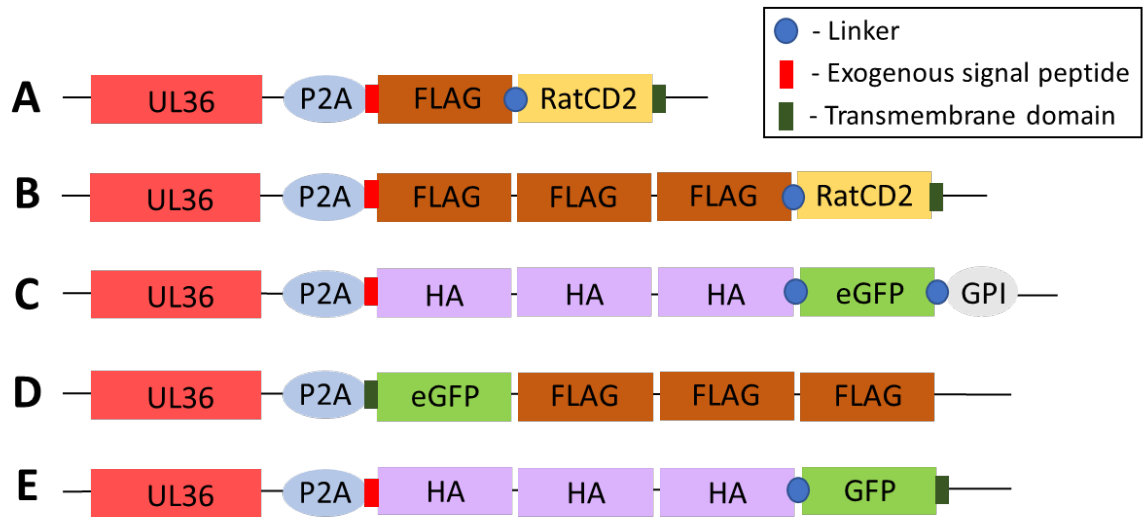


Figure 4.7 – Five UL36 constructs containing epitope tags. A) Single FLAG tag inserted before RatCD2. B) Triple FLAG tag inserted before RatCD2. C) RatCD2 replaced with triple HA tag, linked to eGFP and GPI anchor. D) RatCD2 and exogenous signal peptide replaced with eGFP and triple FLAG tag with a transmembrane domain. E) RatCD2 replaced with a triple HA tag, linked to GFP and a transmembrane domain.

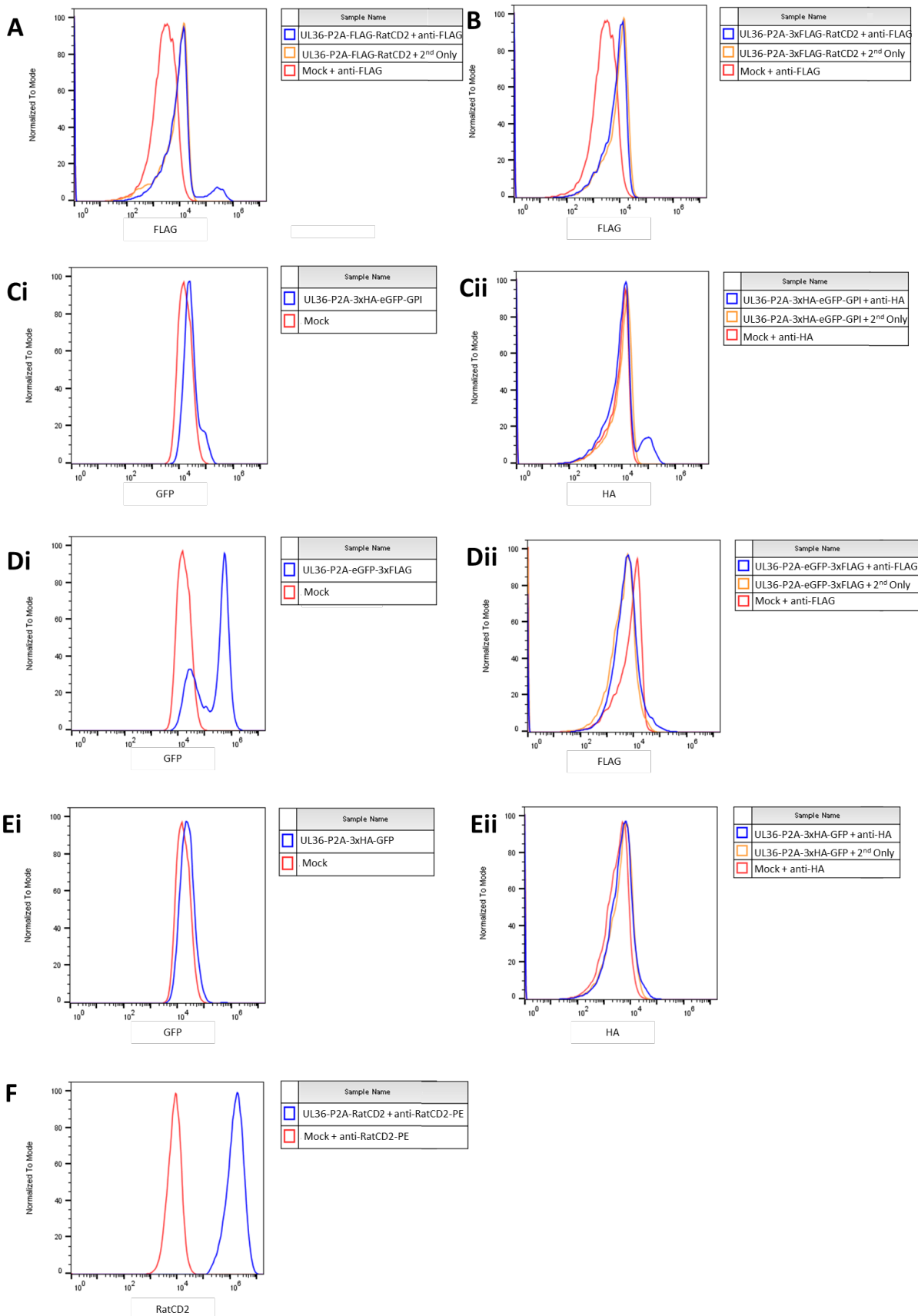


Figure 4.8 – Expression of the new UL36 tags in HFFFs is poor compared to the UL36-P2A-RatCD2 tag. HFFFs were infected with the supernatant from cells transfected with the constructs shown and analysed by flow cytometry (including surface staining for FLAG, HA and RatCD2). A) UL36-P2A-

FLAG-RatCD2 (*pAL2544*). B) *UL36-P2A-3xFLAG-RatCD2* (*pAL2545*). C) *UL36-P2A-3xHA-eGFP-GPI* (*pAL2546*). D) *UL36-P2A-eGFP-3xFLAG* (*pAL2547*). E) *UL36-P2A-3xHA-GFP* (*pAL2550*). F) *UL36-P2A-RatCD2* (*pAL2310*).

In initial experiments, DCs and fibroblasts were separated 24h after co-culture, then infected DCs were separated from bystanders at the time of analysis (24-72 hours later). However, at 48-72h there was poor separation of populations (Figure 4.9). Examination of staining patterns indicated that ‘bystander’ DCs started binding the anti-RatCD2-PE antibody if the infected and uninfected DCs were kept together for 48h or longer (Figure 4.10). This may have been due to bystanders acquiring membranes from the infected cells by phagocytosis or trogocytosis. Ideally, for proteomics we needed $\geq 90\%$ pure population of infected dendritic cells. Therefore, in future experiments, infected and bystander cells were separated the same day as separation from fibroblasts (with a resting period between separations), even if they were analysed at later timepoints. As a result, I obtained $>90\%$ pure populations of infected DCs after passing the cells through only one LS column (Figure 4.11).

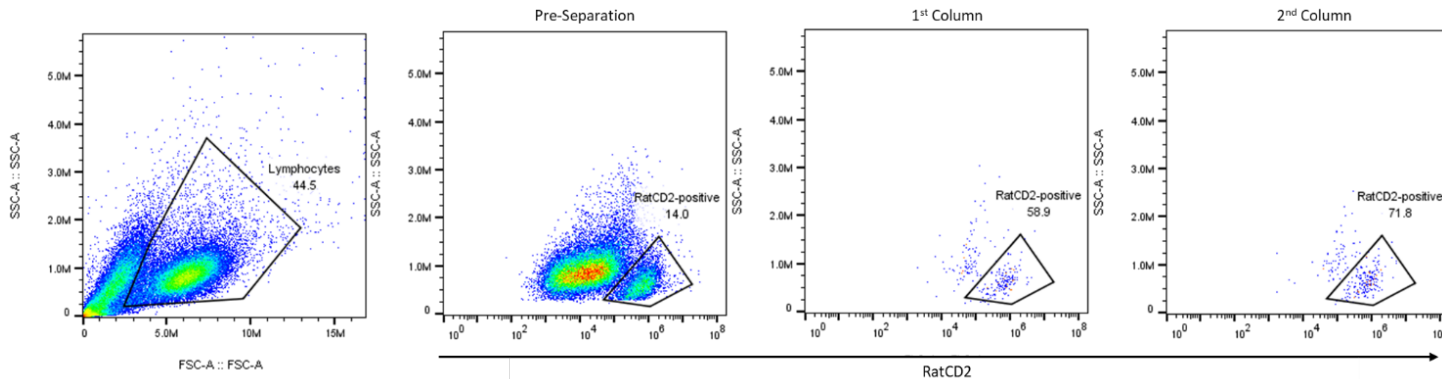


Figure 4.9 – Infected DCs and bystanders separated 72 hours after co-culture and passed through two LS columns. DCs were co-cultured with UL36-P2A-RatCD2 infected HFFF-His cells for 24hrs before being separated by MACS, infected and bystander DCs were kept in culture until 72hrs post co-culture when they were then stained with anti-PE and anti-IgG beads for MACS. When the purity of the desired population is <90%, the retained sample was passed through another LS column.

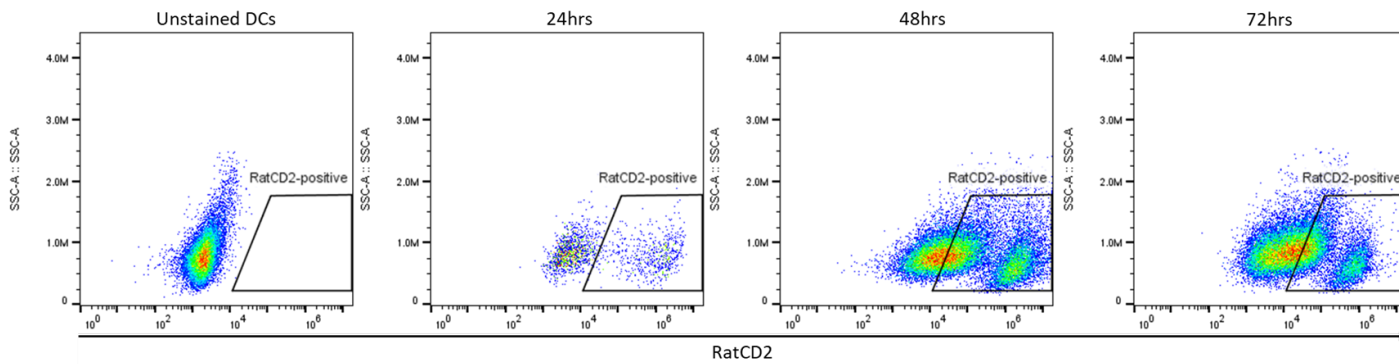


Figure 4.10 – Bystander DCs shift towards the RatCD2+ population during culture. DCs were co-cultured with UL36-P2A-RatCD2 infected HFFF-His cells for 24hrs before being separated by MACS, infected and bystander DCs were kept in culture and samples taken for flow cytometry at 24hr intervals and stained with anti-RatCD2-PE antibody.

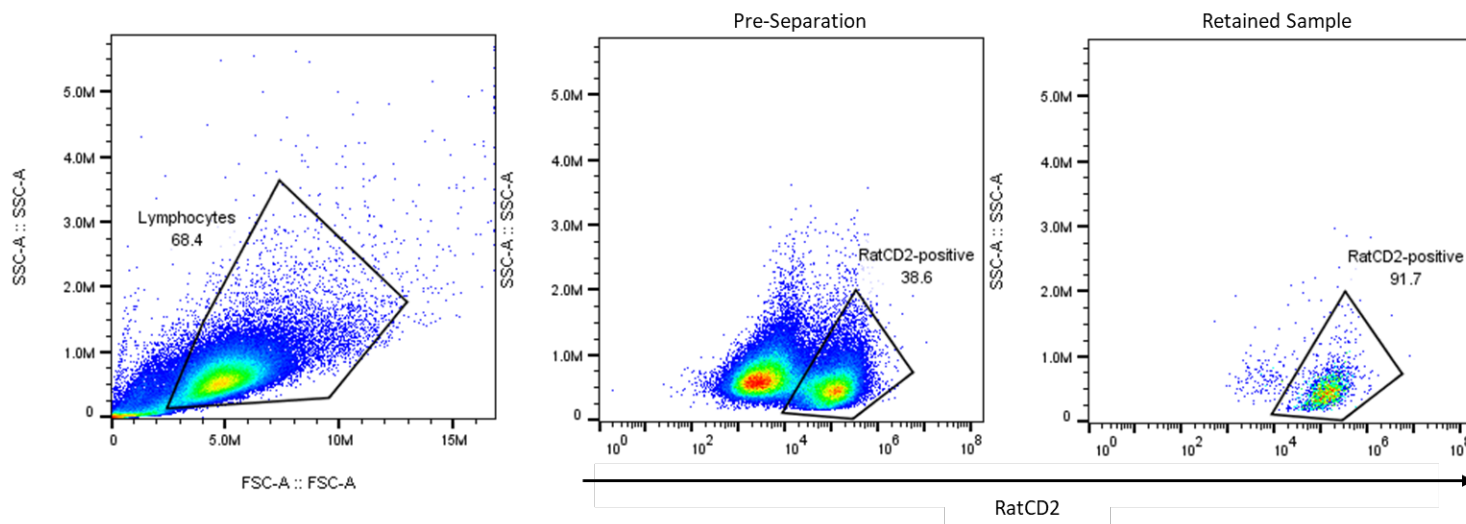


Figure 4.11 – Infected DC population purity can be improved by separating from bystanders at 24hrs post co-culture. Infected DCs and bystanders separated 24 hours after co-culture (2hrs rest after HFFF separation) using anti-PE and anti-IgG beads and MACS, separation required passing the cells through only one LS column.

4.1.3 Preparing Dendritic Cells for Proteomic Analysis

Following separation, the pure populations of infected, bystander and uninfected dendritic cells can either be lysed directly in a guanidine buffer to obtain whole cell lysates (WCL), or cells can be fractionated into subcellular compartments prior to lysis. Given that many functions of DCs depend on interactions of cell-surface proteins with other ligands and cell types, we also isolated plasma membrane proteins. This also enabled us to identify proteins that are retained within the cell by viral proteins – such proteins are downregulated at the cell surface, but maintain the same level in whole-cell lysates.

To isolate proteins found on the cell surface of the DCs, glycoproteins on the plasma membrane (PM) are oxidised and biotinylated, the cells lysed, then streptavidin beads used to purify biotinylated proteins¹⁷². This technique has previously been optimised and shown to provide a much higher level of plasma membrane protein purification than other techniques. Prior to labelling, cells were purified on histopaque to remove any dead or dying cells. When using this technique on fibroblasts, oxidation and aminoxy-biotinylation were performed at the same time, in the presence of aniline, which catalyses the biotinylation. With DCs however, all cells lysed during the procedure. By incubating cells with each reagent individually, we determined that it was a combination of the Aniline and the mixing method that caused the problems; this could be avoided by including FCS in the aniline, however FCS was incompatible with the oxidation step. Therefore, on further samples a two-step method was used: oxidation was performed first (without FCS), then aminoxy-biotinylation with FCS (and Aniline) on a Falcon roller at slow speed, with PBS + 5% FCS washes in between steps.

The samples, either WCL or PM, were then digested into peptides and labelled with 10-plex TMT reagents, before being mixed together and analysed by mass spectrometry. The combination of 10-plex TMT reagents and the ‘MS3’ method of analysis on an Orbitrap Fusion MS, enables accurate comparative quantitation to be performed between samples that are mixed together in a single run on the MS. We compared protein levels in uninfected DCs (to provide a baseline for protein expression), as well as infected or bystander cells. The bystander samples permit identification of protein changes that have occurred in a DC that has detected HCMV infection, but not become infected itself.

4.2 Quantitative Proteomics of Wildtype HCMV-Infected Dendritic Cells

4.2.1 Whole Cell Lysate

Whole cell lysates were generated previously in the lab. In analysis, uninfected DCs were compared to infected or bystander cells at multiple timepoints – 24, 48 or 72h. These timepoints represent the immediate early, early and late phases in fibroblasts. We used two uninfected samples – one taken immediately prior to co-culture, and one from 24h later, when the fibroblast and DCs were separated. We also included a sample of DCs that had been treated with LPS, in order to determine how protein levels compare in immature to mature DCs. 7992 proteins were quantified, 99 of which were downregulated at least 3-fold by HCMV. 63 of these were not quantified in previous HFFF proteomic analysis¹⁷², and therefore may to be specifically involved in DC function. Hierarchical cluster analysis (Figure 4.12) showed that the infected samples all clustered together, but clustered separately to the bystander samples, indicating that HCMV is actively modulating protein levels in DCs. Furthermore, the LPS samples were clearly distinct to the bystanders (which were themselves distinct to uninfected cells), indicating that bystanders are not simply undergoing maturation in response to infection, but may themselves be ‘modulated’ as a result of infection.

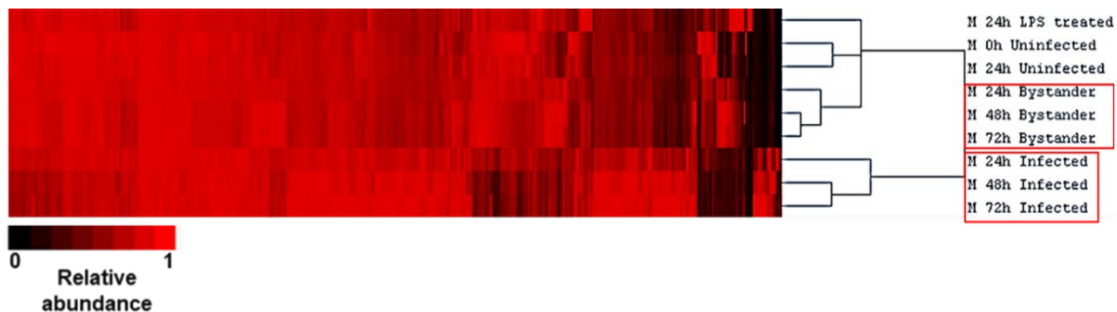


Figure 4.12 – Hierarchical cluster of DC whole cell lysate. This shows the relative abundance of proteins across all samples.

4.2.2 Plasma Membrane

For the plasma membrane analysis, the isolation of a sub-fraction of the cell means that higher cell numbers were required as compared to the WCL. Therefore only a single timepoint was analysed. 72h was chosen since viability of DCs reduces over time, yet most viral genes should be expressed by this time. Two donors were used, to provide a test of inter-donor variation. When the samples were processed, 703 proteins were quantified, 43 of which were downregulated (28 of these were not quantified in HFFFs), and 53 upregulated (15 were not quantified in previous HFFF analyses). The fact that many proteins from both datasets were not quantified in fibroblasts suggests that HCMV infection is specifically modulating DC function. As with the WCL, hierarchical cluster (Figure 4.13) showed a clear difference between the infected and bystander samples, with the two donors clustering together. Thus there is limited inter-donor variation.

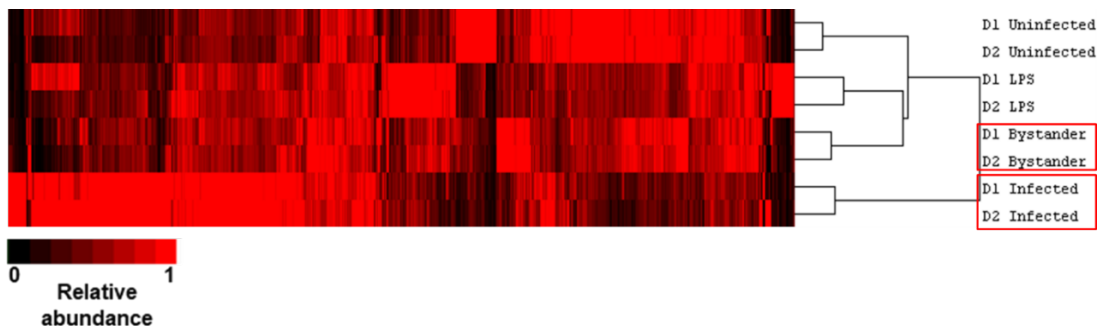


Figure 4.13 – Hierarchical cluster of DC plasma membrane. This shows the relative abundance of proteins across all samples.

4.2.3 Positive Controls

In order to validate the proteomics data, we compared the levels of proteins in our dataset to published data. CD1b and CD1c are both expressed on antigen presenting cells (APCs), and are involved in presenting lipids to T cells. These proteins are known to be downregulated by HCMV¹⁹³, and were similarly downregulated >2-fold when compared to uninfected and bystander samples (Figure 4.14). Other positive controls used for validation included CD1a¹⁹³, Sp100¹⁹⁴, and human leukocyte antigens (HLAs)^{195, 196} (Figure 4.14).

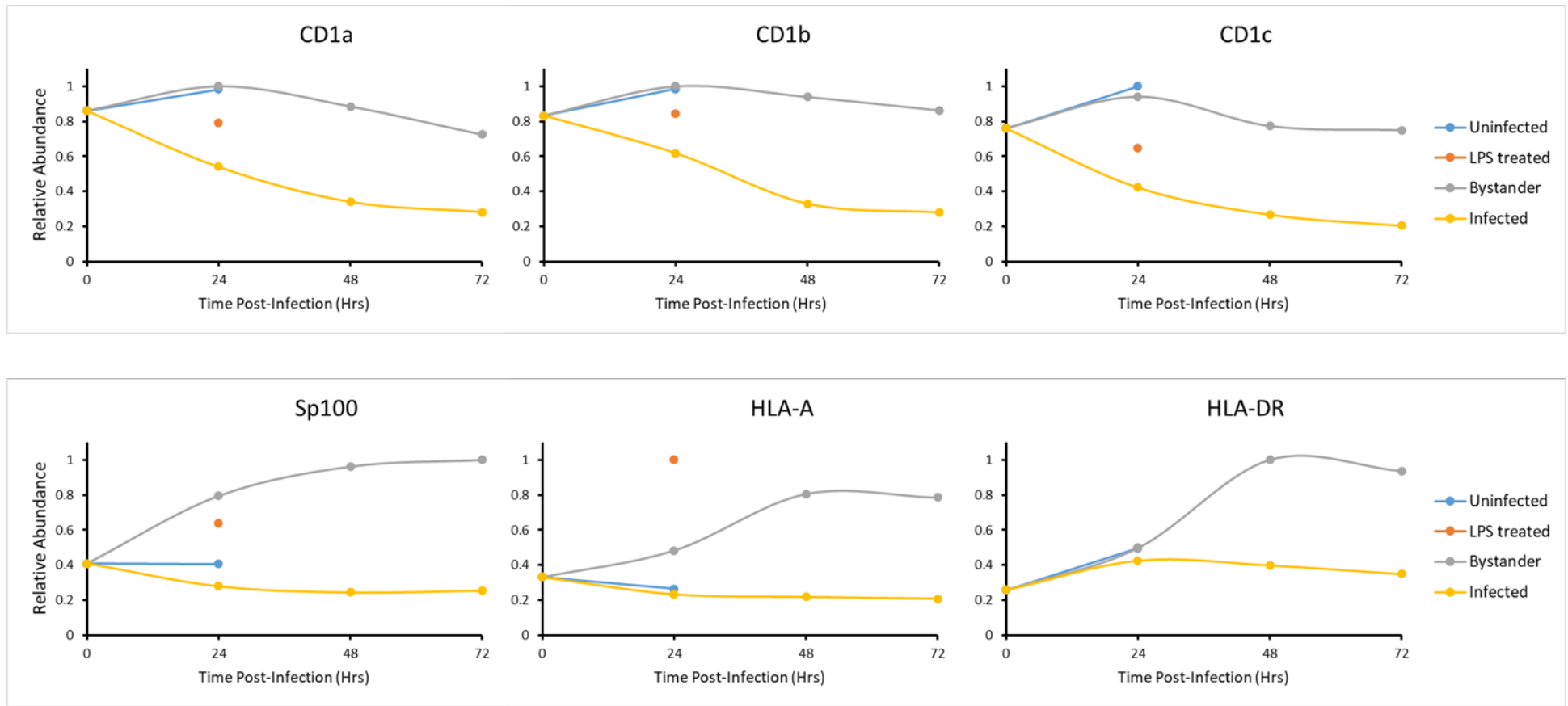


Figure 4.14 – Relative abundance of several proteins in dendritic cells, which are known to be downregulated by HCMV^{193, 194, 195, 196}

4.2.4 DAVID Pathway Analysis

Database for annotation, visualization and integrated discovery (DAVID) pathway analysis (Figure 4.15) groups proteins that are modified in a dataset by function. Analysis of the proteomics datasets showed that downregulated proteins were enriched for those involved in innate and adaptive immunity, while upregulated proteins were enriched for endopeptidase inhibitor activity – endopeptidases are involved in toll-like receptor (TLR) signalling and anti-influenza immune responses^{197, 198}. This further underlined that HCMV modulation of proteins in DCs is likely to result in inhibition of the ability of DCs to mount an optimal adaptive immune response.

Whole Cell Lysate				Plasma Membrane ↓			
Term	Count	Fold Enrichment	Benjamini	Term	Fold Enrichment	Benjamini	
topological domain:Extracellular	29	5.0	1.70E-10	topological domain:Extracellular	1.82	4.30E-07	
Adaptive immune response	8	10.3	0.001438	IPR013783:Immunoglobulin-like fold	2.91	9.71E-06	
Innate immunity	9	5.0	0.004868	transmembrane region	1.47	6.58E-05	
domain:C-type lectin	5	30.9	0.001007	GO:0002250:adaptive immune response	6.02	0.0019446	
interferon-gamma-mediated signaling pathway	8	12.7	4.76E-04	IPR03599:Immunoglobulin subtype	3.35	0.0012798	
External side of plasma membrane	9	9.9	1.66E-04	Plasma Membrane ↑			
Systemic lupus erythematosus	5	10.1	0.028412	Term	Fold Enrichment	Benjamini	
Secreted	12	3.1	0.016373	GO:0010951:negative regulation of endopeptidase activity	6.75	2.43E-04	
Chemotaxis	4	9.3	0.254991	GO:0004866:endopeptidase inhibitor activity	7.37	0.008437	
MHC classes I/I-like antigen recognition protein	4	14.3	0.061285	GO:0005576:extracellular region	3.14	3.52E-07	
Type I interferon signaling pathway	6	12.9	0.008231	GO:0004867:serine-type endopeptidase inhibitor activity	7.22	0.004075	
Ligase activity	3	1.5	0.999072	hsa04610:Complement and coagulation cascades	6.01	0.001318	

Figure 4.15 – DAVID pathway analysis of fractionated DC whole cell lysate and plasma membrane samples shows enrichment of proteins involved in the immune response.

4.2.5 Target Proteins

Many of the proteins that were modulated by infection in the proteomics data were involved in DC maturation and T and B cell activation. From the large list of potential targets that could be followed up in greater detail, we compiled a list of 15 target proteins (Table 4.1) – see Figure 4.16 for selection criteria. Six proteins from the plasma membrane dataset, 5 proteins from whole cell lysate, and 4 from both datasets. The functions of each protein were identified using UniProt¹⁹⁹, NCBI Gene and literature.

- Activated leukocyte cell adhesion molecule (ALCAM), expressed on APCs, binds to CD6 on T cells at the point of contact between the DC and T cell. This interaction promotes early DC-T cell binding and DC-induced T cell

proliferation²⁰⁰. ALCAM was found to be downregulated at the plasma membrane of infected DCs, but not in fibroblasts (Table 4.1).

- Caspase 10 (CASP10) is involved in both Fas- and TNFR-mediated apoptosis. This proteolytic enzyme was found to be downregulated in the whole cell lysate – and this effect was specific to DCs (Table 4.1). It is unsurprising that Caspase 10 is downregulated as HCMV encodes several apoptosis inhibitors, however none have been shown to target Caspase 10.
- CD84 (SLAM family) promotes autophagy in monocyte-derived DCs via regulation of IRF8²⁰¹. Autophagy is linked to multiple DC functions including maturation, antigen stimulation and T cell activation²⁰². CD84 is downregulated in DCs by HCMV at the plasma membrane and in the whole cell lysate (Table 4.1).
- Dectin-1 (CLEC7A) is a pattern recognition receptor (PRR) found on DCs that signals via the Syk pathway – signalling through this pathway activates DCs and allows them to prime Th1, Th17 and CD8+ T cell responses²⁰³. This protein was downregulated >3-fold in the whole cell lysates of infected DCs, and was not quantified in the HFFF dataset (Table 4.1).
- ICAM3 is found expressed on all leukocytes and is a ligand for LFA-1 – it is not only involved in cell adhesion, but also in the generation of the adaptive immune response²⁰⁴. Table 4.1 shows that ICAM3 was downregulated following HCMV infection.
- ICOSL (ICOSLG) is the ligand for ICOS expressed on activated T cells. The engagement of ICOSL and ICOS provides a co-stimulatory signal that results in T cell proliferation. Modulation of this interaction allows HCMV to manipulate the secondary immune response via DC infection.
- Interferon regulatory factor 7 (IRF7), in response to viral infection, triggers the activation of the type I interferon (IFN) genes. Kaposi's sarcoma-associated herpesvirus (KSHV) modulates the type I IFN response by preventing accumulation of IRF7 in the nucleus²⁰⁵ – in contrast HCMV infection results in downregulation of IRF7.
- Lymphocyte activating gene 3 (LAG3) has multiple functions. It is able to trigger maturation of DCs following binding to MHC-II^{206,207}, but overall, this protein has a negative regulatory role in the immune system. It is surprising

then, that LAG3 is downregulated both in the cell lysate and at the plasma membrane.

- c-Met (MET), the only protein selected that has been upregulated (25-fold at cell surface), is a receptor for hepatocyte growth factor. The addition of hepatocyte growth factor to DCs reduces antigen presentation and therefore T cell proliferation²⁰⁸.
- Osteoclast-associated immunoglobulin-like receptor (OSCAR) is expressed on the cell surface of DCs, and was found in the plasma membrane proteomic dataset. Upon binding of antigen to OSCAR, DCs are activated, and the antigen is processed and presented to CD4 T cells²⁰⁹.
- PECAM1 is involved in the reverse transmigration of DCs, where DCs enter the lymphatic system from peripheral tissues – a crucial step in priming the adaptive arm of immunity²¹⁰. This protein is downregulated following HCMV infection, further underlining that HCMV is modulating the immune response by manipulating DCs.
- SCIMP regulates Dectin-1-dependent MAP kinase activation, which in turn regulates downstream production of TNFa, IL6 and pro-inflammatory cytokines in dendritic cells²¹¹. SCIMP was found to be downregulated by HCMV but not quantified in HFFFs (Table 4.1).
- SECTM1 is found as both membrane-bound and soluble forms, is a ligand for CD7 and synergises with CD28 on T cells. Recent studies have shown that the soluble form of this protein enhances CD4 and CD8 T cell proliferation and IL2 production²¹².
- Semaphorin-4A (SEMA4A) expressed on dendritic cells plays a role in activating and differentiating T cells *in vitro*, and in priming antigen-specific T cells *in vivo* via TIM2²¹³. SEMA4A is downregulated at both the plasma membrane and in the whole cell lysate (Table 4.1).
- Leukosialin (CD43, SPN) is expressed on most cells of haematopoietic lineage and was also found in the HFFF dataset. Cross-linking of leukosialin expressed on DCs results in their maturation, leading to a decrease in endocytic activity and an increase in antigen presentation to T cells²¹⁴. Table 4.1 shows that leukosialin is only downregulated in the dendritic cells.

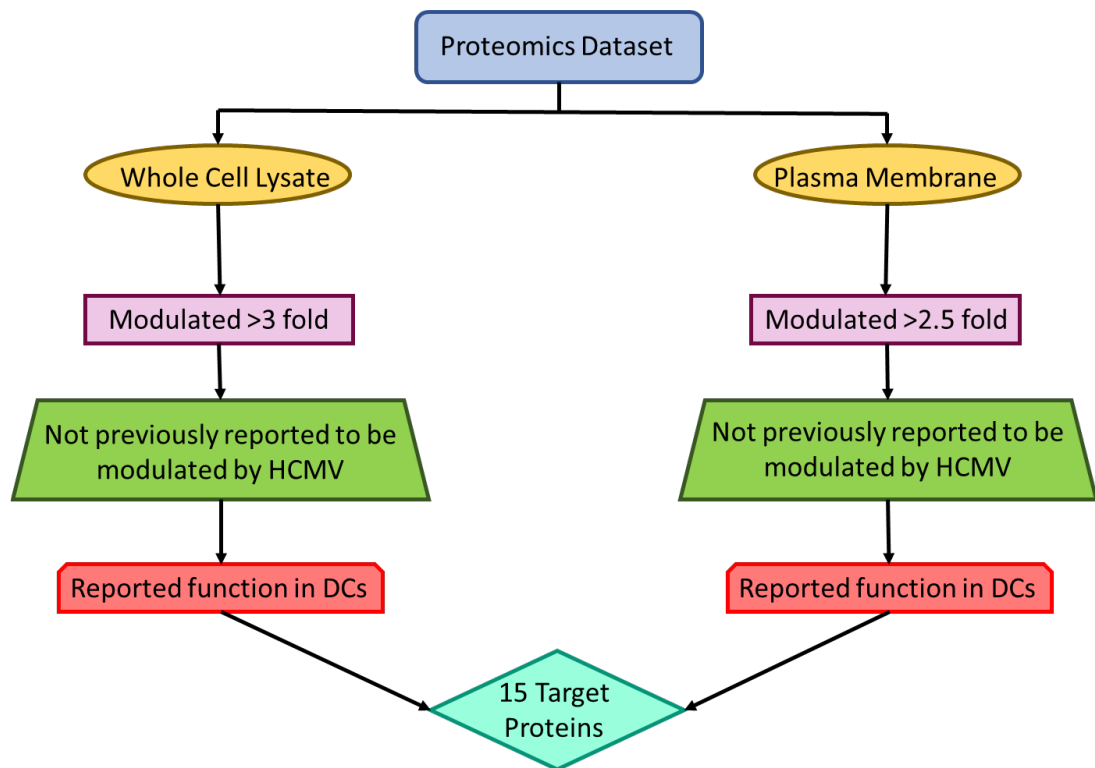


Figure 4.16 – Flow diagram of selection criteria for target proteins identified in proteomics data sets.

Gene Symbol	Description	Downregulated?	Upregulated?	Effects in DCs only?	Not Quantified in HFFFs	PM & WCL?
<i>ALCAM</i>	Activated leukocyte cell adhesion molecule, isoform 2 of CD166 antigen	✓				PM
<i>CASP10</i>	Caspase 10	✓			✓	WCL
<i>CD84</i>	Self-ligand receptor of the signalling lymphocytic activation molecule (SLAM) family member 5	✓			✓	Both
<i>CLEC7A</i>	Dectin-1, C-type lectin domain family 7 member A, CD369	✓			✓	WCL
<i>ICAM3</i>	Intracellular adhesion molecule 3	✓			✓	WCL
<i>ICOSLG</i>	Inducible T-cell co-stimulator ligand (ICOSL), CD275	✓				Both
<i>IRF7</i>	Interferon regulatory factor 7	✓			✓	WCL
<i>LAG3</i>	Lymphocyte activation gene 3 protein, CD223	✓			✓	Both
<i>MET</i>	c-Met, tyrosine-protein kinase Met, hepatocyte growth factor (scatter factor) receptor		✓	✓		PM
<i>OSCAR</i>	Isoform 3 of Osteoclast-associated immunoglobulin-like receptor	✓			✓	PM
<i>PECAMI</i>	Platelet endothelial cell adhesion molecule, CD31	✓		✓		PM
<i>SCIMP</i>	SLP adapter and CSK-interacting membrane protein	✓			✓	WCL
<i>SECTM1</i>	Secreted and transmembrane protein 1	✓			✓	Both
<i>SEMA4A</i>	Semaphorin-4A	✓			✓	PM
<i>SPN</i>	Leukosialin/CD43	✓		✓		PM

Table 4.1 – Targets chosen from list of proteomic hits from both data sets. PM = plasma membrane. WCL = whole cell lysate.

4.2.6 Validation of Target Proteins

To validate the accuracy of the proteomics dataset, the level of knockdown for the selected proteins was determined by an alternative method. DCs were co-cultured with HFFFs for 24 hours, and then infected DCs were purified as before – however, for Dectin-1, downregulation was clearer when using a UL36-GFP tagged virus (pAL2344), and in this case, infected and bystander DCs were not separated. Infected, bystander and uninfected DCs were stained at 48 hours post co-culture with the relevant antibodies either intracellularly or on the surface, fixed and analysed.

Flow cytometry has confirmed what was seen in the proteomics for 10 out of 15 of the identified target proteins so far. The protein levels of targets that were not validated by flow cytometry were then analysed by Western Blot, however the antibodies used did not stain the membranes. The validation for each of the identified proteins is summarised in Table 4.2.

Protein	Validation Method
<i>ALCAM</i>	Flow cytometry – surface staining
<i>Caspase 10</i>	Not yet validated
<i>CD84</i>	Flow cytometry – surface staining
<i>Dectin-1</i>	Flow cytometry – surface staining
<i>ICAM3</i>	Not yet validated
<i>ICOSL</i>	Flow cytometry – surface staining
<i>IRF7</i>	Not yet validated
<i>LAG3</i>	Not yet validated
<i>c-Met</i>	Flow cytometry – surface staining
<i>OSCAR</i>	Flow cytometry – surface staining
<i>PECAM1</i>	Flow cytometry – surface staining
<i>SCIMP</i>	Flow cytometry – intracellular staining
<i>SECTM1</i>	Not yet validated
<i>Semaphorin-4A</i>	Flow cytometry – surface staining
<i>Leukosialin</i>	Flow cytometry – surface staining

Table 4.2 – Summary of how each of the selected proteins was validated.

4.2.6.1 ALCAM

As in the proteomics, levels of ALCAM on the surface of dendritic cells were reduced following infection (Figure 4.17), although the magnitude of the reduction was relatively small.

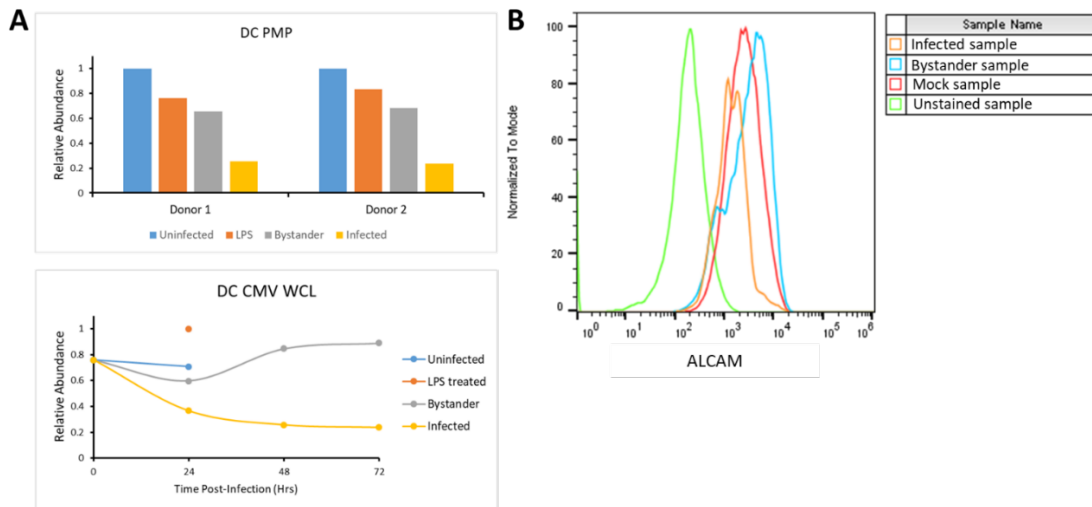


Figure 4.17 – Validation of ALCAM downregulation using flow cytometry. A) Modulation seen in proteomics data sets. B) ALCAM expression in bystander, mock and infected DC samples.

4.2.6.2 Caspase 10

Intracellular staining of the DC samples with Caspase 10 antibody did not convincingly show downregulation of the protein in infected cells (Figure 4.18), and attempts to use Western Blot for validation were unsuccessful (not shown).

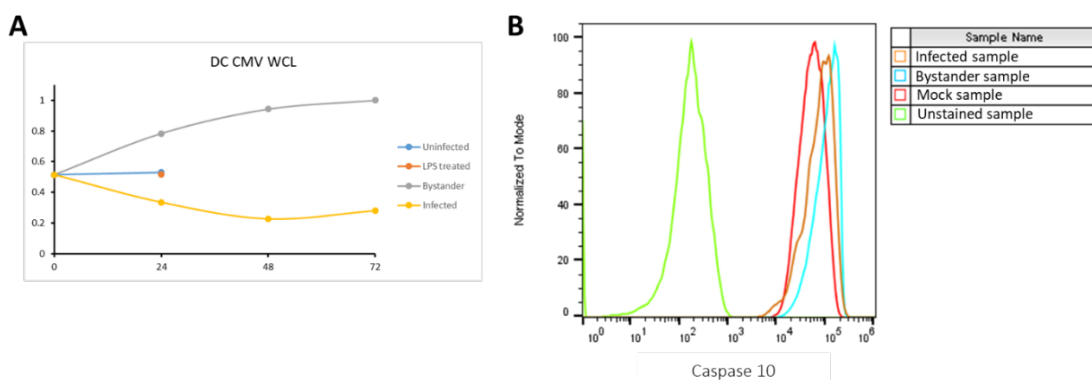


Figure 4.18 – Validation of Caspase 10 downregulation using flow cytometry. A) Modulation seen in proteomics data sets. B) Caspase 10 expression in bystander, mock and infected DC samples.

4.2.6.3 CD84

Staining of CD84 shows that this protein is substantially downregulated in infected cells, as was seen in the proteomics data (Figure 4.19).

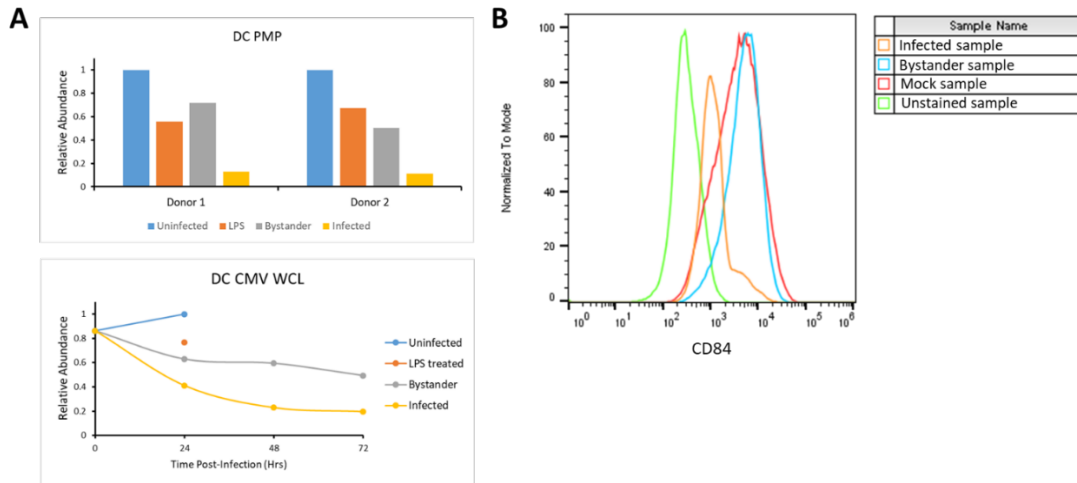


Figure 4.19 – Validation of CD84 downregulation using flow cytometry. A) Modulation seen in proteomics data sets. B) CD84 expression in bystander, mock and infected DC samples.

4.2.6.4 Dectin-1

When analysing Dectin-1 expression by flow cytometry, it was clear that there was a difference between the infected and bystander DCs, as seen in Figure 4.20, which correlated with the effects seen in the proteomics data.

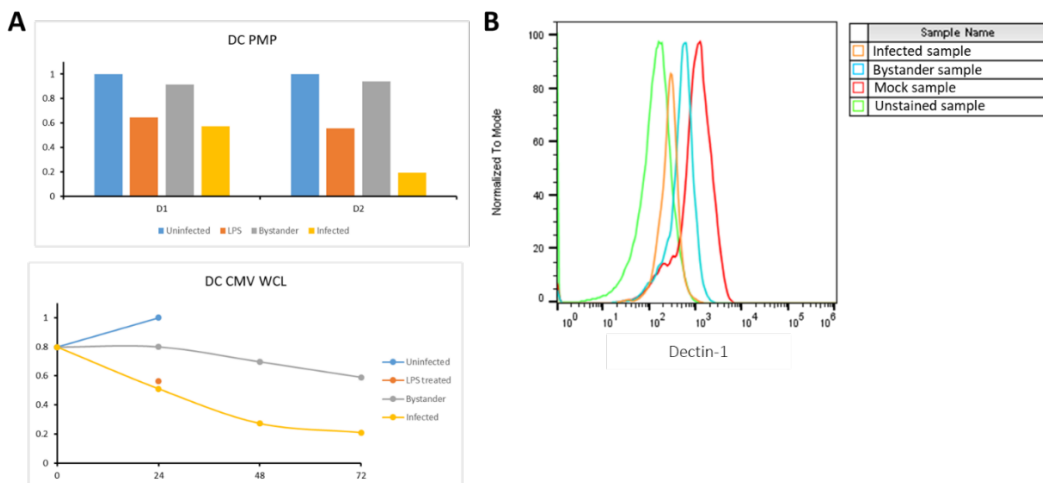


Figure 4.20 – Validation of Dectin-1 downregulation using flow cytometry. A) Modulation seen in proteomics data sets. B) Dectin-1 expression in bystander, mock and pAL2344-infected DC samples.

4.2.6.5 ICAM3

Similarly to Caspase 10, analysis using flow cytometry failed to validate the difference of ICAM3 expression levels between samples, shown in Figure 4.21. However staining levels were weak, and attempts to use Western Blot also showed poor staining for ICAM3 (not shown).

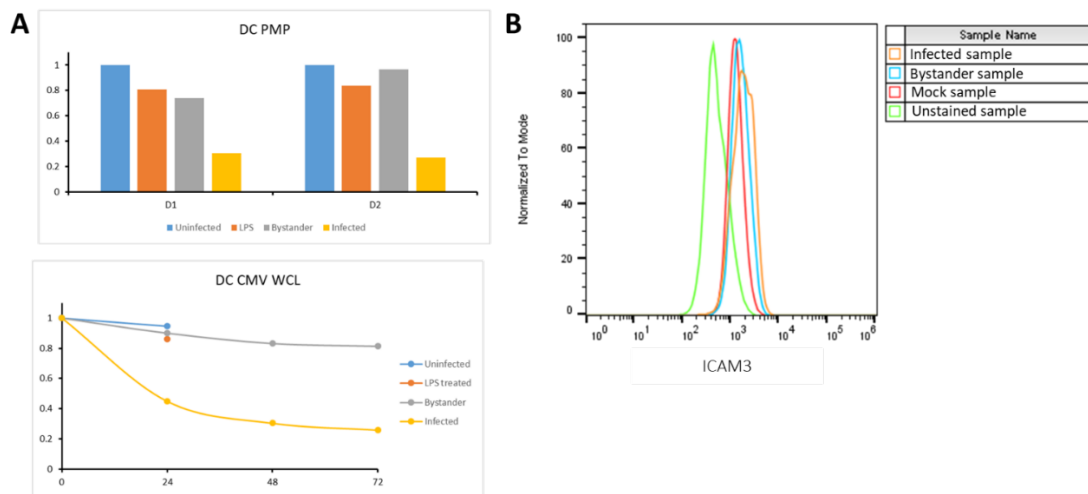


Figure 4.21 – Validation of ICAM3 downregulation using flow cytometry. A) Modulation seen in proteomics data sets. B) ICAM3 expression in bystander, mock and infected DC samples.

4.2.6.6 ICOSL

Expression levels of ICOSL saw substantial downregulation in infected DCs compared to uninfected and bystander samples (Figure 4.22), which matches nicely with what was seen in the proteomics dataset.

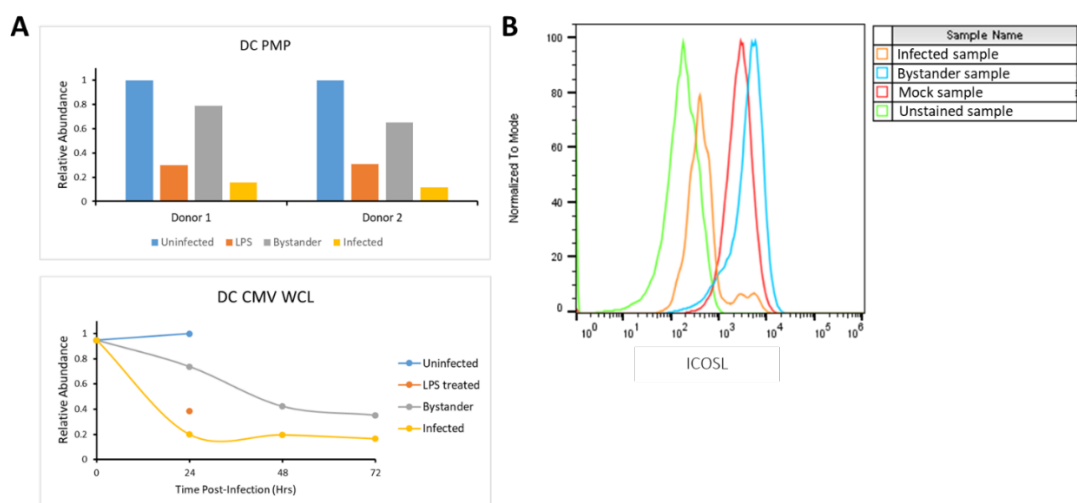


Figure 4.22 – Validation of ICOSL downregulation using flow cytometry. A) Modulation seen in proteomics data sets. B) ICOSL expression in bystander, mock and infected DC samples.

4.2.6.7 IRF7

Validation of IRF7 downregulation was attempted using an immunofluorescence assay. However, staining was inadequate and it was difficult to establish what was background fluorescence and what was real IRF7 expression (Figure 4.23). When using Western Blot to validate IRF7 expression, the antibody failed to stain the membrane (not shown).

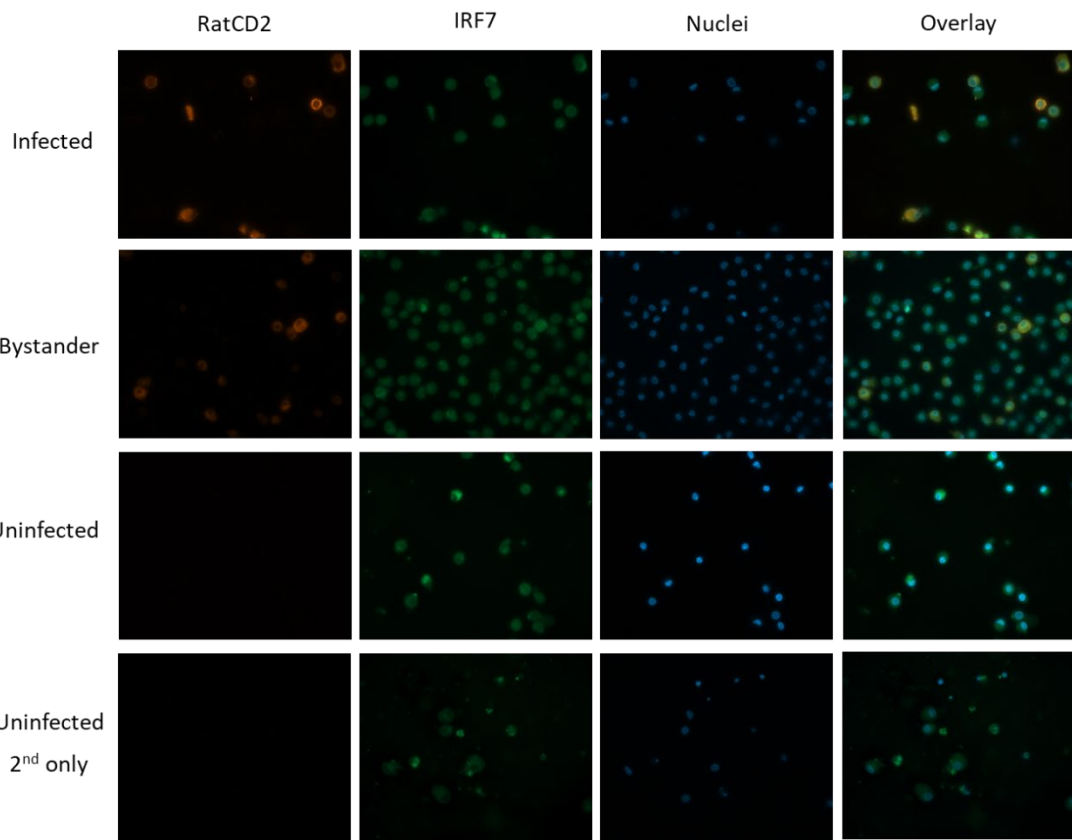


Figure 4.23 – Validation of IRF7 using IFA. DCs were co-cultured with UL36-RatCD2 infected HFFF-His cells for 24hrs before being separated by MACS; infected and bystander DCs were separated by MACS 2hrs after HFFF separation. DCs were seeded onto glass-bottomed 96-well plates treated with poly-D-lysine hydrobromide before being fixed, permeabilised and stained with RatCD2-PE, rabbit anti-IRF7, anti-rabbit AF488 and DAPI after 24hrs.

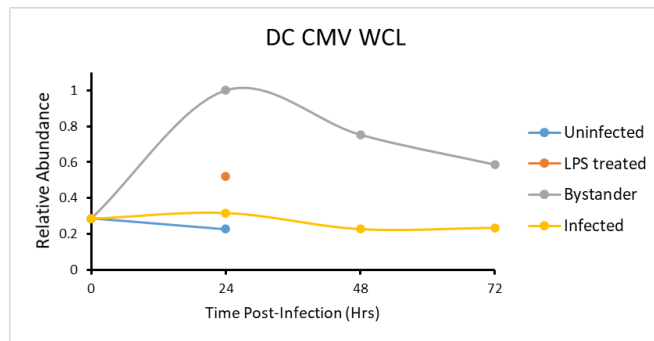


Figure 4.24 – Modulation of IRF7 seen in whole cell proteomics data set.

4.2.6.8 LAG3

When validating the expression of LAG3 following HCMV infection, the result seen was the opposite to that observed in the proteomics dataset – LAG3 was weakly

upregulated in the infected DCs (Figure 4.25). The expression of LAG3 was not able to be confirmed by Western Blot either (not shown).

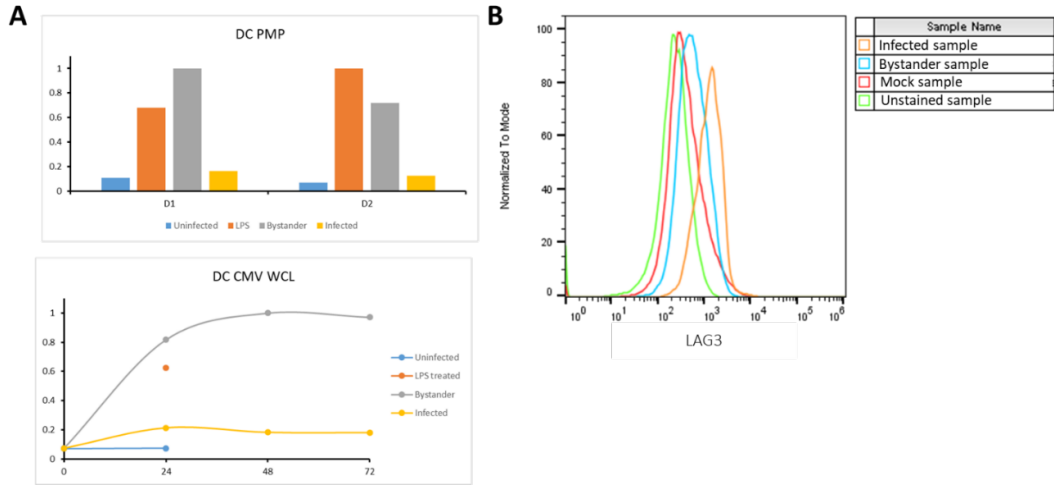


Figure 4.25 – Validation of LAG3 downregulation using flow cytometry. A) Modulation seen in proteomics data sets. B) LAG3 expression in bystander, mock and infected DC samples.

4.2.6.9 c-Met

The expression of c-Met on the dendritic cell membrane confirmed what was observed in the proteomics, expression on infected DCs is higher than that on uninfected and bystander cells (Figure 4.26).

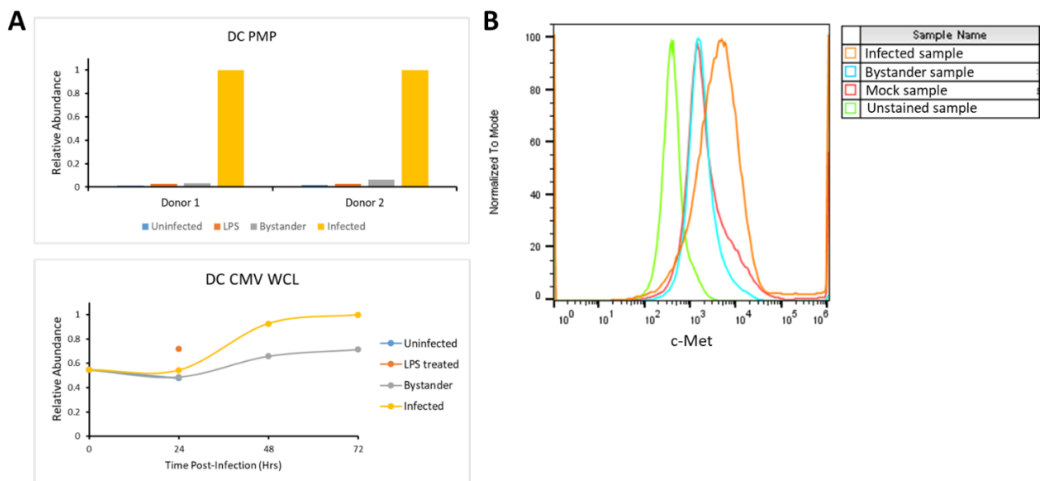


Figure 4.26 – Validation of c-Met upregulation using flow cytometry. A) Modulation seen in proteomics data sets. B) c-Met expression in bystander, mock and infected DC samples.

4.2.6.10 OSCAR

Figure 4.27 demonstrates that the downregulation of OSCAR that was seen in the proteomics can also be seen when analysed by flow cytometry.

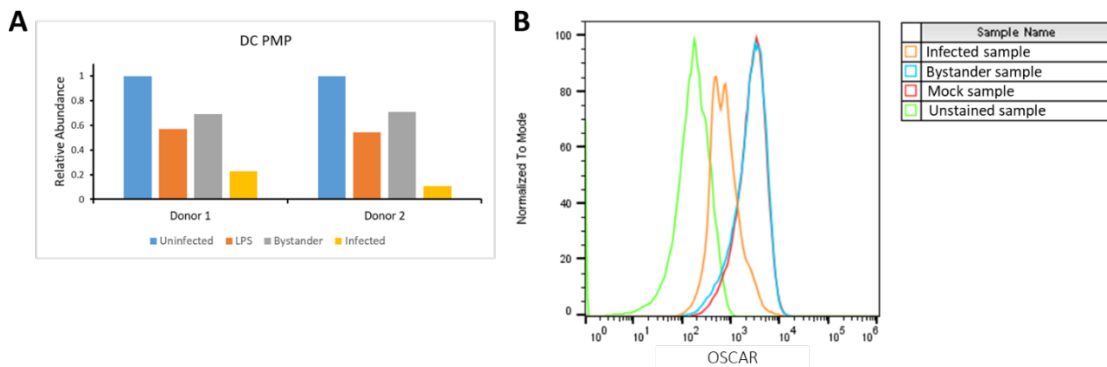


Figure 4.27 – Validation of OSCAR downregulation using flow cytometry. A) Modulation seen in proteomics data sets. B) OSCAR expression in bystander, mock and infected DC samples.

4.2.6.11 PECAM1

PECAM1 expression was downregulated in infected DCs when compared to infected and bystander DCs, this correlates with the proteomics dataset (Figure 4.28).

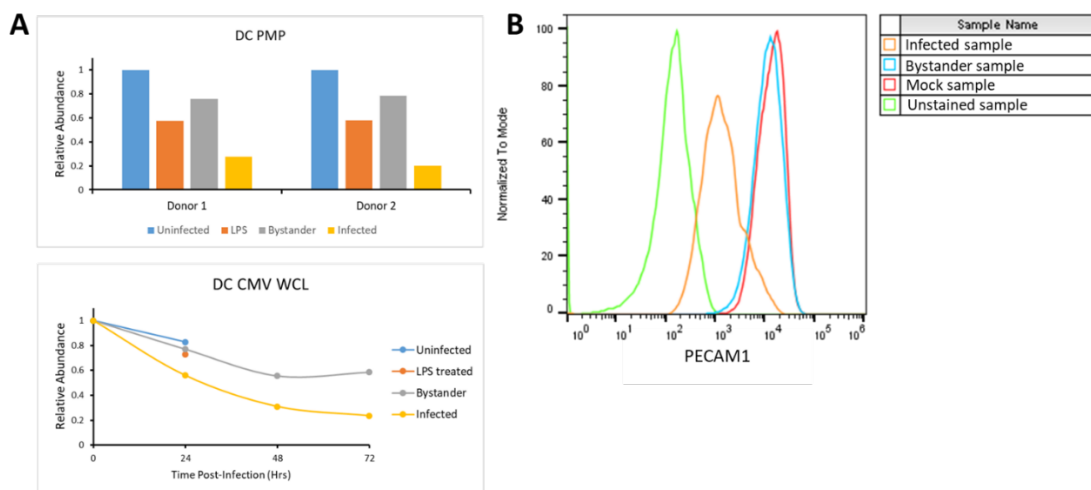


Figure 4.28 – Validation of PECAM1 downregulation using flow cytometry. A) Modulation seen in proteomics data sets. B) PECAM1 expression in bystander, mock and infected DC samples.

4.2.6.12 SCIMP

The protein levels of SCIMP when analysed by intracellular flow cytometry were higher in infected DCs than in the mock sample (Figure 4.29). This does not completely match with the proteomics data, however, the intracellular levels of SCIMP in infected DCs were lower than in the bystanders.

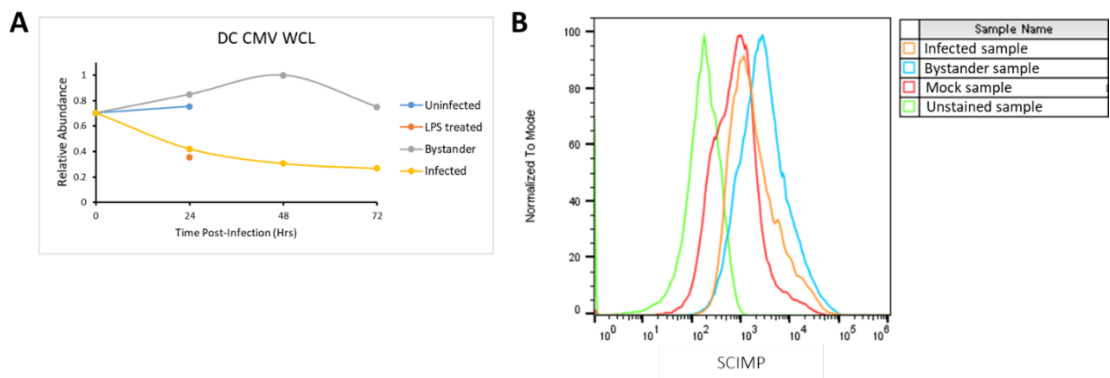


Figure 4.29 – Validation of SCIMP downregulation using flow cytometry. A) Modulation seen in proteomics data sets. B) SCIMP expression in bystander, mock and infected DC samples.

4.2.6.13 SECTM1

When analysing the expression levels of SECTM1, this protein was not downregulated convincingly when comparing the infected to bystander DCs, as shown in Figure 4.30. Western Blot was then attempted to validate SECTM1 expression in infected DCs, however this was not successful (not shown).

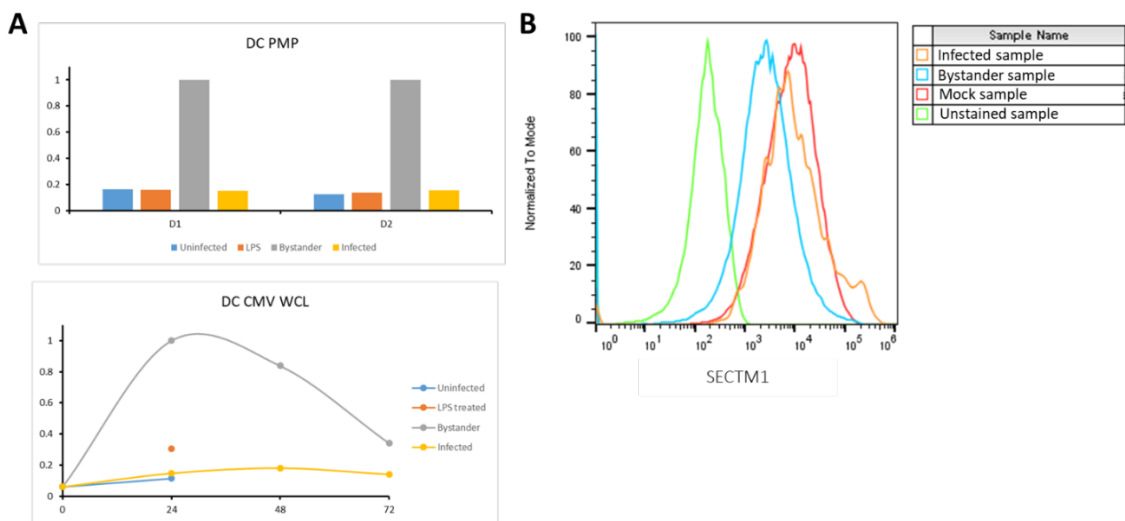


Figure 4.30 – Validation of SECTM1 downregulation using flow cytometry. A) Modulation seen in proteomics data sets. B) SECTM1 expression in bystander, mock and infected DC samples.

4.2.6.14 Semaphorin-4A

Flow cytometric analysis of Semaphorin-4A showed that the expression of this protein complemented the results of the proteomic analysis (Figure 4.31). Semaphorin-4A is downregulated on the surface of infected dendritic cells.

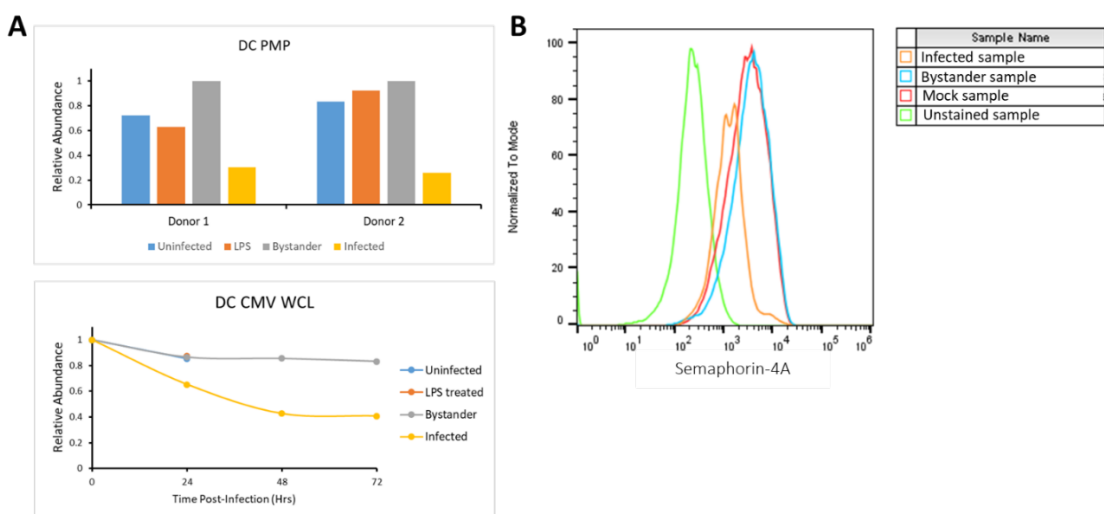


Figure 4.31 – Validation of Semaphorin-4A downregulation using flow cytometry. A) Modulation seen in proteomics data sets. B) Semaphorin-4A expression in bystander, mock and infected DC samples.

4.2.6.15 Leukosialin

Expression levels of Leukosialin were markedly decreased in the infected sample, which corresponds to the effects seen in the proteomics datasets, as seen in Figure 4.32.

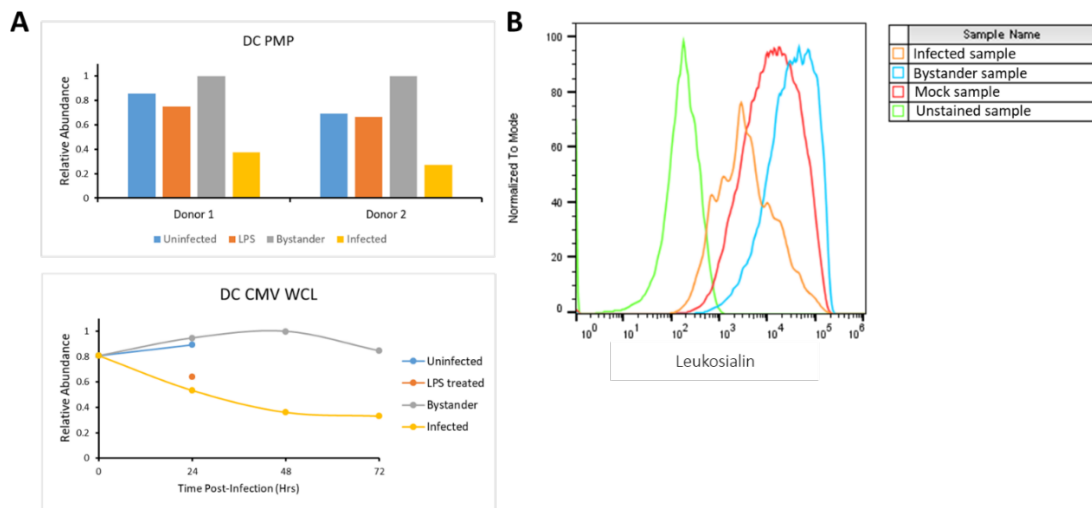


Figure 4.32 – Validation of Leukosialin downregulation using flow cytometry. A) Modulation seen in proteomics data sets. B) Leukosialin expression in bystander, mock and infected DC samples.

4.3 Interactions between Single Deletion Mutants and ICOSL and ALCAM

In order to determine the functional importance of the modifications HCMV causes to DCs following infection, it is necessary to map the viral gene responsible for targeting each cellular gene. We have previously used the approach of making large deletions in the HCMV genome, across a series of different viruses^{24, 153}. Each virus lacks a section containing 2-8 non-essential virus genes. Between this panel of 15 viruses, 45% of the 170 viral genes are knocked out. Using these viruses, it is possible to rapidly shortlist the genes that might be involved in any particular process. To enable this process in DCs, the same large-scale deletions were made in the UL36-P2A-RatCD2 virus (Figure 4.33). All viruses were successfully recovered, and can now be used in experiments (Table 4.3). Due to the COVID-19 pandemic, Dr Andrew Davison's lab in Glasgow University were unable to sequence 14 of the block deletion mutants, hence, Dr Angela Marchbank's group in Cardiff University ran the samples using the same protocol, and the sequenced genomes were then analysed by myself using GRACy and Geneious, as shown in Table 4.4 and Figure 4.34.

GRACy identifies SNPs between a reference sequence, and the data for each particular mutant, and indicates what percentage of reads contain each SNP. Each set of reads were aligned to the 'intended' Merlin genome sequence. Any SNPs present in <10% reads were excluded from analysis. The sequence of UL32 present in the BAC differs from the sequence found in the Merlin genome used as the reference for screening, thus 100% of the SNPs in each of the deletion mutants appears to have a mutated UL32 gene. Aside from this, only two viruses demonstrated SNPs. For UL48 in ΔUS16 (pAL3060), a mutation was observed that replaced a Cytosine with a Guanine, but did not result in a change in the amino acid sequence – this was suspected to have occurred during recombination, but as the substitution did not affect the amino acid sequence the virus is fine for use in infections. A UL78 mutation was seen in ΔUL139-UL150 (pAL3130), but was rare enough that it was not found when reads were manually aligned to the reference sequence, and as such is not a cause for concern.

Reads were also aligned to the wildtype Merlin reference sequence using Geneious, and inspected manually in the region containing the intended modification (Figure

4.33). This was to ensure that where a gene had been deleted, no reads were present. If any reads were present, it would indicate a contaminating wildtype genome in the stock. No such contaminants were seen.

The US12 gene family has been reported to be involved in natural killer (NK) cell evasion²⁴ – this paper performed proteomic analysis of HCMV infection in HFFFs and found that infection with a Δ US12-US21 virus rescued both ALCAM and ICOSL. When investigated with proteomics of single gene deletion mutants, Fielding et al. found Δ US18 and Δ US20 increased the relative abundance of ALCAM, while Δ US16 and Δ US20 were responsible for that of ICOSL, however levels of these proteins were below the limit of detection by flow cytometry, thus we were unable to validate these results in HFFF. However since we were able to detect ICOSL and ALCAM in DCs (Figure 4.17 & Figure 4.22), deletions of US16, US18 and US20 were also made in the UL36-P2A-RatCD2 virus (Table 4.3).

Description	Titre (pfu/ml)	Potential Interactions
$\Delta RL1-RL6$	1.6×10^5	-
$\Delta RL10-UL1$	3.0×10^6	-
$\Delta UL2-UL11$	1.0×10^7	-
$\Delta UL13-UL20$	1.5×10^6	-
$\Delta UL22A-UL25$	1.55×10^7	-
$\Delta UL148-UL140$	1.3×10^6	-
$\Delta UL139-UL150$	4.0×10^5	-
$\Delta US1-US11$	2.0×10^6	-
$\Delta US12-US17$	3.0×10^7	ICOSL
$\Delta US12-US21$	5.5×10^6	ICOSL/ALCAM
$\Delta US16$	5.5×10^5	ICOSL
$\Delta US16 & \Delta US20$	5.5×10^7	ICOSL/ALCAM
$\Delta US18$	4.0×10^7	ALCAM
$\Delta US18 & \Delta US20$	2.1×10^6	ICOSL/ALCAM
$\Delta US18-US22$	7.0×10^5	ICOSL/ALCAM
$\Delta US20$	1.0×10^7	ICOSL/ALCAM
$\Delta US27-US28$	4.0×10^6	-
$\Delta US29-US34A$	1.25×10^7	-

Table 4.3 – List of UL36-P2A-RatCD2 block deletion mutants engineered for proteomic analysis. Potential interactions with targets based on previous data²⁴.

Deletion Mutant	Mutation	Percentage of SNPs with Mutation
$\Delta RL1-RL6$ (<i>pAL2839</i>)	UL32	100
	UL32	12.12121
$\Delta UL2-UL11$ (<i>pAL3032</i>)	UL32	99.5283
$\Delta UL13-UL20$ (<i>pAL2857</i>)	UL32	100
$\Delta UL148-UL140$ (<i>pAL3068</i>)	UL32	100
$\Delta UL139-UL150$ (<i>pAL3130</i>)	UL32	100
	UL78	16.66667
$\Delta US1-US11$ (<i>pAL3114</i>)	UL32	100
$\Delta US12-US21$ (<i>pAL3137</i>)	UL32	100
$\Delta US16$ (<i>pAL3060</i>)	UL32	100
	UL48	100
$\Delta US16 \& \Delta US20$ (<i>pAL3080</i>)	UL32	100
$\Delta US18$ (<i>pAL2993</i>)	UL32	100
$\Delta US18 \& \Delta US20$ (<i>pAL3186</i>)	UL32	100
$\Delta US18-US22$ (<i>pAL2858</i>)	UL32	100
$\Delta US20$ (<i>pAL3132</i>)	UL32	100
$\Delta US29-US34A$ (<i>pAL2906</i>)	UL32	100

Table 4.4 – GRACy SNP analysis of the UL36-P2A-RatCD2 block deletion mutants. Only mutations that were found in >10% of SNPs are noted h

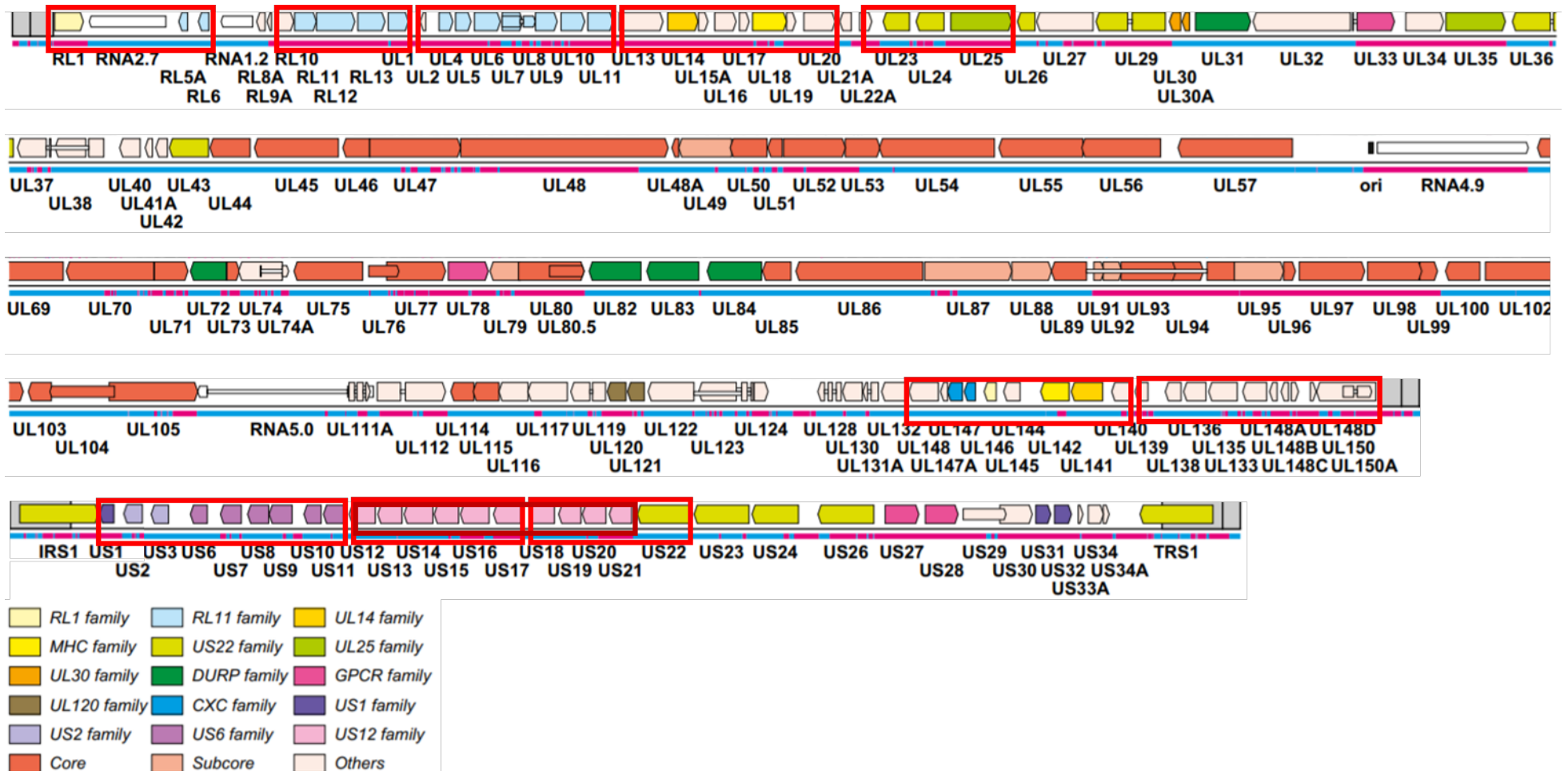


Figure 4.33 – The HCMV strain Merlin genome arrangement, adapted from Gatherer et al⁹. Red rectangles indicate groups of genes that were removed in the block deletion mutants.



Figure 4.34 - Example of analysis of the sequenced block deletion mutant genomes using Geneious. Δ US16 virus (pAL3060) aligned to the Merlin genome, A) the whole alignment; B) a close up of the US16 gene, showing no reads in the area of the deletion.

Based on the previous noted interactions of the single deletion mutant viruses and ICOSL and ALCAM in HFFFs (Table 4.3), the expression of these proteins in DCs was measured 48hrs following co-culture with infected HFFF-His. Unfortunately, at the time of the assay not all of the single deletion mutants had a high enough titre to be used.

The data from this experiment correlated nicely with proteomics of the HFFFs; single deletion mutants Δ US16&US20, Δ US20 and Δ US18&US20 saw greater recovery of ICOSL in infected DCs when compared to the wildtype and the Δ US18 mutant, shown in Figure 4.35A – this experiment will need to be repeated using the Δ US16 virus to determine if US16 has as much control as US20 over ICOSL. For ALCAM (Figure 4.35B), each of the deletion mutants shifted the peak slightly to the right, with the Δ US20 mutant causing a slightly larger shift than the others; the right-most “positive” peak in the DCs infected with Δ US18&US20 is the highest, which could mean that in a small percentage of the cells there is full recovery of ALCAM. As with US16 and ICOSL, the Δ US18 virus will need to be used to evaluate its effect on ALCAM in the presence of US20.

Despite the single deletion mutants interacting with ICOSL and ALCAM as previously seen in HFFFs²⁴, none of the mutants completely restored the level of expression of these proteins. This suggests that there are more viral genes/proteins involved in the downregulation of ICOSL and ALCAM than initially thought; this can be investigated when performing the proteomics with the block and single gene deletion mutants.

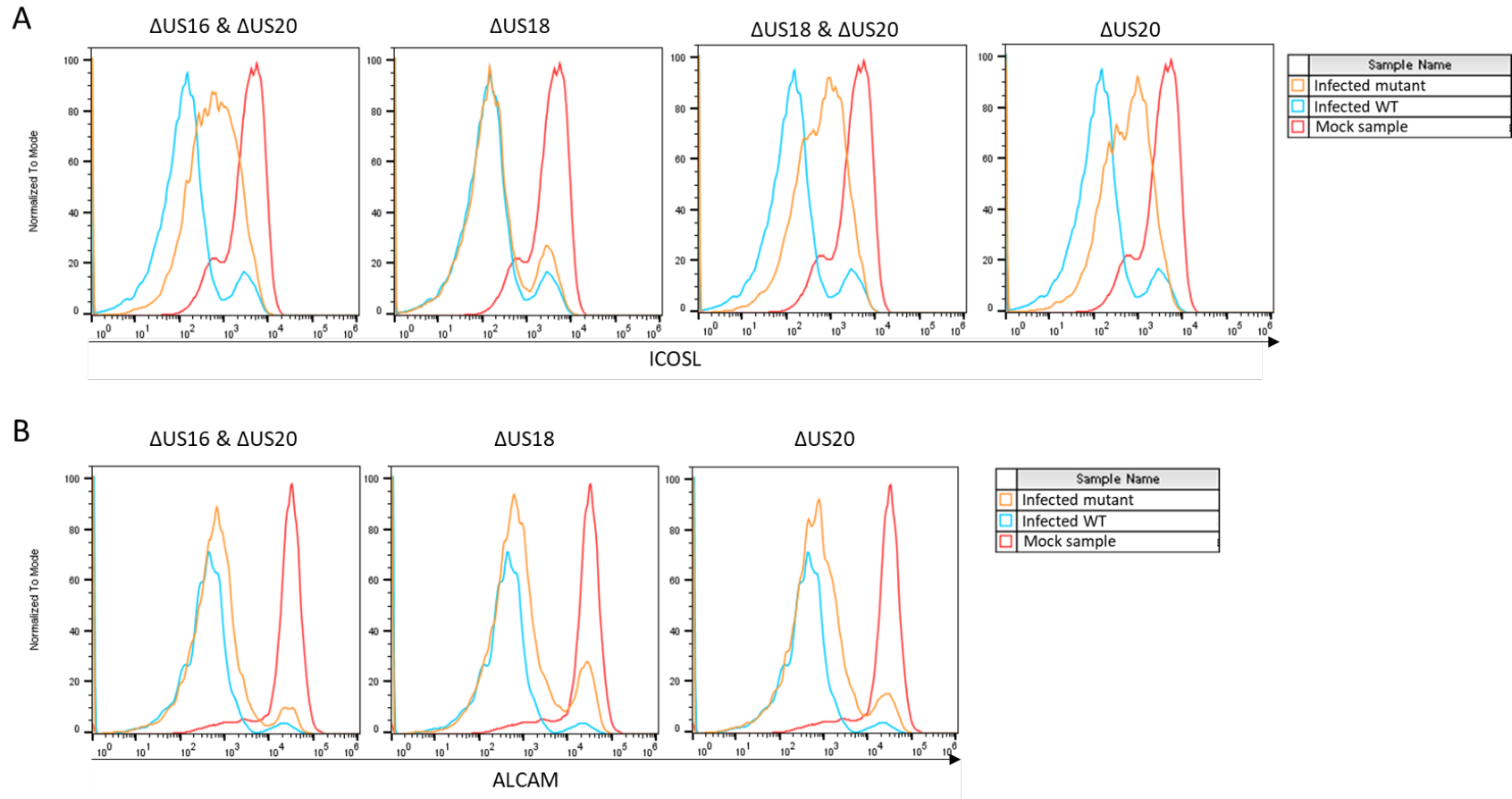


Figure 4.35 – Using single deletion mutants to confirm the genes responsible for downregulating ICOSL and ALCAM. DCs were co-cultured for 24hrs with infected HFFF-His cells, protein expression in mock, infected and bystander DCs was analysed by flow cytometry at 48hrs post co-culture. A) Manipulation of ICOSL with pAL2310 (WT), pAL3080 (Δ US16 & Δ US20), pAL2993 (Δ US18), pAL3186 (Δ US18 & Δ US20), and pAL3132 (Δ US20). B) Manipulation of ALCAM with pAL2310 (WT), pAL3080 (Δ US16 & Δ US20), pAL2993 (Δ US18), and pAL3132 (Δ US20).

4.4 Summary

The data in this chapter show that when purifying a population of cells from a mixed co-culture, that it is best to do this at 24hrs post co-culture, as it can become increasingly difficult to separate HFFFs, infected DCs and bystander DCs at later time points, and there is very little benefit to leaving the HFFFs and DCs in co-culture past this point as the number of infected DCs does not increase.

The proteomic analysis of the DC plasma membrane and whole cell lysate quantified thousands of proteins, of which 15 were selected to be validated. These proteins were chosen based on their roles in DC maturation and T and B cell activation, which understandably make them targets for modulation by HCMV. Of the 15 proteins, 10 have been validated using flow cytometry; and a further two, ICOSL and ALCAM, were investigated using single deletion mutants. This demonstrated that US16, US18 and US20 play roles in downregulation of these proteins in DCs, but other viral genes may also play a role. A series of viral mutants in which blocks of genes have been deleted were constructed, sequenced, and validated, and can now be used to identify other viral genes involved in modulating DC proteins.

Chapter 5.

Intrinsic

Antiviral

Mechanisms in

Dendritic Cells

It was evident while setting up primary dendritic cells for the proteomics screen that these cells undergo extreme levels of cell death *in vitro*. While uninfected DCs are susceptible to cell death, with approximately half the cells dying while differentiating from monocytes, it was clear that HCMV infection exacerbates this.

HCMV is known to extend the lifespan of monocytes, which usually survive only up to 3 days, by blocking apoptosis in these cells – but it was clear that infected dendritic cells rapidly undergo cell death during cell culture. This was unexpected since HCMV encodes apoptosis inhibitors, which can directly or indirectly affect the activation of caspases, thereby blocking caspase-mediated cell death, and also inhibitors of necroptosis²¹⁵.

While analysing the proteomic datasets, it was also noted that there was a surprising phenomenon relating to viral gene expression, HCMV late genes were expressed with different kinetics between HFFFs and DCs – that, based on the literature, is not seen in other strains such as TB40¹⁶⁵. This led to the investigation of novel intrinsic mechanisms that promote apoptosis and/or prevent the full lytic cycle of the Merlin strain in primary DCs.

5.1 Caspase-Mediated Apoptosis and Necroptosis

5.1.1 Investigation into Cause of Dendritic Cell Death

When preparing the dendritic cells for the plasma membrane profiling (PMP) for the proteomics analysis, it was difficult to maintain a reasonable number of infected cells for the PMP after co-culture. Dead and dying cells had to be removed by layering over histopaque before preparing the plasma membranes of the infected DCs.

Death could have occurred due to an intrinsic property of the co-culture set up, or due to the way that the cells were handled during the process of co-culture and separation. To differentiate between these possibilities, cell numbers were calculated at various stages of the co-culture and separation procedure, and at 72hrs post co-culture. The purpose of this was to determine whether cells were lost as a direct result of the separation technique, as well as other theories (Figure 5.1, Table 5.1). The conditioned media was supernatant from Merlin-infected HFFFs, which had been passed through a 0.2 μ m filter to remove virions; DCs were matured as described in methods; cell-free infections were performed using 200 μ l concentrated pAL2344 (UL36-P2A-GFP) grown in RPE cells; the anti-TNF drug Etanercept²¹⁶ (Enbrel) was used at a concentration of 33 μ g/ml. ‘2 separations’ refers to separation of DC from HFFF, and also infected from uninfected DCs.

Conditions Tested	Rationale	Outcome
No co-culture (uninfected)	Assess lifespan of uninfected DCs from 0hrs to 72hrs	60-70% of DCs die during cell culture
No co-culture + conditioned media (uninfected)	Are the HFFFs releasing cytokines that affect DC cell survival?	No alteration in DC cell death compared to the no-coculture condition
No co-culture + 2 ‘mock’ separation processes (uninfected)	Is the separation process stressing the dendritic cells and leading to death?	No alteration in DC cell death compared to the no co-culture condition
No co-culture, cell-free pAL2344	Is it specific to the RatCD2 virus in co-culture?	Caused 80-90% of DCs to die
Co-culture, \pm virus, no separations	Is the separation process stressing the DCs?	Slight improvement of survival for both infected and uninfected DCs, but not dramatic
Co-culture, \pm virus, + 2 separations	Used for processing the DCs for any experiment using the RatCD2 virus	Less death seen in uninfected DCs

<i>Co-culture, +pAL2344, + 2 separations</i>	Is it specific to the RatCD2 expressing virus?	No alteration in DC death compared to RatCD2 virus
<i>Co-culture, ±virus, + 2 separations + conditioned media</i>	Are the HFs releasing cytokines affecting dendritic cell survival?	No alteration in DC death compared to normal media
<i>Co-culture, + virus, + HFFF separation only</i>	Are the bystanders keeping the infected DCs alive?	Slight improvement of infected DC survival
<i>Co-culture, + virus, + RatCD2 separation</i>	Are the bystanders killing infected DCs?	Increased DC death, but could have been due to lower cell density
<i>Mature DC co-culture, no separations</i>	Are mature DCs more resilient?	Maturation increased survival overall but decreased infectivity
<i>Mature DC co-culture, ±virus, + 2 separations</i>	Are mature DCs more resilient?	Maturation increased survival overall but decreased infectivity
<i>Co-culture, ±virus, + 2 separations + anti-TNF (Etanercept)</i>	Are DCs releasing TNF to kill HFFFs but feedback is killing DCs too?	Did not improve infected DC survival

Table 5.1 – Conditions tested during DC death investigations. Dendritic cells were co-cultured for 24hrs with HFFF-His cells infected with UL36-RatCD2 virus unless stated otherwise, before undergoing separation from the HFFFs, and then separation of infected and bystander DCs. DC death was measured by using flow cytometry to count the number of DCs before and after each step of the separation process and up to 72hrs post co-culture; and by staining the DCs with a viability stain. Each condition was tested with a minimum of two different donors.

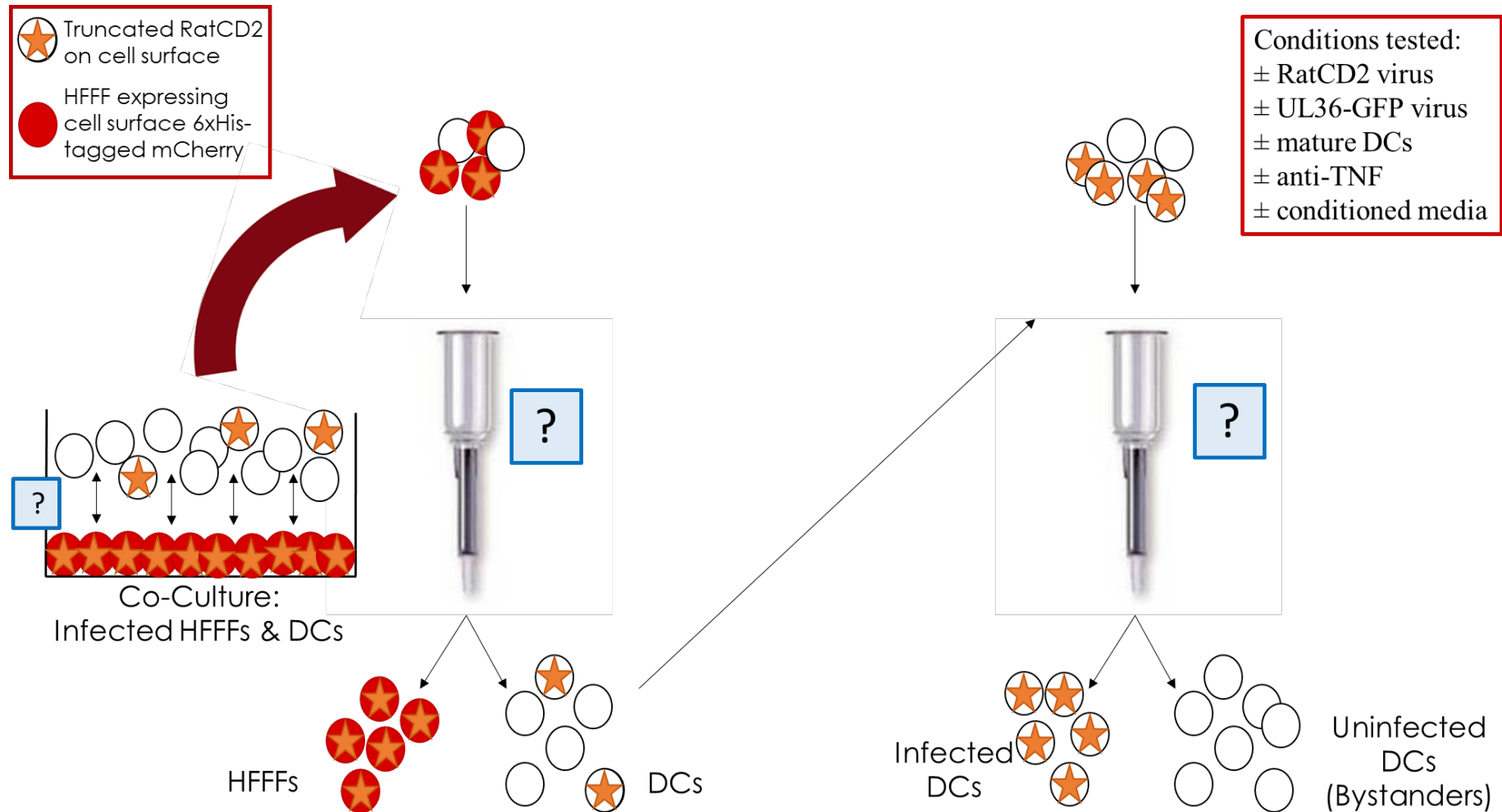


Figure 5.1 – Diagram depicting the stages of the co-culture and separation process that were modified when investigating the cause of DC death.

The conclusion of these experiments was that while the separation process itself may have had a minor impact, it did not appear that either the fibroblasts or bystander DCs were negatively impacting the survival of the infected DCs; whether cells were kept together or separated made little difference, and the presence or absence of RatCD2 made no difference.

While DCs matured with either LPS or TNF α overall had increased survival rates, these cells were also less susceptible to infection (Figure 5.2), contradictory to that previously published by Raftery et al.²¹⁷ – hence all work was continued using immature DCs.

Overall, this extensive panel of troubleshooting conditions indicated that the technical design of the experiment was not responsible for inducing DC death following HCMV infection, and therefore there was no simple way to improve DC survival through altering the experimental setup. Attention therefore turned to investigating the molecular causes of cell death.

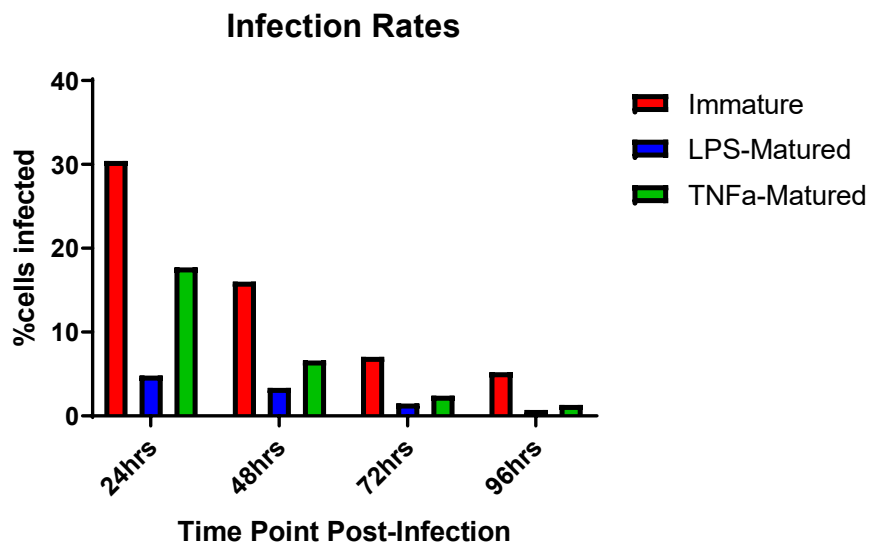


Figure 5.2 – HCMV infection rates in immature and mature DCs. DCs were co-cultured with UL36-GFP infected HFFF-His cells for 24hrs before separation of HFFFs and DCs. The percentage of infected cells calculated from live cells at each time point, by staining the DCs with a viability stain and analysing fluorescence using flow cytometry. DCs were matured with either LPS or TNF- α 24hrs prior to co-culture.

5.1.2 Z-VAD & Nec-1s

When investigating the effects of maturing the DCs on HCMV infection rates and improving survival in Figure 5.2, the percentage of infected cells drops at each time point rather than remaining level. Thus infected DCs perish at a greater rate than the bystanders, and using the percentage of infected cells provides a simple readout for this process. As a result, further experiments utilised a HCMV containing a UL36-GFP tag, negating the need to stain with the RatCD2 antibody. Following infection by co-culture, DCs were separated from HFFF, however infected and bystander DCs were not separated. Figure 5.3 demonstrates the same effect seen in Figure 5.2, where the percentage of live cells that are infected decreases over time.

The two best studied pathways of cell death are caspase-mediated apoptosis, and necroptosis. To establish whether either of these was being triggered in the DCs, cells were treated with either the pan-caspase inhibitor Z-VAD (50 μ M, R&D Systems FMK001) or the necroptosis inhibitor Nec-1s (10 μ M, Generon 2263-1) immediately after separation from HFFFs. As seen in Figure 5.4, DCs that had been treated with Z-VAD saw increased survival of infected cells up to 72hrs when compared to untreated cells, and it had a greater effect than that seen in the DCs treated with Nec-1s. The addition of Nec-1s to Z-VAD gave a small increase in survival compared to Z-VAD alone. Thus caspase-dependent apoptosis is responsible for most of the cell death observed, with necroptosis playing a smaller role.

Z-VAD is a pan-caspase inhibitor, and therefore affects multiple pathways within the cell. Research therefore focussed on determining which caspases associated with apoptosis were activated in the DCs following infection with Merlin.

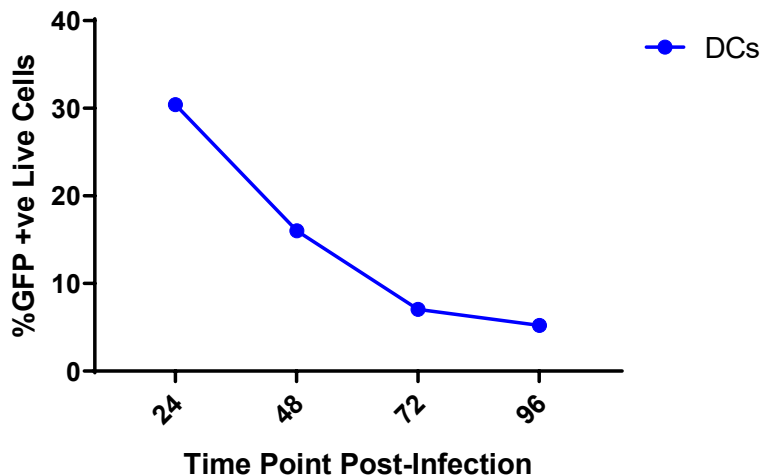


Figure 5.3 – Survival of immature DCs infected with HCMV-GFP via co-culture, up to 96hrs post co-culture. DCs were co-cultured with UL36-GFP infected HFFF-His cells for 24hrs before separation of HFFFs and DCs. The percentage of GFP+ cells was calculated from live dendritic cells at each time point, by staining the DCs with a viability stain and analysing fluorescence using flow cytometry. Representative of two donors.

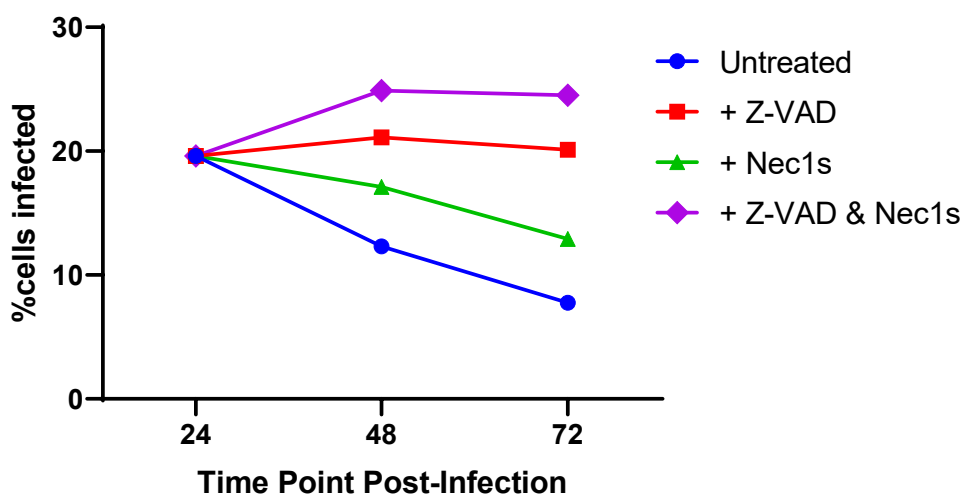


Figure 5.4 – Survival of HCMV-infected DCs following treatment with caspase and necroptosis inhibitors. DCs were co-cultured with UL36-GFP infected HFFF-His cells for 24hrs before separation of HFFFs and DCs. Z-VAD and Nec-1s were added to the media of the DCs immediately after separation from HFFFs. The percentage of infected cells was calculated from live dendritic cells at each time point, by staining the DCs with a viability stain and analysing fluorescence using flow cytometry.

5.1.3 Multiple Caspase Inhibitors

In human cells there are initiator and executioner caspases, both types are originally synthesised as inactive pro-caspases. The initiator caspases – caspases 2, 8, 9 and 10 – are present in the cell in their inactive pro-caspase form; following stimulation via binding of tumour necrosis factor (TNF) superfamily members to the death receptors, release of cytochrome C from the mitochondria, or DNA damage, these are cleaved to their active forms (Figure 5.5). These initiator caspases can then trigger the executioner/effectort caspases – caspases 3, 6 and 7 – which set off caspase-dependent apoptosis; a single executioner caspase can also start a positive feedback loop which drives activation of the other executioner caspases²¹⁸.

To investigate which caspases HCMV may be modulating, cellular levels of each caspase were investigated in the proteomics data. However, it must be remembered that the proteomics data provide the relative abundance of the caspases, and not information relating to the cleavage and activation of these proteins.

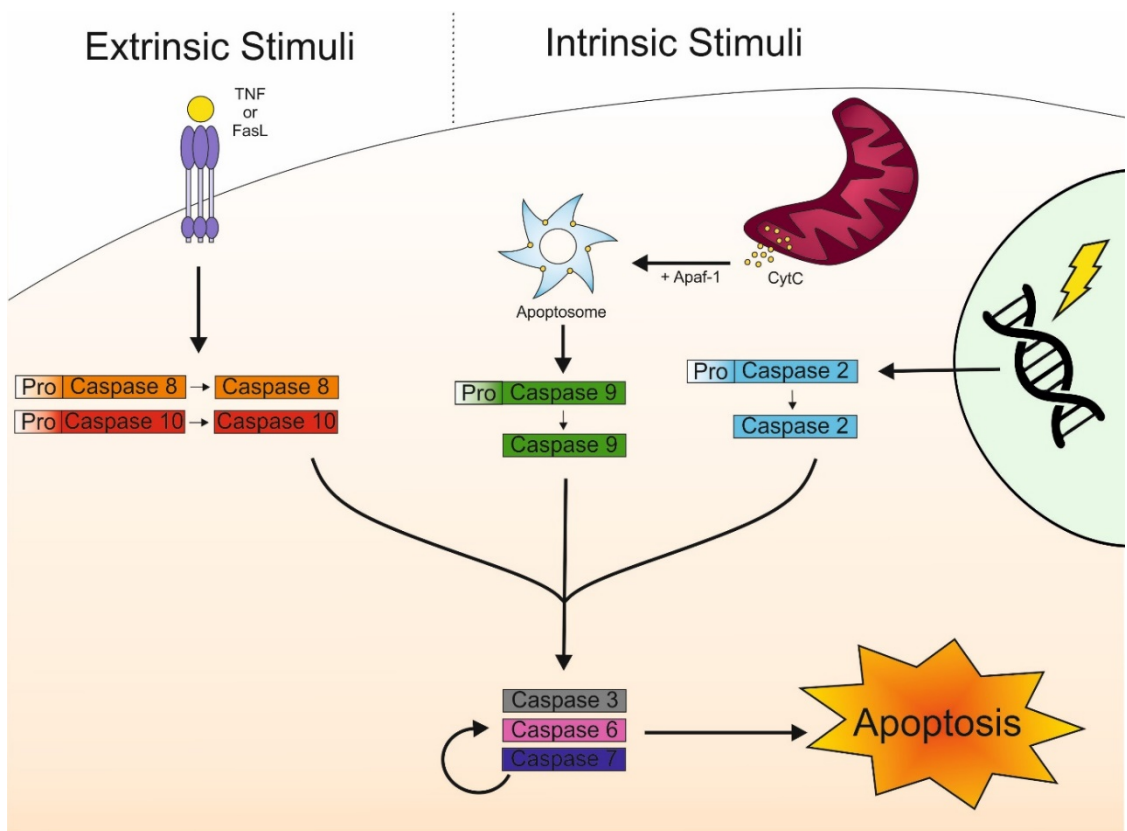


Figure 5.5 – Simple schematic of caspase-dependent apoptosis and the stimuli which trigger the cascade.

5.1.3.1 Caspase 2

Caspase 2 is mostly associated with the control of cell death following DNA damage, but it has also been linked to ER stress-related apoptosis induced by viral infection²¹⁹. In the proteomics (Figure 5.6), the relative abundance of Caspase 2 in both infected and bystander cells remains somewhat level throughout the time course, suggesting that HCMV does not downregulate this protein. However, HCMV is able to act upstream of Caspase 2, the UL38 protein is responsible for preventing ER stress-related apoptosis during the late stage of infection (72hours and later) by acting on the unfolded protein response (UPR)²²⁰, therefore preventing the cleavage of Caspase 2 to its mature form.

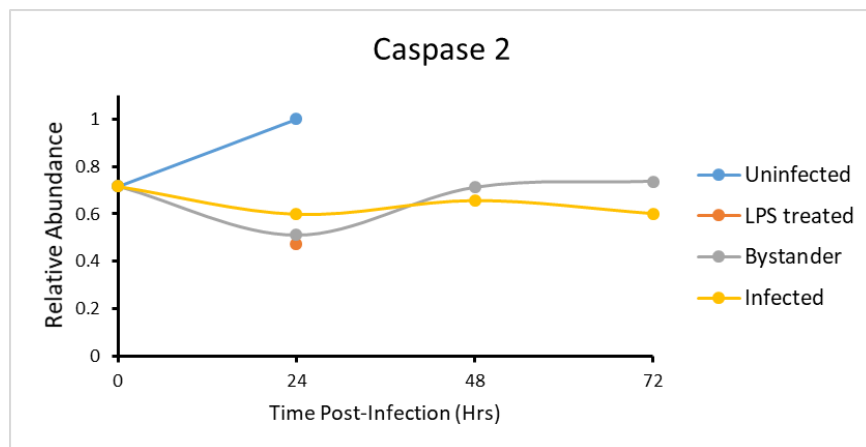


Figure 5.6 – Modulation of Caspase 2 seen in DC whole cell lysate proteomics dataset. DCs were co-cultured with UL36-RatCD2 infected HFFF-His cells for 24hrs before separation of HFFFs and DCs, and separation of infected and bystander DCs. DCs were lysed and the whole cell lysates analysed for protein abundance.

5.1.3.2 Caspase 3

Caspase 3 is an effector caspase, and is activated following cleavage by Caspases 8, 9 and 10. Caspase 3, once activated, is responsible for organising DNA fragmentation and the breakdown of the cytoskeleton during apoptosis. In the proteomics data, it appears that Caspase 3 is weakly upregulated in the bystander DCs, but not in the infected DCs (Figure 5.7), suggesting that HCMV may encode a mechanism to prevent upregulation in infected cells.

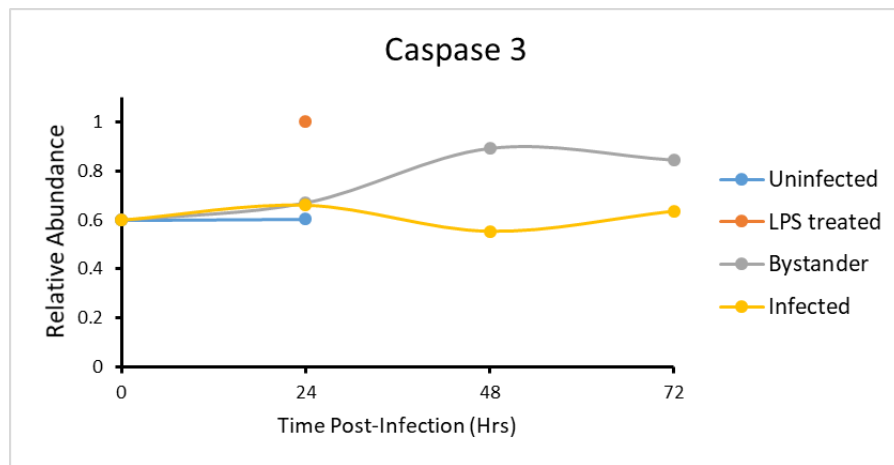


Figure 5.7 – Modulation of Caspase 3 seen in DC whole cell lysate proteomics dataset. DCs were co-cultured with UL36-RatCD2 infected HFFF-His cells for 24hrs before separation of HFFFs and DCs, and separation of infected and bystander DCs. DCs were lysed and the whole cell lysates analysed for protein abundance.

5.1.3.3 Caspase 6

Caspase 6 is another executioner caspase, activated by Caspases 7, 8 and 10, which triggers nuclear shrinkage during apoptosis. Similarly to Caspase 2, the abundance of Caspase 6 within both infected and uninfected cells remains unchanged, as seen in Figure 5.8. It appears that HCMV is not modulating Caspase 6 levels directly, but the virus could be manipulating a pathway upstream of this protein.

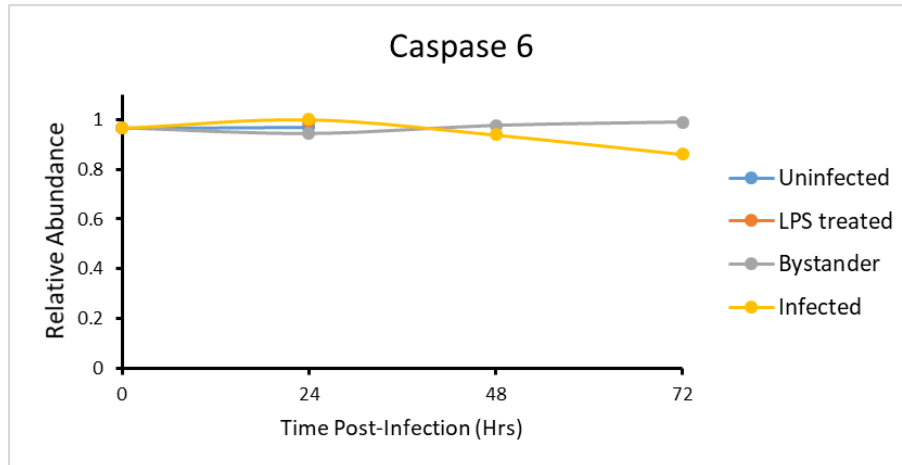


Figure 5.8 – Modulation of Caspase 6 seen in DC whole cell lysate proteomics dataset. DCs were co-cultured with UL36-RatCD2 infected HFFF-His cells for 24hrs before separation of HFFFs and DCs, and separation of infected and bystander DCs. DCs were lysed and the whole cell lysates analysed for protein abundance.

5.1.3.4 Caspase 7

The final effector caspase is Caspase 7, previously thought to be redundant in apoptosis due to its many similarities to Caspase 3. Caspase 7, like Caspase 3, is processed by Caspase 8, 9 and Caspase 10, however, Caspase 7 causes cell detachment from the extracellular matrix (ECM) during apoptosis²²¹ and can also cleave and activate Caspase 6. HCMV appears to directly modulate Caspase 7 levels, as upregulation is specifically prevented in infected DCs when compared to the bystanders.

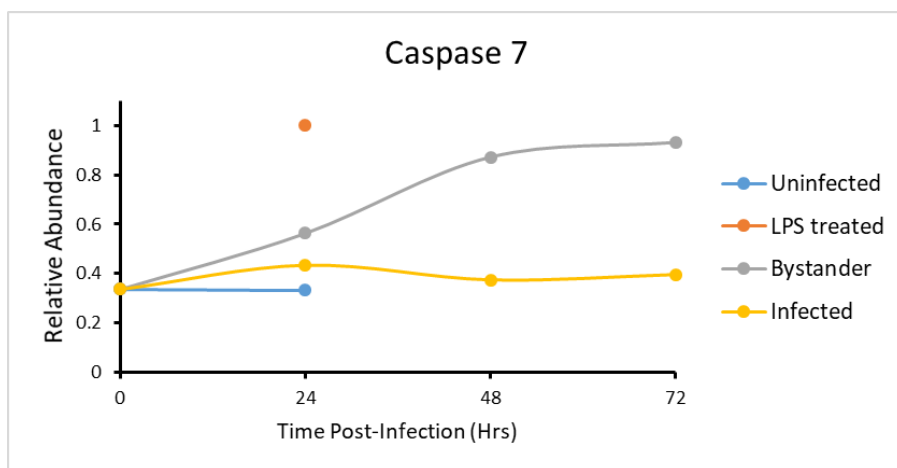


Figure 5.9 – Modulation of Caspase 7 seen in DC whole cell lysate proteomics dataset. DCs were co-cultured with UL36-RatCD2 infected HFFF-His cells for 24hrs before separation of HFFFs and DCs, and separation of infected and bystander DCs. DCs were lysed and the whole cell lysates analysed for protein abundance.

5.1.3.5 Caspase 8

Caspase 8 is an initiator caspase activated by the death receptors TNF receptor 1 (TNFR1) and Fas upon binding of their ligands TNF and Fas ligand (FasL), respectively. Caspase 8 then cleaves pro-Caspase 3, coordinates downstream activation of other effector caspases and Caspase 9, and is also able to block necroptosis. HCMV UL36 gene encodes a specific inhibitor of Caspase 8, viral inhibitor of caspase 8-induced apoptosis (vICA), which binds to and prevents cleavage of pro-Caspase 8²⁶. Additionally, IE1 and IE2 are involved in the inhibition of apoptosis induced by TNF α ²²². In dendritic cells, the expression levels of Caspase 8 are very slightly lower in infected cells than the bystanders, although this increases at 72 hours (Figure 5.10), suggesting minimal modulation of levels by HCMV.

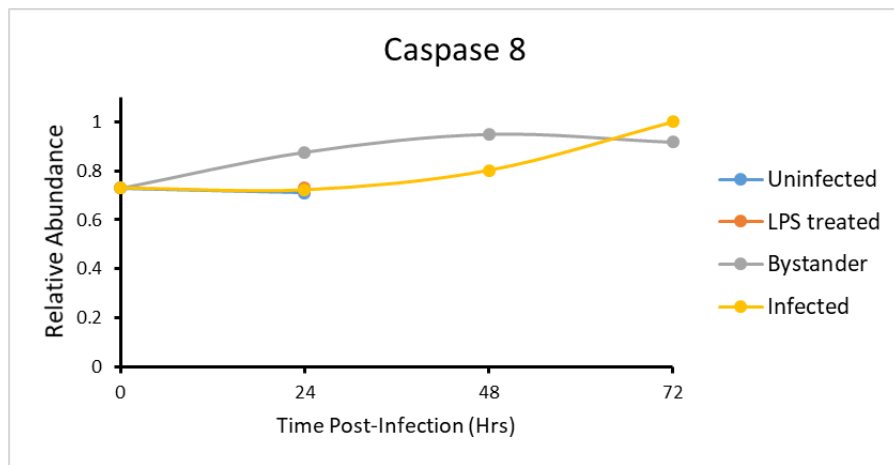


Figure 5.10 – Modulation of Caspase 8 seen in DC whole cell lysate proteomics dataset. DCs were co-cultured with UL36-RatCD2 infected HFFF-His cells for 24hrs before separation of HFFFs and DCs, and separation of infected and bystander DCs. DCs were lysed and the whole cell lysates analysed for protein abundance.

5.1.3.6 Caspase 9

Caspase 9 is another initiator caspase; when the mitochondria releases Cytochrome C, this forms the apoptosome with Apaf-1, which then binds to and activates Caspase 9. HCMV encodes another apoptosis inhibitor, UL37. This gene encodes viral mitochondria inhibitor of apoptosis (vMIA), which indirectly blocks Caspase 9 activation by impeding Cytochrome C release^{223, 224}. Caspase 9 was not detected in the proteomics data, which could mean that the protein is expressed at very low levels in dendritic cells.

5.1.3.7 Caspase 10

Caspase 10 is an initiator of apoptosis following extrinsic stimuli, binding of TNF or FasL to the death receptors, just as Caspase 8 is. HCMV is not known to encode a specific Caspase 10 inhibitor, but the abundance of Caspase 10 in infected dendritic cells is robustly reduced (Figure 5.11). Caspase 10 was also identified as a novel target protein during the proteomics screen.

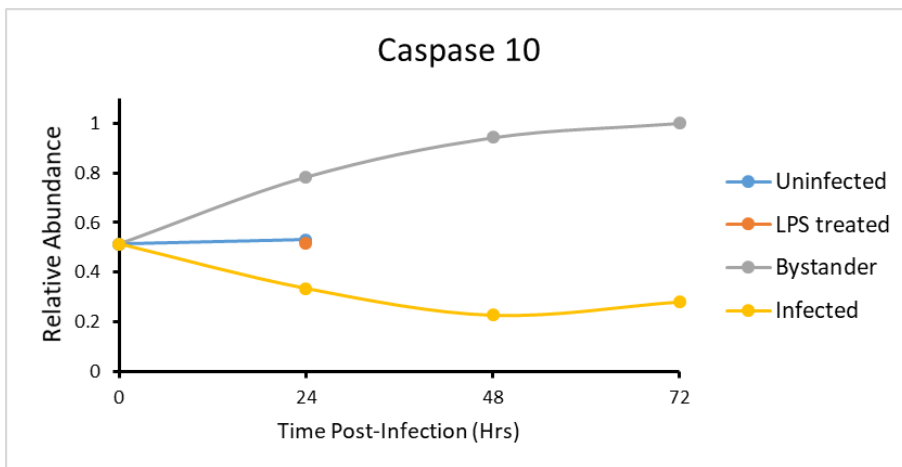


Figure 5.11 – Modulation of Caspase 10 seen in DC whole cell lysate proteomics dataset. DCs were co-cultured with UL36-RatCD2 infected HFFF-His cells for 24hrs before separation of HFFFs and DCs, and separation of infected and bystander DCs. DCs were lysed and the whole cell lysates analysed for protein abundance.

In summary, HCMV appears to modulate the abundance of several initiator and executioner caspases, which is unsurprising as HCMV is known to encode inhibitors of apoptosis, many of which operate by inhibiting the activation of caspases. It is possible that in some cases the virus is also manipulating other elements of the caspase-dependent apoptosis pathway, by acting on proteins that are responsible for activating and cleaving the caspases. However, despite attempts by HCMV to block the apoptosis pathway, infected DCs are still more susceptible to cell death than DCs that have detected infection but remained uninfected (bystanders). It is possible that the abundance of initiator and executioner caspases in DCs are greater than expected, and so despite downregulation within the caspase-mediated cell death pathways, levels of the caspases within the cell are high enough to trigger apoptosis.

5.1.3.8 Treatment with Caspase Inhibitors and Z-VAD

To investigate which caspases were being activated in the DCs following HCMV infection, infected cells were first treated with inhibitors for the initiator caspases (seen in Table 5.2). DCs were co-cultured with HFFFs infected with a UL36-GFP-tagged virus, following a 24hr co-culture the DCs were separated from the fibroblasts, and at this point the caspase inhibitors were added. Z-VAD was used as a positive control for apoptosis inhibition.

When analysing the data from these experiments by flow cytometry, survival of HCMV-infected DCs was determined by the percentage of live cells that were GFP positive within the mixed bystander and infected DC culture (Figure 5.12). The ability of inhibitors to prevent cell death varied between donors, however Z-IETD and Z-AEVD – inhibiting Caspase 8 and Caspase 10, respectively – consistently reduced the death seen in infected DCs, but not always to the same level as Z-VAD. Inhibitors targeting caspases 2 and 9, showed very little effect when compared to untreated cells.

<i>Target</i>	<i>Inhibitor</i>	<i>Concentration</i>	<i>Manufacturer</i>	<i>Cat. Number</i>
<i>All caspases</i>	Z-VAD	50µM	R&D Systems	FMK001
<i>Caspase 2</i>	Z-VDVAD	50µM	Generon	A1922-1mg
<i>Caspase 8</i>	Z-IETD	50µM	BD Biosciences	550380
<i>Caspase 9</i>	Z-LEHD	50µM	BD Biosciences	550381
<i>Caspase 10</i>	Z-AEVD	50µM	Cambridge Bioscience	14987-1 mg

Table 5.2 – List of specific caspase inhibitors used in this study.

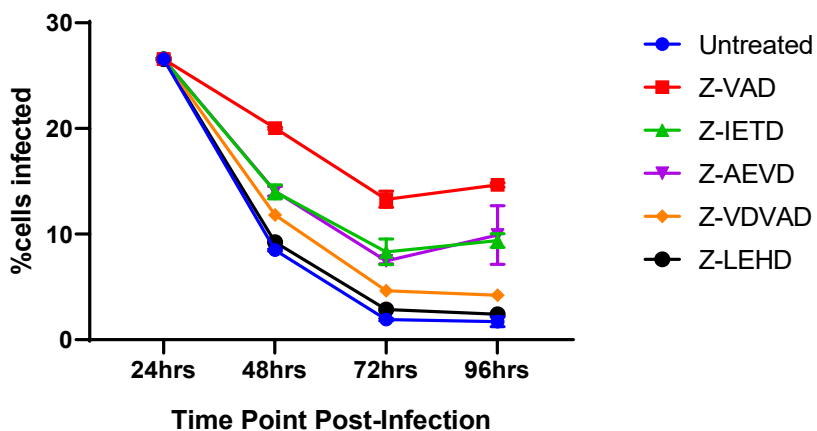


Figure 5.12 - Survival of HCMV-infected DCs following treatment with caspase inhibitors. Dendritic DCs were co-cultured with UL36-GFP infected HFFF-His cells for 24hrs before separation of HFFFs and DCs. Caspase inhibitors were added to the DC media immediately after separation from HFFFs. The percentage of GFP+ cells was calculated from live dendritic cells at each time point, by staining the DCs with a viability stain and analysing fluorescence using flow cytometry. Untreated, Z-VAD, Z-IETD and Z-AEVD samples were performed in triplicate, Z-VDVAD and Z-LEHD performed in singlicate. Representative of four donors. Error bars refer to mean + SD of triplicate samples.

The inability of Z-IETD and Z-AEVD to individually inhibit apoptosis to the same extent as Z-VAD may reflect redundancy in cellular pathways. Therefore, we

compared Z-VAD to treatment with Z-IETD and Z-AEVD in combination. In addition, HCMV UL36 is known to inhibit Caspase 8, however the fact that Z-IETD inhibited cell death implied that this block was incomplete in DCs. A potential concern was that this could be due to the virus having a P2A-GFP tag after UL36-GFP, which was affecting UL36 function. We have previously shown that this tag does not affect the ability of UL36 to inhibit Fas-mediated apoptosis in fibroblasts, making this unlikely¹⁹². Nevertheless, to exclude the possibility that tagging UL36 affected its function in DCs, in addition to the combination of Z-IETD and Z-AEVD, I tested viruses with an IE2-GFP tag (instead of UL36-P2A-GFP) and a virus lacking UL36 (but which still expresses GFP from the UL36 promoter).

There was only a slight increase in rates of death when UL36 was deleted, indicating that any ability of UL36 to mediate inhibition of caspase 8 was a small component of the processes occurring here. Furthermore, viruses with tags on either UL36 or IE2, did not display major differences in the rate at which infected cells died, and certainly did not recover the rate of live cells in the same way that addition of Z-VAD did in previous experiments. Therefore, tagging UL36 was unlikely to be responsible for the phenotype observed (Figure 5.13).

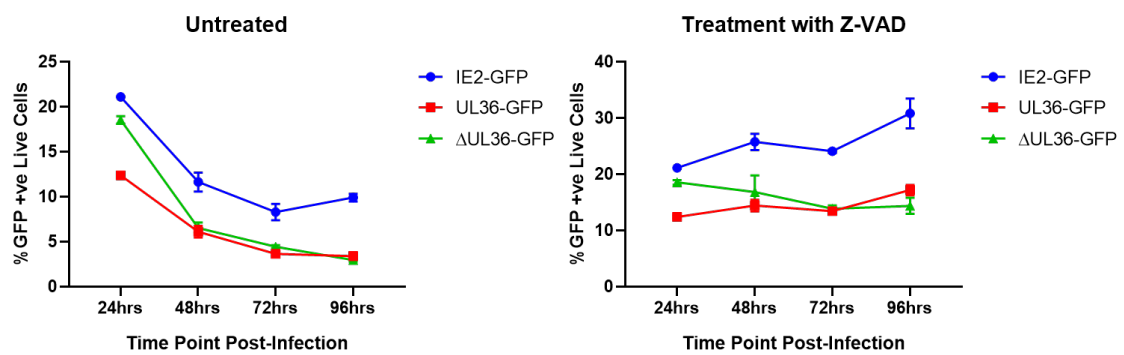


Figure 5.13 - Survival of HCMV-infected DCs using tagged, untagged and ΔUL36 strains, in control conditions (left) or following treatment with Z-VAD (right). DCs were co-cultured with UL36-GFP, IE2-GFP or ΔUL36-GFP infected HFFF-His cells for 24hrs before separation of HFFFs and DCs. Z-VAD was added to the media of the DCs immediately after separation from HFFFs. The percentage of infected cells was calculated from live dendritic cells at each time point, by staining the DCs with a viability stain and analysing fluorescence using flow cytometry. Each sample was performed in triplicate. Error bars refer to mean + SD of triplicate samples.

When comparing the abilities of Z-IETD and Z-AEVD to prevent cell death, with all viruses the combination of the two was either better than or equal to Z-VAD (Figure 5.14), suggesting that inhibition of both caspase 8 and caspase 10 is sufficient to block apoptosis in HCMV-infected DCs. However, caspase inhibitors are known to have some off-target effects on other caspases, so the combination of both Z-IETD and Z-AEVD may have resulted in inhibition equivalent to that of Z-VAD coincidentally. Hence, it would not be appropriate to state that HCMV triggers apoptosis in dendritic cells via the activation of caspases 8 and 10. Despite this, the data clearly show that the cell death occurring in the DCs is caspase-mediated, and the caspase 8 and 10 inhibitors did have an effect individually, while caspase 9 and 2 inhibitors did not; therefore, Z-VAD can be used to extend the lifespan of HCMV-infected DCs for use in experiments, even if the full pathway of caspase-mediated death is unknown.

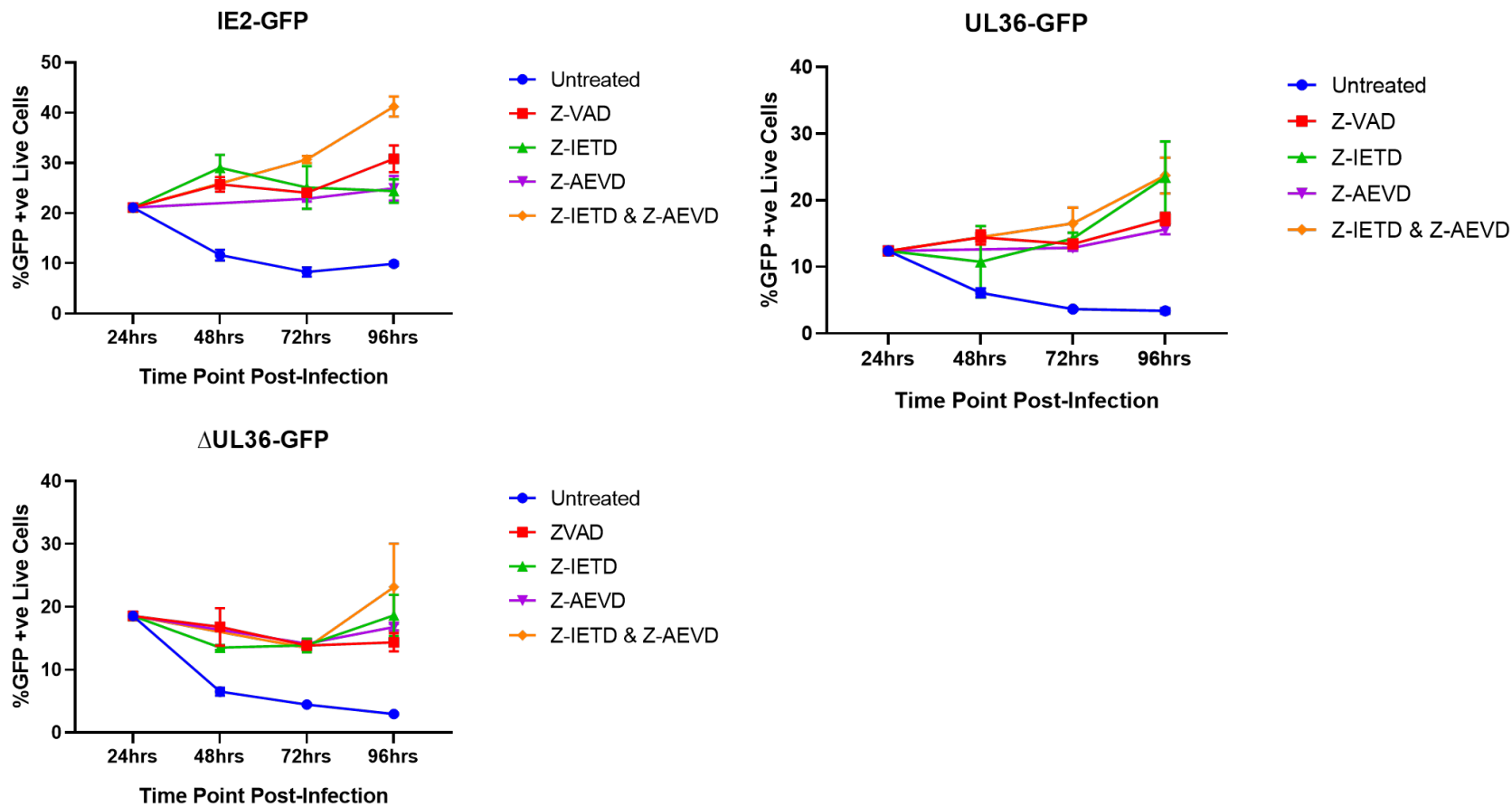


Figure 5.14 – Survival of HCMV-infected DCs using tagged, untagged and Δ UL36 strains, following treatment with caspase inhibitors. DCs were co-cultured with UL36-GFP, IE2-GFP or Δ UL36-GFP infected HFFF-His cells for 24hrs before separation of HFFFs and DCs. Caspase inhibitors were added to the media of the DCs immediately after separation from HFFFs. The percentage of infected cells was calculated from live dendritic cells at each time point, by staining the DCs with a viability stain and analysing fluorescence using flow cytometry. Each sample was performed in triplicate, error bars refer to mean + SD of triplicate samples.

5.2 Late Gene Expression

The proteomics also revealed an unusual observation regarding the kinetics of viral gene expression. Productive HCMV infection can be separated into four phases of gene expression: immediate-early (IE), early (E), early-late (EL) and late (L). The protein expression that occurs in these phases was further classified into five temporal protein (Tp) profiles by Weekes et al¹⁷². Immediate-early proteins in Tp1 are expressed within the first 24hrs following infection; expression of early proteins in Tp2 also begins within 24hrs, however levels continue to increase up to 48hrs; early-late proteins in Tp3 and Tp4 are expressed after 48hrs, although levels of expression of proteins in Tp3 increase up to 72hrs; finally, late genes/proteins in Tp5 are only expressed to their highest level from 72hrs¹⁷².

When the late time point of HCMV replication in fibroblasts occurs from 72hrs post-infection, late genes have been expressed and new virions have begun to be assembled, ready to infect new cells. However, this is not the case for dendritic cells infected with Merlin via the cell-cell route, despite previous publications showing that TB40 is able to undergo the full lytic life cycle in DCs albeit with delayed kinetics¹⁶⁵.

Immediate early (IE) and early gene expression is similar between HFFFs and DCs (Figure 5.15A); Tp1 genes expressed rapidly following infection, Tp2 expressed from 24-48hrs, and Tp3 gene expression increasing over the three time points in both cell types. However, Figure 5.15A & B show strong upregulation of late genes in HFFFs, this is not the case in DCs – Tp4 expression in DCs is delayed until 72hrs, and Tp5 proteins are not expressed at 72hrs as they are in HFFFs.

In Figure 5.15B, the relative abundance of UL32 appears higher in DCs at 24hrs than in HFFFs, however, this is likely to be due to the protein being present in the input virion. By plotting abundance relative to the maximal expression level at any timepoint, levels appear high throughout due to the lack of upregulation of the gene at later time points. Therefore, it is likely that all late genes that are present at the earlier time points are from input virions. At 72hrs there is no increase in levels, and therefore no *de novo* expression of the late genes.

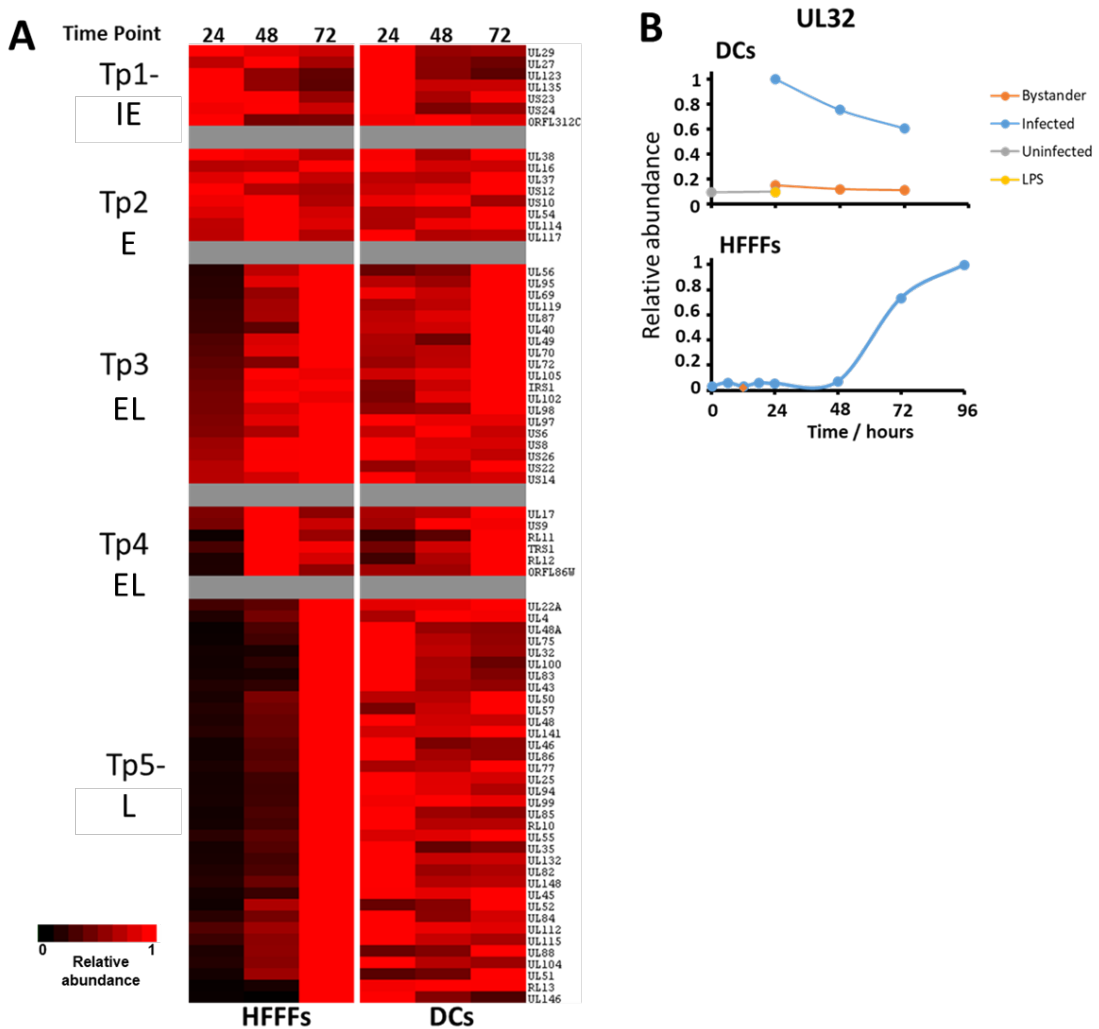
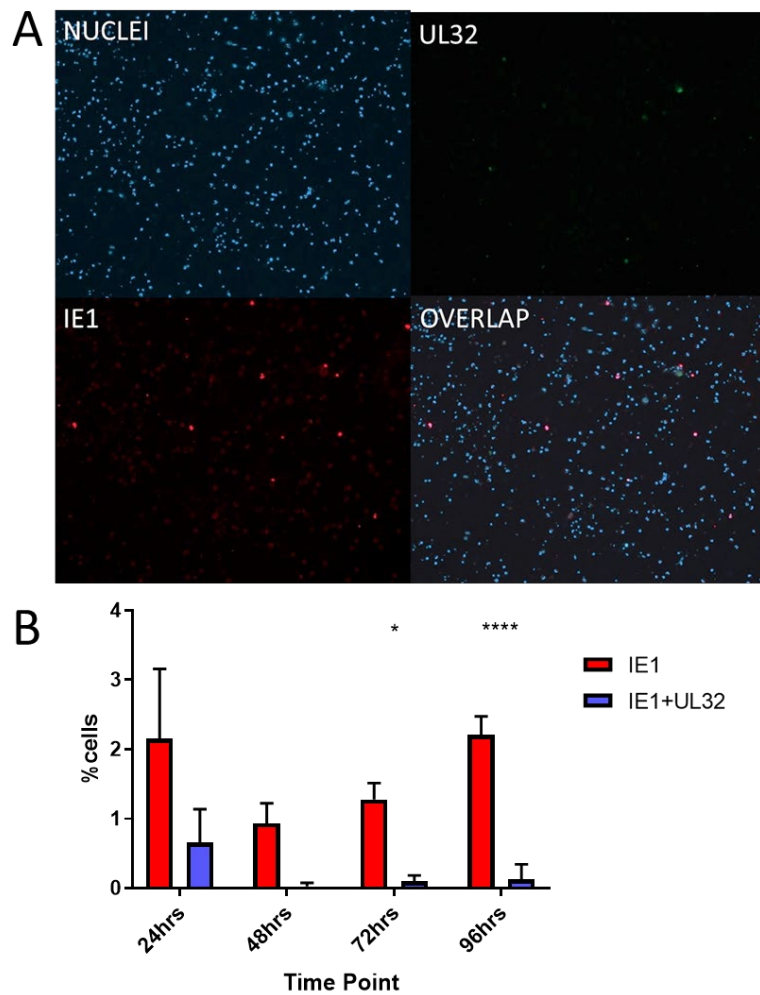


Figure 5.15 – Comparison of HCMV gene expression in HFFFs and DCs from whole cell lysate data; infected via the cell-free and cell-associated routes, respectively. A) Temporal expression profiles showing relative abundance of HCMV genes. B) Graph showing relative abundance of the late gene UL32 in DCs and HFFFs.

5.2.1 Immunofluorescence Assay

One possibility was simply that late gene expression was delayed in DCs; in support of this observation, the Tp4 class of viral genes showed maximal expression at 48h in HFFF, but 72h in DCs. To investigate this, co-cultures were set up in a similar manner to those used for the proteomics. Samples were taken for immunofluorescence (IF) for IE1 (a Tp1 gene) and UL32 (a Tp5 gene) at 24, 48 & 72hrs post co-culture, and also at a later time point of 96hrs (Figure 5.16A). The IF data from each time point is quantified in Figure 5.16B, where there is significant difference between IE1⁺ single positive cells and IE1⁺UL32⁺ double positive cells at 72hrs and 96hrs post co-culture.

The presence of IE1 demonstrates that DCs are infected at the later time points, however late genes are not expressed even by 96h. However, this method of measuring late gene expression suffered from complications, primarily because dead and dying DCs in the culture were hard to exclude, resulting in a low number of infected DCs overall (2-3% instead of the 20-30% usually seen at 24hrs by flow cytometry).



*Figure 5.16 – Immediate early (IE1) and late gene (UL32) expression in dendritic cells co-cultured with Merlin-infected HFFFs, then the DCs separated from the HFFF. A) Immunofluorescence (IF) image taken 96hrs post co-culture, nuclei stained with DAPI, IE1 stained with anti- IE1-AF647, UL32 tagged with GFP in virus. B) IF data from each time point quantified in chart. Error bars refer to mean + SD of triplicate samples. *P < 0.05, ****P < 0.0001 by 1-way ANOVA.*

5.2.2 Intracellular Flow Cytometry

As measuring late gene expression by IFA was unreliable due to the presence of dead cells, expression was then measured at each time point by performing intracellular flow cytometry and staining for gB (a late gene). By using this method I was able to stain and therefore exclude dead DCs from the analysis. DCs were infected with a UL36-GFP expressing virus (providing a Tp1 marker), and stained for gB at 24, 72 and 96hrs post co-culture; infected HFFFs that had been stained for gB at 72hrs were used as a positive control in this experiment. Figure 5.17 compares the level of gB in infected DCs to that seen in the positive control; Z-VAD was also added to one sample as previously described, and stained for gB at 96hrs. The gB present at the earlier time points in DCs is likely to be from incoming virions, as this gene is not expressed until at least 72hrs post infection, at which point the shift in DCs is smaller than that seen in lytically infected fibroblasts. Unfortunately this assay suffered from high background signals, making robust conclusions difficult; future experiments will use a virus with a fluorescently-tagged late gene. Nevertheless, combined with the IFA, it does not appear that Tp5 gene expression is simply delayed in DCs.

While the addition of Z-VAD did improve survival of infected DCs up until 96hrs post co-culture, there was also no upregulation of gB at this time point, suggesting that caspase-mediated cell death is not the only factor involved in limiting late gene expression in DCs infected with the Merlin strain.

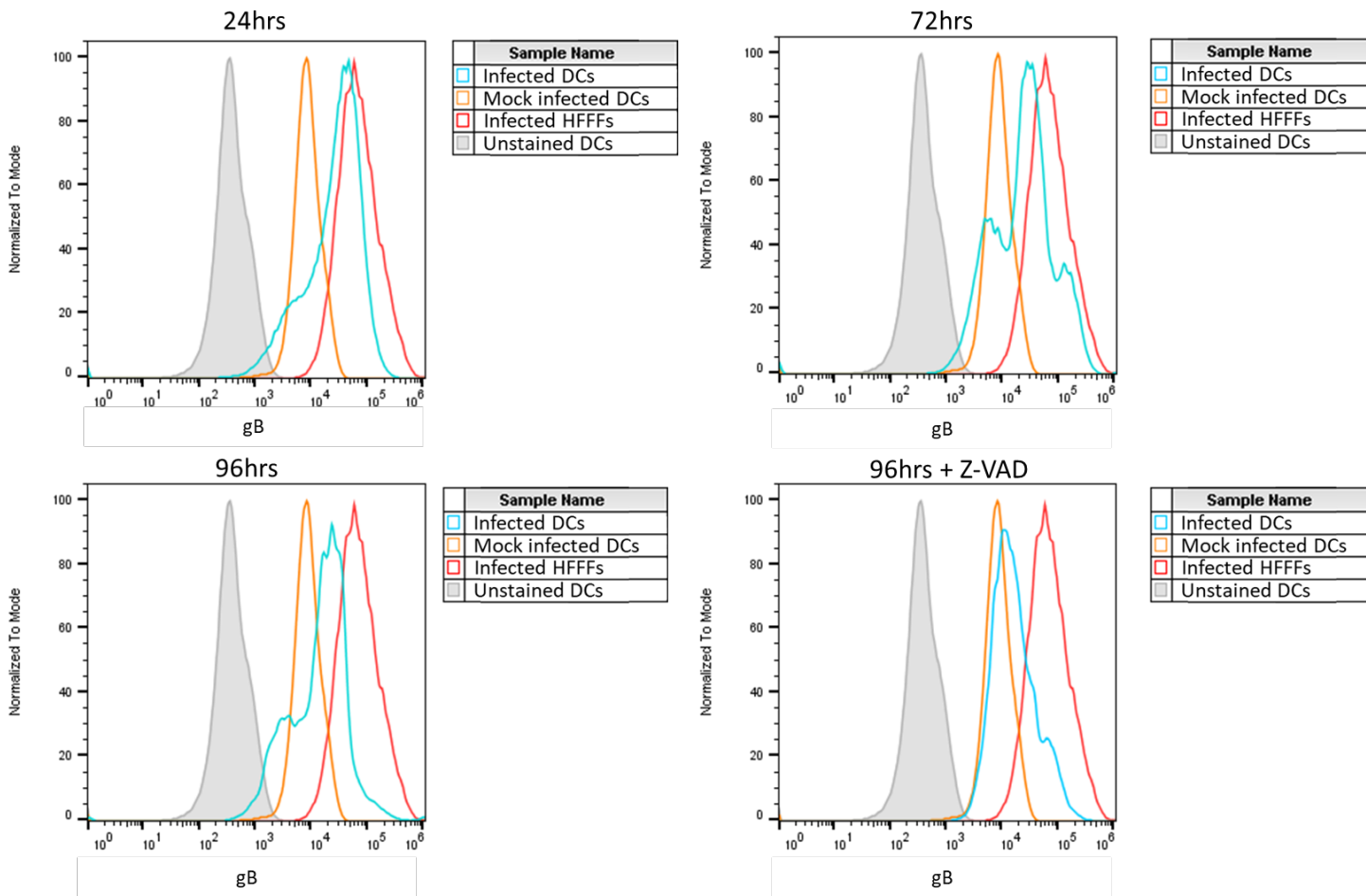


Figure 5.17 – Histogram plots comparing gB expression DCs to positive control over a time course. DCs were co-cultured with UL36-GFP infected HFFF-His cells for 24hrs before separation of HFFFs and DCs. gB was stained for intracellularly and fluorescence was analysed by flow cytometry. HFFFs at 72hrs post-infection used as positive control for gB staining. “Mock” = DCs co-cultured with uninfected HFFFs. CMV -ve serum used as Fc block. Representative of two donors.

5.2.3 Comparing Infection Methods

As all experiments up to this point had used co-culture to infect dendritic cells, and had failed to observe expression of late genes, it was important to determine if this phenomenon was specific to cell-cell infection. TB40 is able to infect dendritic cells without co-culture, albeit with lower efficiency than cell-cell spread of Merlin, and has been shown to undergo the complete lytic cycle¹⁶⁵. Therefore a Merlin virus expressing UL36-GFP was grown in RPE-1 cells, then used to infect DCs via the cell-free route alongside TB40. As Merlin grown in RPE-1 cells produces poor titres (few virions are released into the supernatant) the DCs were infected with 200µl concentrated virus at an unknown MOI, TB40 was used at a MOI 50. Staining for the late gene gB was performed at 96hr post-infection.

As expected, there were problems obtaining a reasonable level of infection with cell-free virus, although this was also the case for the TB40 strain, as shown in Figure 5.18. In the case of the cell-free Merlin, the inoculum used would have contained large amounts of debris, potentially causing premature death of the DCs; similarly, using TB40 at an MOI of 50 could also introduce a large amount of debris to the cells. As infection rates at 24hrs were so low, it was impossible to obtain accurate gB staining at 96hrs post-infection, as many of the infected cells were dead by this timepoint (Figure S.2).

To improve the survival of the dendritic cells, when repeating this experiment, Z-VAD will be added to the DCs at the same time as the virus. Also, to reliably measure late gene expression, instead of using intracellular staining of gB, a dual-tagged UL36-BFP and UL32-GFP Merlin virus will be grown in RPE-1 cells.

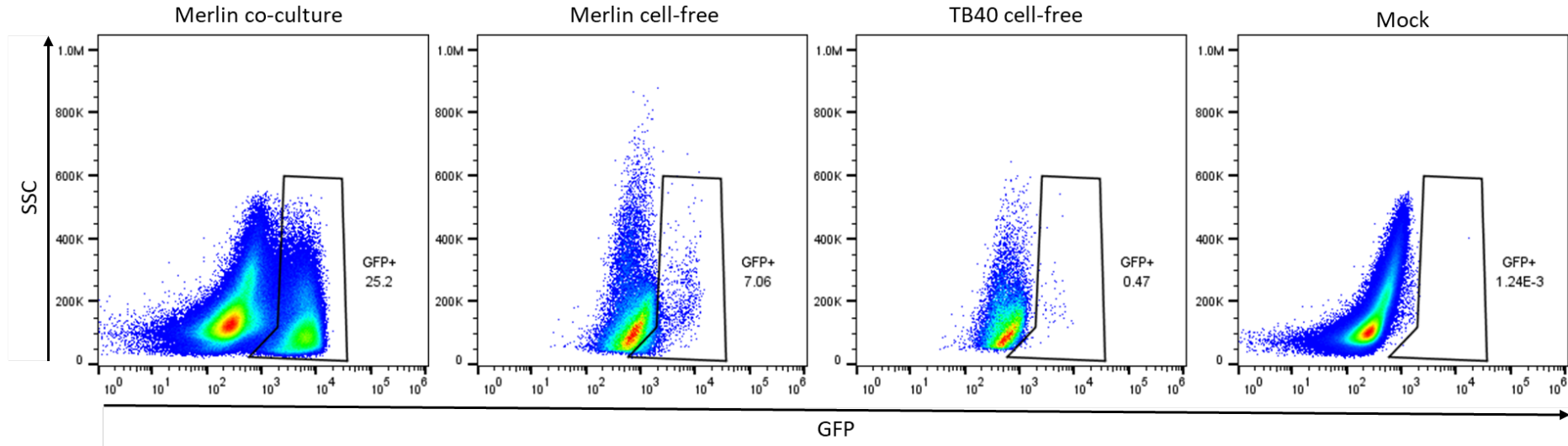


Figure 5.18 – Comparing cell-cell and cell-free infection rates of dendritic cells at 24hrs post-infection. Both Merlin (pAL2344) and TB40 (pAL2413) contained a UL36-P2A-GFP tag. DCs infected cell-free with Merlin at unknown MOI, or with TB40 at MOI 50. DCs infected cell-cell with Merlin were co-cultured with infected HFFF-His cells for 24hrs before separation of HFFFs and DCs. “Mock” = uninfected DCs not co-cultured with HFFFs. DCs were stained with a viability stain and live cells gated before analysing GFP fluorescence using flow cytometry.

5.2.4 APOBEC3A

In fibroblasts, HCMV late genes are expressed by 72hrs post-infection, but this did not occur in DCs, nor did it occur at a delayed time point of 96hrs. When caspase-mediated apoptosis is blocked, there is still no *de novo* expression of the late genes, which gives reason to believe that there is another factor which is blocking the late gene expression. The transition to the late phase of infection is dependent on DNA replication. The fact that viruses were expressing IE and E genes, but were not progressing to the late stage, suggested a specific block at the stage of DNA replication. A literature search of viral restriction factors suggested that the APOBEC proteins would have this affect. APOBEC proteins are a family of cytidine deaminases, which are utilised by the innate immune system against both DNA and RNA viruses, mutating the viral genomes during replication²²⁵. This prompted us to look again at the proteomics data set; when all known restriction factors were compared, only APOBEC3A (A3A) and APOBEC3G (A3G) are upregulated in infected cells when compared to uninfected DCs, albeit this does not occur to the same degree as the bystanders (Figure 5.19). Thus, HCMV may encode a factor that inhibits their expression levels to an extent, but this inhibition is incomplete. Furthermore, Weisblum et. al investigated the effect of A3A on HCMV replication in decidual tissue²²⁶. They found that this protein becomes upregulated in response to infection, and that exogenous overexpression of APOBEC3A generates hypermutations within the viral genome which hinders HCMV replication – there is limited expression of immediate early genes but not of late genes.

Putting all of this evidence together suggested that APOBEC3A could explain the limited late gene expression in DCs. We investigated whether this was the case using siRNA to knockdown A3A.

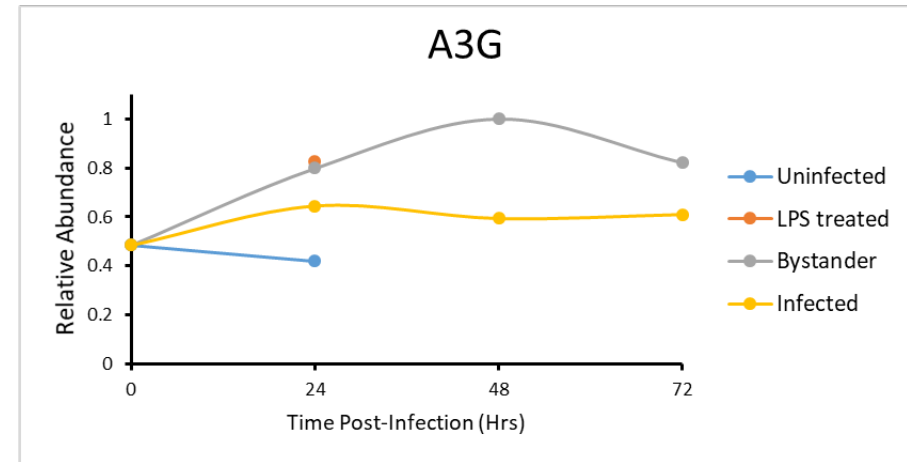
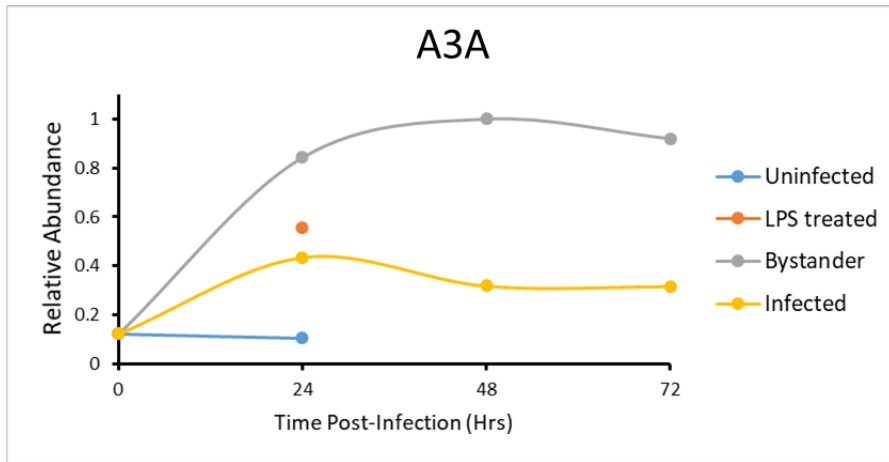


Figure 5.19 – Modulation of APOBEC3A (A3A) and APOBEC3G (A3G) seen in the DC whole cell lysate proteomics dataset. DCs were co-cultured with UL36-RatCD2 infected HFFF-His cells for 24hrs before separation of HFFFs and DCs, and separation of infected and bystander DCs. DCs were lysed and the whole cell lysates analysed for protein abundance.

5.2.4.1 Validating siRNA Knockdown of A3A

Knockdown of A3A in primary DCs was performed using sequential transfections of siRNA on two consecutive days; two days following the second transfection, RNA was extracted from the DCs and RT-QPCR was used to measure the fold change of A3A compared to GAPDH (housekeeping gene).

To calculate the expression change following treatment of DCs with A3A siRNA, the CT was used in the following equations:

$2^{-(\Delta\Delta CT)}$
$\Delta CT = CT \text{ (gene of interest)} - CT \text{ (housekeeping gene)}$
$\Delta\Delta CT = \Delta CT \text{ (treated sample)} - \Delta CT \text{ (untreated sample)}$

Equation 5.1 – Equations used to calculate expression change of target gene in treated sample vs untreated sample.

siRNA Target	RT-QPCR Target	CT	ΔCT	$\Delta\Delta CT$	$2^{-(\Delta\Delta CT)}$	% Reduction
A3A	A3A	32.435	15.041	2.712	0.152618	85%
	GAPDH	17.394	-	-	-	
GAPDH	A3A	29.686	-	-	-	
	GAPDH	18.688	-10.998	1.331	0.397493	60%
Negative	A3A	28.014	12.329	-	-	
	GAPDH	15.685	-12.329	-	-	

Table 5.3 – Percentage reduction of A3A or GAPDH following siRNA knockdown in DCs. CT values and $2^{-(\Delta\Delta CT)}$ values using equations listed in Equation 5.1.

The $2^{-(\Delta\Delta CT)}$ values in Table 5.3 show the target gene expression level in the treated sample as a percentage of that in the control sample²²⁷. I.e. treatment with A3A siRNA knocks down expression of A3A to 15% of that in DCs treated with AllStars Negative siRNA.

5.2.4.2 Measuring HCMV Genome Replication with QPCR

To measure HCMV genome replication in DCs treated with A3A siRNA, siRNA transfected DCs were co-cultured with mCherry-HFFFs infected with a UL36-

RatCD2 tagged virus. Following a 24hr co-culture, infected DCs were purified and the DNA extracted at 24hrs, 48hrs, 72hrs and 96hrs post co-culture. Levels of DNA replication were assessed by QPCR for gB.

According to the data in Figure 5.20A, knockdown of A3A in primary DCs prior to infection by co-culture allowed some genome replication at 96hrs. However, there were only around 80 copies per cell at 96hrs, compared to the >500 copies at 24hrs in HFFFs (Figure 5.20B) – this may reflect the fact that many of the infected cells were undergoing caspase-mediated death by 96h. Hence, when this experiment is repeated, the DCs will be treated with Z-VAD and purified over histopaque to remove dead cells prior to DNA extraction; that should provide more information to determine the effect of A3A knock down on gB expression.

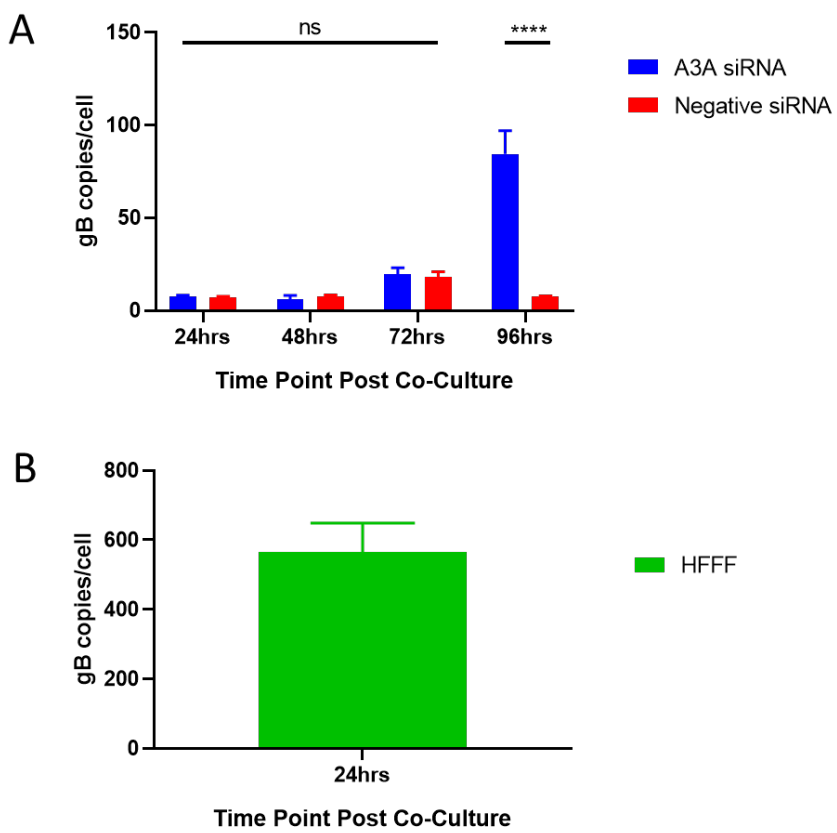


Figure 5.20 – Comparing gB expression in DCs with knocked down A3A to untreated DCs and HFFFs. QPCR used to measure gB copies per cell in each sample. Target cells A) DCs, and B) HFFFs were separated from HFFF-His cells at 24hrs post co-culture. Error bars refer to mean + SD of triplicate samples. ***P < 0.0001 by 1-way ANOVA.

5.3 Summary

This chapter investigated the cell death seen in dendritic cells, and confirmed that the experimental setup was not the cause of this cell death, rather that it was more likely a response of the cell to infection. Z-VAD was able to alleviate the death, suggesting that the pathway is caspase-mediated rather than necroptosis. In addition to the premature cell death, DCs do not express the full repertoire of HCMV genes when infected with the Merlin strain, in particular the genes normally expressed during the late time point in HFFFs. A3A may play a role in blocking late gene expression in DCs.

Chapter 6.

General

Discussion

6.1 Cell-Associated Infection

Cell-cell spread is believed to be a major method by which HCMV spreads within the host; recent clinical isolates spread predominantly by cell-cell infection, and cell-free virus is extremely difficult to isolate from the blood. Cell-associated infection is more efficient than cell-free infection, is also able to conceal the virus from neutralising antibodies, and offers some protection from the IFN response and intrinsic cellular restriction factors^{121, 122}.

The presence of the pentameric complex (gH/gL/UL128L) in the virion is a key factor that determines the ability of the virus to infect and spread in a cell-associated manner in non-HFFF cell types. Lab-adapted strains of human cytomegalovirus that have been passaged in HFFFs contain mutations in the UL128L; these mutations are not only found in heavily passaged strain but also in commonly used low-passage stains¹². When the UL128L is disrupted, HCMV becomes less efficient at infecting epithelial, endothelial and myeloid cells, and disseminates predominantly by the cell-free route *in vitro*^{113, 118, 176}.

The mechanism of cell-associated infection in a wildtype virus is currently unknown. What has been published regarding the mechanism suggests that entry into endothelial and epithelial cells requires the presence of the trimer to facilitate fusion at the cellular membrane by gB following an initiation event dependent on the pentamer which triggers endocytosis and low pH-dependent fusion of the virion with the endosomal membrane^{118, 228}.

6.1.1 Fluorescently-Tagged Virions

The Merlin strain has had its genome repaired so that it has an intact UL128L under the control of a tetracycline repressor system¹⁰². Using this strain I attempted to tag the viral genome with fluorescent proteins, with the aim of visualising both entry and egress of HCMV in HFFFs – building upon the work by Sampaio et al^{181, 182}. UL32, a tegument protein expressed in the late timepoint of infection, was tagged with GFP; the C-terminus of the envelope protein gM was tagged with mCherry; and as a marker of infection, the immediate-early UL36 gene was tagged with UL36-BFP (pAL2479). Unfortunately, this virus suffered from a severe growth defect and the gM protein

appeared mis-localised. Viruses tagged individually with UL32-GFP or UL36-P2A-GFP/mCherry have previously shown no growth defects, therefore it seems likely that the mCherry tag affected the function of gM. Therefore alternative envelope glycoproteins were investigated.

The glycoproteins gB and gH in HSV were previously tagged with a fluorescent protein¹⁸³, hence these were tagged with mCherry in HCMV, however both viruses also suffered serious growth issues. Tagging gH (pAL2566) seemed to impact both cell-free and cell-cell infection. As this glycoprotein is key to both the trimeric and pentameric complexes, it is clear that the tag negatively affected the function of this protein. The gB-mCherry (pAL2605) virus demonstrated similar mis-localisation to gM-mCherry throughout the cell, and also failed to reach 100% CPE. The same 9 amino acid long flexible linker sequence was used when adding the fluorescent tags, it is possible that the linker sequence and/or fluorescent tag affected the folding or trafficking of the selected. Using a longer or more flexible linker may reduce this issue. Nevertheless, it is clear that these molecules are highly sensitive to the addition of bulky tags, thus considerable care and optimisation needs to be taken when tagging them in HCMV.

Due to the unsuccessful attempts to tag gM, gB and gH, Dr Christian Sinzger gifted us a construct that had previously been used to investigate viral entry: the UL32-GFP/gM (external loop)-mCherry virus¹⁸² (pAL2624) – they found that by placing the mCherry tag after the first transmembrane loop of gM, instead of at the C-terminus, they were able to circumvent major growth problems. Nevertheless, this virus still experienced a 1-log reduction in titre, indicating that there remains a functional impact of tagging gM in this way. I then attempted to insert the third fluorescent tag. The resulting virus, UL32-GFP/UL36-P2A-BFP/gM-mCherry-gM (pAL2759), was successfully recovered in culture, however the titre obtained was far worse than that of the parent strain. I concluded that the cumulative effects of each of the fluorescent tags severely impact the growth of HCMV, regardless of where the tags were located. However arguing against this, a recent publication by Rand et al has demonstrated that the TB40/E strain can be tagged with three fluorescent proteins (HCMV^{3F}), apparently with only a slight growth defect when compared to wildtype²²⁹; each of the three proteins (UL148A, UL112/UL113 and UL122/UL123) was linked using a self-cleaving 2A peptide, as the sole purpose for this virus was to detect the immediate

early (IE), early (E), and late (L) phases of lytic replication, and not to track individual virions. Interestingly, although a UL32-GFP virus had previously been grown in the lab without problems in the context of a virus mutated for UL128, when I grew RCMV2422 (which contains a single UL32-GFP tag in a virus expressing UL128), titres were consistently lower than expected. This may indicate that tagging UL32 with GFP impacts virus growth in the context of a fully wildtype virus, and could have partially contributed to the problems I observed. Alternatively, another tegument protein such as pp28 (encoded by UL99) could be tagged with a fluorescent protein; pp28 has previously been tagged in the AD169 strain with minimal impact on the growth of the virus²³⁰, this protein could be tagged in Merlin but whether this has a similar effect to tagging UL32 would need to be assessed.

The single-tagged UL32-GFP (pAL2422) was therefore used to optimise long-term fluorescent microscopy in live cells. Real-time imaging of live cells over several days with the addition of fluorescently tagged virions was intended to visualise viral entry, egress and the stages at which viral particles acquire and lose tegument and envelope. Despite using different combinations of binning, exposure, and power at a frequency of 30 minutes, imaging with Z-stacks caused phototoxicity in HFFFs before the full lytic cycle had run its course. The phototoxicity was only exacerbated when Hoechst was added to the cells, which meant that it would be extremely difficult to capture the entire lifecycle of the triple-tagged virus in these cells. As there was only a single fluorescent tag incorporated into the virions, it was difficult to tell at what stage a cell was at when imaging began. With these issues, it was not possible to continue working with HFFFs, so attention turned to RPE-1s.

The RPE-1 cells were far less sensitive to phototoxicity than HFFFs, and I was able to image using the dual-tagged UL32-GFP/gM-mCherry virus (pAL2624) over several days. Virions could be seen moving within the cell in real-time, which has not previously been published for HCMV, but has been documented for other viruses. For example Ward et al tracked the saltatory movement of fluorescent Vaccinia particles and determined that they were most likely hijacking microtubules in order to be transported throughout the cell²³¹ – it was not possible to track the movement of the HCMV virions during this project, however UL32 has previously been shown to be associated with microtubules when infected cells were treated with the microtubule-

depolymerising drug nocodazole²³², hence future work to track virions in real-time could involve both the dual-tagged virus and nocodazole.

While imaging virus particle movement, some of the infected RPE1 cells formed membrane extensions, in which virions could be seen moving. HTLV-1 utilises membrane extensions for cell-cell infection of neighbouring cells, it is possible that in certain cell types HCMV does this too¹²³. Epithelial cells, including retinal pigment epithelium, have primary cilia, which are membrane extensions supported by microtubules²³³; other herpesviruses hijack microtubules to traffic bidirectionally within the cell²³⁴, thus HCMV could be utilising these microtubule-rich extensions in epithelial cells to spread within epithelial tissues. Had the UL36-BFP/UL32-GFP/gM-mCherry virus grown to reasonable titres, then this could have been used to determine if contact with these membrane extensions led to infection of neighbouring uninfected cells, and to quantitate how common this phenomenon was.

6.1.2 The Mechanism of Cell-Associated Infection

To complement the fluorescence microscopy, TEM was used to obtain detailed images of the junctions formed between neighbouring HFFFs and DCs. Both HIV and HTLV-1 can infect cells via a “virological synapse”, a niche similar in structure to the immunological synapse that protects virions from extracellular defences such as neutralising antibodies^{123, 178, 179}. The TEM showed that a structure forms between an infected HFFF and an uninfected DC, in which there are mature virions and dense bodies. This may be a virological synapse, and potentially the mechanism used by wildtype HCMV to spread both *in vitro* and *in vivo*. Gerna et al have previously reported that HCMV cell-cell spread occurs via microfusions in the cellular membrane. However the strain used contained large deletions in the genome, and did not contain the wildtype UL128L required to force the virus into the cell-cell spread that is characteristic of clinical isolates¹⁸⁰. Furthermore, more recent work demonstrated that a full complement of virus entry glycoproteins are required for cell-cell spread of Merlin to occur¹²⁰. This is more consistent with a virological synapse, where intact virions exit and enter adjacent cells, than transfer of capsids between cells without membrane fusion. While the TEM was informative regarding the mechanism of transfer, I was not able to determine whether the transfer was directional. More

images will need to be taken of the co-cultures, especially of the cell membrane of the infected HFFFs; if viral particles are released evenly from the cell then the cell-cell spread is non-directional, and may simply represent virions released from the infected cell and captured non-specifically at the interface between cells. Alternatively there may be clear polarisation of the new virions towards the neighbouring uninfected cell, as has been observed in HIV and HSV^{116, 235 236}. This could have been determined by using cryo-SXT had there not been mechanical issues and technical difficulties due to restrictions imposed as a result of the COVID-19 pandemic; cryo-SXT has very recently been used by Nahas et al during HSV-1 infection, where virions were seen along the junctions between cells²³⁷.

In addition to protecting viral particles, the virological synapse could increase the efficiency of cell-cell spread by enabling a larger number of virions to enter the cell. In support of this, cell-cell infection of HCMV delivers well over ten times the number of genomes compared to cell-free infection with an MOI of 10. In other viruses this is believed to occur by causing virions to accumulate on the cell surface at the site of infection, and reducing the distance that they need to travel¹¹⁶. It seems likely that the same is true for HCMV. Further work will be needed to discover whether the ability of cell-cell spreading HCMV to overcome innate and intrinsic immunity is related to this large number of genomes (and associated tegument proteins) delivered.

Neutralising antibodies produced during a natural infection are able to reduce the infectivity of multiple HCMV strains *in vitro*, including AD169, TR, Toledo and VR1814^{75, 112}; the majority of antibodies target glycoproteins and envelope complexes, and are very effective against cell-free infection¹⁰. In the context of cell-cell infection, however, viral particles are protected from the detrimental effects of neutralising antibodies, as long as UL128L is expressed at high levels^{121, 122, 177}. Merck developed monoclonal antibodies against the pentamer and gH/gL which are active against cell-free virus at much lower concentrations than the polyclonal response arising from natural infection^{185, 186}. This provided an opportunity to investigate whether cell-cell spread is completely resistant to neutralising antibodies, or whether this resistance can be overcome. Both antibodies reduced cell-associated infection, although the amount of antibody required was significantly higher than for cell-free virus. This implies that antibodies do have access to cell-cell spreading virus, however this process requires high concentrations of very potent antibody, and inhibition

remains incomplete. I also investigated whether, in those cells that did become infected, these antibodies reduced the number of virions delivered. Surprisingly, it appeared that genome delivery was actually enhanced. There are two hypotheses for this are: 1) the antibodies are coating the virus particles and as such, there is increased internalisation of these particles which are then degraded in endosomes, and are consequently unable to cause productive infection in the RPE-1s; or 2) the antibodies are interrupting viral transfer in a proportion, but not all, of the cell-cell junctions, therefore reducing the rate of infection of epithelial cells, while the cells that do become infected receive more genomes. To differentiate these possibilities, genomes were isolated from the nuclei of cells, rather than from the entire cell. Unfortunately, experimental variation prevented this question from being answered conclusively. Further repeats could not be done as the potent neutralising antibodies have been discontinued by Merck. I was able to find the sequences of their antibodies in a patent, and began cloning them, however I was unable to complete production before the end of the project.

The generation of new antibody stocks will also enable further questions to be addressed regarding the mechanisms of resistance of cell-cell spreading virions to antibodies. In particular, it will be possible to generate Fab fragments²³⁸, to investigate whether smaller antibody fragments may be better able to enter virological synapses, increasing antibody effectiveness. Alternatively, it is possible that neutralisation of cell-cell spread occurs through active antibody transport via molecules such as the intracellular antibody receptor tripartite motif containing-21 (TRIM21), which targets virions for proteasomal degradation^{239, 240}. If this is the case, removal of the Fc domain will result in failure to inhibit cell-associated spread of HCMV.

6.1.3 Superinfection and Recombination

Strains of HCMV are able to superinfect the same host, and it is clear from genetic data that recombination between different strains plays a major part in the generation of genetically distinct strains worldwide^{188, 189}. The ability of HCMV to superinfect is unusual, and is dependent on the virus' ability to downregulate MHC-I, and to overcome the CD8⁺ T cell response^{188, 189, 241}. A pre-requisite for recombination is that two viruses must co-infect the same cell *in vivo*. Given that cell-cell infection was

highly efficient, and delivered a greater number of genomes to the uninfected cell, I wondered whether infection via this route could lead to greater rates of superinfection and/or recombination than cell-free infection. This process was investigated using cell-free infection with viruses containing different fluorescent tags at opposite ends of the genome (UL36, and US28). Given that the viruses were otherwise identical, there should have been a high probability of recombination occurring at any point along their length. PDGFR α , one of the predominant receptors used for cell-free infection in HFFFs^{117, 119, 190}, was downregulated from the cell surface rapidly following infection, which could make it increasingly difficult to superinfect. In line with this, although cells could be readily co-infected if infected at the same time, superinfection by cell-free virus did not convincingly produce a large population of double-positive cells. When the same experiment was carried out using cell-cell infection, double-positive cells were again difficult to demonstrate convincingly. This provides further support for the fact that cell-cell spread is dependent on the transfer of intact virions, but also raises the question of what conditions are required for two viruses to co-infect the same cell and recombine *in vivo*. Superinfection of the same cell is clearly inefficient, and can only occur within a very small time-window.

Another interesting observation was that UL36-GFP expression levels were clearly lower from one of the viruses when it was co-infected at the same time as a second virus. This phenomenon is hard to explain, but may indicate that the expression of each virus is partially suppressed by the other. However, it also raised the possibility that superinfection was occurring (and could potentially lead to recombination), but was undetectable due to suppression of expression of the fluorescent tag in the co-infecting virus. When the supernatant from ‘superinfected’ cells was used to infect a new monolayer, cells co-expressing both tags were detected, albeit at a fairly low level (~10%). This could indicate co-infection of the same cell with two viruses, or genuine recombination; it would be interesting to plaque purify these viruses and sequence them, to determine whether recombination had occurred.

In summary, superinfection and recombination does not occur readily or at a high level. As a result it was not possible to determine whether cell-cell spread specifically contributed to enhancing this process.

6.2 Manipulation of Proteins in Dendritic Cells

HCMV causes a life-long infection in the host and encodes numerous immune evasion proteins that inhibit the activation of NK cells, T cells and other elements of the immune response^{24, 148, 191}. Clinical strains of HCMV are able to infect DCs, a cell type that bridges the innate and adaptive immune responses, and plays a major role in the induction of adaptive immunity. Hence there is likely to be an advantage to the virus in manipulating the function of these cells following infection; indeed, previous work has shown that the virus downregulates co-stimulatory molecules (such as MHC-I, MHC-II, CD40 and CD80), and inhibits the ability of DCs to stimulate T cells^{167, 168}. Given the size of the HCMV genome, and the number of proteins it encodes, it seemed likely that viral manipulation of DC functions encompassed a much broader number of mechanisms than have been discovered to date. Multiplexed quantitative proteomics has proven to be a robust technology to discover novel proteins involved in the cell's antiviral response, and the ways that HCMV antagonises this response in cultured fibroblasts¹⁷². This same approach was therefore used to provide an unbiased proteome-wide view of the impact of virus infection on both the whole-cell, and plasma membrane, of primary DCs infected with a HCMV strain expressing the complete complement of viral genes.

This required considerable technical optimisation, but was ultimately successful in generating a high quality dataset. The whole cell lysate dataset revealed that HCMV downregulated 99 proteins in the DCs by at least 3-fold, and that 63 of these had not been previously quantified in the HFFF proteomic analysis¹⁷². Furthermore, there were also novel proteins detected when the plasma membrane samples were processed; of the 43 proteins downregulated and 53 upregulated, 28 and 15 were not quantified in HFFF, respectively. This indicates that HCMV likely encodes proteins that specifically target proteins required for DC function, for modulation. Differences were also observed between the bystanders and uninfected cells, however there were also differences between bystanders and LPS treated cells. This indicated that despite not becoming infected themselves, the bystander DCs were not simply undergoing maturation in response to infection, but were also being modulated, possibly by immune-regulatory cytokines and other soluble mediators. However it should be remembered that DCs can mature in response to multiple different stimuli, and we only tested one (LPS); a full investigation of how HCMV infection impacts bystander

maturation would ideally incorporate DCs matured with multiple different stimuli, such as TNF, IL-1 β , IL-6 and prostaglandin E2 (PGE2).

The modulated proteins were grouped by function using DAVID pathway analysis, revealing that the majority of proteins were involved in or altered the immune response to some extent; this includes DC maturation and T and B cell activation. Of the thousands of proteins identified in both the WCL and PMP datasets, 15 proteins were selected for further investigation: ALCAM, Caspase 10, CD84, Dectin-1, ICAM3, ICOSL, IRF7, LAG3, c-Met, OSCAR, PECAM1, SCIMP, SECTM1, Semaphorin-4A, and Leukosialin. These proteins were selected based on their clear manipulation by the virus. We also focussed on proteins that have not previously been reported to have been modulated by HCMV, but that had reported functions in DCs, so that they could be followed up using functional studies.

- ALCAM, a protein responsible for promoting the interaction between DCs and T cells and therefore T cell proliferation²⁰⁰, was downregulated in the plasma membrane dataset. This was confirmed by flow cytometry. Further investigation of the effect that HCMV has on this protein would involve both T cell proliferation assays and visualisation of DC-T cell contacts in the presence of infection +/- blocking antibodies, as has been previously published²⁰⁰.
- Caspase 10 is a proteolytic enzyme involved in initiating apoptosis, and was downregulated in the whole cell lysate. HCMV is known to encode several apoptosis inhibitors including vMIA and vICA, however, none yet have been identified that specifically target Caspase 10, either directly or indirectly^{26, 223, 224}. I was unable to validate the downregulation of Caspase 10 in the DCs; intracellular staining and subsequent flow cytometric analysis did not definitively show downregulation, and antibodies did not work in Western Blot. A screen of more antibodies will be needed to identify one that works well.
- CD84 drives autophagy and therefore DC maturation and T cell activation^{201, 202}, making it a logical target for HCMV. This protein was downregulated in both datasets, and was clearly downregulated when analysed by flow cytometry.

- Dectin-1 is a pattern recognition receptor that signals via the Syk pathway, and SCIMP regulates Dectin-1-dependent MAP kinase activation, which leads to priming of cytotoxic T cells and production of pro-inflammatory cytokines^{203, 211}. The downregulation of both proteins was validated using flow cytometry.
- ICAM3 is the ligand for LFA-1 expressed on T cells, is involved in the initial DC-T cell interaction²⁰⁴ and was seen to be downregulated in the proteomics dataset. However, when staining for flow cytometry, there was no obvious difference between any of the samples. However staining overall was weak, and antibodies did not work in western blot. Additional antibodies are needed to confirm this effect.
- ICOSL is another ligand for a receptor expressed on T cells (ICOS); co-stimulation via ICOS results in the proliferation of activated T cells. The downregulation of this protein was confirmed using flow cytometry. A recent publication has shown that in mice, MCMV leads to the downregulation of ICOSL, interfering in the T cell response and reducing MCMV-specific antibody production, underlining the importance that modulation of ICOSL has to the virus²⁴².
- HCMV is able to hamper activation of the IFN pathway, and in accordance with this, proteomic analysis revealed that IRF7 is downregulated following infection. As this protein is expressed in the nucleus, I used an immunofluorescence assay to attempt to validate the modulation of IRF7 – unfortunately, the background fluorescence was very high, so it was difficult to establish what was real IRF7 expression. The anti-IRF7 antibody also failed to stain a Western Blot membrane, which suggests that there was an issue with this antibody. Nevertheless, another herpesvirus, Kaposi's sarcoma-associated herpesvirus, also prevents phosphorylation and accumulation of IRF7 in the nucleus, therefore impeding induction of the IFN genes²⁰⁵. Thus modulation of IRF7 may be a common mechanism amongst the herpesviruses to inhibit IFN activation.
- LAG3 generally has a negative regulatory role in the immune response but can promote maturation of DCs^{206, 207}. Despite being downregulated in both the whole cell and plasma membrane proteomics, flow cytometry showed a slight upregulation in infected cells; this result needs to be repeated as there was very

poor staining. When LAG3 was investigated in mice, it was found to be uniquely expressed on plasmacytoid DCs²⁴³; as the proteomics uses relative abundance of the proteins, it could be that expression levels of LAG3 in these monocyte-derived DCs is actually very low and that downregulation by HCMV has very little effect on the cells.

- c-Met is upregulated 25-fold on the DC cell surface following infection, and hence was the only upregulated protein that was selected for follow up. c-Met is the receptor for hepatocyte growth factor, the addition of which to dendritic cells reduces antigen presentation and ultimately affects T cell proliferation²⁰⁸. Flow cytometry confirmed that the expression of c-Met is higher on the surface of infected DCs than the bystanders or mock-infected cells.
- OSCAR, a receptor found on both immature and mature DCs, allows exogenous antigen presentation and activation of DCs²⁰⁹. The plasma membrane dataset shows that this protein is downregulated on the cell surface of infected cells, and this was validated by flow cytometry.
- PECAM1 becomes downregulated on DCs during the maturation process²⁴⁴, which can be seen when comparing the uninfected DCs to the bystanders and LPS-treated sample in both proteomic datasets. PECAM1 is also involved in the reverse transmigration of dendritic cells and other leukocytes across the lymphatic endothelia, a requirement for peripheral DCs to be able to prime the adaptive immune response^{210, 245}. In infected DCs, the level of PECAM1 was below that of the bystanders, suggesting that further downregulation of this protein is advantageous to HCMV; this was confirmed using flow cytometry.
- SECTM1 co-stimulates T cells via CD28, and its soluble form enhances CD4 and CD8 T cell proliferation as well as IL2 production²¹². Despite both proteomics datasets appearing to show that SECTM1 is massively upregulated in the bystander cells, staining with an anti-SECTM1 antibody and analysing the cells using flow cytometry showed the opposite result, where expression of the protein in the mock and infected samples was higher than in the bystanders. Attempts to then use Western Blot were unsuccessful, indicating that a different antibody will need to be used to obtain reliable results.
- Semaphorin-4A is a transmembrane protein expressed on DCs that primes T cells via the Tim-2 receptor, and also co-stimulates activated CD4⁺ T cells

using the ILT-4 receptor, therefore driving Th2 responses^{213, 246}. In Semaphorin-4A knockout mice, there is an impairment of T cell-priming and antibody responses to T cell-dependent antigens²⁴⁷, hence downregulation by HCMV likely has the same goal. This downregulation was also seen in the flow cytometric analysis.

- Finally, Leukosialin was previously quantified in HFFFs, despite being expressed on most haematopoietic cells. When this protein is cross-linked on DCs it triggers maturation of the cells and therefore increases antigen presentation to T cells²¹⁴. The downregulation of Leukosialin was validated using flow cytometry.

Thus where reliable staining was observed, modulation of the selected target proteins was nearly always validated, providing confidence in the proteomic datasets. The next step will be to determine the functional importance of these modulations. This requires identifying the viral gene that is responsible for manipulating each of the proteins. Publications by Fielding and Wang have previously used the approach of generating a series of viruses lacking large sections of the HCMV genome to screen for the genome region responsible^{24, 153}. However these viruses were all constructed on the background of a virus lacking UL128L. I therefore created the same block deletion mutants in virus containing an intact UL128L for infection of DCs, and a UL36-P2A-RatCD2 tag to enable purification of infected cells. Between the 15 viruses made, 45% of the 170 viral genes are knocked out, with each virus lacking 2-8 non-essential genes. Fielding et al used block deletion mutants to identify the US12 gene family as key players in NK evasion, following infection of HFFF. Interestingly, they also found that knockdown of three specific genes increased the relative abundance of two of the genes (ALCAM and ICOSL) identified in our DC dataset²⁴. However, they were unable to validate these effects in HFFF. As the downregulation of ICOSL and ALCAM was clearly observable in infected DCs, I then made Δ US16, Δ US16&US20, Δ US18, Δ US18&US20 and Δ US20 viruses on the background of a DC-tropic virus expressing RatCD2.

Not all viruses were grown to sufficient titre for analysis. Nevertheless, for ALCAM, mutants lacking US20, or US18 and US20, were tested. A very slight recovery of the

protein was observed with these viruses. US16 and US20 were indicated to be involved in the downregulation of ICOSL, and cells infected with the ΔUS16&US20, ΔUS20 and ΔUS18&US20 viruses all showed a greater level of ICOSL expression than the ΔUS18 mutant and wildtype. Despite these effects, the levels of ICOSL or ALCAM were not restored to that seen in the mock cells in any mutant. This suggests that there are other viral genes/proteins that interact with and downregulate these proteins, either directly or indirectly. Since the proteomics screen and validation of ICOSL downregulation, an investigation into ICOSL in mice following MCMV infection has been published; in this paper, the product of the m138 gene targets ICOSL to the lysosome for downregulation in a range of APCs including DCs and macrophages, demonstrating the importance of ICOSLG modulation²⁴². There is no homolog of m138 in HCMV, thus the block deletion mutant proteomics screen in DCs will be required to identify additional viral antagonists.

The block deletion mutants were successfully made and grown, for the purpose of doing another proteomics screen. Each of the sequenced genomes have now been analysed and are ready for use in the proteomics screen.

6.3 Are DCs Able to Block the Lytic Cycle?

6.3.1 Premature Cell Death

HCMV encodes multiple inhibitors of cell death such as apoptosis, including proteins that directly or indirectly affect the activation of caspases, and necroptosis^{26, 215, 222, 223, 224}. HCMV uses these inhibitors to extend the lifespan of cells, including monocytes. However, primary monocyte-derived dendritic cells infected with HCMV strain Merlin *in vitro* demonstrated exacerbated levels of cell death. This was evident when preparing the DCs for the PMP for the proteomics analysis; it was difficult to maintain sufficient live infected cells, necessitating dead cell removal by histopaque prior to analysis. Extensive analysis of samples at multiple stages of the separation protocol demonstrated that this was not due to the separation process *per se*. The level of death was somewhat unexpected, since cell-free infection of DCs has been reported before, and this phenomenon has not been reported¹⁶⁵. A number of potential reasons exist for this difference. It could have been due to the analysis method used. Previous publications have used an indirect immunoperoxidase staining of a single protein to demonstrate infection¹⁶⁵. By following both IE and late gene expression over time, we may have observed this where others didn't. Alternatively, the difference could be due to our use of cell-cell infection. Unfortunately, when I attempted to verify this by comparing cell-cell with cell-free infection, almost all of the DCs died. This may have been due to the high levels of cellular debris in the concentrated 200µl that was added to the DCs. A major difference between cell-cell and cell-free infection is the number of DCs that become infected. I also therefore tested the effect of co-culturing DCs with HFFFs that had been infected at a lower MOI (MOI 0.2 & 1, instead of MOI 5)(data not shown). This did appear to improve the survival of infected DCs at 72hrs; however as this was a single experiment, it will need to be repeated before any conclusions can be drawn.

Mature DCs have previously been reported by Raftery et al to be susceptible to infection by HCMV²¹⁷, however in contradiction to that publication, while maturation of the DCs improved the overall survival of the cells, these cells were less infectable than the immature cells in our hands – hence immature cells were used in all future experiments. In addition to this, treatment with Etanercept had no effect on the survival

of the infected DCs, so TNF induced by infection did not appear to be triggering apoptosis.

As there was nothing obvious that could be changed technically to reduce cell death, attention turned to molecular causes of cell death such as apoptosis and necroptosis. HCMV encodes inhibitors of these cell death pathways, but it is possible that the DCs mount such a strong response that the viral genes are unable to overcome this. DCs were treated with Z-VAD and Nec-1s which are inhibitors of caspase-mediated apoptosis and necroptosis, respectively. Treatment of the DCs immediately after separation from the HFFFs with Z-VAD was able to prevent a decline in the number of infected DCs up to 72hrs post co-culture, while treatment with Nec-1s had only a small impact. This suggests that the DCs are undergoing caspase-mediated death. Blocking of apoptosis would usually direct cells to undergo necroptosis, however the ineffectiveness of Nec-1s indicates that this did not occur, consistent with HCMV inhibiting necroptosis – in MCMV, the viral inhibitor of RIP activation (vIRA) is responsible for interrupting the necroptotic pathway when triggered by vICA suppressing caspase 8, while in HCMV UL36 has been shown to be sufficient to inhibit necroptosis by degrading MLKL, in addition to its roles in inhibiting apoptosis^{10, 248}.

Caspase-mediated apoptosis in human cells is controlled by initiator and executioner/effectector caspase. The initiator caspases – caspases 2, 8, 9 and 10 – are originally synthesised in their inactive pro-caspase form, which are activated following cleavage as a result of extrinsic (binding of TNF or FasL to death receptors) or intrinsic stimulation (DNA damage or release of cytochrome C from mitochondria). Once an initiator caspase has been activated, this promotes cleavage of the effector caspases – caspases 3, 6 and 7 – which triggers caspase-dependent apoptosis²¹⁸. To investigate the caspase-mediated apoptotic pathway further, each of the initiator and effector caspases were examined; the cellular levels of each caspase were reviewed in the proteomics data, however this did not provide any information regarding cleavage or activation. Individual inhibitors of the initiator caspases were used to treat infected DCs to determine which was involved in the processes seen in these cells.

- Caspase 2 is activated following DNA damage and has been linked to ER stress-related apoptosis in response to viral infection²¹⁹. This initiator caspase

was present at relatively low levels in both infected and bystander DCs, and didn't seem to be directly modulated by HCMV – although the UL38 protein acts upstream of Caspase 2 and prevents its cleavage^{220, 249}. Treatment of dendritic cells with the caspase 2 inhibitor Z-VDVAD had very little effect on their survival, indicating that caspase 2 is not responsible triggering apoptosis, potentially because this protein is already inhibited indirectly by UL38.

- Caspase 3 is an effector caspase which promotes DNA fragmentation and breakdown of the cytoskeleton following activation. Caspase 3 is slightly upregulated in bystander DCs but not in the infected cells, which implies that HCMV is blocking upregulation of this protein and possibly activation too.
- Caspase 6, the executioner caspase responsible for nuclear shrinkage, does not appear to be modulated by HCMV; it is possible that HCMV acts upstream of this caspase to prevent apoptosis.
- Caspase 7 is the third effector caspase. Activation of this caspase leads to cell detachment from the ECM; Caspase 7 is also able to start a positive feedback loop which drives activation of Caspase 6. This caspase was seen to be greatly downregulated in infected cells in the proteomics data – this suggests that HCMV is preventing upregulation of Caspase 7, however, it is unknown whether it undergoes cleavage and maturation following infection despite its modulation.
- Caspase 8 is the initiator caspase activated by binding of TNF and FASL binding to TNFR1 and Fas, respectively. Caspase 8 coordinates the activation of the effector caspases, and blocks necroptosis. HCMV encodes the vICA which prevents cleavage of pro-Caspase 8²⁶. The difference of expression levels of Caspase 8 in infected and bystander cells was quite small, with the relative abundance in infected cells being slightly lower; this indicates that HCMV doesn't require downregulation of this protein as it inhibits activation instead. Although the vICA's function is to block Caspase 8 and therefore apoptosis, treatment of DCs with the inhibitor Z-IETD saw a vast improvement in the survival of these cells, albeit not always to the extent as the pan caspase inhibitor Z-VAD.
- Caspase 9, activated following release of cytochrome C from mitochondria, is indirectly inhibited by vMIA encoded by HCMV – vMIA blocks the release

of cytochrome C^{223, 224}. Caspase 9 was not detected in the proteomics, which could mean that it is expressed at very low levels in DCs; regardless, Z-LEHD was used to inhibit Caspase 9 in DCs to determine if this protein did play a role in apoptosis. This inhibitor had no significant effect when compared to untreated cells, so it is likely that the abundance of Caspase 9 in DCs is too low to trigger apoptosis.

- Finally, Caspase 10 is another initiator caspase, triggered by extrinsic stimuli such as TNF and FasL. As mentioned previously, this protein was selected for validation as it was shown to be downregulated greatly in infected DCs when compared to bystander DCs; however, I was unable to successfully stain for Caspase 10 using flow cytometry or Western Blot. Treatment of DCs with the Caspase 10 inhibitor Z-AEVD consistently reduced the death seen in infected DCs, similarly to Z-IETD (Caspase 8 inhibitor).

It seemed surprising that viral inhibitors of necroptosis would function in DCs, while inhibitors of caspase 8/10 mediated apoptosis wouldn't, especially given that UL36 inhibits both caspase-8 mediated apoptosis and necroptosis, while caspase 10 was clearly downregulated by infection. Given that the virus used for most of these experiments contained a GFP tag on UL36, I was concerned that UL36 was not functioning completely in DCs, despite a previous publication demonstrated that incorporating a UL36-tag did not affect HCMV's ability to impede Fas-mediated apoptosis¹⁹². This concern proved unfounded, because moving the GFP tag onto IE2 retained identical levels of cell death. A further complication was that caspase inhibitors are not fully specific, making it difficult to know whether the caspases identified by the inhibitors (i.e. caspase 8/10) are truly responsible. Future work could measure activation of these caspases specifically. Nevertheless, it is clear that the pathway responsible for the death seen in infected DCs involves caspases in some capacity. One possibility is that the DCs were undergoing pyroptosis – an inflammatory pathway dependent on Caspase 1, mechanistically distinct from apoptosis and not involving the apoptotic caspases²⁵⁰. HCMV has previously been shown to induce pyroptosis in macrophages by triggering the assembly of the absent in melanoma 2 (AIM2) inflammasome²⁵¹, this complex binds dsDNA and is also found in dendritic cells²⁵². It would be straightforward to determine if pyroptosis were

the pathway responsible for the cell death in HCMV-infected DCs: as a result of pyroptosis, the cytokines IL-18 and IL-1 β are released into the supernatant in their mature forms²⁵³, these cytokines have been shown to be produced following HCMV infection and could be detected by running a sample of the supernatants from the co-culture and post-HFFF separation through a Luminex^{254, 255}; furthermore, gasdermin D (GSDMD) is activated following cleavage, this pore-forming molecule could be detected in its immature and mature forms by Western Blot²⁵⁶.

6.3.2 Inhibition of Late Gene Expression

While analysing the proteomic data from DCs, we noticed a surprising phenomenon relating to viral gene expression in dendritic cells: Merlin-infected DCs showed slightly delayed kinetics of viral gene expression compared to HFFF, with the Tp4 class of proteins delayed by 24hrs, and Tp5 proteins were not expressed at all at 72hrs. Experiments to validate this result, and to extend the timepoint to 96h were subject to some technical issues. Nonetheless it did not appear that Tp5 gene expression occurred at 96hr either, even when DCs were treated with Z-VAD to improve their survival rates. This suggested that the lytic cycle in DCs is blocked. This contradicts the current literature, where TB40 has been shown able to complete its full lytic life cycle, albeit with delayed kinetics¹⁶⁵.

I therefore investigated differences between my experimental setup, and that of Riegler et al: the strain of HCMV used and the route of infection. Hence, I compared cell-free infection of Merlin to that of TB40; cell-free titres of wildtype Merlin when harvested from HFFF are negligible, this can be improved somewhat by growing it in RPE1 cells. Nevertheless, titres remain low, so the DCs were infected with 200 μ l concentrated virus. Even using this protocol, levels of infection were low, and combined with high levels of cell death (likely due to the large amount of debris in the inoculum), I was unable to answer this question. Surprisingly, similar issues were observed with TB40 infection. As a result, intracellular staining for gB was unsuccessful and a conclusion could not be drawn from the data. To obtain compelling data, these late gene expression experiments will need to be repeated using the dual-tagged Merlin virus – this should also be grown in RPE-1 cells – to avoid the need for intracellular staining, and Z-VAD will need to be included in all cell-free infections.

The use of cell-free TB40 will be important to enable comparisons to the existing literature.

One potential explanation for the block to the viral lifecycle was Apobec3A (A3A). This was the only viral restriction factor upregulated in infected cells when examining the proteomics datasets – it is responsible for introducing hypermutations into viral genomes during replication, and may potentially block late gene expression of HCMV in decidual tissue^{225, 226}. Interestingly, although A3A was upregulated in infected cells, it was upregulated to a greater extent in bystander DCs. This suggests that an unidentified HCMV protein targets it for degradation, but this inhibition may be incomplete and/or unable to completely prevent A3A from functioning²⁵⁷.

To evaluate the effect of A3A on late gene expression in DCs, I used siRNA to knock down the protein in primary cells; using RT-QPCR, A3A RNA levels in the cell were reduced by 85%. Extraction of DNA from infected DCs with or without A3A siRNA at multiple timepoints suggested that knockdown of A3A increased the copies of gB per cell. However overall the levels of genome were far below that observed in HFFFs – this could possibly be due to dead and dying cells being included in the DNA extraction. This experiment needs to be repeated using Z-VAD, and cells purified over histopaque prior to DNA extraction. If, following these modifications to the experimental setup, the copies of gB at 96hrs post co-culture in A3A siRNA-treated DCs are still restricted, then this would imply that there is more than one viral restriction factor involved in the blocking of HCMV replication; another APOBEC protein detected in the proteomics data is A3G, however data published by Pautasso et al suggest that this protein does not affect the Merlin strain²⁵⁸. It would also be interesting to measure virus release from DCs, by co-culturing with fibroblasts, to determine whether the block on late gene expression is complete or not.

6.4 Future Directions and Concluding Remarks

This thesis aimed to characterise the intra-host spread of HCMV by investigating the mechanism of cell-cell spread, and the interactions between HCMV and primary immature dendritic cells following cell-cell spread.

The observation that HCMV may infect via virological synapses contradicts previous theories that the virus may transmit through microfusions in the membrane between different cells, but is supported by recent studies from other labs using the Merlin strain. As the Merlin strain encodes the complete repertoire of viral genes, it seems likely that the virological synapse is a mechanism used *in vivo*¹⁸⁰. Nevertheless, further work is needed to support this claim. Ideally, a 3D reconstruction of the virological synapse using cryo-X-ray tomography would provide improved detail of the junction formed between the infected and uninfected cell, avoiding the limitations resulting from the thin sectioning of TEM. Furthermore, investigating the frequency and duration of the virological synapses, along with the directionality of virus egress, would also provide valuable supportive mechanistic information.

Clinical strains of HCMV are able to superinfect immunocompromised hosts and recombine, producing more genetically distinct strains that circulate in the population^{188, 189}. Unfortunately, I was unable to convincingly superinfect cells or detect high levels of recombination *in vitro*. Future work would need to use methodologies designed to detect low frequency events, and potentially enrich for recombinants – for example by designing viruses that are selectable following recombination. It was also interesting that co-infection of two viruses resulted in partial suppression of gene expression; this implies a previously unrecognised mechanism that limits the number of genomes that successfully express protein on a per-cell basis.

The proteomic analysis provides an important dataset for future mining. I have already identified 15 proteins involved in DC function that are modulated by HCMV and could be instrumental in directing the immune response following infection. Having generated viral mutants lacking multiple genome regions, the impact of these modulations can now be investigated. In line with published data by Fielding et al, I have shown that the US16, US18 and US20 genes are involved in the downregulation of ICOSL, and possibly ALCAM, in primary infected DCs²⁴ – with the complete set

of single, and double, mutants, the control of viral genes over ICOSL and ALCAM (and ultimately priming of the adaptive immune response) can be determined by co-culturing infected DCs and naïve T cells in an assay to measure T cell activation and expansion.

The ability of dendritic cells to inhibit the full lytic life cycle of the Merlin strain is a novel observation. It remains unclear whether this blockade is strain-specific or specific to cell-associated infection. Furthermore, primary DCs infected with HCMV undergo extreme levels of cell death which is caspase-mediated. Should pyroptosis be the key pathway responsible then this inflammatory form of programmed cell death may contribute to the subsequent adaptive immune response seen in HCMV seropositive individuals. Further to this, A3A was identified as a potential factor in these processes, something which has previously only been demonstrated to occur in artificial culture systems^{226, 257}. The compounding effects of premature cell death and expression of viral restriction factors suggest that DCs have evolved powerful intrinsic antiviral mechanisms that are capable of interfering with the spread of HCMV within the host. However, the ability of HCMV to interfere with multiple pathways required for adaptive immunity within DCs implies that even with these host measures, HCMV is likely to disrupt priming of the antiviral immune response.

Chapter 7.

Appendix

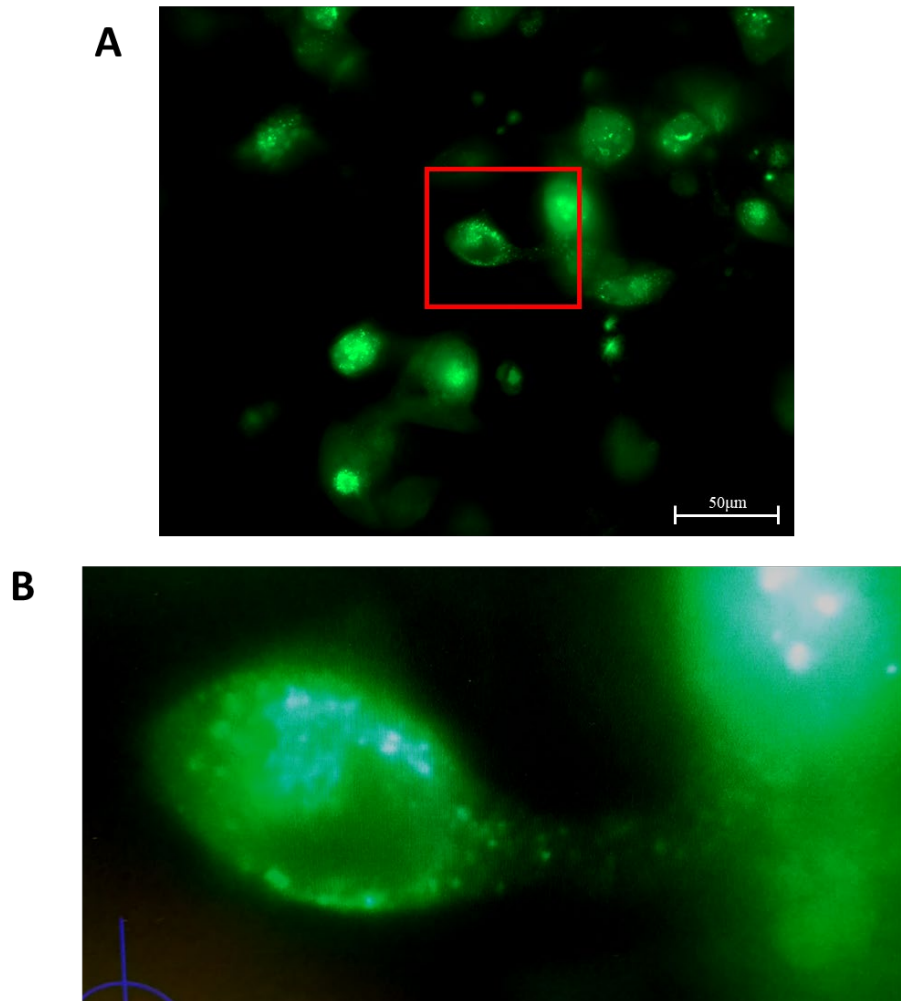


Figure S.1 – Virion movement in RPE-1 cells. RPE-1 cells infected with UL32-GFP by co-culture with HFFFs. A) Images captured every 0.1 seconds. B) Video captured in real time. Follow this link for videos: <https://photos.app.goo.gl/QAsvTYuDeGosSFNu5>

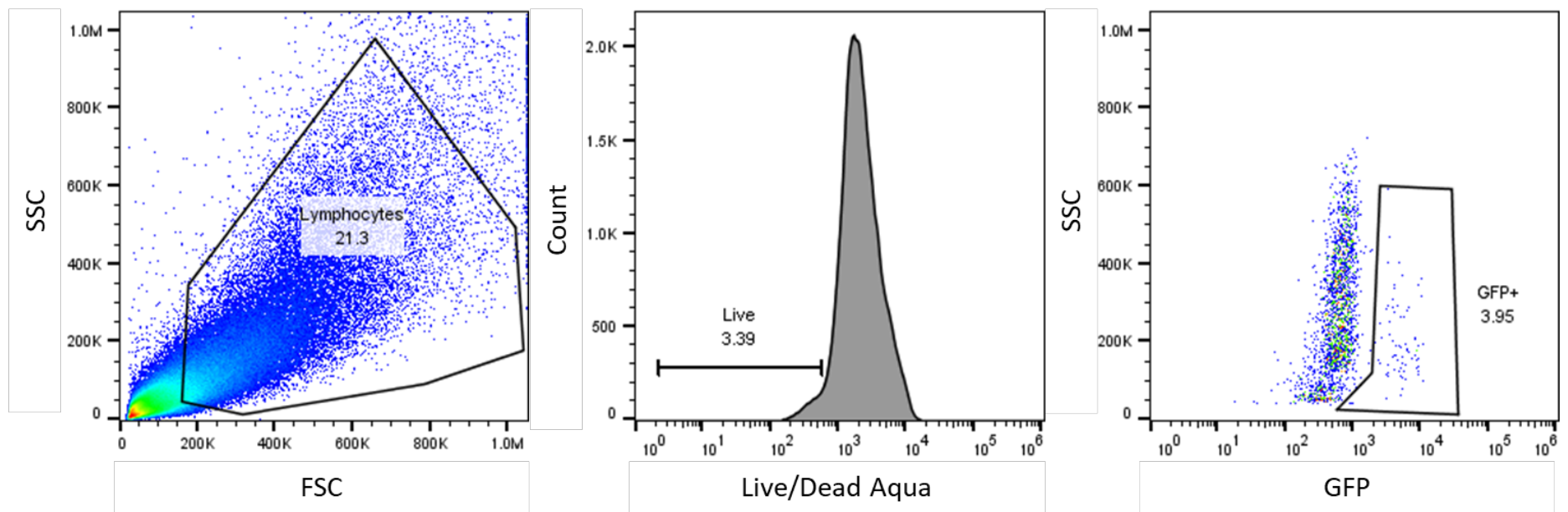


Figure S.2– Gating strategy showing poor viability of DCs at 96hrs post-infection with cell-free UL36-GFP (*pAL2344*).

Chapter 8.

References

1. Davison, A. Herpesviruses: general features. (2014).
2. Davison, A.J. *et al.* The order herpesvirales. *Archives of virology* **154**, 171-177 (2009).
3. Wilkie, G.S. *et al.* First fatality associated with elephant endotheliotropic herpesvirus 5 in an Asian elephant: pathological findings and complete viral genome sequence. *Scientific reports* **4**, 6299 (2014).
4. Davison, A.J. Comparative analysis of the genomes. *Human herpesviruses: Biology, therapy, and immunoprophylaxis*. Cambridge University Press, 2007.
5. Murphy, E. & Shenk, T.E. Human cytomegalovirus genome. *Human cytomegalovirus*. Springer, 2008, pp 1-19.
6. Dolan, A. *et al.* Genetic content of wild-type human cytomegalovirus. *Journal of General Virology* **85**, 1301-1312 (2004).
7. Tamashiro, J.C. & Spector, D.H. Terminal structure and heterogeneity in human cytomegalovirus strain AD169. *Journal of virology* **59**, 591-604 (1986).
8. Pellet, P. & Roizman, B. Herpesviridae, p 1802–1822. *Fields virology* **2** (2014).
9. Gatherer, D. *et al.* High-resolution human cytomegalovirus transcriptome. *Proceedings of the National Academy of Sciences* **108**, 19755-19760 (2011).
10. Mocarski, E.S., Shenk, T. & Pass, R. Cytomegaloviruses. *Fields Virology*, eds Knipe DM, Howley PM. Lippincott Williams & Wilkins, Philadelphia); 2007.
11. Chee, M. *et al.* Analysis of the protein-coding content of the sequence of human cytomegalovirus strain AD169. *Cytomegaloviruses*. Springer, 1990, pp 125-169.
12. Akter, P. *et al.* Two novel spliced genes in human cytomegalovirus. *Journal of General Virology* **84**, 1117-1122 (2003).
13. Dargan, D.J. *et al.* Sequential mutations associated with adaptation of human cytomegalovirus to growth in cell culture. *Journal of General Virology* **91**, 1535-1546 (2010).

14. Sijmons, S. *et al.* A method enabling high-throughput sequencing of human cytomegalovirus complete genomes from clinical isolates. *PLoS One* **9**, e95501 (2014).
15. Suárez, N.M. *et al.* Human cytomegalovirus genomes sequenced directly from clinical material: variation, multiple-strain infection, recombination, and gene loss. *The Journal of infectious diseases* **220**, 781-791 (2019).
16. Dunn, W. *et al.* Functional profiling of a human cytomegalovirus genome. *Proceedings of the National Academy of Sciences* **100**, 14223-14228 (2003).
17. Salsman, J. *et al.* Proteomic profiling of the human cytomegalovirus UL35 gene products reveals a role for UL35 in the DNA repair response. *Journal of virology* **86**, 806-820 (2012).
18. Le-Trilling, V.T.K. *et al.* The human Cytomegalovirus pUL145 isoforms act as viral DDB1-Cullin-Associated factors to instruct host protein degradation to impede innate immunity. *Cell reports* **30**, 2248-2260. e2245 (2020).
19. Ye, L. *et al.* Functional profile of human cytomegalovirus genes and their associated diseases: a review. *Frontiers in Microbiology* **11**, 2104 (2020).
20. Kim, S. *et al.* Human cytomegalovirus microRNA miR-US4-1 inhibits CD8+ T cell responses by targeting the aminopeptidase ERAP1. *Nature immunology* **12**, 984-991 (2011).
21. Van der Wal, F., Kikkert, M. & Wiertz, E. The HCMV gene products US2 and US11 target MHC class I molecules for degradation in the cytosol. *Viral Proteins Counteracting Host Defenses*, 37-55 (2002).
22. Nobre, L.V. *et al.* Human cytomegalovirus interactome analysis identifies degradation hubs, domain associations and viral protein functions. *eLife* **8**, e49894 (2019).
23. Davison, A.J. *et al.* Homology between the human cytomegalovirus RL11 gene family and human adenovirus E3 genes. *Journal of General Virology* **84**, 657-663 (2003).
24. Fielding, C.A. *et al.* Control of immune ligands by members of a cytomegalovirus gene expansion suppresses natural killer cell activation. *Elife* **6**, e22206 (2017).

25. Sijmons, S., Van Ranst, M. & Maes, P. Genomic and functional characteristics of human cytomegalovirus revealed by next-generation sequencing. *Viruses* **6**, 1049-1072 (2014).
26. Skaletskaya, A. *et al.* A cytomegalovirus-encoded inhibitor of apoptosis that suppresses caspase-8 activation. *Proceedings of the National Academy of Sciences* **98**, 7829-7834 (2001).
27. Krishna, B.A., Miller, W.E. & O'Connor, C.M. US28: HCMV's Swiss army knife. *Viruses* **10**, 445 (2018).
28. Cha, T.-a. *et al.* Human cytomegalovirus clinical isolates carry at least 19 genes not found in laboratory strains. *Journal of virology* **70**, 78-83 (1996).
29. Davison, A.J. *et al.* The human cytomegalovirus genome revisited: comparison with the chimpanzee cytomegalovirus genomeFN1. *Journal of General Virology* **84**, 17-28 (2003).
30. Wallace, P.R., Janet, W.H., Samuel, W., Horace, C.T. & Robert, J.H. Cytopathogenic agent resembling human salivary gland virus recovered from tissue cultures of human adenoids. *Proceedings of the Society for Experimental Biology and Medicine* **92**, 418-424 (1956).
31. Murphy, E. *et al.* Coding potential of laboratory and clinical strains of human cytomegalovirus. *Proceedings of the National Academy of Sciences* **100**, 14976-14981 (2003).
32. Wilkinson, G.W.G. *et al.* Human cytomegalovirus: taking the strain. *Medical microbiology and immunology* **204**, 273-284 (2015).
33. Revollo, M.G. *et al.* In vitro selection of human cytomegalovirus variants unable to transfer virus and virus products from infected cells to polymorphonuclear leukocytes and to grow in endothelial cells. *Journal of General Virology* **82**, 1429-1438 (2001).
34. Hahn, G. *et al.* The human cytomegalovirus ribonucleotide reductase homolog UL45 is dispensable for growth in endothelial cells, as determined by a BAC-cloned clinical isolate of human cytomegalovirus with preserved wild-type characteristics. *Journal of virology* **76**, 9551-9555 (2002).

35. Tomasec, P. *et al.* Surface expression of HLA-E, an inhibitor of natural killer cells, enhanced by human cytomegalovirus gpUL40. *Science* **287**, 1031-1033 (2000).
36. McSharry, B.P., Tomasec, P., Neale, M.L. & Wilkinson, G.W. The most abundantly transcribed human cytomegalovirus gene (β 2. 7) is non-essential for growth in vitro. *Journal of general virology* **84**, 2511-2516 (2003).
37. Tomasec, P. *et al.* Downregulation of natural killer cell-activating ligand CD155 by human cytomegalovirus UL141. *Nature immunology* **6**, 181-188 (2005).
38. Sinzger, C. *et al.* Cloning and sequencing of a highly productive, endotheliotropic virus strain derived from human cytomegalovirus TB40/E. *Journal of General Virology* **89**, 359-368 (2008).
39. Sinzger, C. *et al.* Modification of human cytomegalovirus tropism through propagation in vitro is associated with changes in the viral genome. *Journal of General Virology* **80**, 2867-2877 (1999).
40. QUINNAN Jr, G.V. *et al.* Comparative virulence and immunogenicity of the Towne strain and a nonattenuated strain of cytomegalovirus. *Annals of internal medicine* **101**, 478-483 (1984).
41. Prichard, M., Penfold, M., Duke, G., Spaete, R. & Kemble, G. A review of genetic differences between limited and extensively passaged human cytomegalovirus strains. *Reviews in medical virology* **11**, 191-200 (2001).
42. Plotkin, S., Furukawa, T., Zygraich, N. & Huygelen, C. Candidate cytomegalovirus strain for human vaccination. *Infection and immunity* **12**, 521-527 (1975).
43. Smith, I.L. *et al.* Clinical failure of CMV retinitis with intravitreal cidofovir is associated with antiviral resistance. *Archives of Ophthalmology* **116**, 178-185 (1998).
44. Reddehase, M.J. Margaret Gladys Smith, mother of cytomegalovirus: 60th anniversary of cytomegalovirus isolation. Springer; 2015.
45. Jesionek, A., Jesionek, A. & Kiolemenoglou, B. Ueber einen Befund von protozoenartigen Gebilden in den Organen eines hereditar-luetischen Foetus. (1904).

46. Ribbert, H. Über protozoenartige Zellen in der Niere eines syphilitischen Neugeborenen und in der Parotis von Kindern. *Zbl Allg Pathol.* **15**, 945-948 (1904).
47. VonGlahn, W.C. & Pappenheimer, A.M. Intranuclear inclusions in visceral disease. *The American journal of pathology* **1**, 445 (1925).
48. Wyatt, J.P., Saxton, J., Lee, R. & Pinkerton, H. Generalized cytomegalic inclusion disease. *Journal of Pediatrics* **36**, 271-294 (1950).
49. Minder, W. Etiology of cytomegaly in infants. *Schweizerische medizinische Wochenschrift* **83**, 1180 (1953).
50. Smith, M.G. Propagation in tissue cultures of a cytopathogenic virus from human salivary gland virus (SGV) disease. *Proceedings of the Society for Experimental Biology and Medicine* **92**, 424-430 (1956).
51. Weller, T.H., Macauley, J., Craig, J. & Wirth, P. Isolation of intranuclear inclusion producing agents from infants with illnesses resembling cytomegalic inclusion disease. *Proceedings of the Society for Experimental Biology and Medicine* **94**, 4-12 (1957).
52. Ho, M. The history of cytomegalovirus and its diseases. *Medical microbiology and immunology* **197**, 65-73 (2008).
53. Weller, T.H., Hanshaw, J.B. & Scott, D. Serologie Differentiation of Viruses responsible for Cytomegalic Inclusion Disease. *Virology* **12**, 130-132 (1960).
54. Boppana, S.B. & Fowler, K.B. Persistence in the population: epidemiology and transmisson. *Human herpesviruses: biology, therapy, and immunoprophylaxis* (2007).
55. Krech, U. & Tobin, J. A collaborative study of cytomegalovirus antibodies in mothers and young children in 19 countries. *Bulletin of the World Health Organization* **59**, 605 (1981).
56. Pomeroy, C. & Englund, J.A. Cytomegalovirus: epidemiology and infection control. *American journal of infection control* **15**, 107-119 (1987).

57. Kenneson, A. & Cannon, M.J. Review and meta-analysis of the epidemiology of congenital cytomegalovirus (CMV) infection. *Reviews in medical virology* **17**, 253-276 (2007).
58. Griffiths, P.D., Baboonian, C., Rutter, D. & Peckham, C. Congenital and maternal cytomegalovirus infections in a London population. *BJOG: An International Journal of Obstetrics & Gynaecology* **98**, 135-140 (1991).
59. Schottstedt, V. *et al.* Human cytomegalovirus (HCMV)-revised. *Transfusion medicine and hemotherapy* **37**, 365 (2010).
60. Jacobson, M.A., Stanley, H., Holtzer, C., Margolis, T.P. & Cunningham, E.T. Natural history and outcome of new AIDS-related cytomegalovirus retinitis diagnosed in the era of highly active antiretroviral therapy. *Clinical infectious diseases* **30**, 231-233 (2000).
61. Jabs, D.A., Enger, C. & Bartlett, J.G. Cytomegalovirus retinitis and acquired immunodeficiency syndrome. *Archives of Ophthalmology* **107**, 75-80 (1989).
62. Jacobson, M.A. *et al.* Cytomegalovirus (CMV)-specific CD4+ T lymphocyte immune function in long-term survivors of AIDS-related CMV end-organ disease who are receiving potent antiretroviral therapy. *The Journal of infectious diseases* **183**, 1399-1404 (2001).
63. Azevedo, L.S. *et al.* Cytomegalovirus infection in transplant recipients. *Clinics* **70**, 515-523 (2015).
64. Razonable, R.R. Epidemiology of cytomegalovirus disease in solid organ and hematopoietic stem cell transplant recipients. *American journal of health-system pharmacy* **62**, S7-S13 (2005).
65. Wingard, J. Opportunistic infections after blood and marrow transplantation. *Transplant infectious disease* **1**, 3-20 (1999).
66. Stratton, K.R., Durch, J.S. & Lawrence, R.S. Committee to Study Priorities for Vaccine Development, Division of Health Promotion and Disease Prevention Institute of Medicine. *Vaccines for the 21st century: a tool for decision making*. Washington: National Academies Press; 2000.
67. Fu, T.-M., An, Z. & Wang, D. Progress on pursuit of human cytomegalovirus vaccines for prevention of congenital infection and disease. *Vaccine* **32**, 2525-2533 (2014).

68. Elek, S. & Stern, H. Development of a vaccine against mental retardation caused by cytomegalovirus infection in utero. *The Lancet* **303**, 1-5 (1974).
69. Plotkin, S. *et al.* Towne-vaccine-induced prevention of cytomegalovirus disease after renal transplants. *The Lancet* **323**, 528-530 (1984).
70. Liu, Y. *et al.* A replication-defective human cytomegalovirus vaccine elicits humoral immune responses analogous to those with natural infection. *Journal of virology* **93**, e00747-00719 (2019).
71. Merck, S. & Dohme, C. Double-Blind, Randomized, Placebo-Controlled Phase 2b, Multi-Center Study to Evaluate the Safety, Tolerability, Efficacy and Immunogenicity of a 2-Dose and a 3—Dose Regimen of V160 (Cytomegalovirus [CMV] Vaccine) in Healthy Seronegative Women, 16 to 35 Years of Age; Clinical Trial Registration NCT03486834. 2021.
72. Pass, R.F. *et al.* Vaccine prevention of maternal cytomegalovirus infection. *New England Journal of Medicine* **360**, 1191-1199 (2009).
73. Sabbaj, S., Pass, R.F., Pichon, S. & Goepfert, P.A. Glycoprotein B vaccine is capable of boosting both antibody and CD4 T-cell responses to cytomegalovirus in chronically infected women. *Journal of Infectious Diseases* **203**, 1534-1541 (2011).
74. Griffiths, P.D. *et al.* Cytomegalovirus glycoprotein-B vaccine with MF59 adjuvant in transplant recipients: a phase 2 randomised placebo-controlled trial. *The Lancet* **377**, 1256-1263 (2011).
75. Macagno, A. *et al.* Isolation of human monoclonal antibodies that potently neutralize human cytomegalovirus infection by targeting different epitopes on the gH/gL/UL128-131A complex. *Journal of virology* **84**, 1005-1013 (2010).
76. John, S. *et al.* Multi-antigenic human cytomegalovirus mRNA vaccines that elicit potent humoral and cell-mediated immunity. *Vaccine* **36**, 1689-1699 (2018).
77. Biron, K.K. Antiviral drugs for cytomegalovirus diseases. *Antiviral research* **71**, 154-163 (2006).
78. Erice, A. Resistance of human cytomegalovirus to antiviral drugs. *Clinical Microbiology Reviews* **12**, 286-297 (1999).

79. Åsberg, A. *et al.* Oral valganciclovir is noninferior to intravenous ganciclovir for the treatment of cytomegalovirus disease in solid organ transplant recipients. *American Journal of Transplantation* **7**, 2106-2113 (2007).
80. Jung, S., Michel, M., Stamminger, T. & Michel, D. Fast breakthrough of resistant cytomegalovirus during secondary letermovir prophylaxis in a hematopoietic stem cell transplant recipient. *BMC infectious diseases* **19**, 1-5 (2019).
81. D Vadlapudi, A., K Vadlapatla, R. & K Mitra, A. Current and emerging antivirals for the treatment of cytomegalovirus (CMV) retinitis: an update on recent patents. *Recent patents on anti-infective drug discovery* **7**, 8-18 (2012).
82. Marty, F.M. *et al.* Letermovir prophylaxis for cytomegalovirus in hematopoietic-cell transplantation. *New England Journal of Medicine* **377**, 2433-2444 (2017).
83. Gibson, W. Structure and formation of the cytomegalovirus virion. *Human cytomegalovirus*. Springer, 2008, pp 187-204.
84. Liu, F. & Zhou, Z.H. Comparative virion structures of human herpesviruses. *Human Herpesviruses: Biology, Therapy, and Immunoprophylaxis*. Cambridge University Press, 2007.
85. Kalejta, R.F. Tegument proteins of human cytomegalovirus. *Microbiology and molecular biology reviews* **72**, 249-265 (2008).
86. Grunewald, K. *et al.* Three-dimensional structure of herpes simplex virus from cryo-electron tomography. *Science* **302**, 1396-1398 (2003).
87. Davison, A.J. & Bhella, D. Comparative genome and virion structure. *Human herpesviruses: biology, therapy, and immunoprophylaxis*. Cambridge University Press, 2007.
88. Gibson, W. & Roizman, B. Proteins specified by herpes simplex virus VIII. Characterization and composition of multiple capsid forms of subtypes 1 and 2. *Journal of virology* **10**, 1044-1052 (1972).
89. Irmiere, A. & Gibson, W. Isolation of human cytomegalovirus intranuclear capsids, characterization of their protein constituents, and demonstration

that the B-capsid assembly protein is also abundant in noninfectious enveloped particles. *Journal of virology* **56**, 277-283 (1985).

90. Heming, J.D., Conway, J.F. & Homa, F.L. Herpesvirus capsid assembly and DNA packaging. *Cell biology of herpes viruses*, 119-142 (2017).
91. Gibson, W. & Bogner, E. Morphogenesis of the Cytomegalovirus Virion and Subviral 945 Particles, p 230-246. *Cytomegaloviruses: from molecular* **946** (2013).
92. Varnum, S.M. *et al.* Identification of proteins in human cytomegalovirus (HCMV) particles: the HCMV proteome. *Journal of virology* **78**, 10960-10966 (2004).
93. Schmolke, S., Drescher, P., Jahn, G. & Plachter, B. Nuclear targeting of the tegument protein pp65 (UL83) of human cytomegalovirus: an unusual bipartite nuclear localization signal functions with other portions of the protein to mediate its efficient nuclear transport. *Journal of virology* **69**, 1071-1078 (1995).
94. Tomtishen III, J.P. Human cytomegalovirus tegument proteins (pp65, pp71, pp150, pp28). *Virology journal* **9**, 1-9 (2012).
95. Odeberg, J., Plachter, B., Brandén, L. & Söderberg-Nauclér, C. Human cytomegalovirus protein pp65 mediates accumulation of HLA-DR in lysosomes and destruction of the HLA-DR α -chain. *Blood* **101**, 4870-4877 (2003).
96. Gilbert, M.J., Riddell, S.R., Plachter, B. & Greenberg, P.D. Cytomegalovirus selectively blocks antigen processing and presentation of its immediate-early gene product. *Nature* **383**, 720-722 (1996).
97. Hensel, G.M. *et al.* Intracellular localization and expression of the human cytomegalovirus matrix phosphoprotein pp71 (ppUL82): evidence for its translocation into the nucleus. *Journal of General Virology* **77**, 3087-3097 (1996).
98. Weng, C. *et al.* Human cytomegalovirus productively replicates in vitro in undifferentiated oral epithelial cells. *Journal of virology* **92**, e00903-00918 (2018).

99. Kalejta, R.F. & Albright, E.R. Expanding the known functional repertoire of the human cytomegalovirus pp71 protein. *Frontiers in cellular and infection microbiology* **10**, 95 (2020).
100. Trgovcich, J., Cebulla, C., Zimmerman, P. & Sedmak, D.D. Human cytomegalovirus protein pp71 disrupts major histocompatibility complex class I cell surface expression. *Journal of virology* **80**, 951-963 (2006).
101. Meyer, H.H. et al. Human cytomegalovirus late-phase maturation is blocked by stably expressed UL32 antisense mRNA in astrocytoma cells. *Journal of general virology* **78**, 2621-2631 (1997).
102. Stanton, R.J. et al. Reconstruction of the complete human cytomegalovirus genome in a BAC reveals RL13 to be a potent inhibitor of replication. *The Journal of clinical investigation* **120**, 3191 (2010).
103. Murrell, I. et al. Genetic stability of bacterial artificial Chromosome-Derived human Cytomegalovirus during culture in vitro. *Journal of virology* **90**, 3929-3943 (2016).
104. Crough, T. & Khanna, R. Immunobiology of human cytomegalovirus: from bench to bedside. *Clinical microbiology reviews* **22**, 76-98 (2009).
105. Sinzger, C., Digel, M. & Jahn, G. Cytomegalovirus cell tropism. *Human cytomegalovirus*, 63-83 (2008).
106. Compton, T., Nepomuceno, R.R. & Nowlin, D.M. Human cytomegalovirus penetrates host cells by pH-independent fusion at the cell surface. *Virology* **191**, 387-395 (1992).
107. Compton, T., Nowlin, D.M. & Cooper, N.R. Initiation of human cytomegalovirus infection requires initial interaction with cell surface heparan sulfate. *Virology* **193**, 834-841 (1993).
108. Isaacson, M.K. & Compton, T. Human cytomegalovirus glycoprotein B is required for virus entry and cell-to-cell spread but not for virion attachment, assembly, or egress. *Journal of virology* **83**, 3891-3903 (2009).
109. Mach, M., Kropff, B., Dal Monte, P. & Britt, W. Complex formation by human cytomegalovirus glycoproteins M (gpUL100) and N (gpUL73). *Journal of virology* **74**, 11881-11892 (2000).

110. Britt, W.J. & Auger, D. Synthesis and processing of the envelope gp55-116 complex of human cytomegalovirus. *Journal of virology* **58**, 185-191 (1986).
111. Compton, T. Receptors and immune sensors: the complex entry path of human cytomegalovirus. *Trends in cell biology* **14**, 5-8 (2004).
112. Shimamura, M., Mach, M. & Britt, W.J. Human cytomegalovirus infection elicits a glycoprotein M (gM)/gN-specific virus-neutralizing antibody response. *Journal of virology* **80**, 4591-4600 (2006).
113. Murrell, I. et al. Impact of sequence variation in the UL128 locus on production of human cytomegalovirus in fibroblast and epithelial cells. *Journal of virology* **87**, 10489-10500 (2013).
114. Zhou, M., Yu, Q., Wechsler, A. & Ryckman, B.J. Comparative analysis of gO isoforms reveals that strains of human cytomegalovirus differ in the ratio of gH/gL/gO and gH/gL/UL128-131 in the virion envelope. *Journal of virology* **87**, 9680-9690 (2013).
115. Zhang, L., Zhou, M., Stanton, R., Kamil, J. & Ryckman, B.J. Expression levels of glycoprotein O (gO) vary between strains of human cytomegalovirus, influencing the assembly of gH/gL complexes and virion infectivity. *Journal of virology* **92**, e00606-00618 (2018).
116. Zhong, P., Agosto, L.M., Munro, J.B. & Mothes, W. Cell-to-cell transmission of viruses. *Current opinion in virology* **3**, 44-50 (2013).
117. Soroceanu, L., Akhavan, A. & Cobbs, C.S. Platelet-derived growth factor- α receptor activation is required for human cytomegalovirus infection. *Nature* **455**, 391-395 (2008).
118. Ryckman, B.J., Jarvis, M.A., Drummond, D.D., Nelson, J.A. & Johnson, D.C. Human cytomegalovirus entry into epithelial and endothelial cells depends on genes UL128 to UL150 and occurs by endocytosis and low-pH fusion. *Journal of virology* **80**, 710-722 (2006).
119. Wu, Y. et al. Human cytomegalovirus glycoprotein complex gH/gL/gO uses PDGFR- α as a key for entry. *PLoS pathogens* **13** (2017).
120. Weiler, N. et al. Role of Envelope Glycoprotein Complexes in Cell-Associated Spread of Human Cytomegalovirus. *Viruses* **13**, 614 (2021).

121. Murrell, I. *et al.* The pentameric complex drives immunologically covert cell-cell transmission of wild-type human cytomegalovirus. *Proceedings of the National Academy of Sciences*, 201704809 (2017).
122. Falk, J. *et al.* Large-Scale Screening of HCMV-Seropositive Blood Donors Indicates that HCMV Effectively Escapes from Antibodies by Cell-Associated Spread. *Viruses* **10**, 500 (2018).
123. Pique, C. & Jones, K.S. Pathways of cell-cell transmission of HTLV-1. *Frontiers in microbiology* **3**, 378 (2012).
124. Vanarsdall, A.L. & Johnson, D.C. Human cytomegalovirus entry into cells. *Current opinion in virology* **2** (2012).
125. McVOY, M.A. & Adler, S.P. Human cytomegalovirus DNA replicates after early circularization by concatemer formation, and inversion occurs within the concatemer. *Journal of virology* **68**, 1040-1051 (1994).
126. Mocarski, E.S. & Roizman, B. Structure and role of the herpes simplex virus DNA termini in inversion, circularization and generation of virion DNA. *Cell* **31**, 89-97 (1982).
127. Chambers, J. *et al.* DNA microarrays of the complex human cytomegalovirus genome: profiling kinetic class with drug sensitivity of viral gene expression. *Journal of virology* **73**, 5757-5766 (1999).
128. Das, S., Vasanji, A. & Pellett, P.E. Three-dimensional structure of the human cytomegalovirus cytoplasmic virion assembly complex includes a reoriented secretory apparatus. *Journal of virology* **81**, 11861-11869 (2007).
129. Sanchez, V., Greis, K.D., Sztul, E. & Britt, W.J. Accumulation of virion tegument and envelope proteins in a stable cytoplasmic compartment during human cytomegalovirus replication: characterization of a potential site of virus assembly. *Journal of virology* **74**, 975-986 (2000).
130. Procter, D.J. *et al.* The HCMV assembly compartment is a dynamic Golgi-derived MTOC that controls nuclear rotation and virus spread. *Developmental cell* **45**, 83-100. e107 (2018).

131. Alwine, J.C. The human cytomegalovirus assembly compartment: a masterpiece of viral manipulation of cellular processes that facilitates assembly and egress. (2012).
132. Sinclair, J. & Sissons, P. Latency and reactivation of human cytomegalovirus. *Journal of General Virology* **87**, 1763-1779 (2006).
133. Zhu, D. *et al.* Human cytomegalovirus reprogrammes haematopoietic progenitor cells into immunosuppressive monocytes to achieve latency. *Nature Microbiology* **3**, 503 (2018).
134. Reeves, M. & Sinclair, J. Aspects of human cytomegalovirus latency and reactivation. *Human Cytomegalovirus*, 297-313 (2008).
135. Bego, M., Maciejewski, J., Khaiboullina, S., Pari, G. & St. Jeor, S. Characterization of an antisense transcript spanning the UL81-82 locus of human cytomegalovirus. *Journal of virology* **79**, 11022-11034 (2005).
136. Beisser, P.S., Laurent, L., Virelizier, J.-L. & Michelson, S. Human cytomegalovirus chemokine receptor gene US28 is transcribed in latently infected THP-1 monocytes. *Journal of virology* **75**, 5949-5957 (2001).
137. Avdic, S., Cao, J.Z., Cheung, A.K., Abendroth, A. & Slobedman, B. Viral interleukin-10 expressed by human cytomegalovirus during the latent phase of infection modulates latently infected myeloid cell differentiation. *Journal of virology* **85**, 7465-7471 (2011).
138. Poole, E. *et al.* The myeloid transcription factor GATA-2 regulates the viral UL144 gene during human cytomegalovirus latency in an isolate-specific manner. *Journal of virology* **87**, 4261-4271 (2013).
139. Goodrum, F., Reeves, M., Sinclair, J., High, K. & Shenk, T. Human cytomegalovirus sequences expressed in latently infected individuals promote a latent infection in vitro. *Blood, The Journal of the American Society of Hematology* **110**, 937-945 (2007).
140. Reeves, M., MacAry, P., Lehner, P., Sissons, J. & Sinclair, J. Latency, chromatin remodeling, and reactivation of human cytomegalovirus in the dendritic cells of healthy carriers. *Proceedings of the National Academy of Sciences* **102**, 4140-4145 (2005).

141. Forte, E., Zhang, Z., Thorp, E.B. & Hummel, M. Cytomegalovirus latency and reactivation: an intricate interplay with the host immune response. *Frontiers in cellular and infection microbiology* **10**, 130 (2020).
142. Takeuchi, O. & Akira, S. Innate immunity to virus infection. *Immunological reviews* **227**, 75-86 (2009).
143. Thompson, M.R., Kaminski, J.J., Kurt-Jones, E.A. & Fitzgerald, K.A. Pattern recognition receptors and the innate immune response to viral infection. *Viruses* **3**, 920-940 (2011).
144. Powers, C., DeFilippis, V., Malouli, D. & Früh, K. Cytomegalovirus immune evasion. *Human cytomegalovirus*, 333-359 (2008).
145. Batista, F.D. & Harwood, N.E. The who, how and where of antigen presentation to B cells. *Nature Reviews Immunology* **9**, 15-27 (2009).
146. Isaacson, M., Juckem, L. & Compton, T. Virus entry and innate immune activation. *Human Cytomegalovirus*, 85-100 (2008).
147. Prod'homme, V. *et al.* The human cytomegalovirus MHC class I homolog UL18 inhibits LIR-1+ but activates LIR-1- NK cells. *The Journal of Immunology* **178**, 4473-4481 (2007).
148. Fielding, C.A. *et al.* Two novel human cytomegalovirus NK cell evasion functions target MICA for lysosomal degradation. *PLoS pathogens* **10** (2014).
149. Patel, M. *et al.* HCMV-encoded NK modulators: lessons from in vitro and in vivo genetic variation. *Frontiers in immunology* **9**, 2214 (2018).
150. Wu, J. *et al.* Intracellular retention of the MHC class I-related chain B ligand of NKG2D by the human cytomegalovirus UL16 glycoprotein. *The Journal of Immunology* **170**, 4196-4200 (2003).
151. Wang, E.C. *et al.* UL40-mediated NK evasion during productive infection with human cytomegalovirus. *Proceedings of the National Academy of Sciences* **99**, 7570-7575 (2002).
152. Wiertz, E.J., Devlin, R., Collins, H.L. & Ressing, M.E. Herpesvirus interference with major histocompatibility complex class II-restricted T-cell activation. *Journal of virology* **81**, 4389-4396 (2007).

153. Wang, E.C. *et al.* Suppression of costimulation by human cytomegalovirus promotes evasion of cellular immune defenses. *Proceedings of the National Academy of Sciences* **115**, 4998-5003 (2018).
154. Atalay, R. *et al.* Identification and expression of human cytomegalovirus transcription units coding for two distinct Fc_y receptor homologs. *Journal of virology* **76**, 8596-8608 (2002).
155. Wykes, M., Pombo, A., Jenkins, C. & MacPherson, G.G. Dendritic cells interact directly with naive B lymphocytes to transfer antigen and initiate class switching in a primary T-dependent response. *The Journal of Immunology* **161**, 1313-1319 (1998).
156. Patente, T.A. *et al.* Human dendritic cells: their heterogeneity and clinical application potential in cancer immunotherapy. *Frontiers in immunology* **9**, 3176 (2019).
157. Ishikawa, F. *et al.* The developmental program of human dendritic cells is operated independently of conventional myeloid and lymphoid pathways. *Blood, The Journal of the American Society of Hematology* **110**, 3591-3660 (2007).
158. Chow, K.V., Lew, A.M., Sutherland, R.M. & Zhan, Y. Monocyte-derived dendritic cells promote Th polarization, whereas conventional dendritic cells promote Th proliferation. *The Journal of Immunology* **196**, 624-636 (2016).
159. Castell-Rodríguez, A., Piñón-Zárate, G., Herrera-Enríquez, M., Jarquín-Yáñez, K. & Medina-Solares, I. Dendritic cells: location, function, and clinical implications. *Biology of myelomonocytic cells*, 21-50 (2017).
160. Shortman, K. & Liu, Y.-J. Mouse and human dendritic cell subtypes. *Nature Reviews Immunology* **2**, 151-161 (2002).
161. Beck, K., Meyer-König, U., Weidmann, M., Nern, C. & Hufert, F.T. Human cytomegalovirus impairs dendritic cell function: a novel mechanism of human cytomegalovirus immune escape. *European journal of immunology* **33**, 1528-1538 (2003).
162. Halary, F. *et al.* Human cytomegalovirus binding to DC-SIGN is required for dendritic cell infection and target cell trans-infection. *Immunity* **17**, 653-664 (2002).

163. Geijtenbeek, T.B. *et al.* DC-SIGN, a dendritic cell-specific HIV-1-binding protein that enhances trans-infection of T cells. *Cell* **100**, 587-597 (2000).
164. Alvarez, C.P. *et al.* C-type lectins DC-SIGN and L-SIGN mediate cellular entry by Ebola virus in cis and in trans. *Journal of virology* **76**, 6841-6844 (2002).
165. Riegler, S. *et al.* Monocyte-derived dendritic cells are permissive to the complete replicative cycle of human cytomegalovirus. *Journal of General Virology* **81**, 393-399 (2000).
166. Grigoleit, U. *et al.* Human cytomegalovirus induces a direct inhibitory effect on antigen presentation by monocyte-derived immature dendritic cells. *British journal of haematology* **119**, 189-198 (2002).
167. Moutaftsi, M., Mehl, A.M., Borysiewicz, L.K. & Tabi, Z. Human cytomegalovirus inhibits maturation and impairs function of monocyte-derived dendritic cells. *Blood* **99**, 2913-2921 (2002).
168. Tabi, Z., Moutaftsi, M. & Borysiewicz, L.K. Human cytomegalovirus pp65-and immediate early 1 antigen-specific HLA class I-restricted cytotoxic T cell responses induced by cross-presentation of viral antigens. *The Journal of Immunology* **166**, 5695-5703 (2001).
169. Gredmark-Russ, S. & Söderberg-Nauclér, C. Dendritic cell biology in human cytomegalovirus infection and the clinical consequences for host immunity and pathology. *Virulence* **3**, 621-634 (2012).
170. McSharry, B.P. *et al.* Adenovirus E3/19K promotes evasion of NK cell recognition by intracellular sequestration of the NKG2D ligands major histocompatibility complex class I chain-related proteins A and B. *Journal of virology* **82**, 4585-4594 (2008).
171. McSharry, B., Jones, C., Skinner, J., Kipling, D. & Wilkinson, G. Human telomerase reverse transcriptase-immortalized MRC-5 and HCA2 human fibroblasts are fully permissive for human cytomegalovirus. *Journal of General Virology* **82**, 855-863 (2001).
172. Weekes, M.P. *et al.* Quantitative temporal viromics: an approach to investigate host-pathogen interaction. *Cell* **157**, 1460-1472 (2014).

173. Soday, L. *et al.* Quantitative temporal proteomic analysis of vaccinia virus infection reveals regulation of histone deacetylases by an interferon antagonist. *Cell reports* **27**, 1920-1933. e1927 (2019).
174. Fu, T.-M., Wang, D. & An, Z. CMV neutralizing antigen binding proteins. Google Patents; 2018.
175. Tischer, B.K., Smith, G.A. & Osterrieder, N. En passant mutagenesis: a two step markerless red recombination system. *In vitro mutagenesis protocols*. Springer, 2010, pp 421-430.
176. Straschewski, S. *et al.* Protein pUL128 of human cytomegalovirus is necessary for monocyte infection and blocking of migration. *Journal of virology* **85**, 5150-5158 (2011).
177. Jacob, C.L. *et al.* Neutralizing antibodies are unable to inhibit direct viral cell-to-cell spread of human cytomegalovirus. *Virology* **444**, 140-147 (2013).
178. Vasiliver-Shamis, G., Dustin, M.L. & Hioe, C.E. HIV-1 virological synapse is not simply a copycat of the immunological synapse. *Viruses* **2**, 1239-1260 (2010).
179. Jolly, C., Kashefi, K., Hollinshead, M. & Sattentau, Q.J. HIV-1 cell to cell transfer across an Env-induced, actin-dependent synapse. *Journal of Experimental Medicine* **199**, 283-293 (2004).
180. Gerna, G. *et al.* Human cytomegalovirus replicates abortively in polymorphonuclear leukocytes after transfer from infected endothelial cells via transient microfusion events. *Journal of virology* **74**, 5629-5638 (2000).
181. Sampaio, K.L., Cavignac, Y., Stierhof, Y.-D. & Sinzger, C. Human cytomegalovirus labeled with green fluorescent protein for live analysis of intracellular particle movements. *Journal of virology* **79**, 2754-2767 (2005).
182. Sampaio, K.L., Jahn, G. & Sinzger, C. Applications for a dual fluorescent human cytomegalovirus in the analysis of viral entry. *Virus-Host Interactions: Methods and Protocols*, 201-209 (2013).
183. Atanasiu, D. *et al.* Bimolecular complementation reveals that glycoproteins gB and gH/gL of herpes simplex virus interact with each other during cell fusion. *Proceedings of the National Academy of Sciences* **104**, 18718-18723 (2007).

184. Harkiolaki, M. *et al.* Cryo-soft X-ray tomography: using soft X-rays to explore the ultrastructure of whole cells. *Emerging Topics in Life Sciences* **2**, 81-92 (2018).
185. Xia, L. *et al.* Active evolution of memory B-cells specific to viral gH/gL/pUL128/130/131 pentameric complex in healthy subjects with silent human cytomegalovirus infection. *Oncotarget* **8**, 73654 (2017).
186. Cui, X. *et al.* Impact of antibodies and strain polymorphisms on cytomegalovirus entry and spread in fibroblasts and epithelial cells. *Journal of virology* **91**, e01650-01616 (2017).
187. Ha, S. *et al.* Neutralization of diverse human cytomegalovirus strains conferred by antibodies targeting viral gH/gL/pUL128-131 pentameric complex. *Journal of virology* **91**, e02033-02016 (2017).
188. Cudini, J. *et al.* Human cytomegalovirus haplotype reconstruction reveals high diversity due to superinfection and evidence of within-host recombination. *Proceedings of the National Academy of Sciences* **116**, 5693-5698 (2019).
189. Baldanti, F. *et al.* Coinfection of the immunocompromised but not the immunocompetent host by multiple human cytomegalovirus strains. *Archives of virology* **143**, 1701-1709 (1998).
190. Kabanova, A. *et al.* Platelet-derived growth factor- α receptor is the cellular receptor for human cytomegalovirus gHgLgO trimer. *Nature microbiology* **1**, 1-8 (2016).
191. Stanton, R.J. *et al.* HCMV pUL135 remodels the actin cytoskeleton to impair immune recognition of infected cells. *Cell host & microbe* **16**, 201-214 (2014).
192. Nightingale, K. *et al.* High-definition analysis of host protein stability during human cytomegalovirus infection reveals antiviral factors and viral evasion mechanisms. *Cell host & microbe* **24**, 447-460. e411 (2018).
193. Raftery, M.J. *et al.* Inhibition of CD1 antigen presentation by human cytomegalovirus. *Journal of virology* **82**, 4308-4319 (2008).
194. Kim, Y.-E. *et al.* Human cytomegalovirus infection causes degradation of Sp100 proteins that suppress viral gene expression. *Journal of virology* **85**, 11928-11937 (2011).

195. Lin, A., Xu, H. & Yan, W. Modulation of HLA expression in human cytomegalovirus immune evasion. *Cell Mol Immunol* **4**, 91-98 (2007).
196. Halenius, A., Gerke, C. & Hengel, H. Classical and non-classical MHC I molecule manipulation by human cytomegalovirus: so many targets—but how many arrows in the quiver? *Cellular & molecular immunology* **12**, 139-153 (2015).
197. Maschalidi, S. *et al.* Asparagine endopeptidase controls anti-influenza virus immune responses through TLR7 activation. *PLoS pathogens* **8**, e1002841 (2012).
198. Alvarez, R.A., Barría, M.I. & Chen, B.K. Unique features of HIV-1 spread through T cell virological synapses. *PLoS pathogens* **10**, e1004513 (2014).
199. Consortium, U. UniProt: a worldwide hub of protein knowledge. *Nucleic acids research* **47**, D506-D515 (2018).
200. Zimmerman, A.W. *et al.* Long-term engagement of CD6 and ALCAM is essential for T-cell proliferation induced by dendritic cells. *Blood* **107**, 3212-3220 (2006).
201. Cuenca, M., Sintes, J., Lányi, Á. & Engel, P. CD84 cell surface signaling molecule: An emerging biomarker and target for cancer and autoimmune disorders. *Clinical Immunology* (2018).
202. Ghislat, G. & Lawrence, T. Autophagy in dendritic cells. *Cellular & molecular immunology* (2018).
203. LeibundGut-Landmann, S., Osorio, F., Brown, G.D. & e Sousa, C.R. Stimulation of dendritic cells via the dectin-1/Syk pathway allows priming of cytotoxic T-cell responses. *Blood* **112**, 4971-4980 (2008).
204. Starling, G.C. *et al.* Intercellular adhesion molecule-3 is the predominant co-stimulatory ligand for leukocyte function antigen-1 on human blood dendritic cells. *European journal of immunology* **25**, 2528-2532 (1995).
205. Zhu, F.X., King, S.M., Smith, E.J., Levy, D.E. & Yuan, Y. A Kaposi's sarcoma-associated herpesviral protein inhibits virus-mediated induction of type I interferon by blocking IRF-7 phosphorylation and nuclear accumulation. *Proceedings of the National Academy of Sciences* **99**, 5573-5578 (2002).

206. Andreea, S., Piras, F., Burdin, N. & Triebel, F. Maturation and activation of dendritic cells induced by lymphocyte activation gene-3 (CD223). *The Journal of Immunology* **168**, 3874-3880 (2002).
207. Andreea, S., Buisson, S. & Triebel, F. MHC class II signal transduction in human dendritic cells induced by a natural ligand, the LAG-3 protein (CD223). *Blood* **102**, 2130-2137 (2003).
208. Okunishi, K. *et al.* A novel role of hepatocyte growth factor as an immune regulator through suppressing dendritic cell function. *The Journal of Immunology* **175**, 4745-4753 (2005).
209. Merck, E. *et al.* OSCAR is an FcR γ -associated receptor that is expressed by myeloid cells and is involved in antigen presentation and activation of human dendritic cells. *Blood* **104**, 1386-1395 (2004).
210. Torzicky, M. *et al.* Platelet endothelial cell adhesion molecule-1 (PECAM-1/CD31) and CD99 are critical in lymphatic transmigration of human dendritic cells. *Journal of Investigative Dermatology* **132**, 1149-1157 (2012).
211. Kralova, J. *et al.* The transmembrane adaptor protein SCIMP facilitates sustained dectin-1 signaling in dendritic cells. *Journal of Biological Chemistry* **291**, 16530-16540 (2016).
212. Wang, T. *et al.* K12/SECTM1, an interferon- γ regulated molecule, synergizes with CD28 to costimulate human T cell proliferation. *Journal of leukocyte biology* **91**, 449-459 (2012).
213. Kumanogoh, A. *et al.* Class IV semaphorin Sema4A enhances T-cell activation and interacts with Tim-2. *Nature* **419**, 629 (2002).
214. Corinti, S. *et al.* Cross-linking of membrane CD43 mediates dendritic cell maturation. *The Journal of Immunology* **162**, 6331-6336 (1999).
215. Fletcher-Etherington, A. *et al.* Human cytomegalovirus protein pUL36: a dual cell death pathway inhibitor. *BioRxiv* (2020).
216. Grattendick, K., Nakashima, J., Feng, L., Giri, S. & Margolin, S. Effects of three anti-TNF- α drugs: etanercept, infliximab and pirfenidone on release of TNF- α in medium and TNF- α associated with the cell in vitro. *International immunopharmacology* **8**, 679-687 (2008).

217. Raftery, M.J. *et al.* Targeting the function of mature dendritic cells by human cytomegalovirus: a multilayered viral defense strategy. *Immunity* **15**, 997-1009 (2001).
218. McIlwain, D.R., Berger, T. & Mak, T.W. Caspase functions in cell death and disease. *Cold Spring Harbor perspectives in biology* **5**, a008656 (2013).
219. Mahoney, D.J. *et al.* Virus-tumor interactome screen reveals ER stress response can reprogram resistant cancers for oncolytic virus-triggered caspase-2 cell death. *Cancer cell* **20**, 443-456 (2011).
220. Xuan, B., Qian, Z., Torigoi, E. & Yu, D. Human cytomegalovirus protein pUL38 induces ATF4 expression, inhibits persistent JNK phosphorylation, and suppresses endoplasmic reticulum stress-induced cell death. *Journal of virology* **83**, 3463-3474 (2009).
221. Brentnall, M., Rodriguez-Menocal, L., De Guevara, R.L., Cepero, E. & Boise, L.H. Caspase-9, caspase-3 and caspase-7 have distinct roles during intrinsic apoptosis. *BMC cell biology* **14**, 32 (2013).
222. Zhu, H., Shen, Y. & Shenk, T. Human cytomegalovirus IE1 and IE2 proteins block apoptosis. *Journal of virology* **69**, 7960-7970 (1995).
223. Goldmacher, V.S. *et al.* A cytomegalovirus-encoded mitochondria-localized inhibitor of apoptosis structurally unrelated to Bcl-2. *Proceedings of the National Academy of Sciences* **96**, 12536-12541 (1999).
224. Goldmacher, V.S. vMIA, a viral inhibitor of apoptosis targeting mitochondria. *Biochimie* **84**, 177-185 (2002).
225. Salter, J.D., Bennett, R.P. & Smith, H.C. The APOBEC protein family: united by structure, divergent in function. *Trends in biochemical sciences* **41**, 578-594 (2016).
226. Weisblum, Y. *et al.* APOBEC3A is upregulated by human cytomegalovirus (HCMV) in the maternal-fetal interface, acting as an innate anti-HCMV effector. *Journal of virology* **91**, e01296-01217 (2017).
227. Wilhelm, J. Re: What does a value of 0.1 fold change in qRT-PCR represent? How do I put it in a percentage? (2019).

228. Zhou, M., Lanchy, J.-M. & Ryckman, B.J. Human cytomegalovirus gH/gL/gO promotes the fusion step of entry into all cell types, whereas gH/gL/UL128-131 broadens virus tropism through a distinct mechanism. *Journal of virology* **89**, 8999-9009 (2015).
229. Rand, U., Kubsch, T., Kasmapour, B. & Cicin-Sain, L. A novel triple-fluorescent HCMV strain reveals gene expression dynamics and anti-herpesviral drug mechanisms. *Frontiers in Cellular and Infection Microbiology* **10** (2020).
230. Moorman, N.J., Sharon-Friling, R., Shenk, T. & Cristea, I.M. A targeted spatial-temporal proteomics approach implicates multiple cellular trafficking pathways in human cytomegalovirus virion maturation. *Molecular & Cellular Proteomics* **9**, 851-860 (2010).
231. Ward, B.M. & Moss, B. Visualization of intracellular movement of vaccinia virus virions containing a green fluorescent protein-B5R membrane protein chimera. *Journal of Virology* **75**, 4802-4813 (2001).
232. Ogawa-Goto, K. *et al.* Microtubule network facilitates nuclear targeting of human cytomegalovirus capsid. *Journal of virology* **77**, 8541-8547 (2003).
233. May-Simera, H.L. *et al.* Primary cilium-mediated retinal pigment epithelium maturation is disrupted in ciliopathy patient cells. *Cell reports* **22**, 189-205 (2018).
234. Smith, G.A., Gross, S.P. & Enquist, L.W. Herpesviruses use bidirectional fast-axonal transport to spread in sensory neurons. *Proceedings of the National Academy of Sciences* **98**, 3466-3470 (2001).
235. Johnson, D.C. & Huber, M.T. Directed egress of animal viruses promotes cell-to-cell spread. *Journal of virology* **76**, 1-8 (2002).
236. Johnson, D.C., Webb, M., Wisner, T.W. & Brunetti, C. Herpes simplex virus gE/gI sorts nascent virions to epithelial cell junctions, promoting virus spread. *Journal of virology* **75**, 821-833 (2001).
237. Nahas, K.L., Connor, V., Harkiolaki, M., Crump, C.M. & Graham, S.C. Near-native state imaging by cryo-soft-X-ray tomography reveals remodelling of cytoplasmic vesicles and mitochondria during HSV-1 infection. *bioRxiv* (2021).

238. Porter, R. The hydrolysis of rabbit γ -globulin and antibodies with crystalline papain. *Biochemical Journal* **73**, 119-127 (1959).
239. Mallery, D.L. *et al.* Antibodies mediate intracellular immunity through tripartite motif-containing 21 (TRIM21). *Proceedings of the National Academy of Sciences* **107**, 19985-19990 (2010).
240. Bournazos, S. *et al.* Broadly neutralizing anti-HIV-1 antibodies require Fc effector functions for in vivo activity. *Cell* **158**, 1243-1253 (2014).
241. Hansen, S.G. *et al.* Evasion of CD8+ T cells is critical for superinfection by cytomegalovirus. *Science* **328**, 102-106 (2010).
242. Angulo, G. *et al.* Cytomegalovirus restricts ICOSL expression on antigen-presenting cells disabling T cell co-stimulation and contributing to immune evasion. *eLife* **10** (2021).
243. Workman, C.J. *et al.* LAG-3 regulates plasmacytoid dendritic cell homeostasis. *The Journal of Immunology* **182**, 1885-1891 (2009).
244. Clement, M. *et al.* CD31 is a key coinhibitory receptor in the development of immunogenic dendritic cells. *Proceedings of the National Academy of Sciences* **111**, E1101-E1110 (2014).
245. Muller, W.A., Weigl, S.A., Deng, X. & Phillips, D.M. PECAM-1 is required for transendothelial migration of leukocytes. *Journal of Experimental Medicine* **178**, 449-460 (1993).
246. Lu, N. *et al.* Human Semaphorin-4A drives Th2 responses by binding to receptor ILT-4. *Nature communications* **9**, 1-11 (2018).
247. Kumanogoh, A. *et al.* Nonredundant roles of Sema4A in the immune system: defective T cell priming and Th1/Th2 regulation in Sema4A-deficient mice. *Immunity* **22**, 305-316 (2005).
248. Fletcher-Etherington, A. *et al.* Human cytomegalovirus protein pUL36: A dual cell death pathway inhibitor. *Proceedings of the National Academy of Sciences* **117**, 18771-18779 (2020).
249. Qian, Z., Xuan, B., Gualberto, N. & Yu, D. The human cytomegalovirus protein pUL38 suppresses endoplasmic reticulum stress-mediated cell death

- independently of its ability to induce mTORC1 activation. *Journal of virology* **85**, 9103-9113 (2011).
250. Bergsbaken, T., Fink, S.L. & Cookson, B.T. Pyroptosis: host cell death and inflammation. *Nature Reviews Microbiology* **7**, 99-109 (2009).
 251. Huang, Y. *et al.* Human cytomegalovirus triggers the assembly of AIM2 inflammasome in THP-1-derived macrophages. *Journal of medical virology* **89**, 2188-2195 (2017).
 252. Eichholz, K. *et al.* Immune-complexed adenovirus induce AIM2-mediated pyroptosis in human dendritic cells. *PLoS pathogens* **12**, e1005871 (2016).
 253. Yu, P. *et al.* Pyroptosis: mechanisms and diseases. *Signal transduction and targeted therapy* **6**, 1-21 (2021).
 254. van de Berg, P.J. *et al.* Human cytomegalovirus induces systemic immune activation characterized by a type 1 cytokine signature. *The Journal of infectious diseases* **202**, 690-699 (2010).
 255. Botero, J., Contreras, A. & Parra, B. Profiling of inflammatory cytokines produced by gingival fibroblasts after human cytomegalovirus infection. *Oral microbiology and immunology* **23**, 291-298 (2008).
 256. Kovacs, S.B. & Miao, E.A. Gasdermins: effectors of pyroptosis. *Trends in cell biology* **27**, 673-684 (2017).
 257. Xu, W.K., Byun, H. & Dudley, J.P. The role of APOBECs in viral replication. *Microorganisms* **8**, 1899 (2020).
 258. Pautasso, S. *et al.* Strategy of human cytomegalovirus to escape interferon beta-induced APOBEC3G editing activity. *Journal of virology* **92**, e01224-01218 (2018).